# Redox-Active Ligand-Mediated Radical Coupling Reactions at High-Valent Oxorhenium Complexes: Reactions Relevant to Water Oxidation for Artificial Photosynthesis

A Dissertation
Presented to
The Academic Faculty

by

Cameron A. Lippert

In Partial Fulfillment
of the Requirements for the Degree
Doctor of Philosophy in the
School of Chemistry and Biochemistry

Georgia Institute of Technology
August, 2011

**REDOX-ACTIVE LIGAND-MEDIATED RADICAL COUPLING REACTIONS AT HIGH-VALENT OXORHENIUM COMPLEXES: REACTIONS RELEVANT TO WATER OXIDATION FOR ARTIFICIAL PHOTOSYNTHESIS**

Approved by:

Dr. Jake D. Soper, Advisor
School of Chemistry and Biochemistry
*Georgia Institute of Technology*

Dr. Z. John Zhang
School of Chemistry and Biochemistry
*Georgia Institute of Technology*

Dr. Kent E. Barefield
School of Chemistry and Biochemistry
*Georgia Institute of Technology*

Dr. Christopher W. Jones
School of Chemical and Biomolecular Engineering
*Georgia Institute of Technology*

Dr. Angus P. Wilkinson
School of Chemistry and Biochemistry
*Georgia Institute of Technology*

Date Approved: June 28, 2011

## ACKNOWLEDGEMENTS

I wish to thank Professor Jake D. Soper for his guidance and advisement through my graduate career. I highly appreciate his persistence and support during the arduous times throughout my development and maturation as a scientist. I appreciate the support and friendship of the past and current members of the Soper lab with whom it has been a pleasure to work with. I am extremely appreciative to Dr. Adam Offenbacher for his unconditional support and friendship as well as providing stimulating discussions throughout my graduate career. I would also like to thank Mr. Peter Delaune for his friendship and providing endless entertainment, which made life as a graduate student much easier. I would like to express my gratitude to my family for their endless support, and to my committee for their guidance throughout the years.

I am grateful for the financial support provided by Georgia Institute of Technology, American Chemical Society Petroleum Research Fund (Grant 45130-G3), and Defense Advanced Research Projects Agency Young Faculty Award (N6600-1-09-1-2094).

## TABLE OF CONTENTS


Page

ACKNOWLEDGEMENTS iii

LIST OF TABLES x

LIST OF FIGURES xi

LIST OF SYMBOLS AND ABBREVIATIONS xv

SUMMARY xviii

CHAPTER

1 Introduction 1

1.1 The Significance and Challenges of the Assembly and Disassembly of Dioxygen 1

1.1.1 $O_2$ Assembly 1

1.1.2 Introduction to $O_2$ Activation: Dioxygen Disassembly 4

1.2 Nature's Solution to the $O_2$ Challenge 5

1.2.1 Oxygen Evolution 5

1.2.2 Activation of Dioxygen Through $O_2$ Cleavage 9

1.2.2.1 Monooxygenase 9

1.2.2.2 Dioxygenase 11

1.3 Synthetic Approaches to $O_2$ Assembly and Disassembly 11

1.3.1 Water Oxidation Catalyst 11

1.3.2 Oxygen Activation Catalysts 16

1.4 Introduction to Redox-Active Ligands 16

1.4.1 Historical Overview 17

1.4.2 Determination of Metal and Ligand Oxidation State 19

1.4.3 Electronic Coupling and Valence Tautomerism 20

1.5 Reactivity Studies Utilizing Redox-Active Ligands 21

1.5.1 Redox-Active Ligand-Mediated Small Molecules Activation 22

1.6 Goals 26

1.7 References 28

2 Redox-Active Ligand-Mediated Bimetallic Homolysis of Dioxygen 36

2.1 Introduction 36

2.2 Results 41

2.2.1 Preparation and Characterization of Oxorhenium(V) Complexes 41

2.2.2 Preparation and Characterization of Dioxorhenium(VII) Complexes 46

2.2.3 Reactions of $[Re^{V}(O)(cat)_2]^-$ with $O_2$ 49

2.2.4 Computational Studies of $O_2$ Homolysis by $[Re^{V}(O)(cat)_2]^-$ 53

2.2.5 Reactions of Oxorhenium(V) Homologs with $O_2$ 56

2.3 Discussion 60

2.3.1 Mechanism of $O_2$ Homolysis by $[Re^{V}(O)(cat)_2]^-$ 60

2.3.2 Ligand Redox Activity in $1e^-$ Reactions with Oxygenic Radicals 65

2.3.3 $1e^-$ Versus $2e^-$ Redox in $O_2$ Homolysis 67

2.3.4 Implications for Bimetallic Activation and Assembly of $O_2$ 69

2.4 Conclusion 71

2.5 Experimental Details and Supplementary Material 72

2.5.1 General Considerations 72

2.5.2 Methods and Materials 73

2.5.3 Preparation of $(Me_4N)[Re^{V}(O)(ap^{Ph})_2]$ 73

2.5.4 Preparation of $(Et_3NH)[Re^{V}(O)(PPh_3)(ox)_2]$ 74

2.5.5 Preparation of $(Et_4N)[Re^{VII}(O)_2(Br_4cat)_2]$ 75

2.5.6 Preparation of $(Et_4N)[Re^{VII}(O)_2(ap^{Ph})_2]$ 75

2.5.7 Reactions with Dioxygen 76

2.5.8 X–ray Crystallography 77

2.6 References 80

3 Deoxygenation of Nitroxyl Radicals by Oxorhenium(V) Complexes with Redox-Active Ligands 86

3.1 Introduction 86

3.2 Results 86

3.3 Discussion 97

3.4 Conclusion 101

3.5 Experimental Details and Supplementary Material 102

3.5.1 General Considerations 102

3.5.2 Methods and Materials 103

3.5.3 Synthesis of $(Et_4N)[Re^{V}(O)(3,5\text{-}^{t}Bu_2cat)_2]$ 103

3.5.4 Reactions of Oxorhenium(V) Complexes with Nitroxyl Radicals. Stoichiometric Reactions 104

3.5.5 Reactions of $W^{II}Cl_2(PMe_3)_4$ with TEMPO$^{\bullet}$ 105

3.6 References 109

4 Redox-Active Ligand-Mediated Bond-Forming Reactions at a High-Valent Oxorhenium(V) Center 111

4.1 Introduction 111

4.2 Results 113

4.2.1 Preparation of Oxorhenium(VI) Complexes with Ligand-Centered Radicals 113

4.2.2 Electronic Properties 119

4.2.2.1 Nuclear Magnetic Resonance Spectroscopy 119

4.2.2.2 Magnetism 122

4.2.2.3 Electrochemistry 123

4.2.3 Attempted preparation of the S = ½ Congener 125

4.3 Discussion 131

4.3.1 Structural Parameters of Oxorhenium Complexes Containing Ligand-Centered Radicals 131

4.3.2 Ligand Radical Involvement in Re–X Bond-Forming Reactions 132

4.4 Conclusion 135

4.5 Experimental Details and Supplementary Material 136

4.5.1 General Considerations 136

4.5.2 Methods and Materials 137

4.5.3 Synthesis of $Re^{VI}(O)(ap^{Ph})(isq^{Ph})(OC_6Cl_5)$ 137

4.5.4 Synthesis of $Re^{VI}(O)(ap^{Ph})(isq^{Ph})Cl$ 138

4.5.5 Synthesis of $Re_2(\mu\text{-}O)_2(ap^{Ph})_2(isq^{Ph})_2$ 140

4.5.6 X-ray Crystallography 141

4.6 References 143

5 “Masked” Oxyl Radicals: Synthesis, Stabilization, and Reactivity 146

5.1 Introduction 146

5.2 Results 148

5.2.1 Preparation and Characterization of Coordinatively Saturated Oxorhenium Complexes 148

5.2.2 Attempted Synthesis of $[Re(O)(ap^{Ph})(isq^{Ph})(Cl)]^-$ 154

5.3.3 Preparation and Characterization of “Masked” Oxyl Radicals 155

5.3.4 Radical Coupling of “Masked” Oxyls 161

5.3.4.1 Reactions with Hydrogen Atom Donors, $H^\bullet$ 163

5.3.4.2 Reactions with Azobisisobutyronitrile, $C^\bullet$ 164

5.3.4.3 Reactions with $PhMe_2SiB(N^iPr_2)_2$, $Si^\bullet$ and $B^\bullet$ 164

5.3.4.4 Reaction with Gomberg’s Dimer, $C^\bullet$ 166

5.3 Discussion 168

5.3.1 Re–O Bond Formation via Metal-Centered Radical Trapping 168

5.3.2 Radical Coupling at Oxyl-Like Terminal Oxo Ligands 172

5.3.3 Common Properties of "Masked" Oxyls Capable of Radical Coupling at a Terminal Oxo Ligand 176

5.4 Conclusion 178

5.5 Experimental Details and Supplementary Material 179

5.5.1 General Considerations 179

5.5.2 Methods and Materials 180

5.5.3 Synthesis of $TpRe^{V}(O)(cat)$ 180

5.5.4 Synthesis of $TpRe^{V}(O)(3,5\text{-}^{t}Bu_2cat)$ 181

5.5.5 Synthesis of $TpRe^{V}(O)(ap^{Ph})$ 182

5.5.6 Synthesis of $TpRe^{V}(O)(O_2C_2H_4)$ 183

5.5.7 Synthesis of $[TpRe^{V}(O)(isq^{Ph})][BF_4]\bullet 0.28\ CH_2Cl_2$ 183

5.5.8 Synthesis of $Re^{VII}(O)_2(ap^{Ph})(isq^{Ph})$ 184

5.5.9 Synthesis of $Re_2{}^{VI}(O)_2(\mu\text{-}O)(ap^{Ph})_2(isq^{Ph})_2$ 184

5.5.10 Synthesis of $Re^{V}(Cl)_2(ap^{Ph})(isq^{Ph})$ 185

5.5.11 Radical Coupling with Dimethylphenylsilylbis(diisopropylamino)borane 185

5.5.12 Radical Coupling with Triphenylmethyl Radical 186

5.5.13 X-ray Crystallography 186

5.6 References 191

6 Conclusions and Future Directions 194

6.1 Conclusions and Summary 194

6.2 Future Directions 194

6.3 References 196

APPENDIX A: Catalytic Aerobic Alcohol Oxidation by Oxorhenium Complexes Containing Redox-Active Ligands 197

A.1 Introduction 197

A.2 Results 198

A.3 Discussion 204

A.3.1 Mechanistic Insights 205

A.3.2 Ligand Effects on Alcohol Oxidation 208

A.4 Conclusion 209

A.5 Experimental Details and Supplementary Material 209

A.5.1 General Considerations 209

A.5.2 Methods and Materials 210

A.5.3 Reactions with Dioxygen in MeOH 211

A.5.4 Formation of $I_B$ With Constant 2 and Variable 1 211

A.5.5 Formation of $I_B$ With Constant [Re] 211

A.5.6 Formation of $I_B$ From Pure Solution of 2 211

A.5.7 Stoichiometric Alcohol Oxidation 212

A.5.8 Catalytic Alcohol Oxidation 212

A.5.9 Catalytic Alcohol Oxidation in the Presence of Base 212

A.6 References 213

## LIST OF TABLES


Page

Table 2.1: Crystallographic Data and Structure Parameters for $(Et_3NH)[Re^{V}(O)(ap^{Ph})2]^{-}$ • 0.25 MeOH, $(Et_3NH)[Re^{V}(O)(ox)_2(PPh_3)]^{-}$ • 1.5 EtOH, and $(Et_4N)[Re^{VII}(O)_2(ap^{Ph})_2]$. 79

Table 3.1: Rate Constants for TEMPO• Oxidations of Oxorhenium(V) 97

Table 3.2: Rate Constants for Reactions of Oxorhenium(V) Complexes with TEMPO• Obtained by Iterative Fitting to a Biexponential A → B → C Integrated Rate Law Model. 106

Table 3.3: Crystallographic Data and Structure Parameters for $[Re^{V}(O)(3,5\text{-}{}^{t}Bu_2cat)_2]^{-}$. 108

Table 4.1: Selected bond lengths (Å) for $Re^{VI}(O)(ap^{Ph})(isq^{Ph})(OC_6Cl_5)$•$CH_3CN$ and $Re^{VI}(O)(ap^{Ph})(isq^{Ph})Cl$. 117

Table 4.2: Crystallographic Data and Structure Parameters for **2**•$CH_3CN$ and **3**. 142

Table 5.1: List of "masked" oxyl sources. 162

Table 5.2: List of Radical Sources and Corresponding "Masked" Oxyl Source for Radical Coupling Reactions. 163

Table 5.3: Crystallographic Data and Structure Parameters for $TpRe^{V}(O)(ap^{Ph})$, $[TpRe^{V}(O)(isq^{Ph})][BF_4]$•0.28 $CH_2Cl_2$, and $TpRe^{V}(O)(O_2(CH_2)_2)$. 188

Table 5.4: Crystallographic Data and Structure Parameters for $[Re^{V}(Cl)_2(ap^{Ph})(isq^{Ph})]$•0.65 $CH_2Cl_2$ and $[Re_2{}^{VI}(O)_2(\mu\text{-}O)(ap^{Ph})_2(isq^{Ph})_2]$•0.5$CH_3CN$. 189

Table A.1: Oxidation of BnOH to PhCHO by oxorhenium complexes. 203

Table A.2: Catalytic oxidation of BnOH to PhCHO by $[Re(O)(cat)_2]^{-}$ in the presence of base. 203

## LIST OF FIGURES


Page

Figure 1.1: Redox potentials of one-, two-, three-, and four-electron oxidation of water 3

Figure 1.2: A ball and stick representation of the structure of the $Mn_4Ca$ cluster in photosystem II. 7

Figure 1.3: Proposed (a) acid–base and (b) radical coupling mechanisms of water oxidation. 8

Figure 1.4: Consensus catalytic cycle for oxygen activation and transfer by cytochrome P450. 10

Figure 1.5: Solid state structure of the "blue dimer", *cis*,*cis*–$[(bpy)_2(H_2O)Ru^{III}ORu^{III}(OH_2)(bpy)_2]^{4+}$. 13

Figure 1.6: Structural models for Co–Pi water oxidation catalysts. 15

Figure 1.7: Proposed pathway for the OER by Co–Pi. 16

Figure 1.8: Relevant bond distances for (A) iminoseniiquinone ($isq^{Ph}$) and (B) amidophenolate ($ap^{Ph}$) ligands of $Mn^{III}(isq^{Ph})_2(ap^{Ph})$. 19

Figure 1.9: Spin–Coupling of copper semiquinone complexes. 20

Figure 1.10: VT equilibria of $Co^{II}(bpy)(^tBu_2sq)_2$ and $Co^{III}(bpy)(^tBu_2cat)(^tBu_2sq)$. 21

Figure 1.11: Proposed reaction pathway for redox-active ligand-mediated cross-coupling. 24

Figure 2.1: $^1H$ NMR spectra of **(a)** $[Re^V(O)(cat)_2]^-$ at 25 °C, **(b)** $[Re^V(O)(PPh_3)(cat)_2]^-$ at 25 °C, and **(c)** $[Re^V(O)(cat)_2(PPh_3)]^-$ at –40 °C. 42

Figure 2.2: Solid–state structure of the anion in $(Et_3NH)[Re^V(O)(ap^{Ph})_2]$•0.25MeOH shown with 50% probability ellipsoids. 44

Figure 2.3: Solid–state structure of the anion in $(Et_3NH)[Re^V(O)(PPh_3)(ox)_2]$•1.5EtOH shown with 50% probability ellipsoids. 46

Figure 2.4: Solid–state structure of the anion in $(Et_4N)[Re^{VII}(O)_2(ap^{Ph})_2]$ shown with 50% probability ellipsoids. 48

Figure 2.5: Plot of % yield of $[Re^{VII}(O)_2(cat)_2]^-$ as a function of molar stoichiometry in reactions of $[Re^V(O)(cat)_2]^-$ with $O_2$. 50

Figure 2.6: UV–vis absorption spectra for a reaction of 8 x $10^{-5}$ M $[Re^{V}(O)(cat)_2]^-$ with 1 atm $O_2$. 52

Figure 2.7: Reaction energy diagram for 2 $[Re^{V}(O)(cat)_2]^-$ + $O_2$ → 2 $[Re^{VII}(O)_2(cat)_2]^-$. 54

Figure 2.8: Surface plots of the two orbitals with unpaired spin density in the *S* = 1 $O_2$–adduct to $[Re^{V}(O)(cat)_2]^-$. 55

Figure 2.9: Selected UV–vis absorption data for a reaction of 2 x $10^{-4}$ M $[Re^{V}(O)(OPPh_3)(Br_4cat)_2]^-$ with 1 atm $O_2$ at 25 °C in $CH_2Cl_2$ to generate $[Re^{VII}(O)_2(Br_4cat)_2]^-$. 58

Figure 2.10: Plot of ln $|A_t - A_f|$ versus time for UV–vis absorption data collected at 554 nm in a reaction of 8 x $10^{-5}$ M $[Re^{V}(O)(cat)_2]^-$ with 1 atm $O_2$ in $CH_2Cl_2$ at 25 °C to generate $[Re^{VII}(O)_2(cat)_2]^-$. 78

Figure 3.1: Gas chromatogram from a reaction of $[Re^{V}(O)(cat)_2]^-$ (0.035 mmol) with TEMPO$^\bullet$ (0.033 mmol) performed in $CH_3CN$. 88

Figure 3.2a: Electron impact mass spectrum (EI–MS) of the TMP-H fraction from the gas chromatogram shown in Figure 3.1. 88

Figure 3.2b: Electron impact mass spectrum (EI–MS) of the TMP-$CH_2CN$ fraction from the gas chromatogram shown in Figure 3.1. 89

Figure 3.3: Gas chromatogram from a reaction of $[Re^{V}(O)(cat)_2]^-$ (0.023 mmol) with TEMPO$^\bullet$ (0.022 mmol) performed in $CD_3CN$. 89

Figure 3.4a: Electron impact mass spectrum (EI–MS) of the TMP-D fraction from the gas chromatogram shown in Figure 3.3. 90

Figure 3.4b: Electron impact mass spectrum (EI–MS) of the TMP-$CD_2CN$ fraction from the gas chromatogram shown in Figure 3.3. 90

Figure 3.5: Solid–state structure of the anion in $(Et_4N)[Re^{V}(O)(3,5\text{-}^{t}Bu_2cat)_2]$ shown with 50% probability ellipsoids. 92

Figure 3.6: UV–vis absorption data for a reaction of 0.14 mM $[Re^{V}(O)(cat)_2]^-$ with 1.5 mM TEMPO$^\bullet$ at 25 $^{o}$C in $CH_3CN$ to generate $[Re^{VII}(O)_2(cat)_2]^-$. 93

Figure 3.7: Computed UV–vis absorption data obtained from iterative global analysis of a reaction of 0.14 mM $[Re^{V}(O)(cat)_2]^-$ with 1.5 mM TEMPO$^\bullet$ at 25 °C in $CH_3CN$ using a biexponential A → B → C integrated rate law model. 94

Figure 3.8: Time resolved UV–vis absorption data collected at 330 nm (orange ○) for a reaction of 0.14 mM $[Re^{V}(O)(cat)_2]^-$ with 1.5 mM TEMPO$^\bullet$ at 25 °C in $CH_3CN$. 94

Figure 3.9: Plot of $k_1$ (orange ○) and $k_2$ (purple □) as a function of [TEMPO•] for reactions with 0.14 mM $[Re^{V}(O)(cat)_2]^-$ to generate $[Re^{VII}(O)_2(cat)_2]^-$ in $CH_3CN$ at 25 °C. 95

Figure 3.10: Selected UV–vis absorption data for a reaction of 0.14 mM $[Re^{V}(O)(3,5\text{-}^{t}Bu_2cat)_2]^-$ with 1.6 mM TEMPO• at 25 °C in $CH_3CN$ to generate $[Re^{VII}(O)_2(3,5\text{-}^{t}Bu_2cat)_2]^-$. 95

Figure 3.11: UV–vis absorption data for reactions of 0.14 mM $[Re^{V}(O)(Br_4cat)_2]^-$ with 1.5 mM TEMPO• at 25 °C in $CH_3CN$ to generate $[Re^{VII}(O)_2(Br_4cat)_2]^-$. 96

Figure 3.12: Gas chromatogram from a reaction of $[Re^{V}(O)(cat)_2]^-$ (0.041 mmol) with TEMPO• (0.040 mmol) performed in $CH_3CN$ containing 9,10-dihydroanthracene (DHA) (0.52 mmol). 107

Figure 4.1: Solid-state structure of $Re^{VI}(O)(ap^{Ph})(isq^{Ph})(OC_6Cl_5)\bullet CH_3CN$ (**2**) shown with 50% probability ellipsoids. 114

Figure 4.2: Schematic drawing showing the bond lengths (Å) for **2**. 115

Figure 4.3: Solid-state structure of $Re^{VI}(O)(ap^{Ph})(isq^{Ph})(Cl)$ (**3**) shown with 50% probability ellipsoids. 116

Figure 4.4: Variable temperature $^1H$ NMR of $Re^{VI}(O)(ap^{Ph})(isq^{Ph})(Cl)$ in $CD_2Cl_2$. 120

Figure 4.5: Two dimensional NMR (COSY) spectrum of $Re(O)(ap^{Ph})(isq^{Ph})(OC_6Cl_5)$. 121

Figure 4.6: Two dimensional NMR (COSY) spectrum of $Re(O)(ap^{Ph})(isq^{Ph})(Cl)$. 122

Figure 4.7: Magnetic susceptibility of $Re^{VI}(O)(ap^{Ph})(isq^{Ph})(Cl)$. 123

Figure 4.8: Cyclic voltammograms of MeCN solutions of $Re^{VI}(O)(ap^{Ph})(isq^{Ph})(Cl)$ 124

Figure 4.9: Cyclic voltammograms of $Re^{VI}(O)(ap^{Ph})(isq^{Ph})(OC_6Cl_5)$ 125

Figure 4.10: UV-vis absorption data in $CH_2Cl_2$ for $Re^{VI}(O)(ap^{Ph})(isq^{Ph})(Cl)$ (purple line) and the isolated product from a reaction of $Re^{VI}(O)(ap^{Ph})(isq^{Ph})(Cl)$ with 1 equiv of bis(benzene)chromium (red line). 126

Figure 4.11: Solid state structure of **4**. Shown with 50% probability ellipsoids. 128

Figure 4.12: Cyclic voltammograms 130

Figure 4.13: Schematic representation of sterics involved in **3** and $[Re^{VII}(O)_2(ap^{Ph})]^-$. 132

Figure 4.14: Qualitative π orbital interactions 135

Figure 5.1: Qualitative MO of “Masled” Oxyls 148

Figure 5.2: Solid-state structure of $TpRe^{V}(O)(ap^{Ph})$•0.3 Pentane shown with 50% probability ellipsoids. 150

Figure 5.3: Solid-state structure of $TpRe^{V}(O)(OCH_2CH_2O)$ shown with 50% probability ellipsoids. 151

Figure 5.4: Cyclic voltammograms 153

Figure 5.5: Solid state structure of $[Re(Cl)_2(ap^{Ph})(isq^{Ph})]$•0.65 $CH_2Cl_2$ show with 50% probability ellipsoids. 155

Figure 5.6: UV-vis absorption spectra of 2 x $10^{-5}$ M $TpRe(O)(ap^{Ph})$ (brown line) and $[TpRe(O)(isq^{Ph})][BF_4]$ (green line) in MeCN. 156

Figure 5.7: Solid-state structure of $[TpRe^{V}(O)(isq^{Ph})][BF_4]$•0.28 $CH_2Cl_2$ shown with 50% probability ellipsoids. 157

Figure 5.8: Solid state structure of $Re_2^{VI}(O)_2(\mu\text{-}O)(ap^{Ph})_2(isq^{Ph})_2$ shown with 50% probability ellipsoids. 160

Figure 5.9: Qualitative π orbital interactions in $Re^{VI}(O)(ap^{Ph})(isq^{Ph})(Cl)$. 177

Figure 5.10: Qualitative π-bonding MO of (a) $Re^{VI}(O)(ap^{Ph})(isq^{Ph})(Cl)$. 178

Figure 5.11: Theoretical splitting pattern for $Re^{VI}(O)(OSiMe_2Ph)(ap^{Ph})(isq^{Ph})$ and (**b**) experimental MALDI-MS of a reaction with $Re^{VI}(O)_2(\mu\text{-}O)(ap^{Ph})_2(isq^{Ph})_2$ and $PhMe_2Si^{\bullet}$. 190

Figure A.1: UV-vis absorption spectra for a reaction of 4.5 × $10^{-4}$ M **1** (green line) with 1 atm air in MeOH. 199

Figure A.2: Plot showing maximum absorbance for a reaction of 1.5 × $10^{-4}$ M **2** and variable concentrations of **1.** 200

Figure A.3: Plot of maximum absorbance at 600 nm ($\mathbf{I_B}$) for a reaction of 4.0 × $10^{-4}$ M total [Re] with variable ratios of **1** and **2**, and (**b**) rate of $\mathbf{I_B}$ formation as a function of [**1**] in MeOH at 25 °C. 200

Figure A.4: Time-resolved data for the formation and decay of $\mathbf{I_B}$ in reactions of 3.6 × $10^{-4}$ M **2** with 0.2 equiv pyridine oxide (●), 20 equiv LiMeOH (■), and 1 equiv **1** (▲) in MeOH at 25 °C. 204

## LIST OF SYMBOLS AND ABBREVIATIONS

| | |
|---|---|
| Å | angstrom |
| AIBN | azobisisobutyronitrile |
| $AsPh_3$ | triphenylarsine |
| BDE | bond dissociation enthalpy |
| BHT | 2,6-di-*tert*-butyl-4-methylphenol |
| $^{o}C$ | degrees Celsius |
| CCSD | cambridge crystal structure database |
| $CH_2Cl_2$ | dichloromethane |
| $CH_3CN$ | acetonitrile |
| $cm^{-1}$ | wavenumber |
| cm | centimeter |
| DFT | density functional theory |
| DMSO | dimethylsulfoxide |
| ε | molar absorptivity |
| EI | electron impact |
| EPR | electron paramagnetic resonance |
| ESI | electrospray ionization |
| EtOH | ethanol |
| FAB | fast atom bombardment |
| FTIR | fourier transform infrared |
| g | gram |
| GC | gas chromatography |
| k | rate constant |
| kcal | kilocalorie |

| | |
|---|---|
| M | molarity |
| MALDI | matrix assisted laser desorption ionization |
| MeCN | acetonitrile |
| MeOH | methanol |
| mg | milligram |
| MHz | megahertz |
| min | minute |
| mL | milliliter |
| mmol | milimole |
| mol | mole |
| MS | mass spectrometry |
| nm | nanometer |
| NMR | nuclear magnetic resonance |
| $O_2$ | dioxygen |
| $OAsPh_3$ | triphenylarsine oxide |
| OAT | oxygen atom transfer |
| OEC | oxygen evolving complex |
| OER | oxygen evolving reaction |
| $OPPh_3$ | triphenylphosphine oxide |
| % | percent |
| $PPh_3$ | triphenylphosphine |
| ppm | parts per million |
| PSII | photosystem II |
| s | second |
| SOMO | semi occupied molecular orbital |
| SQUID | superconducting quantum interference device |

| | |
|---|---|
| t | time |
| TEMPO | 2,2,6,6-dimethylpiperdine-1-oxyl |
| THF | tetrahydrofuran |
| TMP | tetramethylpiperdine |
| TMS | tetramethylsilane |
| UV | ultra-violet |
| vis | visible |
| vt | variable temperature |
| VT | valence tautomerism |
| $\lambda$ | wavelength |
| W | watt |

## SUMMARY

The making and breaking of O–O bonds has implications ranging from artificial photosynthesis and water oxidation to the use of $O_2$ as a selective, green oxidant for transformations of small molecules. Oxidative generation of $O_2$ from coupling of two $H_2O$ molecules remains challenging, and well defined systems that catalytically evolve $O_2$ are exceedingly rare. Recent theoretical studies have invoked metal oxyl radicals ($L_nM{=}O\bullet$) containing a singly occupied M-O π-type orbital as precursors to O–O bond forming events in both biological and synthetic water oxidation catalysts. However, the lack of stable metal oxyl complexes makes it difficult to explore and understand this hypothesis. The activation of dioxygen (breaking of O–O bonds) to produce terminal metal oxos also remains a challenge. There is an inherent kinetic barrier to the spin-forbidden reactions of triplet dioxygen, and features that engender selective $O_2$ reduction are not easily transferable from system to system. The primary thrust of this thesis work has been to elaborate new methods to generate well-defined metal oxyl radicals for studies of their reactions in radical bond-forming reactions.

Chapter 1 discusses a general and broad overview of the relevant background pertaining to the thesis work. Specifically, this chapter touches upon the significance and challenges of making and breaking O–O bonds, the state of the art methods in both biological and synthetic systems for achieving this reactivity, and the use of redox-active "non-innocent" ligands as electron reservoirs.

Chapter 2 highlights how oxorhenium(V) complexes containing redox-active ligands can be utilized to effect clean bimetallic cleavage of dioxygen. Through a rigorous and detailed kinetic study supplemented by computational investigations, it was determined that electronic coupling to the redox-active ligands lowers the kinetic barrier to $O_2$ activation by facilitating formation and stabilization of intermediates containing

reduced oxygen adducts. The dioxygen cleavage occurs by a net $2e^-$ process through a series of $1e^-$ steps mediated by the redox-active ligands.

Chapter 3 details how oxorhenium(V) complexes deoxygenate nitroxide radicals. This reaction is unusual in that nitroxides are poor oxygen atom donors and are used primarily as radical traps. The key to these types of systems is that the coordination to redox-active ligands affords access to $1e^-$ redox reactions while preserving the ability of the metal to mediate $2e^-$ oxo-transfer reactivity. Most importantly, these reactions show how ligand-centered radicals can facilitate radical reactions at a distal site in the same molecule.

Chapter 4 explains how to trap high-valent oxorhenium complexes containing ligand-centered radicals. Isolation of these species can be accomplished by oxidation with strong chemical oxidants in the presence of trapping agents. These diradical complexes are antiferromagnetically coupled to produce a diamagnetic ground state. The redox-active ligands facilitate Re–X radical-like bond forming reactions at the metal center.

Chapter 5 discuses how to make and isolate “masked” oxyl complexes and their reactivity towards radical bond-forming reactions. The previous chapter discussed how coordinatively unsaturated oxorhenium complexes containing redox-active ligands acted like metalloradicals and not the desired oxyl radical. In order to direct the bond-forming reaction at the terminal oxo new synthetic routes were developed to prepare coordinatively saturated oxorhenium(V) and dioxorhenium(VII) analogs that are precursors to six-coordinate S = ½ "masked” oxyl radicals.

Chapter 6 discusses a brief summary of the major results presented in Chapters 2-5. Future directions for this research project are also explained.

# CHAPTER 1

# Introduction

## 1.1 The Significance and Challenges of the Assembly and Disassembly of Dioxygen.

It has been predicted that by the year 2050 the world's energy consumption will increase to be in the range of 30-40 TW, which is more than a 100% increase with regards to what we consumed in the year 2004.[1-3] Fossil fuels are capable of meeting such a demand. However, the elevated $CO_2$ emissions would produce catastrophic consequences for our planet.[2,3] To effectively reach this demand, new methods of using existing carbon fuels as well as new low-carbon fuels must be developed.

The topic of this thesis will address one fundamental reaction behavior that has relevance to clean energy production in regards to the above concern. Specifically, it will address fundamental issues at the oxidative side of water splitting and how to both generate O–O bonds as well as break them. Both 5- and 6-coordinate oxorhenium complexes have propensity for performing multielectron redox reactions,[4,5] however, they are poor at doing single electron radical reactions. The strategy is to utilize redox-active ligands which are capable of providing redox equivalents for multielectron reactions, therefore allowing access to low barrier, radical-like reactivity without inhibiting the $2e^-$ redox selectivity. The next few sections will discuss the challenges of $O_2$ assembly and activation, and how both nature and current synthetic systems address these two reactions, followed by a detailed strategy that we are applying towards this goal.

### 1.1.1 $O_2$ Assembly

The amount of energy that strikes the earth from the sun in one hour could supply the world's energy demands for an entire year,[6] but only a minute fraction is

utilized and applied to the current energy system. The problem in using this energy arises from a lack of sufficient means of capturing and storing the energy from sunlight.[7] To rectify this problem, a lesson can be taken from nature to capture and store the solar energy in a fuel, like sugar. This is the basis of photosynthesis.[3,8]

$$H_2O \longrightarrow \tfrac{1}{2} O_2 + 2 H^+ + 2 e^- \quad (1)$$

$$2 H^+ + 2 e^- \longrightarrow H_2 \quad (2)$$

$$H_2O \longrightarrow \tfrac{1}{2} O_2 + H_2 \quad (3)$$

Photocatalytic splitting of water into hydrogen and oxygen using solar energy is a potentially clean and renewable source for hydrogen fuel (eq. 1-3).[2,3,6-13] Presently, the solar-to-hydrogen energy conversion efficiency is too inefficient to be economically competitive.[14] The more difficult part of the reaction is the oxidation of water to make O–O bonds (eq. 1). At first glance one might think that the synthesis of a diatomic molecule, $O_2$, would be easy, but it is a much more complicated problem. The thermodynamics of making oxygen from water are demanding: 1.23 V (vs. NHE, pH = 0) (Figure 1.1).[15] A reaction pathway involving a single electron transfer and $^{\bullet}OH$ as an intermediate require strong oxidizing agents $E°(^{\bullet}OH/H_2O)$ = 2.31 V (vs. NHE at pH = 0). The two-electron oxidation via hydrogen peroxide intermediate formation would be more favorable, but is still 0.53 V less favorable then the overall four-electron transformation. The reaction pathway becomes more favorable with each additional consecutive electron transfer with transferring all four at once being the most favorable (Figure 1.1). The reaction is

mechanistically challenging and not well understood. This will be discussed in more detail in section 1.3.

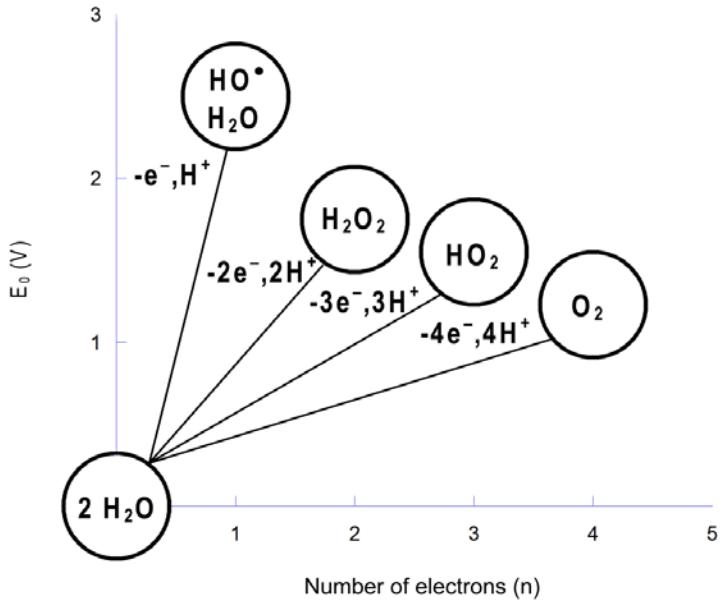


**Figure 1.1.** Redox potentials of one–, two–, three–, and four–electron oxidation of water. Adapted from reference 13.

During the process of water oxidation by metal catalysts, an exceptionally strong metal oxygen ($M=O_{Oxo}$) bond is typically produced prior to $O_2$ generation. In order to complete the catalytic cycle, these highly stable bonds need to be activated by either the direct or indirect capture of solar energy to produce dioxygen and regenerate the catalyst (Scheme 1.1). This step in the oxidation process remains the greatest challenge.[7,16,17] There are two competing hypotheses that will be discussed in section 1.2: The Acid–Base (AB) and Radical–Coupling (RC) hypotheses.

**Scheme 1.1.**

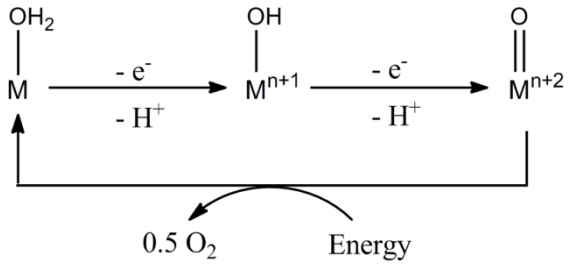


### 1.1.2 Introduction to $O_2$ Activation: Dioxygen Disassembly

The challenges of making O–O bonds were discussed in the previous section. This section will focus on the challenges of the microscopic reverse, breaking O–O bonds. The activation of molecular oxygen is also important and essential to energy demands in that it would serve as the ideal terminal oxidant due to its abundance and benign byproducts.[18- 21] Thermodynamically dioxygen should be reactive. However, under ambient conditions it remains inert towards combustible materials such as wood and fossil fuels. This lack of reactivity derives from a kinetic inertness, resulting from the triplet ground state of $O_2$. This barrier can be overcome when $O_2$ is reacted with species that can undergo single-electron transfer reactions, such as radicals (S = ½), photochemically generated triplet excited states (S = 1), or paramagnetic metal centers (S ≥ ½). But these reactions tend to produce unselective products.[22]

Utilizing $O_2$ as a selective, catalytic oxidant by coupling to transition metals is challenging for several reasons.[23] Reduction of $O_2$ by transition metals to produce two $M{=}O_{Oxo}$ is a $4e^-$ process that typically proceeds in multiple steps. This often leads to O–O bond homolysis and uncontrolled formation of metal oxides in which the oxo-groups are bridged between multiple metal centers.[24] These species tend to be unreactive

towards oxygen atom transfer reactions and thus less useful for selective oxidation chemistry.

## 1.2 Nature's Solution to the $O_2$ Challenge

Over the course of millions of years of evolution, nature has been able to fine tune and perfect the process of making and breaking O–O bonds. Specifically, biological systems have developed classes of enzymes to handle these two different reaction types. For example, photosystem II (PSII) performs water oxidation ($O_2$ assembly) and oxygenases carry out dioxygen activation ($O_2$ cleavage).

### 1.2.1 Oxygen Evolution

Plants, algae, and cyanobacteria harvest solar energy to oxidize water and evolve $O_2$. This process is performed by the oxygen evolving complex (OEC) in PSII.[7,8,25] PS II uses light to produce a charge-separation reaction that results in the reduction of plastiquinone (PQ), the oxidation of water, and the generation of a proton gradient across the chloroplast thylakoid membrane. The overall reaction requires four photochemical, charge-separation reactions (eq. 4).[26-29] This four photon cycle was first observed by Joliot and coworkers in flash experiments, which led to Kok's proposal of the store- or S-state cycle (Scheme 1.2).[30,31] As a direct result of this light-driven reaction, water is oxidized to dioxygen. Each advancement in the S-state has since been correlated with an oxidation state change in the OEC.

$$2\,H_2O + 2\,PQ + 4\,H_{out}^{+} \longrightarrow O_2 + 2\,PQH_2 + 4\,H_{In}^{+} \qquad (4)$$

**Scheme 1.2.** Adapted from reference 24.

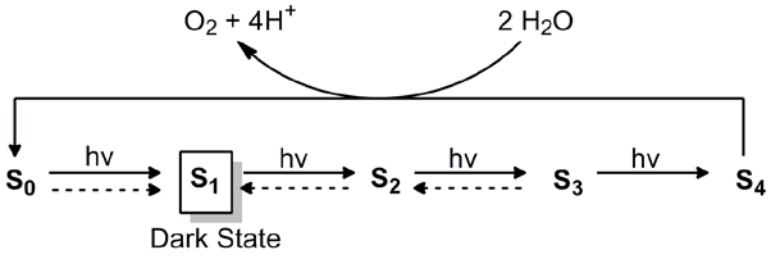


The structure of PSII and the mechanism of $O_2$ evolution in photosynthesis has been the focus of extensive research over the past 30-40 years.[2-13,32-41] However, even with the vast amount of research on the topic, the exact mechanism and structure remain debatable. The OEC consists of a tetranuclear manganese cluster and an associated redox-active tyrosine,[25-29] $Y_Z$. PSII contains a chlorophyll complex, P680 that undergoes a light-induced charge separation, reducing the $PQ_A$, which in turn reduces $PQ_B$. $P680^+$ is then reduce by the redox-active $Y_Z$ to form a neutral tyrosyl radical $Y_Z^\bullet$, and finally $Y_Z^\bullet$ is reduced by the manganese cluster. The exact structure and orientation of the tetranuclear manganese core during oxygen evolution has been the subject of recent spectroscopic studies using X-ray absorption and electron paramagnetic resonance (EPR), which have led to some detailed proposals of the structure.[42] However, the most well accepted structure, today, is the cubane-like structure consisting of 4 manganese atoms, 5 oxygen atoms and one calcium atom all linked in a cluster (Figure 1.2).[43]

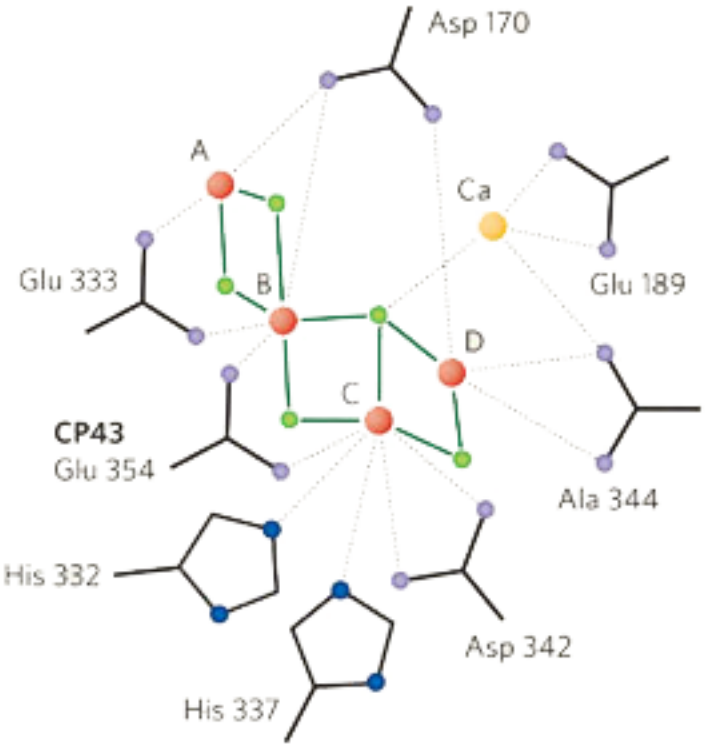


**Figure 1.2.** A ball and stick representation of the structure of the $Mn_4Ca$ cluster in photosystem II. The structure was obtained from X–ray spectroscopy (XANES, XAFS, and X-ray crystallography) of a crystal of the photosystem II reaction centre. Shows four Mn atoms (red; A–D), five O atoms (green), and a Ca atom (yellow).

The exact mechanism of biological O-O bond formation is also under much debate and controversy in the literature. There are two prevalent theories on the mechanism of water oxidation: Acid-base (AB) and radical coupling (RC) (Scheme 1.3).[44] The AB hypothesis of water oxidation consists of a nucleophilic attack by an oxygen nucleophile (hydroxide ion, water, or an M–OH) on a high-valent, electrophilic $M{=}O_{oxo}$ to produce $O_2$ with concomitant reduction of the metal center by four electrons (Figure 1.3a).[45]

**Scheme 1.3.** Adapted from reference 46.

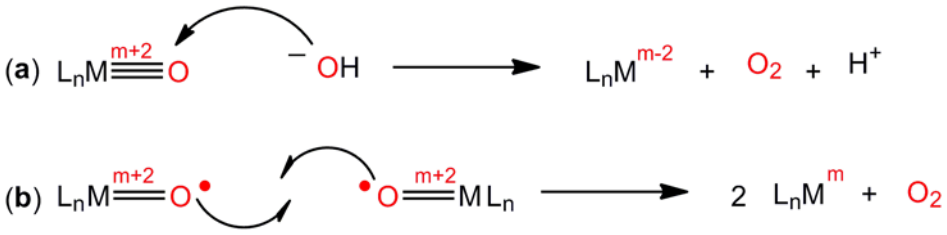


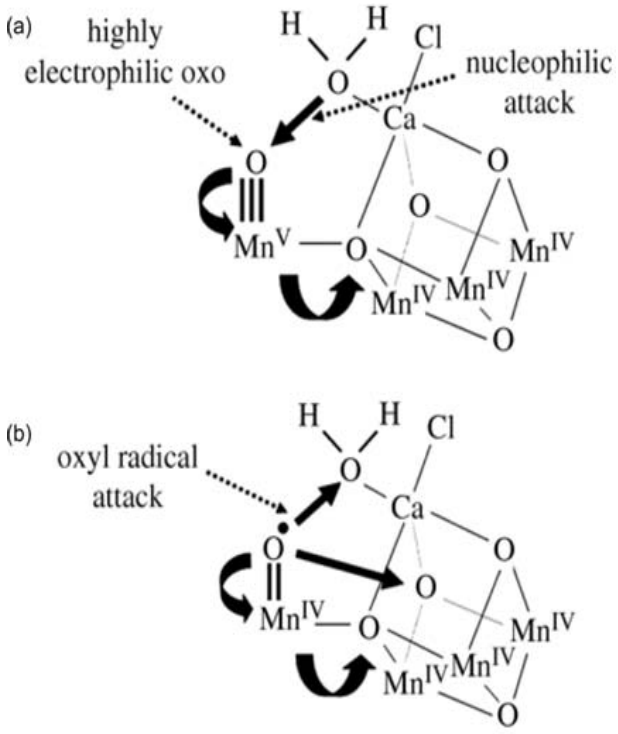


**Figure 1.3.** Proposed (a) acid–base and (b) radical coupling mechanisms of water oxidation.

There have been some recent computational studies that propose an alternative mechanistic possibility of water oxidation that occurs via a RC of two oxygen-based radicals.[40,46- 51] The RC hypothesis consists of radical coupling of a high-valent metal oxyl radical (M=O•) with another oxygenic radical (Figure 1.3b).[45,45]

### 1.2.2 Activation of Dioxygen via $O_2$ Cleavage.

Biological oxidations by molecular oxygen can roughly be divided into two categories: (1) Oxidations where the $O_2$ serves as an electron sink, typically producing $H_2O_2$ or $H_2O$,[15,52,53] and (2) Oxygenations where the $O_2$ is partially or fully incorporated into the oxidation product.[54,55] This section will only discuss the 2nd category. These reactions are carried out by enzymes usually containing transition metals, however, they are not a requirement.[56] There are examples of non-metal based monooxygenases such as flavin (nucleotide)-dependent monooxygenases that will not be discussed.[56] The oxygenation enzymes can be further categorized into monooxygenases, which incorporate only a single oxygen atom from $O_2$ into the substrate and the other is reduced to water, and dioxygenases which incorporate both oxygen atoms into the substrate.[56]

#### 1.2.2.1 Monooxygenase

Monoxygenases are enzymes that incorporate only one oxygen from dioxygen into the oxidized substrate while the other is reduced to water. Cytochromes P450 (P450) will be used as an example to explain how biological systems have tackled the challenge of activating $O_2$. P450 are monooxygenases found in nearly all living organisms. They catalyze a diverse set of oxidations, such as hydroxylation of strong C–H bonds in hydrocarbons, epoxidations of alkenes, and oxidation of primary amines to ketones, among many others.[57] Four electrons are necessary to cleave dioxygen to formally produce two equivalents of oxo anions ($[O]^{2-}$). In hydroxylation reactions, one of these anions combines with two protons to form water while the other is inserted into a C–H bond of the substrate to produce a C–OH bond.

The active site of P450 contains a heme iron center. The iron is tethered to the P450 protein via a thiolate ligand derived from a cysteine residue. P450 catalyzes a vast variety of reactions, however, a generalized mechanism can be proposed (Figure 1.4).[57]

In general, the iron center is reduced by a single electron prior to dioxygen coordination (**3**-**5** in Figure 1.4). Another electron transfer process occurs to produce an iron peroxo species which then undergoes two proton transfer steps to release water and oxidize the iron center by two electrons to produce a highly reactive high-valent iron-oxo containing a porphyrin radical (**6** and **7** in Figure 1.4). This high-valent iron-oxo termed "compound I" is believed to be the oxidizing species, and the reactivity is often attributed to the ground state diradical structure of the active site.[57] This is an overall four-electron process to produce a high-valent M=O, which is then inserted into a C–H bond to produce a C–OH bond and regenerate the catalyst.

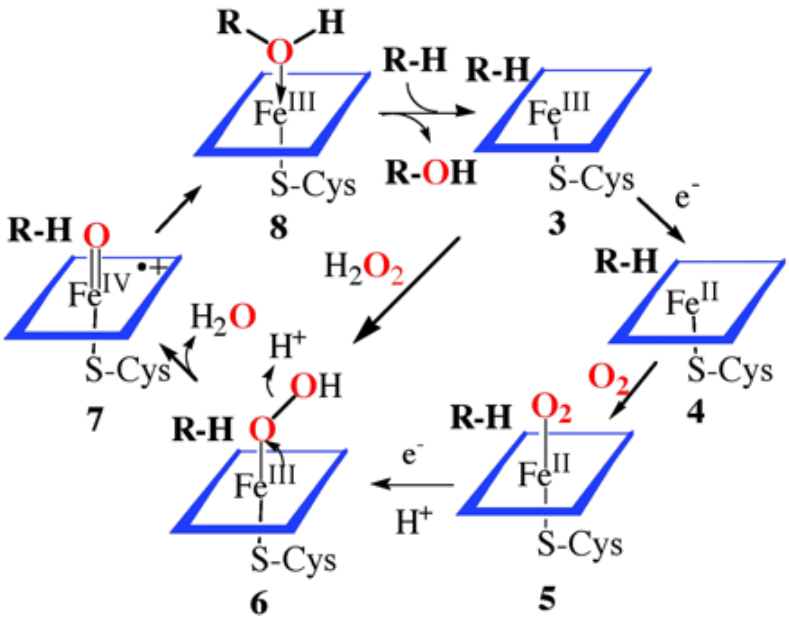


**Figure 1.4.** Consensus catalytic cycle for oxygen activation and transfer by cytochrome P450.

1.2.2.2 Dioxygenase

Dioxygenases catalyze the incorporation of both atoms of $O_2$ into substrates. When both oxygen atoms are incorporated into the same molecule it is referred to as an intramolecular dioxygenase; when the two atoms are incorporated into two products it is an intermolecular dioxygenase.[58] A common step in oxygenase reactivity is cleavage of the dioxygen O–O bond to generate a transition metal oxo complex.[59-62] Bimetallic $O_2$ activation is frequently observed with metalloenzyme dioxygenases.[59,60,63] Despite structural differences between the dioxygenases they tend to share general, key features and proceed by similar mechanisms.[60] The similar mechanisms propose that $O_2$ coordinates with concomitant oxidation of the metal complex by a single electron. Following coordination an electron transfer event takes place to produce a bridging peroxo or superoxo species. From here the O–O bond is cleaved and generates two oxidizing M=O fragments which incorporate the oxygen atom into the substrate(s).[60]

In sum, the general features of dioxygenases that engender dioxygen activation are as follows (1) vacant coordination sites to allow for coordination of the substrate and molecular oxygen, (2) the ability to form a peroxo bridged species, and (3) the ability to perform four sequential one-electron redox events leading to the cleaving of dioxygen.

## 1.3 Synthetic Approaches to $O_2$ Assembly and Disassembly

The previous sections discussed the challenges with molecular assembly and disassembly of $O_2$ and how nature has approached the issue. The following section will discuss how chemists are approaching the challenge synthetically.

### 1.3.1 Water Oxidation Catalysts

The goal of artificial photosynthesis is to use the energy of the sun to produce high-energy chemicals for energy storage and conversion. A key half reaction in both photosynthesis and artificial photosynthesis is water oxidation to dioxygen (eq. 5),

$$2\ H_2O \xrightarrow{-4\ e^-,\ -4\ H^+} O_2 \qquad (5)$$

($E°$ = –1.23 V at pH = 0, –0.82 V at pH = 7). Finding catalysts to carry out this reaction at high rates for sustained periods has been problematic given the mechanistic requirements imposed in removing four electrons and protons from two water molecules with formation of an O-O bond.[64-66] Even though water oxidation has been studied to great extent over the past 30-40 years, there are only a handful of water oxidation catalyst and even less that are well understood mechanistically.[67–78]

There are diverse arrays of methods being undertaken in order to tackle the challenge of water oxidation that range from homogenous catalysis to generation of OEC-like metal cubanes via electrodeposition. The first well-defined water oxidation catalyst was Meyer's "blue dimer" (Figure 1.5).[79] The oxidative equivalents in this system come from Ce(IV) to produce a O=Ru(V)–O–Ru(V)=O dimer, the active species in water oxidation. It was initially unknown if oxygen evolution occurred via coupling of two metal oxos (Scheme 1.4a) or nucleophilic attack of a water molecule on a single oxo ligand (Scheme 1.4b).[80] However, recent detailed labeling studies have shown that the mechanism proceeds by nucleophilic attack of a water molecule on a single oxo ligand to produce $O_2$ (AB-type mechanism).[81-85] This was further supported by the discovery of a single-site water oxidation catalyst.[86]

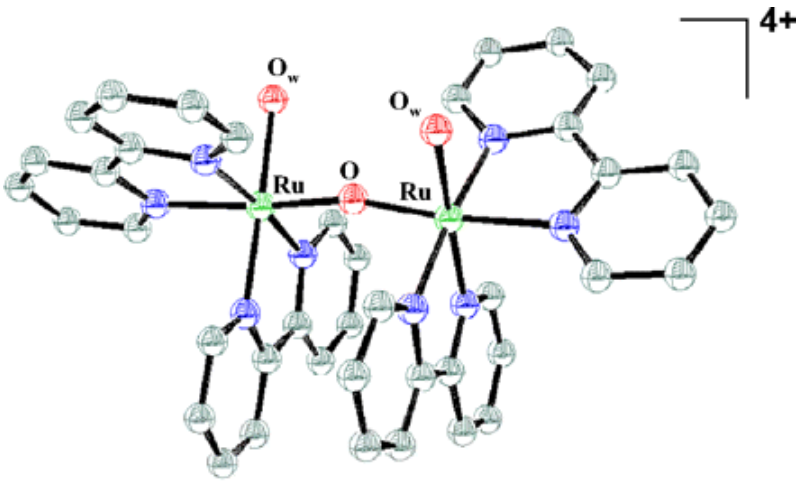


**Figure 1.5.** Solid state structure of the "blue dimer", *cis*,*cis*–$[(bpy)_2(H_2O)Ru^{III}ORu^{III}(OH_2)(bpy)_2]^{4+}$.

**Scheme 1.4**. Adapted from reference 70.

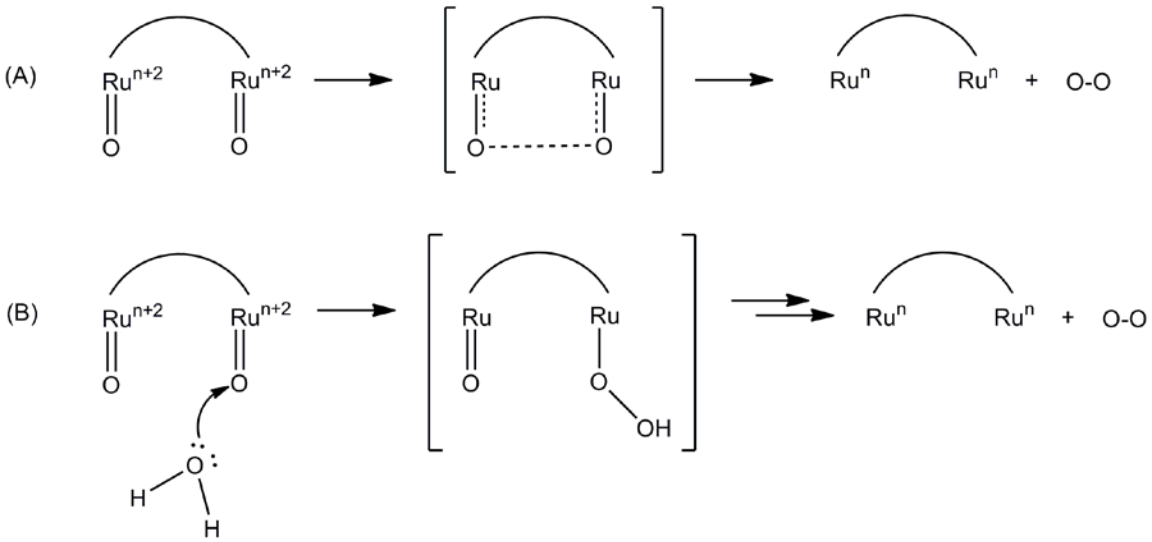


The "blue dimer" has evolved over the years into a more efficient water oxidation catalyst with many derivatives.[86- 90] However, as notable as these catalysts are, there are still many flaws. Ruthenium is a rare and expensive metal which makes it not ideal for

use as a catalyst. This system also requires the use of stoichiometric oxidants to generate the active, oxidizing Ru(V)=O species. Recent progress by Meyer and coworkers has led to the removal of chemical oxidants by attaching the catalyst to an electrode surface.[91-93] This allows for electrochemical, catalytic water oxidation, but still requires a great deal of energy due to the overpotential of ~600 mv.[91] It is noteworthy to mention the more recently developed manganese and iridium catalysts.[94-98] These systems have improved on the efficiency of water oxidation compared to the "blue dimer" and are believed to react by analogous mechanisms.

Nocera and coworkers have developed easily prepared, earth-abundant catalysts consisting of cobalt or nickel that oxidize water.[99,100] They showed that electrolysis of $Co^{2+}$ or $Ni^{2+}$ in pH 7 phosphate (Pi or MePi) or borate (Bi) electrolytes effects the electrodeposition of a highly active water oxidation catalyst as an amorphous thin film on an inert indium-tin-oxide (ITO) or fluorine-tin-oxide (FTO) electrode. [99-102] In contrast to spinel and perovskite metal oxides that oxidize water under highly alkaline conditions[103] or homogenous Ru catalyst that utilize Ce(IV) under acidic conditions, the electrodeposited cobalt-phosphate compound is among the few catalysts for which activity at neutral pH has been demonstrated.[99,101,102,104,106,107] Among the water oxidation catalysts, this system is unique in that it does not involve a precious metal constituent. This catalyst system is made more unique by the fact that it undergoes a self-repair process. Any $Co^{2+}$ formed and released into solution during water-splitting catalysis will be redeposited upon oxidation to $Co^{3+}$ in the presence of phosphate. The ability to self-repair allows for a structurally less stable catalyst without inhibiting its catalytic function.

The exact structure and mechanism of these amorphous films have yet to be determined, however, significant work has been done to elucidate them. There are two proposed structures of the active species in water oxidation that are under debate in the literature (Figure 1.6).[104,105] Dau and coworkers favor a corner-sharing cubane structure

(Figure 1.6 b and d) deduced from XAS data relating to the bulk of the cobalt catalyst film (CoCF). However, Nocera and coworkers favor an edge-sharing molecular cobaltate cluster (MCC) deduced by a variety of in situ X-ray spectroscopy methods.

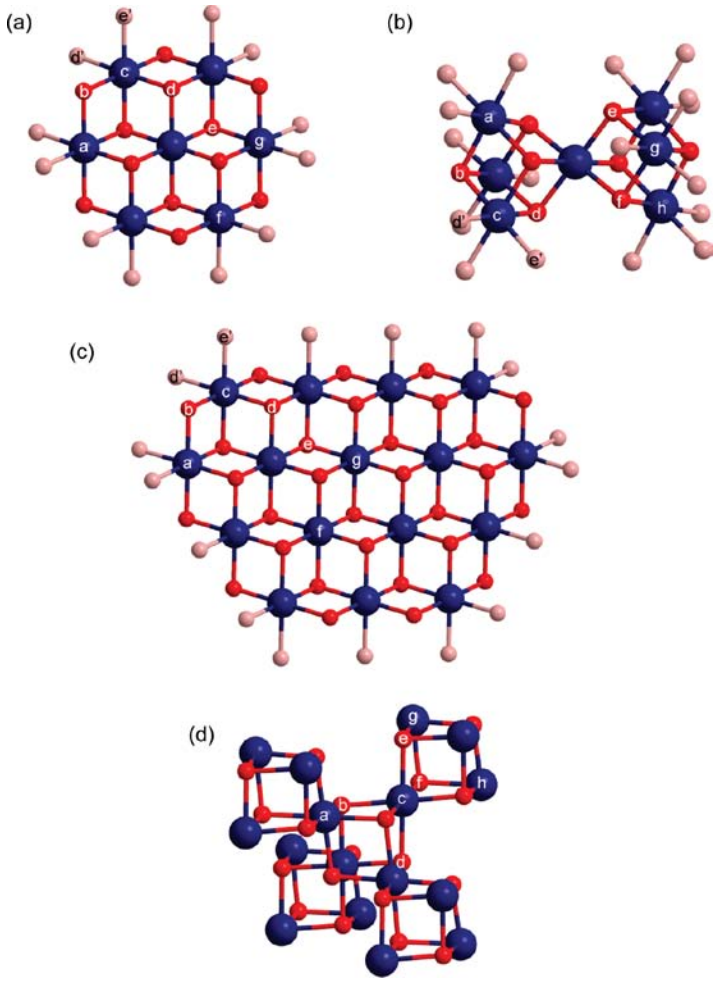


**Figure 1.6.** Structural models for Co–Pi. Bridging oxo/hydroxo ligands are shown in red, nonbridging oxygen ligands (including water, hydroxide, and phosphate) and are shown in light red and Co ions in blue. (a) Edge–sharing molecular cobaltate cluster (MCC) model for surface Co–Pi. (b) Corner–sharing cubane model for surface Co–Pi. (c) Edge–sharing MCC model for bulk Co–Pi. (d) Corner sharing cubane model for bulk Co–Pi.

The exact mechanism of water oxidation by these catalysts has not been determined irrefutably, but mechanistic proposals are supported by XANES,[104] EPR,[106]

electrochemical kinetics,[107] and $^{18}O$ labeling studies.[107] Previous studies on the cobalt valency showed that cobalt centers attained an oxidation state of +IV during water oxidation catalysis. The current mechanistic hypothesis is believed to be a rapid, one electron, one proton equilibrium between $Co^{III}$–OH and $Co^{IV}$–O in which a phosphate species is the proton acceptor, followed by a chemical turnover-limiting process involving O–O bond coupling between two high-valent cobalt oxyl radicals (Figure 1.7).[107] This catalyst appears to have a RC-type mechanism while the homogenous, single-site Ru and Ir catalysts appear to have an AB-type mechanism.[79-90]

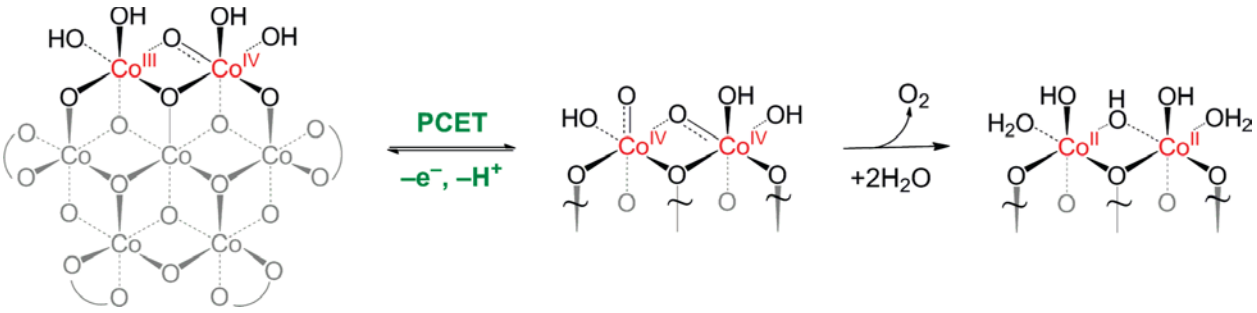


**Figure 1.7.** Proposed pathway for the OER by Co–Pi. A proton coupled electron transfer (PCET) equilibrium proceeded by a turnover-limiting O–O bond forming step is consistent with current dependencies on proton and electron equivalencies. Curved lines denote phosphate, or $OH_x$ terminal or bridging ligands.

### 1.3.2 Oxygen Activation Catalysts

Activation of molecular oxygen is the topic of chapter 2 and will be discussed in more detail then.

## 1.4 Introduction to Redox-Active Ligands

There is a necessity for metal centers to provide two or more redox equivalents in selective multielectron reactions to avoid unfavorable oxidation states or too stable high-valent, multiply bonded metal-substrate intermediates. Biological systems utilize three main strategies for multielectron chemistry at base metals: (1) between two

substrate-binding metal ions working in concert, (2) between the metal ion reaction center and its redox-active ligand, and (3) between the substrate-binding ion and a neighboring redox-active cluster. These three strategies can serve as an inspiration for chemists attempting to approach nature's efficiency, selectivity, and control in small molecule management. Specifically, the vast majority of inorganic chemistry has dealt with metal ions containing redox-inert ligands, which leaves the above three strategies open to experimentation.

This thesis explores strategy (2), that is, the use of a redox-active ligand working together with the metal ion as the redox center. Traditionally, inorganic chemists use ancillary ligands to block coordination sites, and adjust steric and electronic properties at the metal center. By allowing supporting ligands to undergo redox changes unfavorable metal oxidation states can be avoided. This allows for the development of new catalysts where the redox system is not restricted to the metal ion.

### 1.4.1 Historical Overview

The oxidation states of certain ligands in coordination complexes are ambiguous because the most stable oxidation state of the ligand in the free form does not necessarily describe its behavior when coordinated to a metal ion. Nitric oxide, $^{\bullet}NO$, is a good example.[108] Coordination compounds containing nitric oxide usually consider it formally as either the cation $NO^+$, isoelectronic to CO, or the anion $NO^-$, isoelectronic to $O_2$. For example, a reaction of NO gas with iron(III) octaethyl- or tetraphenylporphyrin yields a linear Fe–NO unit formally assigned as Fe(II)($NO^+$).[109,110]

Nitric oxide is considered a redox-active ligand in the sense that its oxidation state in complexes can be different from that of the free ligand form. However, it does not usually show any redox changes once coordinated.[111-114] For that reason they are not used as supporting redox agents in coordination compounds.

Here, “redox-active” ligands will refer to an organic molecule or ion that is able to coordinate to a metal ion in a certain oxidation state, and once coordinated change its oxidation state upon reaction with redox agents.

The first example of such behavior was a nickel dithiolene complex studied in the 1960’s (Scheme 1.5).[128] It was investigated by magnetometry, EPR, and electronic absorption spectroscopy, initially by Schrauzer and Mayweg,[115,116] then in great detail by Davison and Holm[117- 123] and by Gray.[124- 128] Controversy arose because EPR parameters showed the presence of unpaired spin density on the central metal, therefore it cannot be Ni(IV). After debate going back-and-forth in the literature[115-128] it was recognized that the electronic structure consisted of mostly ligand-based radicals with stabilization through covalent binding to the transition metal.[129] This is significant because it showed that the ligand could support a radical.

**Scheme 1.5.** Adapted from reference 118.

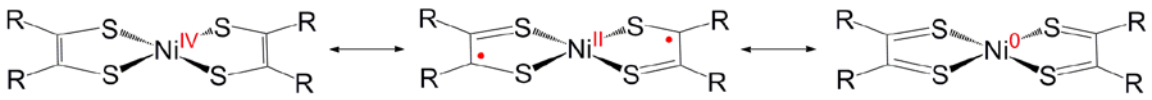

### 1.4.2 Determination of Metal and Ligand Oxidation State

Determination of oxidation states of transition metals containing redox-active ligands is often complicated.[108-129] Redox-active ligands exist in multiple oxidation states which leads to changes in the bond distances of the ligands. This allows for high resolution X-ray crystallography to be used as a tool for identifying oxidation states of the ligand due to distinct bond distances observed for each ligand oxidation state.

A wealth of literature has been compiled over the past 30 years containing metrical parameters for redox-active ligands in various oxidations states as well as coordinated to various metal centers.[130-150] Wieghardt and coworkers are the leading experts in finding and assigning oxidation states of redox-active ligands using X-ray crystallography paired with spectroscopic techniques.[130- 136] For example, they have synthesized a manganese complex with two amidophenol-derived ligands that are distinguishable by their bond lengths (Figure 1.8).[137] The localization of spin density is evident by the loss of aromaticity in the ring. The ring takes on a quinoid-like pattern of four long and two short C–C bonds and contraction of the C–N and C–O bonds (Figure 1.9B). Assignments of ligand oxidation states of non-innocent ligands continue to become easier as more high-quality crystal structures become available.

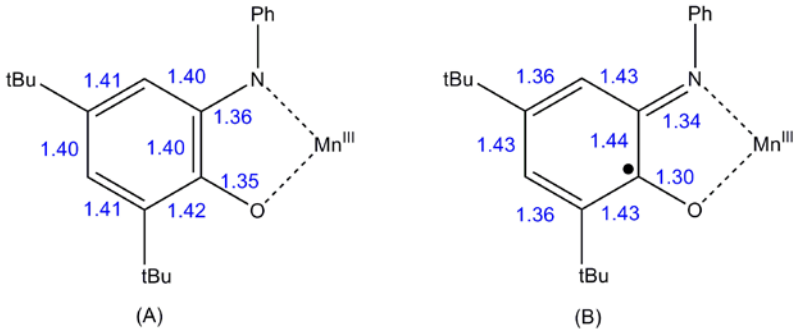


**Figure 1.8.** Relevant bond distances for (A) iminoseniiquinone ($isq^{Ph}$) and (B) amidophenolate ($ap^{Ph}$) ligands of $Mn^{III}(isq^{Ph})_2(ap^{Ph})$. Adapted from reference 127.

### 1.4.3 Electron Coupling and Valence Tautomerism

The presence of multiple resonance structures not only affects oxidation state assignments, but also affects electronic coupling and valence tautomerism. Multiple variables, such as geometry and coordination number, affect the degree and type of electronic interaction between redox-active ligands and metal centers, but their influence is still not fully understood.[138] For example, in a series of copper(II) complexes the antiferromagnetic coupling between two semiquinone ligands and ferromagnetic coupling between the ligand and the metal center is controlled by the addition of a neutral ligand (Figure 1.9).[138] These coupling assignments suggest communication through the linking metal center with disruption by donation into the metal orbitals by the pyridine based ligands. Further research is needed in order to understand these changes and to be able to formulate rational predictions of electronic coupling.

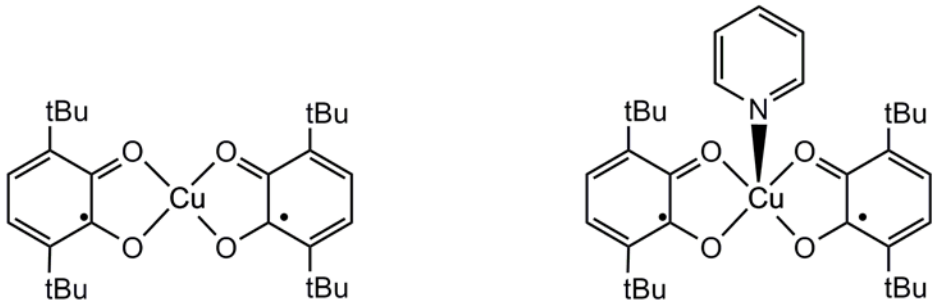


**Figure 1.9.** Spin–Coupling of copper semiquinone complexes.

The frontier π-orbitals of quinoid-like, redox-active ligands are close in energy to properly matched valence d-orbitals of transition metals. The spatial and electronic proximity of these orbitals allows intramolecular, interligand exchange of electrons

between mixed-valent ligand systems. In these systems an equilibrium exists between the $M^{n+1}(L)$ and $M^{n}(L^{\bullet})$ redox isomers.[139–141] For example, the 2,2'-bipyridine (bpy) adduct of $Co(^{t}Bu_2sq)_2$ [Where $^{t}Bu_2sq$ = 3,5-di-*tert*-butylsemiquinone] actually exists as a Co(III) metal center with a mixed-valent ligand set at room temperature in the solid state. However, when in solution and at elevated temperatures, the major species is a Co(II) metal center with two ligand radicals (Figure 1.10).

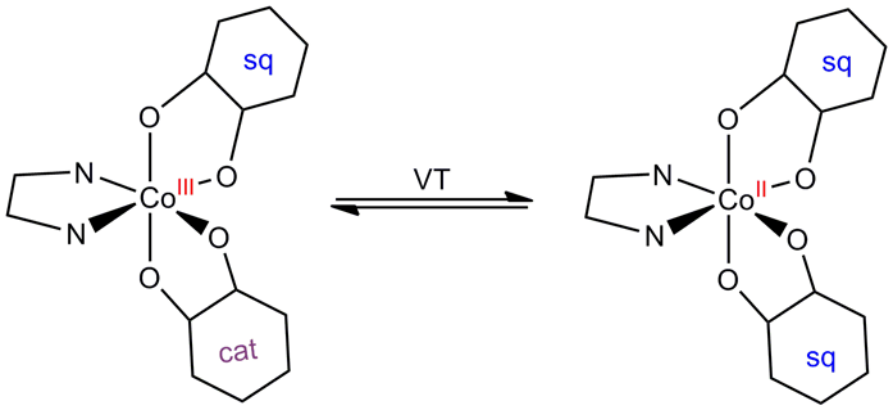


**Figure 1.10.** VT equilibria of $Co^{II}(bpy)(^{t}Bu_2sq)_2$ and $Co^{III}(bpy)(^{t}Bu_2cat)(^{t}Bu_2sq)$.

### 1.5 Reactivity Studies Utilizing Redox-Active Ligands

There is great interest in the activation of small molecules such as $O_2$, $N_2$, and $CO_2$ as well C–H and C–R bonds.[142- 150] The redox-active properties of transition metals have usually been used for the activation of small molecules.[142-146] In general, coordination of small molecules to transition metal centers significantly affects their redox potentials. The binding of small molecules to metal ions enables an inner-sphere electron transfer process which facilitates their oxidation or reduction depending on the electronic and redox properties of the metal center.[140-150] These processes represent the elementary steps behind the metal complex-assisted activation of small molecules.

There are however, limitations to the utility of transition metals for small molecules activation. The reactivity of the 3d metals usually diverges significantly from 4d and 5d metals. The 3d metals prefer changes in oxidation state that vary by a single electron where the 4d and 5d metals tend to avoid odd electron counts and prefer two electron changes in oxidation state.[151-152] From this, the 3d metals tend to activate small molecules via radical pathways. This usually leads to unselective reaction products or they select for undesirable products.[151] On the other hand, the 4d and 5d metals tend to avoid radical pathways facilitating selective and controlled redox reactions. However, this same trait limits their substrate options. For example, they tend to not react with radical species.[153,154] The use of redox-active ligands to store and deliver redox equivalents has shown success in combining the best of early and late metals[147,149,156-160] This method provides a new strategy for activation of small molecules.

### 1.5.1 Redox-Active Ligand-Mediated Small Molecules Activation

Catecholates, amidophenolates, and bis(iminopyridine) ligands have shown great success in the ability to facilitate activation of small molecules.[155-160] These ligands can coordinate as a fully reduced catecholate-like, a singly oxidized semiquinonate-like, or a fully oxidized quinoid-like molecule (Scheme 1.8). The redox potentials of these three oxidation states normally fall within the envelope of metal-centered valence changes, leading to the observation of non-innocent behavior, which has been elucidated by spectroscopic, electrochemical, and reactivity studies.[150] The non-innocence of these ligands derives from the mixing of ligand-based π-orbitals and metal based d-orbitals.

The work of Chirik, Heyduk, and Soper has pioneered the field of small molecule activation facilitated by redox-active ligands. Heyduk's work has focused on using redox-active ligands on $d^0$ metals to bring late-transition-metal reactivity to early metals.[156,157] For example, a $d^0$ Zr(IV) center with two redox-active amidophenolate ligands, $Zr^{IV}(ap^{tBu})_2(THF)_2$ [where ap = 2,4-di-*tert*-butyl-6-*tert*–butylamidophenolate], is capable of

performing oxidative addition of $Cl_2$ to produce $Zr^{IV}(isq^{tBu})_2(Cl)_2$ [where isq = 2,4-di-*tert*-butyl-6-*tert*-butyliminosemiquinonate] (Scheme 1.6). The Zr(IV) center contains zero d-electrons; however, the ligands provide the redox equivalents to perform this two electron reaction.

**Scheme 1.6.**

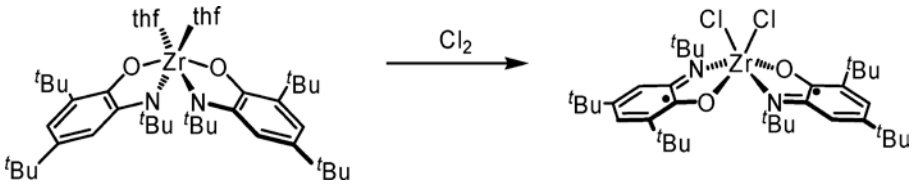


The work of Chirik and coworkers, and Soper and coworkers has focused mainly on later 3d-metals containing redox-active ligands in attempts to mimic the typical 2 electron reactivity of the heavy elements, i.e. Pd and Pt. For example, Chirik and coworkers have had great success in utilizing the redox-active ligand bis(imino)pyridine to perform multielectron $N_2$ and C–H activation on iron, among others.[147-150] The metal typically favors single electron changes in oxidation state that tend to lead towards unselective radical pathways. The ability of the redox-active ligand to store and deliver redox equivalents allows the iron center to perform multielectron reactions while avoiding the unselective, radical pathway.

Recent works from Soper and coworkers have shown the utility of redox-active ligands to mediate bond-forming reactions at 3d metals.[158-160] They have shown that redox-active ligands facilitate $2e^-$ C–C bond-forming reactions at metal centers that typically favor single electron changes in oxidation states. For example, they prepared

square planar cobalt complexes containing redox-active amidophenolate ligands that are strong nucleophiles but mild 2e$^-$ reductants. The redox-active ligands serve as reservoirs that facilitate well-defined 2e$^-$ pseudo-oxidative addition and reductive elimination reactions at cobalt(III), comprising both steps of a catalytic cycle for Negishi-like cross-coupling of alkyl halides with alkyl- and aryl zinc reagents (Figure 1.11).[158]

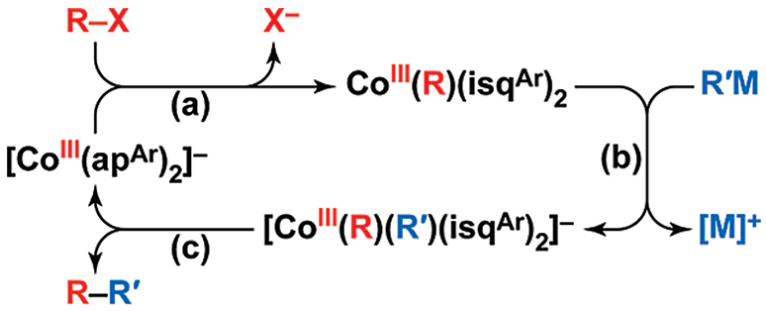


**Figure 1.11.** Proposed reaction pathway for redox-active ligand-mediated cross-coupling showing (a) pseudo oxidative addition of alkyl halide and (b) organozinc reagent followed by (c) pseudo reductive elimination to produce a new C–C bond where the cobalt center maintains a formal oxidation state of +3 throughout the reaction.

The utility of redox-active ligands have also showed recent success in dioxygen activation. However, the features that affect the degree of activation, 1e$^-$ to 4e$^-$, and selectivity are not generalizable. For example, Abu-Omar and coworkers have synthesized a d$^0$, zirconium(IV) complex containing two redox active diamide ligands in which each ligand can be oxidized by two electrons to the diimine.[161] Upon reaction of the amide complex with dioxygen a zirconium(IV) bisperoxo complex is isolated where each of the diamide ligands provided 2e$^-$ to reduce each of two dioxygen molecules by 2e$^-$ to generate peroxides for an overall 4e$^-$ process (Scheme 1.7). On the other hand, Rhode and coworkers have shown that when the redox-active ligand bis(imino)pyridine is coordinated to a Ni(II) metal center it is capable of cleaving the O–O bond giving

ligand centered oxygenation (Scheme 1.8).[162] Unlike the Zr(IV) reaction described above the locus of oxidation is on the ligand. These are only two examples that show the utility of redox-active ligands in $O_2$ activation and how they can differ from system to system.

**Scheme 1.7.**

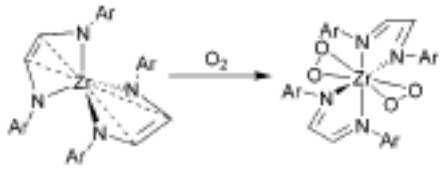


**Scheme 1.8.**

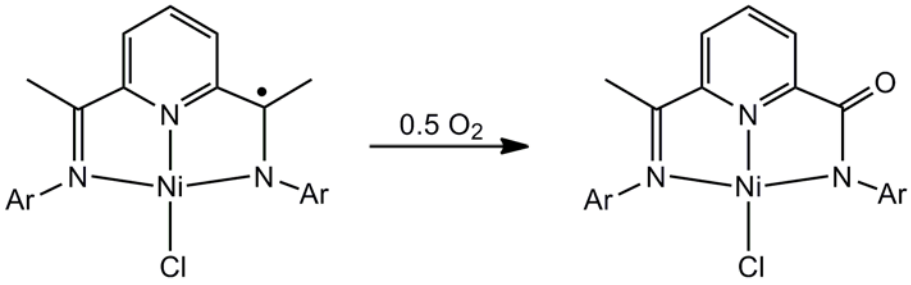

## 1.6 Goals

Simple bond-making and -breaking reactions are overwhelmingly multielectron redox processes.[2] When compared to well-established strategies of single electron transfer, the fundamental understanding of multielectron redox chemistry is underdeveloped.[163- 167] New molecular designs are needed to develop and understand multielectron bond-making and -breaking events to the level of well known single electron processes.

Consequently, this thesis will describe how redox-active ligands can be used to incorporate ligand radicals into reactions that make and break O–O bonds, and to use the ligand radical density for radical like reactivity at other sites in the same molecule. More specifically, this thesis will answer the following five questions:

1. How do you synthesize closed-shell high-valent five- and six-coordinate oxorhenium complexes containing redox-active ligands?
2. How do you synthesize high-valent five- and six-coordinate oxorhenium complexes containing a ligand radical?
3. Can the overall oxidation states be separated into well-defined oxidations states for the metal ion and ligand respectively? What are the electronic structures of these complexes?
4. Is it possible for intraligand charge transfer from redox-active ligands to impart single-electron oxyl radical character to a closed-shell terminal oxo group (Scheme 1.9)?
5. Are redox-active ligands capable of facilitating radical-like reactivity at other sites in the same molecule?

**Scheme 1.9.**

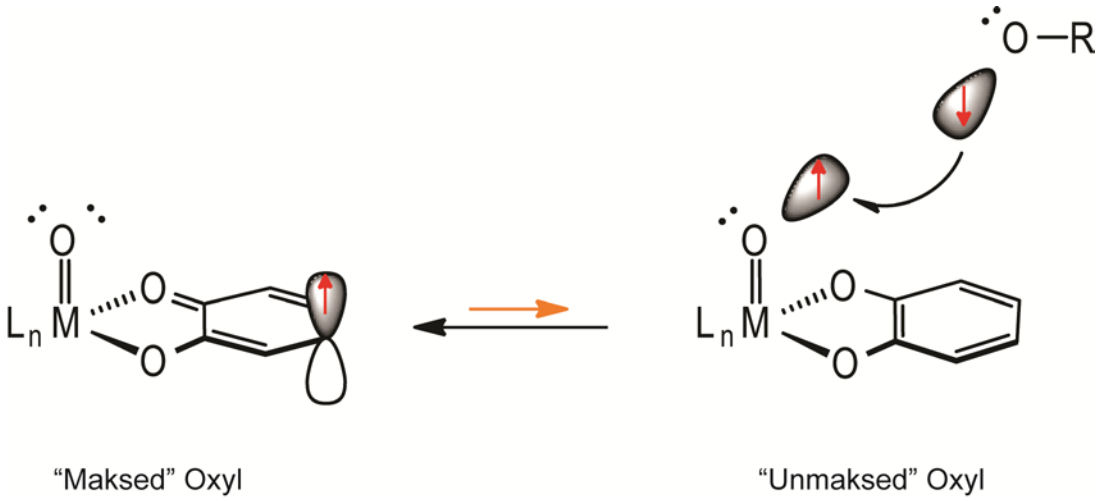


"Maksed" Oxyl

"Unmaksed" Oxyl

## 1.7 References


1. Caldeira, K.; Jain, A. K.; Hoffert, M. I. *Science* **2003**, *299*, 2052.

2. *Basic Research Needs for Solar Energy Utilization*; Report of the Basic Energy Sciences Workshop on Solar Energy Utilization; U.S. Department of Energy; April 18-21, 2005.

3. Lewis, N. S.; Nocera, D. G. "Powering the planet: Chemical challenges in solar energy utilization" *Proc. Natl. Acad. Sci*, **2006**, 103, 43, 15729-15735.

4. Espenson, J. H. *Adv. Inorg. Chem.* **2003**, *54*, 157-202.

5. Huang, R.; Espenson, J. H. *J. Mol. Catal. A: Chem.* **2001**, *168*, 39-46.

6. Lewis, N. S. "Powering the Planet" *MRS Bulletin*, **2007**, 32, 808-820.

7. Eisenberg, R.; Gray, H. B. "Preface on Making Oxygen" *Inorg. Chem.* **2008**, 47, 1697-1699.

8. Eisenberg, R.; Nocera, D. G. Preface: Preview of the Forum on Solar and Renewable Energy. *Inorg. Chem.* **2005**, 44, 6799-6801.

9. Huynh , M. H. V.; Thomas J. M. *Chem. Rev*. **2007,** 107, 5004-5064.

10. Alstrum-Acevedo, J. H.; Brennaman, M. K.; Meyer, T. J. *Inorg. Chem.* **2005**, 44, 6802-6827.

11. Nidhi Dubey, N. K.; Labhsetwar, S. D.; Sadhana S. R. *Catal. Today* **2007**, 129, 428-434.

12. Dempsey, J. L.; Esswein, A. J.; Manke, D. R.; Rosenthal, J.; Soper, J. D.; Nocera, D. G. *Inorg. Chem.* **2005**, 44, 6879-6892.

13. Ryuhei N.; Heinz F. *J. Am. Chem. Soc.* **2006**, 128, 10668-10669.

14. Romm, J.J. *The Hype About Hydrogen*; Island Press: Washington, **2004**.

15. Shilov, A. E. in *Metal Complexes in Biomimetic Chemical Reactions*. CRC press LLC. **1997,** 264-267.

16. Surendranath, Y.; Dinca, M.; Nocera, D. G. *J. Am. Chem. Soc.* **2009**, 131, 2615-2620.

17. Beteley, T. A.; Wu, Q.; Van, V. V.; Nocera, D. G. *Inorg. Chem.* **2008**, 47, 1849-1861.

18. *Oxygen Complexes and Oxygen Activation by Transition Metals*; Martell, A. E., Sawyer, D. T., Eds.; Plenum: New York, **1988**.

19. *The Activation of Dioxygen and Homogeneous Catalytic Oxidation*; Barton, D., H. R., Martell, A. E., Sawyer, D. T., Eds.; Plenum: New York, **1993**.

20. Stahl, S. S. *Science* **2005**, *309*, 1824-1826.

21. *Advances in Catalytic Activation of Dioxygen by Metal Complexes*; Simandi, L. I., Ed.; Kluwer Acadmic Publishers: Norwell, MA, **2003**.

22. Sosnovsky, G.; Zaret, E.H., Dwern, D. Organic Peroxides, Vol. 1, Wiley, NY **1970**, 517-560.

23. Collman, J. P.; Devaraj, N. K.; Decreau, R. A.; Yang, Y.; Yan, Y. L.; Ebina, W.; Eberspacher, T. A.; Chidsey, C. E. D. *Science* **2007**, *315*, 1565.

24. Punniyamurthy, T.; Velusamy, S.; Iqbal, J. *Chem. Rev*. **2005,** 105, 2329-2363.

25. Dau, H.; Haumann, M. *Chem. Rev.* **2008**, 252, 273-295.

26. Rutherford, A. W.; Zimmerman, J. –L.; Boussac, A. in *The Photosystems: Structure, Function and Molecular Biology*, Barber, J., Ed., Elsevier, **1992**, 179.

27. Wieghardt, K. *Angew. Chem. Int. Ed. Engl*., **1994**, 33, 725.

28. Wydrzynki, T. J., in *Photosynthesis,* Govindjee, Ed. Acedemic Press, New York, **1982**, Chap. 10.

29. Hansson, O.; Wydrzynki, T. J., *Photosynth. Res.* **1990**, 23, 131.

30. Joliot, P.; Joliot, A. *Biochim. Biophys. Acta.* **1966**, 153, 625.

31. Kok, B.; Forbush, B.; McGloin, M. *Photochem. Photobiol.* **1970**, 11, 457.

32. Williamson, A.; Conlan, B.; Hillier, W.; Wydrzynski, T. *Photosynth. Res.* **2011**, 107, 71-86.

33. Allen, J. P.; Williams, J. C. *Photosynth. Res.* **2001**, 107, 59-69.

34. Dempsey, Jillian L.; Winkler, Jay R.; Gray, Harry B. *Chem. Rev.* **2010**, 110, 7024-7039.

35. Zhang, T.; Wu, W.; Hu, B.; Man, Y.; Liu, Z. *Advances in Natural Science* **2010**, 3, 291-298.

36. Lemeille, S.; Rochaix, J. *Photosynth. Res.* **2010**, 106, 33-46.

37. Su, H.; Xie, B.; Zhang, X.; Zhou, B.; Zhang, Y. *Photosynth. Res.* **2010**, 106, 73-87.

38. Shutilova, N. I.; Moiseev, D. N. *Protection of Metals and Physical Chemistry of Surfaces* **2010**, 46, 502-507.

39. Fromme, P.; Grotjohann, I. *Curr. Top. Mem.* **2009**, 63, 191-227.

40. Siegbahn, P. E. M.; Blomberg, M. R. A. *Dalton Trans.* **2009**, 30, 5832-5840.

41. Pospisil, P. *Biochim. Biophys. Acta* **2009**, 1787, 1151-1160.

42. McEvoy, J. P.; Brudvig, G. W. *Chem. Rev.* 2006, 106, 4455-4483.

43. Allen, J. F.; Martin, W. *Nature* 2007, 445, 610-612.

44. Betley, T. A.; Wu, Q.; Voorhis, T. V.; Nocera, D. G. *Inorg. Chem.* **2008**, *47*, 1849-1861.

45. Barber, J. *Phil. Trans. R. Soc. B* **2008**, 363, 2665-2674.

46. Yang, X.; Baik, M. –H. *J. Am. Chem. Soc.* **2006,** 128, 23, 7476-7485.

47. Siegbahn, P. E. M.; Crabtree, R. H. *J. Am. Chem. Soc.* **1999**, 121, 1, 117-127.

48. Siegbahn, P. E. M. *Inorg. Chem.* **2000**, 39, 13, 2923-2935.

49. Lundberg, M.; Siegbahn, P. E. M. *Phys. Chem. Chem. Phys.* **2004**, 6, 20, 4772-4780.

50. Siegbahn, P. E. M.; Lundberg, M. *Photochem. Photobiol. Sci.* **2005**, 4, 12, 1035-1043.

51. Lundberg, M.; Blomberg, M. R. A.; Siegbahn, P. E. M. *Inorg. Chem.* **2004**, 43, 1, 264-274.

52. Sheldon, R. A.; Kochi, J. K. *Metal-Catalyzed Oxidations of Organic Compounds*; Academic Press: New York, **1981**.

53. *The Activation of Dioxygen and Homogeneous Catalytic Oxidation*; Barton, D., H. R., Martell, A. E., Sawyer, D. T., Eds.; Plenum: New York, **1993**.

54. *Biomimetic Oxidations Catalyzed by Transition Metal Complexes*; Meunier, B., Ed.; Imperial College: London, **2000**.

55. Special Issue on Dioxygen Activation and Metallozyme Models, *Acc. Chem. Res.* **2007**, *40*, 465-634.

56. Ballou, D. P.; Entsch B.; Cole, L. J. *Biochem Biophys Res Commun* **2005**, 338, 590-598.

57. Ortiz de Montellano, P. R. (ed.) *Cytochrome P450. Structure, Mechanism, and Biochemistry.* Plenum Press, New York, **1995.**

58. Lippard, S. J.; Berg, J. M. *Principles of Bioinorganic Chemistry*, University Science Books, **1994**.

59. Borovik, A. S.; Zinn, P. J.; Zart, M. K. In *Activation of Small Molecules: Organometallic and Bioinorganic Perspectives*; Tolman, W. B., Ed.; Wiley-VCH: Weinheim, Germany, **2006**; 187-234.

60. Nam, W. *Acc. Chem. Res.* **2007**, *40*, 465.

61. *Porphyrin Handbook*; Kadish, K. M., Smith, K. M., Guilard, R., Eds.; Academic Press: San Diego, CA, **2000**.

62. Cornell, C. N.; Sigman, M. S. In *ActiVation of Small Molecules: Organometallic and Bioinorganic Perspectives*; Tolman William, B., Ed.; Wiley-VCH: Weinheim, Germany, **2006**; 159-186.

63. Special Issue on Dioxygen Activation and Metallozyme Models, *Acc. Chem. Res.* **2007**, *40*, 465–634.

64. Gersten, S. W.; Samuels, G. J.; Meyer, T. J. *J. Am. Chem. Soc*. **1982**, 104, 14 4029-4030.

65. Gilbert, J. A.; Eggleston, D. S.; Murphy, W. R., Jr.; Geselowitz, D. A.; Gersten, S. W.; Hodgson, D. J.; Meyer, T. J. *J. Am. Chem. Soc.* **1985**, 107, 13 3855-3864.

66. Hurst, J. K. *Coord. Chem. Rev.* **2005**, 249, (3-4) 313-328.

67. Kadowaki, H.; Saito, N.; Nishiyama, H.; Kobayashi, H.; Shimodaira, Y.; Inoue, Y. *J. Phys. Chem. C* **2007**, 111, 439-444.

68. Hara, M.; Lean, J. T.; Mallouk, T. E. *Chem. Mater.* **2001**, *13*, 4668-4675.

69. Yagi, M.; Narita, K. *J. Am. Chem. Soc.* **2004**, *126*, 26, 8084-8085.

70. Poulsen, A. K.; Rompel, A.; McKenzie, C. J. *Angew. Chem., Int. Ed.* **2005**, *44*, 6916-6920.

71. Limburg, J.; Vrettos, J. S.; Liable-Sands, L. M.; Rheingold, A. L.; Robert, H.; Crabtree, R. H.; Brudvig, G. W. *Science* **1999**, *283*, 1524–1527.

72. Limburg, J.; Vrettos, J. S.; Chen, H.; de Paula, J. C.; Crabtree, R. H.; Brudvig, G. W. *J. Am. Chem. Soc.* **2001**, *123*, 423-430.

73. Zong, R.; Thummel, R. P. *J. Am. Chem. Soc.* **2005**, *127*, 12802-12803.

74. Howells, A. R.; Sankarraj, A.; Shannon, C. *J. Am. Chem. Soc.* **2004**, *126*, 12258-12259

75. Sens, C.; Romero, I.; Rodriguez, M.; Llobet, A.; Parella, T.; Benet-Buchholz, J. *J. Am. Chem. Soc.* **2004**, *126*, 7798-7799.

76. Gersten, S. W.; Samuels, G. J.; Meyer, T. J. *J. Am. Chem. Soc.* **1982**, *104*, 4029-4030.

77. Gilbert, J. A.; Eggleston, D. S.; Murphy, W. R., Jr; Geselowitz, D. A.; Gersten, S. W.; Hodgson, D. J.; Meyer, T. J. *J. Am. Chem. Soc.* **1985**, *107*, 3855-3864.

78. Chronister, C. W.; Binstead, R. A.; Ni, J.; Meyer, T. J. *Inorg. Chem.* **1997**, *36*, 3814-3815.

79. Gilbert, J. A.; Eggleston, D. S.; Murphy, W. R., Jr; Geselowitz, D. A.; Gersten, S. W.; Hodgson, D. J.; Meyer, T. J. *J. Am. Chem. Soc.* **1985**, *107*, 3855-3864.

80. Romero, I.; Rodríguez, M.; Sens, C.; Mola, J.; Kollipara, M. R.; Franca`s, L.; Mas-Marza, E.;Escriche, L.; Llobet, A. *Inorg. Chem.* **2008**, *47*, 1824-1834.

81. Yang, X.; Baik, M. -H. *J. Am. Chem. Soc.* **2006**, *128*, 7476-7485.

82. Geselowitz, D.; Meyer, T. J. *Inorg. Chem.* **1990**, *29*, 3894-3896.

83. Hurst, J. K. *Coord. Chem. Rev.* **2005**, *249*, 313-328.

84. Yamada, H.; Hurst, J. K. *J. Am. Chem. Soc.* **2000**, *122*, 5303-5311.

85. Yamada, H.; Siems, W. F.; Koike, T.; Hurst, J. K. *J. Am. Chem. Soc.* **2004**, *126*, 9786-9795.

86. Concepcion, J. J.; Jurss, J. W.; Templeton, J. L; Meyer, T. J. *J. Am. Chem. Soc.*, **2008**, 130, 16462-16463.

87. McHatton, R. C.; Anson, F. C. *Inorg. Chem.* **1984**, *23*, 3935–3942.

88. Takeuchi, K. J.; Thompson, M. S.; Pipes, D. W.; Meyer, T. J. *Inorg. Chem.* **1984**, *23*, 1845–1851.

89. Wada, T.; Tsuge, K.; Tanaka, K. *Angew. Chem., Int. Ed.* **2001**, *39*, 1479–1482.

90. Wada, T.; Tsuge, K.; Tanaka, K. *Inorg. Chem.* **2001**, *40*, 329–337.

91. Concepcion, J. J.; Jurss, J. W.; Brennaman, M. K.; Hoertz, P. G.; Patrocinio, A. O. T.; Murakami Iha, N. Y.; Templeton J. L.; Meyer, T. J. *Acc. Chem. Res.*, **2009**, 42, 1954-1965.

92. Jurss, J. W.; Concepcion, J. J.; Michael R. Norris, M. R.; Templeton J. L.; Meyer, T. J. *Inorg. Chem.*, **2010**, 49, 3980-3982.

93. Chen, Z.; Concepcion, J. J.; Hull, J. F.; Hoertz, P. G.; J. Meyer, T. J. *J. Chem. Soc. Dalton Trans.*, **2010**, 39, 6950-6952.

94. Shimazaki, Y.; Nagano, T.; Takesue, H.; Ye, B.-H.; Tani, F.; Naruta, Y. *Angew. Chem., Int. Ed.* **2004**, *43*, 98–100.

95. Ruettinger, W.; Yagi, M.; Wolf, K.; Bernasek, S.; Dismukes, G. C. *J. Am. Chem. Soc.* **2000**, *122*, 10353–10357.

96. Poulsen, A. K.; Rompel, A.; McKenzie, C. J. *Angew. Chem., Int. Ed.* **2005**, *44*, 6916–6920.

97. Limburg, J.; Vrettos, J. S.; Liable-Sands, L. M.; Rheingold, A. L.; Crabtree, R. H.; Brudvig, G. W. *Science* **1999**, *283*, 1524–1527.

98. Hull, J. F.; Balcells, D.; Blakemore, J. D.; Incarvito, C. D.; Eisenstein, O.; Brudvig, G. W.; Crabtree, R. H. *J. Am. Chem. Soc.*, **2009**, 131, 25, 8730-8731.

99. Kanan, M. W.; Nocera, D. G. *Science* **2008**, *321*, 1072.

100. Mircea D.; Yogesh S.; Nocera, D. G. *Proc. Natl. Acad. Sci.* **2010,** 107, 10337-10341.

101. Yagi, M.; Tomita, E.; Sakita, S.; Kuwabara, T.; Nagai, K. *J. Phys. Chem. B.* **2005**, *109*, 21489.

102. Hara, M.; Waraksa, C. C.; Lean, J. T.; Lewis, B. A.; Mallouk, T. E. *J. Phys. Chem. A* **2000**, *104*, 5275.

103. Tarasevich, M. R.; Efremov B. N. In *Electrodes of Conductive Metal Oxides*; Trasatti, S., Ed.; Elsevier: Amsterdam, **1980**; Chapter *5*.

104. Kanan, M. W.; Yano, J.; Surendranath, Y.; Dinca, M. Yachandra, V. K.; Nocera, D. G. *J. Am. Chem. Soc.* **2010**, 132, 13692-13701.

105. Risch, M.; Khare, V.; Zaharieva, I.; Gerencser, L.; Chernev, P.; Dau, H. *J. Am. Chem. Soc.* **2009**, *131*, 6936-6937.

106. McAlpin, J. G.; Surendranath, Y.; Dinca, M.; Stich, T. A.; Stoian, S. A.; Casey, W. H.; Nocera, D. G.; Britt, R. D. *J. Am. Chem. Soc.* **2010**, *132*, 6882-6883.

107. Surendranath, Y.; Kanan, M. W.; Nocera, D. G. *J. Am. Chem. Soc.* **2010**, 132, 16501-16509.

108. Richter-Addo, G. B; Legzdins, P. *Metal Nitrosyls*; Oxford University Press: New York, **1992**.

109. Mu, X. H.; Kadish, K. M. *Inorg. Chem.* **1988**, 27, 4120-4125.

110. Ford, P. C.; Lorkovic, I. M. *Chem. Rev.* **2002**, 102, 993-1017.

111. Reingold, J. A.; Virkaitis, K. L.; Carpenter, G. B.; Sun, S.; Sweigart, D. A.; Czech, P. T.; Overly, K. R. *J. Am. Chem. Soc.* **2005**, 127, 11146-11158.

112. Stoll, M. E.; Belanzoni, P.; Calhorda, M. J.; Drew, M. G. B.; Felix, V.; Geiger, W. E.; Gamelas, C. A.; Goncalves, I. S.; Romao, C. C.; Veiros, L. F. *J. Am. Chem. Soc.* **2001**, 123, 10595-10606.

113. Inagaki, A.; Takaya, Y.; Takemori, T.; Suzuki, H.; Tanaka, M.; Haga, M. *J. Am. Chem. Soc.* **1997**, 119, 625-626.

114. Nielson, R. M.; Weaver, M. J. *Organometallics* **1989**, 8, 1636-1643.

115. Schrauzer, G. N.; Mayweg, V. P. *J. Am. Chem. Soc.* **1962**, 84, 3221.

116. Schrauzer, G. N.; Mayweg, V. P. *J. Am. Chem. Soc.* **1965**, 87, 3585-3592.

117. Davison, A.; Edlestein, N.; Holm, R. H.; Maki, A. H. *J. Am. Chem. Soc.***1963,** 85, 2029-2030.

118. Davison, A.; Edlestein, N.; Holm, R. H.; Maki, A. H. *J. Am. Chem. Soc.***1963,** 85, 3049-3050.

119. Davison, A.; Edlestein, N.; Holm, R. H.; Maki, A. H. *Inorg. Chem.* **1964,** 3, 814-82**3.**

120. Davison, A.; Edlestein, N.; Holm, R. H.; Maki, A. H. *J. Am. Chem. Soc.* **1964**, 86, 2799-2805.

121. Maki, A. H.; Edlestein, N.; Davison, A.; Holm, R. H. *J. Am. Chem. Soc.* **1964**, 86, 4580-4587.

122. Davison, A.; Edlestein, N.; Holm, R. H.; Maki, A. H. *Inorg. Chem.***1963**, 2, 1227-1232.

123. Davison, A.; Edlestein, N.; Holm, R. H.; Maki, A. H. *Inorg. Chem.***1965**, 4, 55-59.

124. Latham, A. R.; Hascall, V. C.; Gray, H. B. *Inorg. Chem.***1965**, 4, 788-792.

125. Billig, E.; Williams, R.; Bernal, I.; Waters, J. H.; Gray, H. B. *Inorg. Chem.* **1964**, 3, 663-666.

126. Shupack, S. I.; Billig, E.; Clark, R. J. H.; Williams, R.; Gray, H. B. *J. Am. Chem. Soc.* **1964**, 86, 4594-4602.

127. Gray, H. B.; Billig, E. *J. Am. Chem. Soc.***1963,** 85, 2019-2020.

128. Gray, H. B. *Coord.Chem. Rev.* **1966**, 1, 156-63.

129. Holm, R. H.; Balch, A. L.; Davison, A.; Maki, A. H.; Berry, T. E. *J. Am. Chem. Soc.* **1967**, 89, 1080-1082.

130. E. Bill, E. Bothe, P. Chaudhuri, K. Chlopek,D. Herebian, S. Kokatam, K. Ray, T. Weyhermuller, F. Neese and K. Wieghardt, *Chem.–Eur. J.*, 2004, **11**, 204. 15

131. Ray, K.; Begum, A.; Weyhermuller, T.; Piligkos, S.;Neese, F.; Wieghardt, K. *J. Am. Chem. Soc.* **2005**, 127, 4403.

132. Ray, K.; Bill, E.; Weyhermuller, T.; Wieghardt, K. *J. Am. Chem. Soc.* **2005**, 127, 5641.

133. Ray, K.; Bill, E.; Weyhermuller, T.; Goossens, A.; Craje, M. W. J.; Wieghardt, K. *Inorg. Chem.*, **2003**, 42, 4082.

134. Petrenki, T.; Ray, K.; Wieghardt, K.; Neese, F. *J. Am. Chem. Soc.*, **2006**, 128, 4422.

135. Ray, K.; Weyhermuller, T.; Neese, F.; Wieghardt, K. *Inorg. Chem.*, **2005**, 44, 5345

136. Kapre, R.; Ray, K.; Sylvestre, I.; Weyhermuller, T.; DeBeer, G.; Neese, F.; Wieghardt, K. *Inorg. Chem.* **2006**, 45, 3499.

137. Chun, H.; Chaudhuri, P.; Weyhermueller, T.; Wieghardt, K. *Inorg. Chem.* **2002**, 41, 4295-4303.

138. Abakumov, G. A.; Cherkasov, V. K.; Nevodchikov, V. I.; Kuropatov, V. A.; Yee, G. T.; Peirpont. C. G. *Inorg. Chem.* **2001**, *40*, 2434.

139. Hendrickson, D. N.; Pierpont, C. G.; In *Top. Curr. Chem.* **2004**, 63-95.

140. Pierpont, C. G. *Coord. Chem. Rev.* **2001**, 216-217, 99-125.

141. Pierpont, C. G.; Attia, A. S. *Collect. Czech. Chem. Commun.*, **2001**, **66**, 33-51.

142. Eikey, R. A.; Abu-Omar, M. M. *Coord. Chem. Rev.* **2003**, *243*, 83.

143. Hinnemann, B.; Norskov, J. K. *Top. Catal.* **2006**, *37*, 55.

144. Ertl, G. *Catalytic Ammonia Synthesis*; Plenum: New York, **1991**.

145. DuBois, J.; Tomooka, C. S.; Hong, J.; Carriera, E. M. *Acc. Chem. Res.* **1997**, *30*, 364.

146. Kooistra, T. M.; Knijnenburg, Q.; Smits, J. M. M.; Horton, A. D.; Budzelaar, P. H. M.; Gal, A. W. *Angew. Chem., Int. Ed.* **2001**, 40, 4719.

147. Trovitch, R. J.; Lobkovsky, E.; Bill, E.; Chirik, P. J. *Organometallics* **2008**, *27*, 1470.

148. Bart, S. C.; Lobkovsky, E.; Chirik, P. J. *J. Am. Chem. Soc.* **2004**, 126, 13794.

149. Trovitch, R. J.; Lobkovsky, E.; Bill, E.; Chirik, P. J. *Organometallics* **2008**, *27*, 1470.

150. Bouwkamp, M. W.; Bowman, A. C.; Lobkovsky, E.; Chirik, P. J. *J. Am. Chem. Soc.* **2006**, 128, 13340.

151. Greenwood, N. N.; Earnshaw, A. *Chemistry of the Elements*; Pergamon: New York, **1984**.

152. Holm, R. H. *Chem. Rev.* **1987**, *87*, 1401-1449.

153. Holm, R. H. *Chem. Rev.* **1987**, *87*, 1401-1449.

154. Espenson, J. H. *Adv. Inorg. Chem.* **2003**, *54*, 157-202.

155. Morris, A. M.; Cortlandt G. Pierpont, C. G.; Finke, R. G. *J. Mol. Catal. A: Chem.* **2009**, 137-145.

156. Blacmore, K. J.; Ziller, J. W.; Heyduk, A. F. *Inorg. Chem.* **2005**, 44, 16, 5559-5561.

157. Mason, R. H.; Heyduk, A. F. *J. Am. Chem. Soc.* **2006**, 128, 8410-8411.

158. Smith, A. L.; Hardcastle, K. I.; Soper, J. D. *J. Am. Chem***.** Soc. **2010**, *132*, 14358-14360

159. Rolle, C. J.; Hardcastle, K. I.; Soper, J. D. *Inorg. Chem.*, **2008**, *47*, 6, 1892-1894

160. Smith, A. L.; Clapp, L. A.; Hardcastle, K. I.; Soper, J. D. *Polyhedron,* **2010**, *29*, 164-169.

161. Stanciu, C.; Jones, M. E.; Fanwick, P. E.; Abu-Omar, M. M. *J. Am. Chem. Soc.* **2007**, 129, 12400-12401.

162. Manuel, T. D.; Rohde, J. *J. Am. Chem. Soc.* **2009**, *131*, 15582-15583.

163. Marcus, R. A *Corrd. Chem. Rev.* **1993**, 32, 1111-1222.

164. Marcus, R. A.; Sutin, N. *Biochim. Biophys. Acta.* **1985**, 811, 265-322.

165. Meyer, T. J.; Taube, H. In *Comprehensive Coordination Chemistry*; Wilkinson, G., Ed.; Pergamon: New York, **1987**; Vol 1, 331-384.

166. Barbara, P. F.; Meyer, T. J.; Ratner, M. A. *J. Phys. Chem.* **1996**, 100, 13148-13168.

167. Wherland, S. *Coord. Chem.* **1993**, 123, 169-199.

# CHAPTER 2

# REDOX-ACTIVE LIGAND-MEDIATED BIMETALLIC HOMOLYSIS OF DIOXYGEN

## 2.1 Introduction

Selective oxidation reactions are utilized for transformations of small molecules substrates in applications ranging from benchtop-scale laboratory synthesis, to pharmaceuticals production, to the manufacture of petroleum products.[1-8] In this context, molecular oxygen represents the ideal inexpensive and environmentally benign oxidant.[9-11] Although dioxygen is a thermodynamically strong oxidant, it is kinetically inert, and spontaneous oxidations by $O_2$ are often prone to undesirable free radical autoxidation and over oxidation.[1,10] Therefore, transition metals are typically employed as catalysts to effect selective activation of $O_2$ and to impart control in partial oxidations of organic substrates.[1-4,9,10] There are now many examples of selective and powerful synthetic systems for aerobic oxidation reactions.[9-24] Although these systems are mostly very well understood, the chemical features that engender selective $O_2$ reduction are not easily generalized to other classes of oxidation catalysts. Therefore, the development of broadly applicable methods for selective activation of $O_2$ presages systematic development of new catalytic cycles for aerobic oxidations of small organic molecules.

Biological systems that utilize $O_2$ as a terminal oxidant have received extensive attention for their ability to mediate a wide variety of selective oxidation reactions.[17,19,25-30] These enzymes are classified as oxygenases when one or both oxygen atoms from $O_2$ are incorporated into organic substrates, or oxidases when substrate oxidation is coupled to the reduction of $O_2$ to water or hydrogen peroxide.[11,16,17] The *in vivo* metal-derived oxidants are both powerful and selective. Indeed, the range of accessible

oxidation reactions and the redox-specificity of some enzymes are unparalleled in synthetic systems. Accordingly, many recent efforts to translate enzyme-like selectivity to other aerobic oxidations build on studies of the mechanisms that metalloenzymes employ to generate strong oxidants from $O_2$, which highlight the structural and chemical properties that engender both substrate and redox specificity in reactions with small molecule substrates.[10,17,23,25,30-36]

A common feature of many oxygenase-type redox catalysis cycles is cleavage of the dioxygen O–O bond to generate a transition metal oxo complex.[18,20,25,27,32,37,38] Conversion of two metal ions and one $O_2$ molecule to two oxometal species is formally a $4e^-$ reduction of $O_2$ and a $2e^-$ oxidation of each metal fragment (Scheme 2.1a). Such bimetallic $O_2$ activation is frequently invoked in both metalloenzymes and model systems containing naturally abundant transition metal ions.[18,20,25]Despite the diversity of active site structures, most studies of enzymatic and enzyme-like $O_2$ homolysis invoke a remarkably similar reaction mechanism. This "unified scheme"[20] proposes that O–O bond homolysis occurs by a series of sequential, metal-mediated $1e^-$ steps, via superoxo $[O_2\bullet]^-$ and peroxo $[O_2]^{2-}$ complex intermediates. As illustrated in Scheme 2.1b for bimetallic $O_2$ homolysis, the intermediacy of both mononuclear superoxo complexes and symmetric dinuclear peroxo-bridged intermediates demands formal oxidation of each transition metal ion by $1e^-$. This reaction pattern undoubtedly reflects the fact most first row transition metal ions prefer to exist in oxidation states that vary by only $1e^-$,[39] so the preferred redox reaction for nearly all 3d transition metals is $1e^-$ transfer.

**Scheme 2.1.**

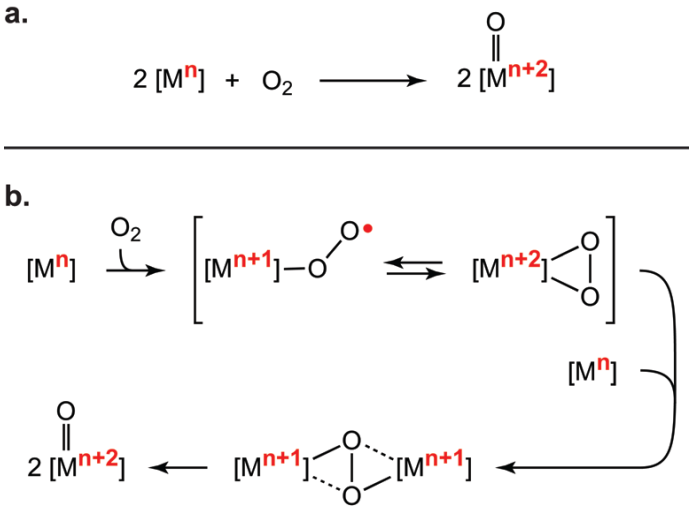


The ability of high-valent terminal oxo complexes of 4d and 5d metals to effect stoichiometric oxidations of small-molecule organic substrates is well-established.[1-5,40] Metal mediated oxygen-atom transfer is a $2e^-$ redox process.[41] The thermodynamics of oxo transfer redox reactions are determined by the bond enthalpies of the oxygen donor and acceptor substrates, so $2e^-$ oxo-transfer reactivity scales have proven useful for prediction of the reaction spontaneity in such metal-mediated oxidation reactions.[41,42] In contrast to 3d metals, most later 4d and 5d metal ions prefer to have oxidation states that vary by $2e^-$.[39]The utility of many coordinatively unsaturated 4d and 5d transition metal complexes in bond–making and bond–breaking oxo transfer reactions therefore derives in part from their ability to mediate the transfer of multiple electrons while avoiding odd-electron intermediates.[41-44] The properties that facilitate oxo transfer processes at unsaturated 2nd and 3rd row transition metal ions also seem conducive to bimetallic $O_2$ cleavage: a strong thermodynamic proclivity for $2e^-$ redox changes, and

low d-electron counts which stabilize the resulting terminal oxo group.[41,45] Although reactions of 2nd and 3rd row transition metals to homolyze $O_2$ are not rare,[41,44,46-48] many thermodynamically strong oxygen-atom acceptors are stable in $O_2$.[41,49] It was speculated that the propensity of some high-valent 4d and 5d metals to avoid odd–electron intermediates might introduce a kinetic barrier to symmetric bimetallic $O_2$ homolysis by inhibiting access to superoxo $[O_2\bullet]^-$ and peroxo $[O_2]^{2-}$ complex intermediates. An emerging strategy for selective redox transformations of small molecules, including $O_2$, utilizes simple redox-active chelates that support charge–localized structures as reservoirs of electrons in reactions at coordinatively unsaturated metal centers.[22,50–64]

As shown in Scheme 2.2, these so–called "non–innocent" ligands can coordinate to metals as fully–reduced catecholates $[cat]^{2-}$, partially–oxidized semiquinonate free radicals $[sq\bullet]^-$, and fully–oxidized benzoquinones [bq].[65,66] Accordingly, when the energies of the redox–active ligand frontier orbitals energies are close to the metal ion frontier orbitals, low energy intravalence charge transfer[66–70] can be utilized for stoichiometric and catalytic reactions at the metal center. In many ways this approach mirrors that widely employed in reactions at metalloporphyrin complexes, especially $O_2$ reduction.[27,32,37]However, the redox–active chelates utilized in this study are easily prepared, and offer the advantages of a high degree of flexibility in coordination environment and electronic tunability. For instance, substitution of the one oxygen in a $[cat]^{2-}$ with an *N*–aryl functional group affords an amidophenolate $[ap^{Ph}]^{2-}$ (Scheme 2.2) ligand that is both more electron rich and sterically demanding.

**Scheme 2.2.**

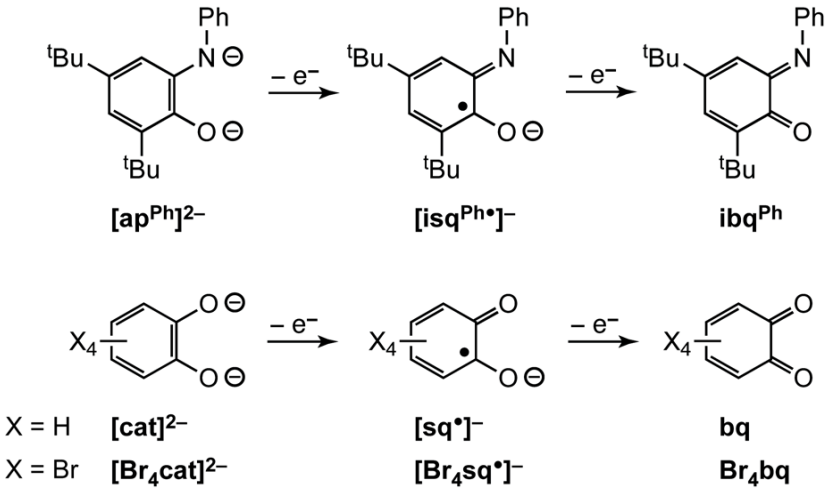


By extension, it seemed that coordination of a redox-active ligand to a high-valent 4d or 5d transition metal ion that is a strong 2e$^-$ oxygen-atom acceptor may give access to the stepwise 1e$^-$ redox steps for enzyme-like bimetallic $O_2$ activation. It was therefore intriguing to find a report on the synthesis and characterization of oxorhenium complexes with redox-active catecholate ligands that noted the five-coordinate monooxo anion $[Re^{V}(O)(cat)_2]^-$ ($[cat]^{2-}$ = 1,2-catecholate; Scheme 2.2) is oxidized to the *cis*-dioxo complex $[Re^{VII}(O)_2(cat)_2]^-$ with exposure to air.[71] Reported herein are mechanistic and computational studies of $O_2$ cleavage by $[Re^{V}(O)(cat)_2]^-$ and related five-coordinate oxorhenium(V) complexes to yield dioxorhenium(VII) products. Data are presented that suggest bimetallic $O_2$ homolysis occurs through redox-active ligand-mediated 1e$^-$ steps that mirror O–O bond cleavage by oxygenase enzymes. This ability of the redox-active ligands to deliver a single electron imparts a remarkable radical-like reactivity to the closed–shell $[Re^{V}(O)(cat)_2]^-$ fragment, which in turn keys efficient Re–O bond formation via reactions with oxygen radicals. Moreover, the ability of the ligands to act as

reservoirs for $1e^-$ does not perturb the ability of the oxorhenium(V) ion to affect $2e^-$ oxygen-atom transfer. This strategy to orthogonalize the $1e^-$ and $2e^-$ redox reactions for $O_2$ cleavage has implications for the design of new oxygenase catalysts, as well as for the microscopic reverse reaction, coupling of oxometal fragments to evolve $O_2$, which is a key step in functional water oxidation catalysts, and in natural and artificial photosynthetic systems.[72– 82]

## 2.2 Results

### 2.2.1 Preparation and Characterization of Oxorhenium(V) Complexes.

To assay the effects of ligand redox–activity on reactions of oxorhenium(V) complexes with dioxygen, a series of structurally similar complex anions were prepared. Using known procedures,[71,83] $[Re^{V}(O)(cat)_2]^-$ ($[cat]^{2-}$ = 1,2–catecholate; Scheme 2.2) can be isolated as either a five–coordinate square pyramidal monomer or a $C_1$–symmetric triphenylphosphine adduct $[Re^{V}(O)(PPh_3)(cat)_2]^-$. The $^1H$ NMR spectrum of $[Re^{V}(O)(cat)_2]^-$ in MeCN–*d*3 features two sharp multiplets for the equivalent $[cat]^{2-}$ ligands at 25 °C. As previously described,[83] the resonances broaden with addition of $PPh_3$ and separate into an eight–line pattern at –40 °C, indicative of two $[cat]^{2-}$ ligands in distinct chemical environments (Figure 2.1). These data indicate that the phosphine ligand in $[Re^{V}(O)(PPh_3)(cat)_2]^-$ is labile in solution at ambient temperature, but that $PPh_3$ binding is accompanied by *cis–trans* isomerization of the $[cat]^{2-}$ ligands, as observed in the solid state structures (eq. 1).[83]

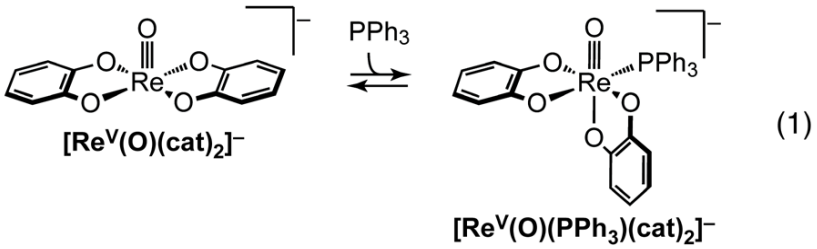


$[Re^{V}(O)(cat)_2]^-$ $[Re^{V}(O)(PPh_3)(cat)_2]^-$ (1)

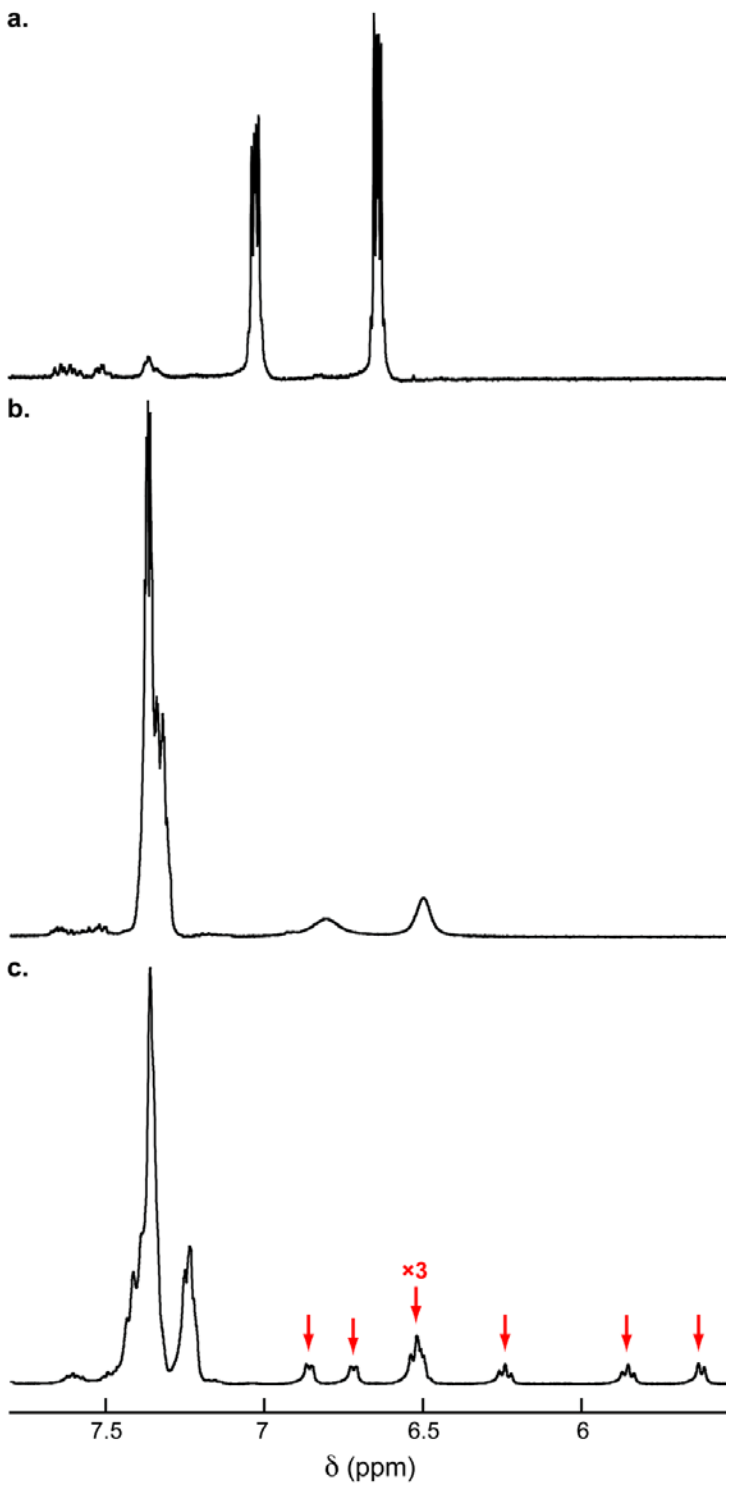


**Figure 2.1.** $^{1}$H NMR spectra of **(a)** $[Re^{V}(O)(cat)_2]^{-}$ at 25 °C, **(b)** $[Re^{V}(O)(PPh_3)(cat)_2]^{-}$ at 25 °C, and **(c)** $[Re^{V}(O)(cat)_2(PPh_3)]^{-}$ at –40 °C. The sample of $[Re^{V}(O)(PPh_3)(cat)_2]^{-}$ was generated *in situ* by addition of 1.3 equiv $PPh_3$ to $[Re^{V}(O)(cat)_2]^{-}$. The red arrows indicate positions of the eight resonances for the two inequivalent $[cat]^{2-}$ ligands at –40 °C. All spectra were recorded in MeCN-*d*3. Signal intensities are not normalized.

Further evidence of the torsional flexibility of the $[Re^{V}(O)(cat)_2]^{-}$ core is manifest in the structures of four homologs. Whereas $[Re^{V}(O)(PPh_3)(Br_4cat)_2]^{-}$ ($[Br_4cat]^{2-}$ = tetrabromo-1,2-catecholate; Scheme 2.2) adopts a $C_1$-symmetric structure with a *cis* arrangement of catecholate ligands, $[Re^{V}(O)(OPPh_3)(Br_4cat)_2]^{-}$ has a pseudo-$C_{2v}$ symmetric *trans* structure in the solid state.[84] The preference for *cis* or *trans* geometry in the six-coordinate complexes can be rationalized by a consideration of the relative π-donor strength of the respective ligands; the strongest π-donor occupies the position *trans* to the oxo group,[45]and the $[X_4cat]^{2-}$ ligand has occupied frontier orbitals of π symmetry.[85] All attempts to isolate the five-coordinate $[Re^{V}(O)(Br_4cat)_2]^{-}$ anion were unsuccessful, presumably due to the electron–withdrawing nature of the $[Br_4cat]^{2-}$ ligand that makes the rhenium center a strong Lewis acid. However, the $OPPh_3$ ligand in $[Re^{V}(O)(OPPh_3)(Br_4cat)_2]^{-}$ is labile, making it a suitable precursor to the $[Re^{V}(O)(Br_4cat)_2]^{-}$ fragment (*vide infra*).

Two new oxorhenium(V) derivatives containing $[ap^{Ph}]^{2-}$ and $[ox]^{2-}$ ligands ($[ap^{Ph}]^{2-}$ = 2,4-di-*tert*-butyl-6-(phenylamido)phenolate; $[ox]^{2-}$ = ethanedioate, $C_2O_4^{2-}$) were prepared by reactions of $[Re^{V}(O)(PPh_3)_2Cl_3]$ with the appropriate acid ligand precursor in basic alcohol solution. Slow cooling of a concentrated solution of $(Et_3NH)[Re^{V}(O)(ap^{Ph})_2]$ deposited dark green crystals suitable for analysis by X-ray diffraction. A single crystal structure of the anion is provided in Figure 2.2. It contains square pyramidal rhenium bound to two crystallographically equivalent aminophenol–derived ligands in the basal positions and an oxo in the apical site. The ligand C–C bond distances are equidistant within 3σ (1.40 ± 0.0Å), and the C –O and C–N bond distances of 1.371(4) and 1.415(5) Å, respectively, suggest that the aminophenol–derived ligands are fully reduced, closed–shell $[ap^{Ph}]^{2-}$ dianions.[86,87] One MeOH solvent molecule is contained in each unit cell, but is not bound to rhenium. The assignment of this complex as

rhenium(V) is additionally supported by the diamagnetic $^{1}$H NMR spectrum and analytical data.

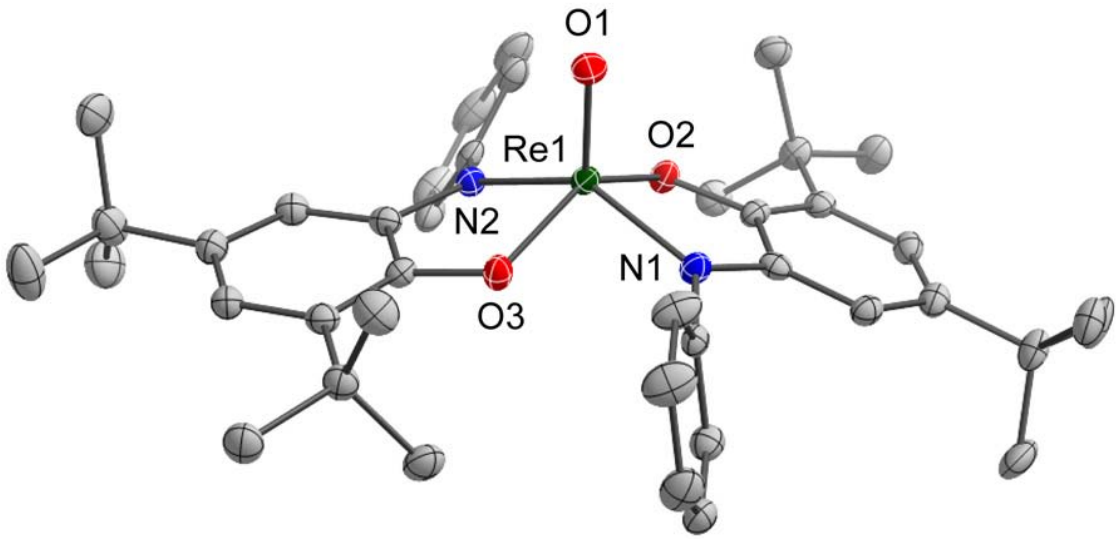


**Figure 2.2.** Solid–state structure of the anion in $(Et_3NH)[Re^{V}(O)(ap^{Ph})_2]$•0.25MeOH shown with 50% probability ellipsoids. Hydrogen atoms, MeOH solvate molecule and countercation omitted for clarity. Selected bond lengths (Å) and angles (deg): Re1–O1 1.715(3), Re1–O2 1.968(3), Re1–O3 1.970(3), Re1–N1 1.980(3), Re1–N2 1.983(3), O1–Re1–O2 111.03(12), O1–Re1–O3 108.88(13), O1–Re1–N1 111.92(14), O1–Re1–N2 108.60(13), O2–Re1–N1 79.35(12), O3–Re1–N2 79.48(12), O2–Re1–N2 87.91(12), O3–Re1–N1 86.06(12), O2–Re1–O3 140.09(11), N1–Re1–N2 139.45(13).

Crystals of $(Et_3NH)[Re^{V}(O)(PPh_3)(ox)_2]$ obtained from concentrated EtOH solution were also analyzed by X-ray diffraction. As shown in Figure 2.3, the anion contains rhenium with pseudo–octahedral geometry. As in the phosphine adducts described above, the $PPh_3$ ligand is *cis* to the oxo, so the two *cis*–oriented $[ox]^{2-}$ ligands are in distinct chemical environments. The $[ox]^{2-}$ ligand that occupies the site *trans* to $PPh_3$ has shorter bonds to rhenium (2.003(3) and 2.035(3) Å) and two pairs of long and short C–O bonds (averaging 1.322(5) and 1.207(5) Å, respectively) typical of a dione/diolate

resonance structure. In contrast, the $[ox]^{2-}$ *trans* to the oxo has elongated Re–O bond distances (2.092(3) and 2.082(3) Å) and a smaller difference between the average bonding and distal C–O bond lengths (1.294(5) and 1.221(5) Å, respectively). The Re–$O_{oxo}$ bond length of 1.671(3) Å is typical of the Re–O triple bond expected for a monooxo $d^2$ ion in a tetragonal ligand field.[45] The diamagnetism of the $[Re^{V}(O)(PPh_3)(ox)_2]^-$ is additionally evidenced by the $^{13}C$ NMR spectrum, which displays four distinct resonances for the $[ox]^{2-}$ ligands in MeCN-*d*3 at 25 °C, implying and isomerization is slow on the NMR timescale. However, addition of tri(4–tolyl)phosphine to NMR tubes containing $[Re^{V}(O)(PPh_3)(ox)_2]^-$ in MeCN-*d*3 gives complete scrambling of the phosphine resonances within in minutes at 25 °C, indicating that the $PPh_3$ ligand in $[Re^{V}(O)(PPh_3)(ox)_2]^-$ is labile at ambient temperature.

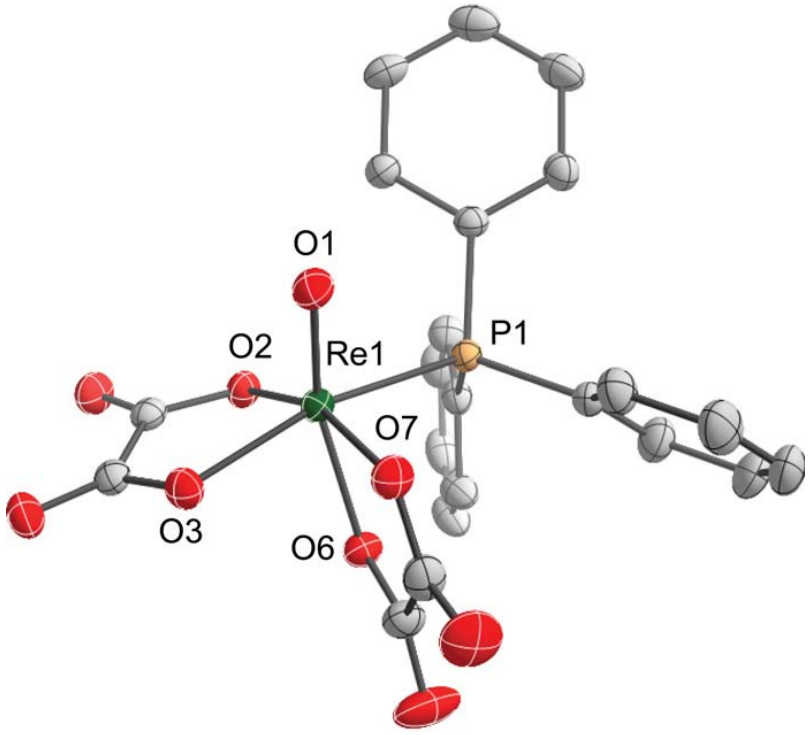


**Figure 2.3.** Solid–state structure of the anion in $(Et_3NH)[Re^{V}(O)(PPh_3)(ox)_2]$•1.5EtOH shown with 50% probability ellipsoids. Hydrogen atoms, EtOH solvate molecule and countercation omitted for clarity. Selected bond lengths (Å) and angles (deg): Re1–O1 1.671(3), Re1–O2 2.003(3), Re1–O3 2.035(3), Re1–O6 2.092(3), Re1–O7 2.082(3), Re1–P1 2.4472(13), O1–Re1–O2 107.95(14), O1–Re1–O3 107.54(14), O1–Re1–O6 162.03(14), O1–Re1–O7 89.30(14).

### 2.2.2 Preparation and Characterization of Dioxorhenium(VII) Complexes.

Addition of 1 equiv of pyridine *N*–oxide, dimethyl sulfoxide (DMSO), or $OAsPh_3$ to $[Re^{V}(O)(cat)_2]^{-}$ in MeCN gives an immediate color change from light tan to dark purple. The purple product is the *cis*–dioxo $[Re^{VII}(O)_2(cat)_2]^{-}$ anion, as evidenced by comparison of the UV–vis and $^1$H NMR spectra to an authentic sample, prepared independently (eq. 2).[71] When the reaction is performed in MeCN-*d*3, integration of the $^1$H NMR resonances confirms quantitative formation of $[Re^{VII}(O)_2(cat)_2]^{-}$ and the deoxygenated organic reagent: pyridine, dimethyl sulfide (DMS), or $AsPh_3$.

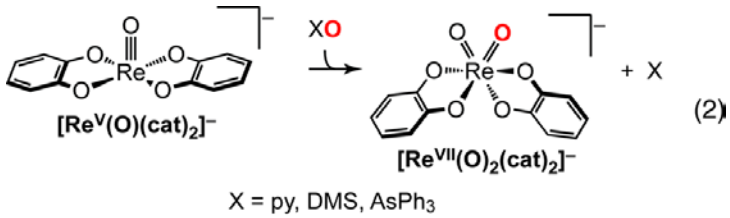


The analogous reaction of 1 equiv of pyridine *N*-oxide, DMSO, or $OAsPh_3$ with $[Re^{V}(O)(OPPh_3)(Br_4cat)_2]^{-}$, or $[Re^{V}(O)(ap^{Ph})_2]^{-}$ rapidly affords the corresponding dioxorhenium(VII) products. The assignment of these materials as the $d^0$ dioxo congeners is supported by spectroscopic and analytical data. Crystals of $(Et_4N)[Re^{VII}(O)_2(ap^{Ph})_2]$ for X-ray diffraction analysis were obtained from concentrated MeOH solution. A thermal ellipsoid plot of the anion is provided in Figure 2.4. The rhenium center has pseudo-octahedral geometry with approximate $C_2$ symmetry. Two terminal oxo ligands occupy a pair of *cis* coordination sites, with a O–Re–O bond angle of 100.78(10)°. The remaining four sites are filled by two crystallographically unique aminophenol–derived ligands. Only one of three possible structural isomers is observed in the solid–state structure. The Re–N bonds are in an approximately *trans* disposition, with each $Re–O_{ap^{Ph}}$ bond in a site *trans* an oxo ligand. The largest distortion from octahedral geometry is manifest in the contracted N–Re–N bond angle of 154.08(10)°. All of the C–C bond distances are identical within experimental error at 1.40 ± 0.01 Å, consistent with a fully-reduced, aromatic $[ap^{Ph}]^{2-}$ ligand.[86,87] The C–O and C–N bond lengths (averaging 1.337(6) and 1.402(6) Å, respectively) are slightly contracted versus those in $[Re^{V}(O)(ap^{Ph})_2]^{-}$ but within the range expected for this ligand oxidation state assignment. Further evidence for the rhenium(VII) assignment is provided by the $Re–O_{oxo}$ bond lengths of 1.742(2) and 1.732(2) Å, which are elongated as compared to $[Re^{V}(O)(ap^{Ph})_2]^{-}$ due to the net decrease in formal bond order (from 3.0 to 2.5 to each

oxo group) with oxygen atom addition.[45]A single crystal structure of the brominated analog $[Re^{VII}(O)_2(Br_4cat)_2]^-$ was not determined, but the structure is assigned as the *cis* conformer based on analogy to $[Re^{VII}(O)_2(cat)_2]^-$ and $[Re^{VII}(O)_2(ap^{Ph})_2]^-$.

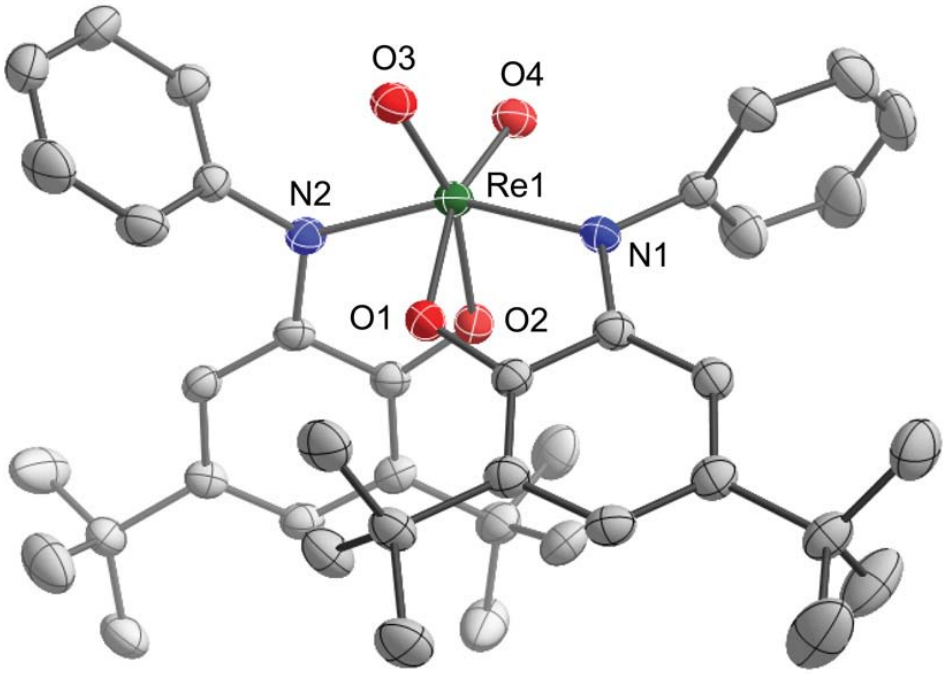


**Figure 2.4.** Solid–state structure of the anion in $(Et_4N)[Re^{VII}(O)_2(ap^{Ph})_2]$ shown with 50% probability ellipsoids. Hydrogen atoms, and countercation omitted for clarity. Selected bond lengths (Å) and angles (deg): Re1–O1 2.049(2), Re1–O2 2.040(2), Re1–O3 1.742(2), Re1–O4 1.732(2),Re1–N1 2.003(2), Re1–N2 2.036(2), O1–Re1–O2 82.23(9), O3–Re1–O4 100.78(10), O1–Re1–N1 75.55(9), O2–Re1–N2 75.23(9), O2–Re1–N1 86.38(9), O1–Re1–N2 83.87(9), O4–Re1–N2 109.73(10), O3–Re1–N1 108.14(10), O1–Re1–O4 162.25(9), O2–Re1–O3 161.95(9), N1–Re1–N2 154.08(10).

Addition of 2 equiv pyridine *N*-oxide or DMSO to violet $[Re^{V}(O)(PPh_3)(ox)_2]^-$ in MeCN rapidly gives a clear, colorless solution containing $OPPh_3$ and $ReO_4^-$ as the only rhenium containing product observable by ESI-MS (eq. 3). The analogous reaction of $[Re^{V}(O)(PPh_3)(ox)_2]^-$ with a stoichiometric amount of the oxidizing agent results only in conversion of the coordinated $PPh_3$ ligand to $OPPh_3$. The $ReO_4^-$ is likely a product of

$[Re^{VII}(O)_2(ox)_2]^-$ decomposition; all other attempts to prepare or isolate the putative dioxo species were unsuccessful.

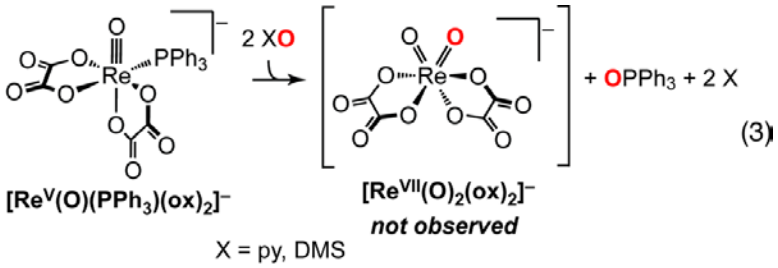


### 2.2.3 Reactions of $[Re^{V}(O)(cat)_2]^-$ with $O_2$.

Consistent with a previous report,[71] exposure of MeCN or $CH_2Cl_2$ solutions of $[Re^{V}(O)(cat)_2]^-$ to 1 atm air or $O_2$ gives conversion to $[Re^{VII}(O)_2(cat)_2]^-$ over hours at ambient temperature. When the reaction is monitored by $^1$H NMR spectroscopy in MeCN-*d*3, no diamagnetic species other than $[Re^{V}(O)(cat)_2]^-$ and $[Re^{VII}(O)_2(cat)_2]^-$ accumulate to an observable concentration, and integration of the $^1$H NMR resonances for $[Re^{V}(O)(cat)_2]^-$ and $[Re^{VII}(O)_2(cat)_2]^-$ indicates that the total concentration of rhenium-containing products is constant throughout the reaction. Quantitative conversion of $[Re^{V}(O)(cat)_2]^-$ to $[Re^{VII}(O)_2(cat)_2]^-$ requires 0.5 equiv $O_2$ (Figure 2.5), implying that both oxygen atoms from $O_2$ are incorporated into $Re^{VII}$=O bonds.

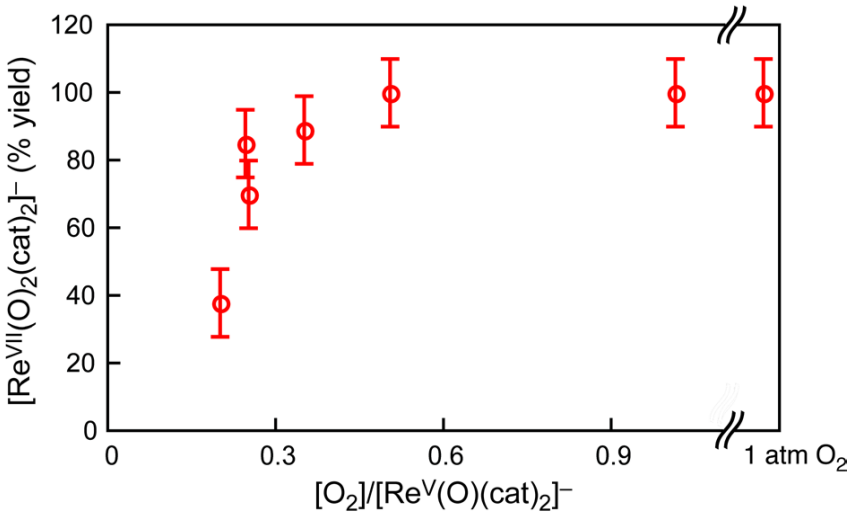


**Figure 2.5.** Plot of % yield of $[Re^{VII}(O)_2(cat)_2]^-$ as a function of molar stoichiometry in reactions of $[Re^{V}(O)(cat)_2]^-$ with $O_2$ in MeCN-*d*3 at 25 °C. All measurements were made in sealable NMR tubes and % conversion was determined by integration of the $^1$H NMR resonance for $[Re^{V}(O)(cat)_2]^-$ and $[Re^{VII}(O)_2(cat)_2]^-$.

Reaction of 1 equiv $PPh_3$ with $[Re^{VII}(O)_2(cat)_2]^-$ in MeCN–*d*3 under $N_2$ gives clean conversion to $[Re^{V}(O)(cat)_2]^-$ and $OPPh_3$ in minutes, as evidenced by $^1$H NMR spectroscopy. This closes a catalytic cycle for aerobic $PPh_3$ oxidation (Scheme 2.3). Accordingly, exposure of the triphenylphosphine adduct $[Re^{V}(O)(PPh_3)(cat)_2]^-$ to 1 atm $O_2$ in MeCN-*d*3 affords complete conversion to $[Re^{VII}(O)_2(cat)_2]^-$ and $OPPh_3$ in <2 h at 25 ºC. In contrast, NMR tubes containing $[Re^{V}(O)(PPh_3)(cat)_2]^-$ and a large excess of $PPh_3$ (50 equiv) in MeCN-*d*3 maintain their green color indefinitely in air at ambient temperature, and generation of trace $OPPh_3$ requires heating to 70 ºC for 3 d. Together, these data imply that the oxidation of $[Re^{V}(O)(PPh_3)(cat)_2]^-$ by $O_2$ proceeds via initial pre equilibrium dissociation of $PPh_3$ to generate $[Re^{V}(O)(cat)_2]^-$, and that a vacant site at rhenium is a prerequisite for the reaction with $O_2$.

**Scheme 2.3.**

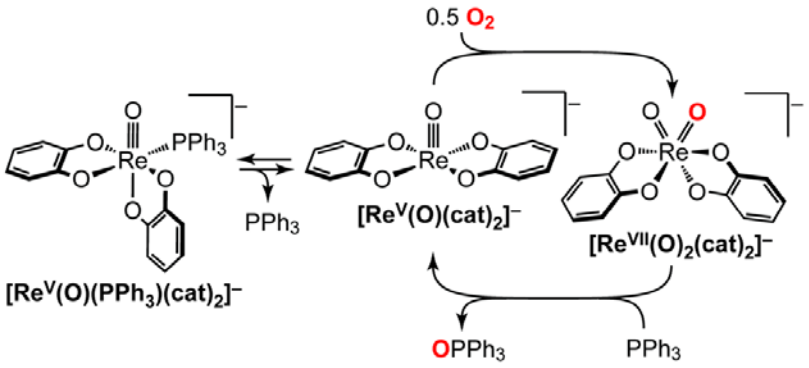


The distinct color change accompanying the aerobic conversion of $[Re^{V}(O)(cat)_2]^-$ to $[Re^{VII}(O)_2(cat)_2]^-$ allows the reaction to be conveniently monitored by UV–vis absorption spectroscopy. Addition of 1 atm $O_2$ to 0.08 mM $[Re^{V}(O)(cat)_2]^-$ in $CH_2Cl_2$ affords quantitative conversion to $[Re^{VII}(O)_2(cat)_2]^-$ in 30 min with apparent isosbestic points at 260, 284 and 312 nm (Figure 2.6a). However, close examination of the kinetics data shows that the conversion of $[Re^{V}(O)(cat)_2]^-$ to $[Re^{VII}(O)_2(cat)_2]^-$ does not proceed in a single phase. The pseudo-first order kinetics plot shows a significant curvature (Figure 2.10), indicative of a biphasic reaction.[88] As shown in Figure 2.6b, the concentration-time data have a sigmoidal shape that are fit best by an ~~A~~ B → C integrated rate law model with two exponential equations corresponding to consecutive first–order processes. The biphasic concentration–time profile, including the length of the apparent induction period, is reproduced exactly using different batches of $[Re^{V}(O)(cat)_2]^-$ and $CH_2Cl_2$ solvent, and in MeCN solutions, suggesting that the biphasic behavior is not due to trace impurities or radical chain kinetics.

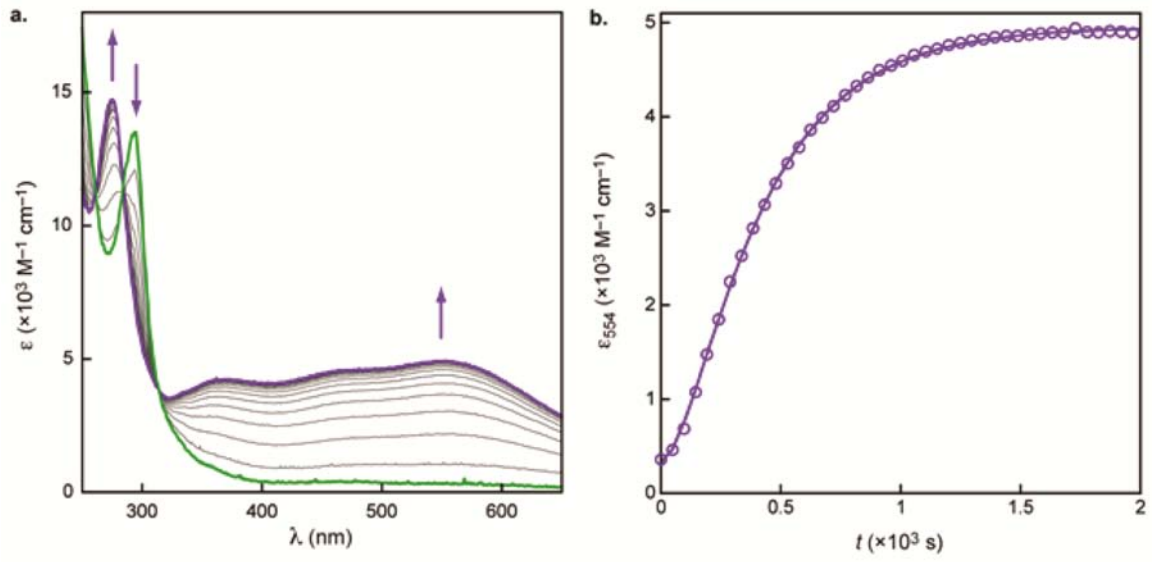


**Figure 2.6. (a)** UV–vis absorption spectra for a reaction of 8 x $10^{-5}$ M $[Re^{V}(O)(cat)_2]^-$ with 1 atm $O_2$ at 25 °C in $CH_2Cl_2$ to generate $[Re^{VII}(O)_2(cat)_2]^-$. Spectra are shown at $t$ = 0 in degassed $CH_2Cl_2$ (green line), and at 2.4 min intervals to $t$ = 33.6 min (purple line) after exposure to $O_2$. **(b)** Selected time–resolved data for the formation of $[Re^{VII}(O)_2(cat)_2]^-$ with $\lambda_{max}$ = 554 nm (purple ○). The fit (purple line) was obtained from iterative analysis of the full spectral window (245–900 nm) using a biexponential A→B→C integrated rate law model, giving $k_{A\rightarrow B}$ = (9 ± 1) x $10^{-3}$ $s^{-1}$ and $k_{B\rightarrow C}$ = (3 ± 1) x $10^{-3}$ $s^{-1}$.

The comparable rate constants for the two phases of the reaction, and the relative small spectral changes during the A → B phase, makes accurate deconvolution of the kinetics data very challenging and comparison of the rate constants problematic. However, consideration of the relative trends in rates with varying concentrations of reactants is informative. When the reaction of 0.08 mM $[Re^{V}(O)(cat)_2]^-$ is performed with dry air as the source of $O_2$, quantitative formation of $[Re^{VII}(O)_2(cat)_2]^-$ requires 150 min (versus 30 min with $O_2$). The five–fold decrease in rate of product formation therefore scales with the relative $O_2$ concentration. However, at a higher initial concentration of $[Re^{V}(O)(cat)_2]^-$ (0.23 mM), both reactions are slow, and the fivefold rate difference is lost: Generation of $[Re^{VII}(O)_2(cat)_2]^-$ from $O_2$ and air requires 120 min and 150 min, respectively. Additionally, the sigmoidal shape of the concentration–time data is

significantly less pronounced, suggesting that varying the initial concentrations of $O_2$ and $[Re^{V}(O)(cat)_2]^-$ impacts the rates of the A→ B and B → C phases of the reaction differently. Indeed, this apparent non–linear dependence of the rate of $[Re^{VII}(O)_2(cat)_2]^-$ formation on both $O_2$ concentration and $[Re^{V}(O)(cat)_2]^-$ concentration are further evidence that, despite the lack of a clearly observable intermediate, the reaction does not proceed in a single step.

### 2.2.4 Computational Studies of $O_2$ Homolysis by $[Re^{V}(O)(cat)_2]^-$.

Attempts to isolate or further characterize intermediate species in the reaction of $[Re^{V}(O)(cat)_2]^-$ with $O_2$ were unsuccessful, prompting us to pursue a computational study of this process. Optimized structures and energies were computed with restricted density functional theory (DFT) with the B3LYP functional and a LACVP+* basis set.[89–91] All calculations were performed with the Jaguar program[92] except for the molecular orbital plots in Figure 2.8, which were computed with MOLPRO[93] and plotted in Molekel[94]. Computed energies and structures are assumed to be in the singlet state unless otherwise noted.

In the absence of a sixth ligand, the *trans* isomer of the $[Re^{V}(O)(cat)_2]^-$ anion optimizes to a stable structure with bond distances and angles that are in excellent agreement with the solid state metrical parameters for $[Re^{V}(O)(cat)_2]^-$.[83]The five-coordinate *cis* isomer of $[Re^{V}(O)(cat)_2]^-$ (Figure 2.7b) was obtained with constrained dihedral angles between the $[cat]^{2-}$ ligands. It is a transition state 26.1 kcal $mol^{-1}$ higher in energy than the *trans* form of the complex (Figure 2.7a). However, as discussed below, this represents an upper limit to the barrier to *cis–trans* isomerization because it does not account for stabilization of the ion by occupancy of the sixth coordination site. The interaction of $[Re^{V}(O)(cat)_2]^-$ with dioxygen was probed by placing $O_2$ in the vacant coordination sites of both the *cis* and *trans* isomers the five–coordinate anion and performing subsequent geometry optimization. Singlet and triplet state minima were

found for dioxygen adducts to both the *cis* and *trans* isomers, but the energies of the *cis* complexes are lower than the *trans* species by 28.9 and 10.2 kcal $mol^{-1}$ for the $S$ = 0 and $S$ = 1 states, respectively. These data imply that $O_2$ addition to $[Re^{V}(O)(cat)_2]^-$ occurs with isomerization to the *cis* conformer, analogous to $PPh_3$ binding (*vide supra*). No stable structures were found with $O_2$ bridges between the rhenium center and quinoid ligands in either the *cis* or *trans* isomers of $[Re^{V}(O)(cat)_2]^-$.

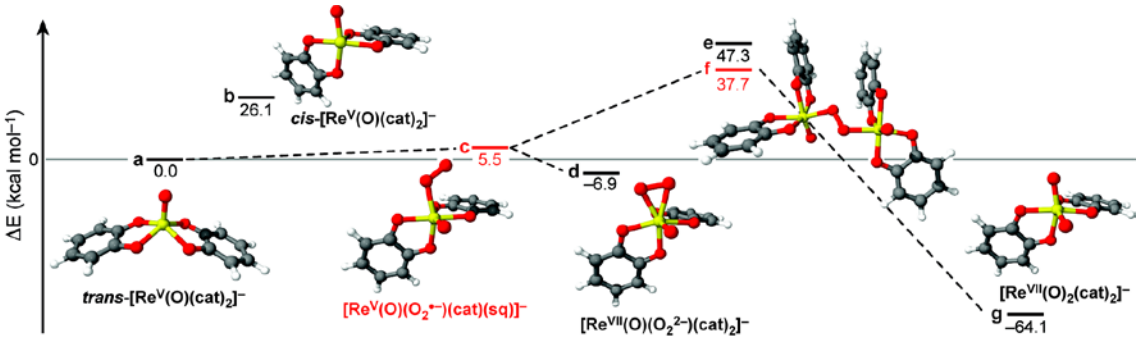


**Figure 2.7.** Reaction energy diagram for 2 $[Re^{V}(O)(cat)_2]^-$ + $O_2$ → 2 $[Re^{VII}(O)_2(cat)_2]^-$. Bold black and red lines represent the $S$ = 0 and $S$ = 1 states, respectively, of the rhenium complexes shown. Reported energies are relative to **(a)** *trans*–$[Re^{V}(O)(cat)_2]^-$ + $O_2$. **(b)** Transition state for isomerization of 1 equiv *trans*–$[Re^{V}(O)(cat)_2]^-$ to 1 equiv *cis*–$[Re^{V}(O)(cat)_2]^-$. **(c)** Formation of the dioxygen adduct in the $S$ = 1 state, and **(d)** in the $S$ = 0 state. **(e)** Relative energy of the $S$ = 0 $O_2$–bridged bimetallic complex. **(f)** Single point energy of the $S$ = 1 state for the $O_2$–bridged complex at the $S$ = 0 geometry. **(g)** Energy of formation of 2 equiv $[Re^{VII}(O)_2(cat)_2]^-$.

The $S$ = 0 and $S$ = 1 states of the *cis* $O_2$ adducts have different geometries. The lower energy, $S$ = 0 state is a minimum 6.9 kcal $mol^{-1}$ below the *trans* form of $[Re^{V}(O)(cat)_2]^-$ (Figure 2.7d). It has an O–O bond distance of 1.42 Å and Re–$O_2$ bond lengths of 1.93 and 2.02 Å. These distances are most consistent with formulation of dioxygen–derived ligand as an $\eta^2$–peroxo $[O_2]^{2-}$ dianion,[95,96] and the seven–coordinate complex anion as $[Re^{VII}(O)(O_2^{2-})(cat)_2]^-$. The $S$ = 1 isomer is 12.4 kcal $mol^{-1}$ higher in

energy than the *cis* $S$ = 0 $O_2$ adduct, 5.5 kcal $mol^{-1}$ above the ground state *trans*-$[Re^{V}(O)(cat)_2]^-$ complex (Figure 2.7c). As compared to the $S$ = 0 complex, the O–O bond length is contracted to 1.32 Å, and there is an enhanced asymmetry in the Re–$O_2$ bond distances (2.06 and 2.88 Å). Examination of the singly occupied molecular orbitals (SOMOs) for this state reveals that one unpaired electron is primarily localized in an orbital that is characteristic of a semiquinonate radical $[sq^{\bullet}]^-$ ligand (Figure 2.8a).[86]The other SOMO has is distributed over both oxygen atoms and the metal center, with contributions from both an O–O π* orbital and a rhenium d–orbital (Figure 2.8b). The large fraction of the oxygen–centered unpaired spin is on the distal atom of the $O_2$-derived ligand, which is antisymmetric to density on the proximal oxygen that partially overlaps with a cloverleaf metal d–orbital. The sum of these data are most consistent with formulation of the complex as rhenium(V) $[Re^{V}(O)(O_2^{\bullet-})(cat)(sq^{\bullet})]^-$ with a $\eta^1$-superoxo $[O_2^{\bullet}]^-$ ligand,[95,96] but covalency in the Re–$O_2$ bond transfers some radical density onto the rhenium center via a weak Re–O π–bonding interaction.

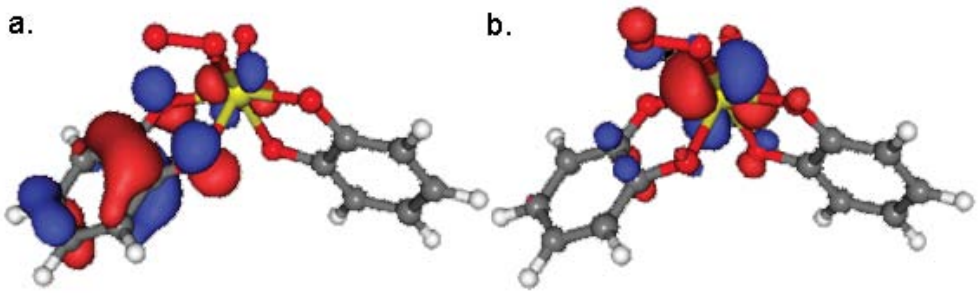


**Figure 2.8. (a–b)** Surface plots of the two orbitals with unpaired spin density in the $S$ = 1 $O_2$–adduct to $[Re^{V}(O)(cat)_2]^-$**.**

Oxygen atom transfer from $[Re^{VII}(O)(O_2^{2-})(cat)_2]^-$ to $[Re^{V}(O)(cat)_2]^-$ was probed by placing the distal oxygen of the bound $O_2$ ligand in the vacant coordination site of a second *cis* isomer of $[Re^{V}(O)(cat)_2]^-$ and performing subsequent geometry optimization. All of the resulting bimetallic structures are higher in energy, consistent with coulombic repulsion of the two anionic fragments. However, minimum energy $O_2$-bridged complexes were located on the potential energy surface. The $S$ = 0 solution is shown in Figure 2.7e. The O–O distance of 1.41 Å, and the asymmetry in the Re–$O_2$ bond distances are most consistent with a *trans*-μ-1,2-peroxo $[O_2]^{2-}$ linkage.[95,96] No stable bimetallic structures were found with side–on, μ–$\eta^2$:$\eta^2$–peroxo linkages. A similar local minimum was not found on the $S$ = 1 potential surface; however, a single point computation of the $S$ = 1 energy at the optimized $S$ = 0 geometry yields a lower energy (Figure 2.7f). This demonstrates that the triplet state potential energy surface is lower in energy than the singlet state in this region, and suggests that an $S$ = 1 peroxo-bridged complex is a precursor to $O_2$ cleavage to generate 2 equiv $[Re^{VII}(O)_2(cat)_2]^-$.

**2.2.5 Reactions of Oxorhenium(V) Homologs with $O_2$.**

The apparent importance of ligand–centered changes in oxidation state during $O_2$ homolysis by $[Re^{V}(O)(cat)_2]^-$ suggested that the reaction rates may be sensitive to substitution of the redox-active ligand. Exposure of green solutions of $[Re^{V}(O)(OPPh_3)(Br_4cat)_2]^-$ in $CH_2Cl_2$, MeCN or acetone to 1 atm air or $O_2$ results in a color change to dark purple over hours at ambient temperature. Monitoring the reaction by UV–vis absorption spectroscopy confirms that the purple product is $[Re^{VII}(O)_2(Br_4cat)_2]^-$, which is formed in quantitative yield (Figure 2.9a). However, in contrast to the reactions of $[Re^{V}(O)(cat)_2]^-$ with $O_2$, under some conditions an intermediate species accumulates to an observable concentration during the course of the reaction. This is best evidenced by examination of the UV–vis concentration-time data from the long wavelength visible portion of the spectrum. For example, a reaction of

0.20 mM $[Re^{V}(O)(OPPh_3)(Br_4cat)_2]^-$ and 1 atm $O_2$ shows a growth in the absorption intensity at 775 nm over the first 3600 s of the reaction, followed by an inflection point and a decay to the $[Re^{VII}(O)_2(Br_4cat)_2]^-$ product spectrum (Figure 2.9b). Global iterative analysis of the full spectral window to an A→ B → C integrated rate law model yields good first–order fits to both the growth and decay phases of the reaction.

As described above, accurate deconvolution of the kinetics data is challenging when the computed rate constants for the two phases of the reaction are similar, making comparison of the rate constants problematic. However, under all conditions examined, the rate of formation of $[Re^{VII}(O)_2(Br_4cat)_2]^-$ from $[Re^{V}(O)(OPPh_3)(Br_4cat)_2]^-$ and $O_2$ is clearly slower than the parent catecholate analog. Quantitative conversion of 0.07 mM $[Re^{V}(O)(OPPh_3)(Br_4cat)_2]^-$ and 1 atm air to $[Re^{VII}(O)_2(Br_4cat)_2]^-$ in $CH_2Cl_2$ requires 1200 min (versus 150 min for the conversion of $[Re^{V}(O)(cat)_2]^-$ to $[Re^{VII}(O)_2(cat)_2]^-$ under similar conditions). All attempts to isolate the intermediate species were unsuccessful. Addition of 1 atm $O_2$ to a $CH_2Cl_2$ solution containing $[Re^{V}(O)(OPPh_3)(Br_4cat)_2]^-$ at –90 °C gives no observable color change over hours, presumably because competitive binding of $OPPh_3$ inhibits the reaction with $O_2$ at low temperatures. Moreover, concentrated solutions of $[Re^{V}(O)(OPPh_3)(Br_4cat)_2]^-$ in $O_2$ convert to $[Re^{VII}(O)_2(Br_4cat)_2]^-$ without accumulation of any observable intermediates, because the putative $O_2$-complex monomers are rapidly trapped by the coordinatively-unsaturated $[Re^{V}(O)(Br_4cat)_2]^-$ fragment.

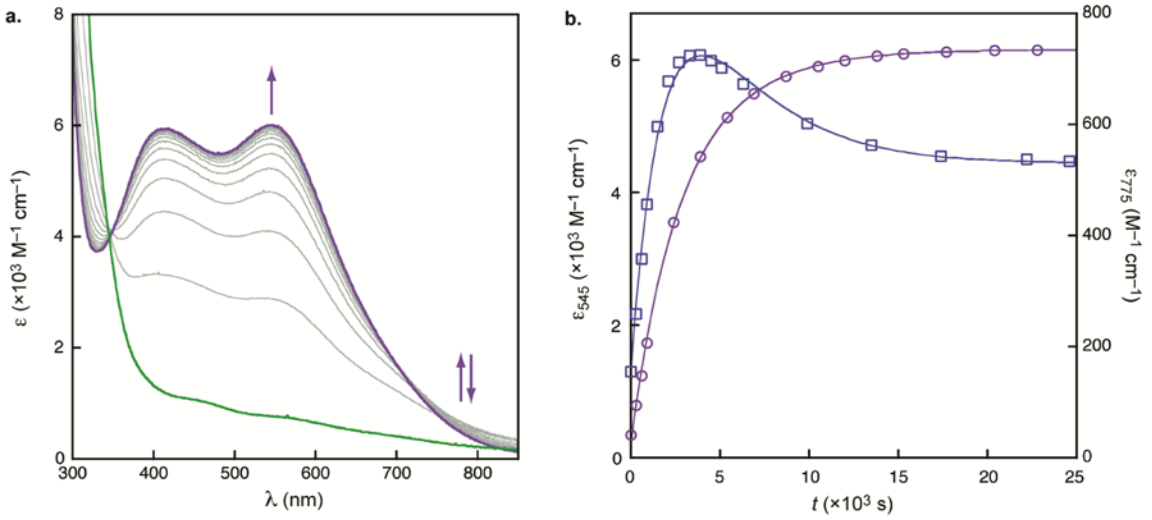


**Figure 2.9.** Selected UV–vis absorption data for a reaction of 2 x $10^{-4}$ M $[Re^{V}(O)(OPPh_3)(Br_4cat)_2]^-$ with 1 atm $O_2$ at 25 °C in $CH_2Cl_2$ to generate $[Re^{VII}(O)_2(Br_4cat)_2]^-$. **(a)** Spectra at $t$ = 0, immediately on addition of $O_2$ (green line), and at 25.0 min intervals to $t$ = 500 min (purple line). **(b)** Selected time–resolved data showing the formation of $[Re^{VII}(O)_2(Br_4cat)_2]^-$ with $\lambda_{max}$ = 554 nm (purple ○), and the formation and decay of an intermediate species at 775 nm (blue □). The fits (purple and blue lines) were obtained simultaneously from iterative analysis of the full spectral window (300–800 nm) using a biexponential A→B→C integrated rate law model, giving $k_{A\rightarrow B}$ = (4.8 ± 0.5) x $10^{-4}$ $s^{-1}$ and $k_{B\rightarrow C}$ = (2.6 ± 0.5) x $10^{-4}$ $s^{-1}$.

Exposure of lime green $[Re^{V}(O)(ap^{Ph})_2]^-$ in MeCN or $CH_2Cl_2$ solutions to air or $O_2$ rapidly generates dark purple solutions containing the $O_2$ homolysis product $[Re^{VII}(O)_2(ap^{Ph})_2]^-$. However, the reaction yields are lower due to a competing oxidative degradation reaction that extrudes the $ibq^{Ph}$ ($ibq^{Ph}$ = 2,4-di-*tert*-butyl-6-(phenylimino)phenol; Scheme 2.2) form of the ligand. For instance, addition of 1 atm air to 0.08 mM $[Re^{V}(O)(apPh)_2]^-$ in $CH_2Cl_2$ affords $[Re^{VII}(O)_2(ap^{Ph})_2]^-$ in <15 min, but the yield is only about 30%. This low yield is not due to an inherent instability of the dioxo product in $O_2$, because independently prepared samples of $[Re^{VII}(O)_2(ap^{Ph})_2]^-$ are indefinitely stable under $O_2$ in solution at ambient temperature.

Notably, the UV–vis spectrum of $[Re^{V}(O)(PPh_3)(ox)_2]^-$ is unchanged under 1 atm $O_2$ in MeCN over weeks at ambient temperature and days at 70 °C. As described above,

oxidation of $[Re^{V}(O)(PPh_3)(ox)_2]^-$ by strong oxo–atom donors leads to rapid composition to $ReO_4^-$, so the comparative stability of $[Re^{V}(O)(PPh_3)(ox)_2]^-$ in $O_2$ suggests that the $[Re^{V}(O)(ox)_2]^-$ core is unable to homolyze $O_2$. Additional experimental data suggests that this inability of $[Re^{V}(O)(PPh_3)(ox)_2]^-$ to effect direct reductive cleavage of $O_2$ arises from kinetic and not thermodynamic factors. Heating $[Re^{V}(O)(PPh_3)(ox)_2]^-$ with 2 equiv $[Re^{VII}(O)_2(cat)_2]^-$ to 60 °C in MeCN–*d*3 affords $OPPh_3$ and 2 equiv $[Re^{V}(O)(cat)_2]^-$ in ~5 h, as the only observable products by $^1H$ NMR spectroscopy (eq. 4). The reactions presumably occur via two sequential oxygen-atom transfer reactions from $[Re^{VII}(O)_2(cat)_2]^-$, first to the labile $PPh_3$ and, then to $[Re^{V}(O)(ox)_2]^-$. The thermodynamics of the second step, oxo transfer from $[Re^{VII}(O)_2(cat)_2]^-$ to $[Re^{V}(O)(ox)_2]^-$ are not determined in this reaction because the equilibrium reaction may driven by the instability

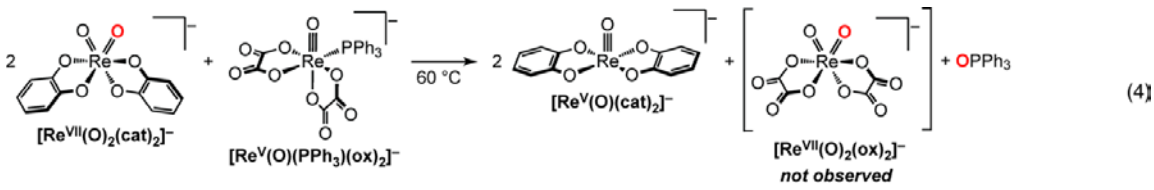


(4)

of $[Re^{VII}(O)_2(ox)_2]^-$. However, because $[Re^{V}(O)(cat)_2]^-$ is rapidly reoxidized under the reaction conditions, the products of eq. 4 imply that $[Re^{VII}(O)_2(cat)_2]^-$ is a catalyst for the aerobic decomposition of the $[Re^{V}(O)(ox)_2]^-$ anion (Scheme 2.4). Indeed, heating a mixture of $[Re^{VII}(O)_2(cat)_2]^-$ and 7 equiv $[Re^{V}(O)(PPh_3)(ox)_2]^-$ under 1 atm $O_2$ results in complete decomposition of the oxalate complex within hours at 60 °C, conditions where $[Re^{V}(O)(PPh_3)(ox)_2]^-$ is itself stable to $O_2$.

**Scheme 2.4.**

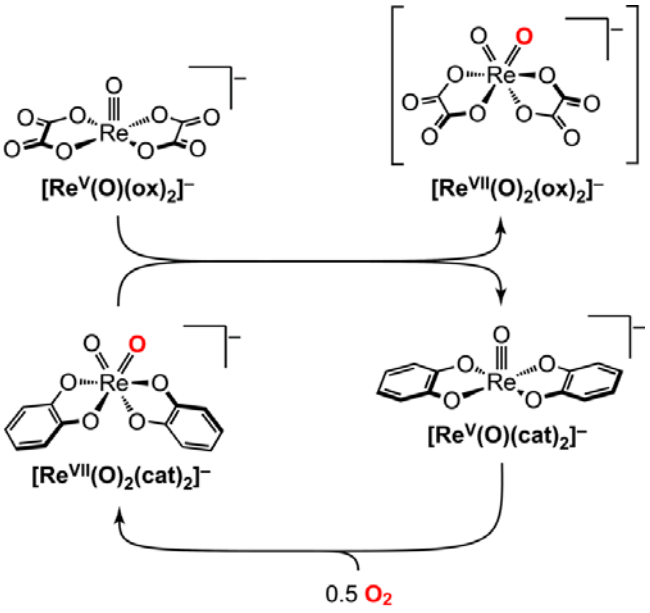


## 2.3 Discussion

### 2.3.1 Mechanism of $O_2$ Homolysis by $[Re^{V}(O)(cat)_2]^-$.

The five-coordinate oxorhenium(V) anion $[Re^{V}(O)(cat)_2]^-$ effects clean reductive cleavage of dioxygen to afford the dioxorhenium(VII) product $[Re^{VII}(O)_2(cat)_2]^-$. The reaction stoichiometry (2 $[Re^{V}(O)(cat)_2]^-$ + 1 $O_2$ → 2 $[Re^{VII}(O)_2(cat)_2]^-$) implies that both of the dioxygen-derived atoms are consumed in formation of two new $Re^{VII}$=O bonds. Although a direct termolecular interaction of the three reactants is consistent with the observed stoichiometry, it is statistically and chemically implausible. Additionally, the UV–vis kinetics data for the reactions with oxygen are multiphasic, and *do not* show a second order dependence on the oxorhenium(V) concentration. The sum of the experimental and computational data reported herein is most consistent with the

stepwise mechanism of bimetallic $O_2$ homolysis shown in Scheme 2.5. Each of these proposed reaction steps is discussed below.

**Scheme 2.5.**

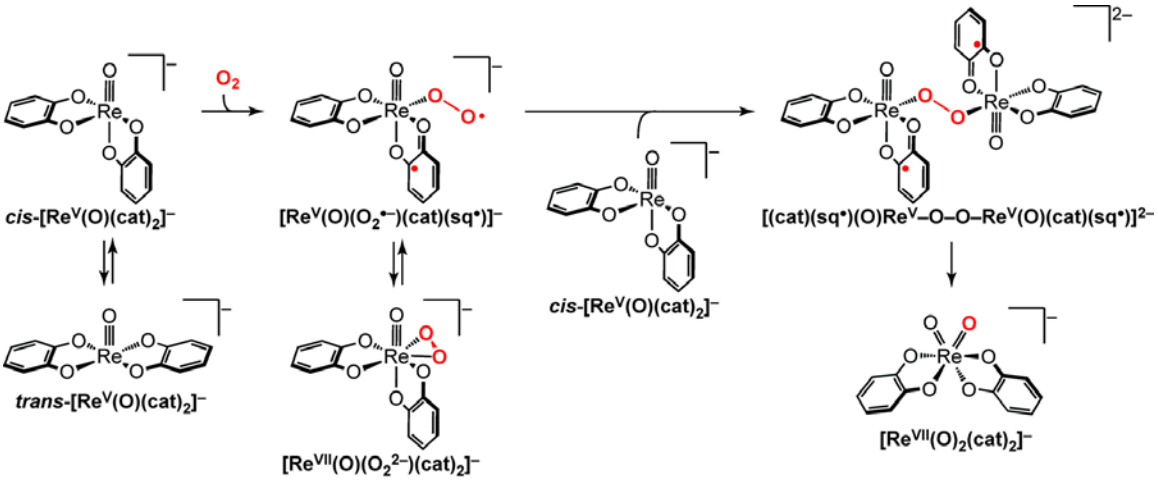


In the first step of the proposed mechanism, $O_2$ binding to $[Re^{V}(O)(cat)_2]^-$ generates a six coordinate dioxygen complex. Evidence for the necessity of a vacant site at rhenium for reaction with $O_2$ comes from the observation that high concentrations of $PPh_3$ stabilize $[Re^{V}(O)(cat)_2]^-$ in $O_2$ atmospheres, presumably via formation of the six-coordinate species $[Re^{V}(O)(PPh_3)(cat)_2]^-$. Dioxygen-adducts to $[Re^{V}(O)(cat)_2]^-$ have not been isolated, but computational studies of these intermediates suggest that $O_2$ binding occurs with isomerization of the $[cat]^{2-}$ ligands to a *cis* conformation. In the absence of a sixth ligand, the *cis* conformer of $[Re^{V}(O)(cat)_2]^-$ is computed to be 26.1 kcal $mol^{-1}$ higher in energy than the *trans* form. However, this value represents an upper limit of the true barrier to *cis-trans* isomerization of $[Re^{V}(O)(cat)_2]^-$, because the $C_1$-symmetric *cis* conformer is stabilized by binding a π-acidic ligand, such as $O_2$, in the vacant

coordination site. This ligand-driven torsional flexibility of the $[Re^{V}(O)(cat)_2]^{-}$ core is additionally manifest in the variable temperature $^1H$ NMR spectra of $[Re^{V}(O)(PPh_3)(cat)_2]^{-}$ in MeCN-*d*3.[84] At –40 °C the two $[cat]^{2-}$ ligands are in distinct chemical environments, consistent with a static structure with local $C_1$ symmetry. However, at 25 °C the resonances for the two $[cat]^{2-}$ ligands coalesce due to $PPh_3$ dissociation, which affords $[Re^{V}(O)(cat)_2]^{-}$. The equivalent $[cat]^{2-}$ $^1H$ NMR resonances in $[Re^{V}(O)(cat)_2]^{-}$ are consistent with either a static $C_{2v}$-symmetric structure or rapid isomerization that equilibrates the ligands on the time scale of the NMR experiment. Either implicates rapid isomerization of $[Re^{V}(O)(cat)_2]^{-}$ with $PPh_3$ binding/dissociation (eq. 1).

Addition of $O_2$ to *cis*–$[Re^{V}(O)(cat)_2]^{-}$ affords two minimum energy $O_2$ complexes with different spin states. As illustrated, end-on approach of triplet $O_2$ first affords a triplet diradical complex $[Re^{V}(O)(O_2^{\bullet-})(cat)(sq^{\bullet})]^{-}$ containing a partially reduced $\eta^1$-superoxide $[O_2^{\bullet}]^{-}$ ligand. Binding and reduction of $O_2$ occurs with concomitant $1e^{-}$ oxidation of the metal fragment, but the oxidation is not metal–centered. Rather, $1e^{-}$ is removed from a redox-active $[cat]^{2-}$ ligand to give a semiquinonate $[sq^{\bullet}]^{-}$ free radical. The $S = 1$ species $[Re^{V}(O)(O_2^{\bullet-})(cat)(sq^{\bullet})]^{-}$ is only 5.5 kcal $mol^{-1}$ above the ground state *trans*–$[Re^{V}(O)(cat)_2]^{-}$, confirming that addition of triplet $O_2$ to *cis*–$[Re^{V}(O)(cat)_2]^{-}$ is exoergic, by 20.6 kcal $mol^{-1}$. Subsequent collapse of the distal oxygen of the $\eta^1$-superoxo ligand forms a seven-coordinate, closed–shell $S = 0$ complex containing a second Re–$O_2$ bond. Isomerization to the singlet state $O_2$–complex isomer is downhill by 12.4 kcal $mol^{-1}$ complex, so $O_2$ binding to form the singlet mononuclear dioxygen complex from *trans*-$[Re^{V}(O)(cat)_2]^{-}$ and $O_2$ is exoergic by 6.9 kcal $mol^{-1}$. The $O_2$ fragment in this minimum energy complex is best described $\eta^2$-peroxo $[O_2]^{2-}$ dianion, implying that the $[Re^{V}(O)(cat)_2]^{-}$ is oxidized by $2e^{-}$. Both of these electrons formally derive from the rhenium center, so the complex anion is $[Re^{VII}(O)(O_2^{2-})(cat)_2]^{-}$, implying that spin

crossover occurs with $1e^-$ reduction of the coordinated $[sq^\bullet]^-$ free radical. The ability of the oxorhenium(V) fragment to undergo metal–centered $2e^-$ oxidation with bond formation is well-established, as exemplified by the facile oxygen atom additions to $[Re^V(O)(cat)_2]^-$ described herein, as well as the rich oxo–transfer reactivity in related species.[41,49,97–99] There is also precedent for formation of $\eta^2$-peroxo complexes of rhenium.[48,97,99,100] The importance of the redox-active $[cat]^{2-}$ ligand as a reservoir for a single electron in these reactions is discussed below.

Reaction of triplet $O_2$ with the closed shell $[Re^V(O)(cat)_2]^-$ anion is formally spin forbidden, but previous reports have suggested that such spin-forbidden reactions of $O_2$ with transition metals are not necessarily intrinsically slow. [101] In particular, the reaction sequence for $O_2$ addition and reduction proposed here closely resembles a reaction of $O_2$ with a mononuclear palladium(0) species to form an $\eta^2$-peroxopalladium(II) complex.[102,103] Binding $O_2$ initially forms a triplet diradical palladium(I) complex with an $\eta^1$-superoxide $[O_2^\bullet]^-$ ligand, which crosses to a singlet surface with formation of the second Pd–$O_2$ bond. Delocalization of unpaired spin density onto the metal ion is proposed to lower the barrier to spin crossover to a singlet product by weakening the exchange interaction. Similarly, the formal transfer of $1e^-$ from $O_2$ to a redox-active catecholate ligand separates the unpaired spins in the triplet diradical complex $[Re^V(O)(O_2^{2-})(cat)(sq^\bullet)]^-$ (Figure 8), providing a mechanism for facile spin crossover to yield the singlet peroxorhenium(VII) product.

The second step of the proposed bimetallic homolysis mechanism is formation of a dinuclear $O_2$–bridged intermediate. The computed minimum-energy singlet state structure contains a *trans*-μ-1,2-peroxo $[O_2]^{2-}$ linkage. Although the net $2e^-$ reduction of $O_2$ could arise from either $2e^-$ oxidation of a single $[Re^V(O)(cat)_2]^-$ anion or from $1e^-$ oxidation of both of the terminal $[Re^V(O)(cat)_2]^-$ fragments, all of the computed bond distances about the two oxorhenium centers are similar, consistent with the latter,

symmetric charge distribution. Accordingly, formation of the second Re–$O_2$ bond likely occurs with ligand–centered 1e$^-$oxidation of $[Re^{V}(O)(cat)_2]^-$, affording $[(cat)(sq^{\bullet})(O)Re^{V}$–O–O–$Re^{V}(O)(cat)(sq^{\bullet})]^{2-}$. The computed barrier to formation of the singlet peroxo–bridge complex is approximately 54 kcal mol$^{-1}$ above singlet state monomeric peroxo complex $[Re^{VII}(O)(O_2^{2-})(cat)_2]^-$. However, calculations suggest that a triplet state potential energy surface is *at least* 9.6 kcal mol$^{-1}$ lower in energy than the singlet state surface. Formation of the dinuclear peroxo-bridged intermediate is therefore proposed to proceed via initial isomerization to the excited–state triplet diradical complex $[Re^{V}(O)(O_2^{2-})(cat)(sq^{\bullet})]^-$, followed by attack of the distal oxygenic radical of the $\eta^1$-superoxide $[O_2^{\bullet}]^-$ ligand on a second equivalent of *cis*-$[Re^{V}(O)(cat)_2]^-$. There are strong similarities in both of the proposed Re–$O_2$ bond forming steps leading to assembly of a dinuclear peroxo–bridged complex: Both invoke attack of an oxygen radical on *cis*-$[Re^{V}(O)(cat)_2]^-$ that proceeds with 1e$^-$ reduction of the incoming $^{\bullet}O_2$ fragment and 1e$^-$ oxidation of a redox-active $[cat]^{2-}$ ligand.

The final reaction step is homolytic cleavage of the peroxo O–O bond in $[(cat)(sq^{\bullet})(O)Re^{V}$–O–O–$Re^{V}(O)(cat)(sq^{\bullet})]^{2-}$ to afford 2 equiv of the dioxorhenium(VII) product $[Re^{VII}(O)_2(cat)_2]^-$. This product–forming step is formally another 2e$^-$ reduction of the *trans*-μ-1,2-peroxo $[O_2]^{2-}$ linkage to two terminal oxo $[O]^{2-}$ ligands. The $d^0$ electron count in the rhenium product suggests that intramolecular transfer of 1e$^-$ from each $[Re^{V}(O)(cat)(sq^{\bullet})]$ fragment to the $[O_2]^{2-}$ group proceeds with intramolecular reduction of the coordinated semiquinonate radical $[sq^{\bullet}]^-$ ligands. As shown in Figure 7, $[Re^{VII}(O)_2(cat)_2]^-$ is the energetic minimum on the potential energy surface. It lies 64.1 kcal mol$^{-1}$ below *trans*-[ReV(O)(cat)2]$^-$ and 57.2 kcal mol$^{-1}$ below the minimum energy $O_2$ adduct $[Re^{VII}(O)(O_2^{2-})(cat)_2]^-$. The computed reaction coordinate therefore agrees well with the observed reaction kinetics: The net reaction proceeds by two sequential exoergic reaction steps, and the second step of the reaction is rate limiting. However,

the observation that mononuclear $O_2$ adducts to $[Re^{V}(O)(cat)_2]^{-}$ do not accumulate to significant concentrations suggests that the computed kinetic barrier to the second step may be overestimated. Indeed, in conditions where the biphasic kinetics are most apparent, the second phase of the reaction is only approximately a factor of 3 slower than the first. Because *cis*-$[Re^{V}(O)(cat)_2]^{-}$ is a reactant common to both steps, it is likely that isomerization of *trans*-$Re^{V}(O)(cat)_2]^{-}$ to the *cis* isomer contributes to the kinetic barrier in both reaction steps. Further support for the intermediacy of ligand–centered oxidation products in reactions of $[Re^{V}(O)(cat)_2]^{-}$ with oxygen radicals, as well as consideration of the relative products of $1e^{-}$ versus $2e^{-}$ oxidation of $[Re^{V}(O)(cat)_2]^{-}$, follows.

**2.3.2 Ligand Redox Activity In $1e^{-}$ Reactions with Oxygenic Radicals.**

In total, the redox–active nature of the $[cat]^{2-}$ ligand is proposed to lower the barrier to $O_2$ homolysis at $[Re^{V}(O)(cat)_2]^{-}$ in two ways. First, both $O_2$ binding to $[Re^{V}(O)(cat)_2]^{-}$ and reaction of $[Re^{V}(O)(O_2^{\bullet-})(cat)(sq^{\bullet})]^{-}$ with $[Re^{V}(O)(cat)_2]^{-}$ formally requires $1e^{-}$ oxidation of $[Re^{V}(O)(cat)_2]^{-}$. With redox–inert ligands, this $1e^{-}$ necessarily derives from the rhenium(V) center, but mononuclear oxorhenium(VI) complexes are comparatively rare versus their $d^0/d^2$ counterparts. Ligand-centered oxidation provides a pathway for $1e^{-}$ redox chemistry at the oxorhenium(V) ion that does not require formation to an oxorhenium(VI) species. Second, delocalization of spin density onto the redox–active ligand likely lowers the barrier to spin crossover in the formally spin–forbidden reaction of $[Re^{V}(O)(cat)_2]^{-}$ with $O_2$. This effect is similarly important in the second step of the reaction, wherein formation of the dinuclear peroxo-bridged complex likely occurs by attack of the radical superoxo group in $[Re^{V}(O)(O_2^{2-})(cat)(sq^{\bullet})]^{-}$ on *cis*-$[Re^{V}(O)(cat)_2]^{-}$. The triplet diradical $\eta^1$-superoxo complex is formally a spin-forbidden excited state. But the principle of microscopic reversibility predicts that the same

electronic properties that facilitate spin crossover with $O_2$ addition also lower the barrier to isomerization to the reactive triplet species.

Direct experimental evidence for the intermediacy of semiquinonate $[sq^{\bullet}]^{-}$ free radical intermediates has been experimentally elusive, and the computed reaction coordinate in fact suggests that they may be in short-lived. But the sum of other data provides strong, indirect support for the importance of ligand-centered redox changes in all of these elementary steps. First, reactions with structural homologs of $[Re^{V}(O)(cat)_2]^{-}$ containing substituted $[cat]^{2-}$ ligands exhibit two important trends: (1) All three oxorhenium(V) complexes with redox-active catecholate and amidophenolate ligands homolyze $O_2$ to generate the corresponding dioxorhenium(VII) products, but $[Re^{V}(O)(ox)_2]^{-}$ with redox-inert oxalate ligands is inert to $O_2$; (2) the relative rates of $O_2$ homolysis parallel the oxidation potentials of the redox–active ligands, with $[ap^{Ph}]^{2-}$ > $[cat]^{2-}$ > $[Br_4cat]^{2-}$.[104,105] As discussed below, these two trends are not rationalized by thermodynamic factors alone, and are most consistent with the redox–active ligand affording access to a kinetically preferred pathway. Moreover, the observation of $[ibq^{Ph}]$ and $[ibq^{Ph}]$-derived products in reactions of with $[Re^{V}(O)(ap^{Ph})_2]^{-}$ with $O_2$ implies that ligand oxidation is viable under the reaction conditions.

Further evidence for ligand–centered changes in oxidation state during $1e^{-}$ redox bond–forming reactions at oxorhenium(V) comes from reactions of $[Re^{V}(O)(cat)_2]^{-}$ with stable nitroxyl radicals.[106] As shown in eq. 5, addition of the stable nitroxyl radical 2,2,6,6-tetramethylpiperidine-1-oxyl ($TEMPO^{\bullet}$) to $[Re^{V}(O)(cat)_2]^{-}$ gives clean conversion to $[Re^{VII}(O)_2(cat)_2]^{-}$ in minutes at ambient temperature. The net reaction is a very unusual oxygen atom transfer from $TEMPO^{\bullet}$ that oxidizes the metal fragment by $2e^{-}$. However, the initial Re–O bond forming reaction is a spin-forbidden $1e^{-}$ process, wherein attack of the nitroxyl radical on *cis*-$[Re^{V}(O)(cat)_2]^{-}$ formally reduces $TEMPO^{\bullet}$ to the closed-shell $[TEMPO]^{-}$ (eq. 6). Mechanistic studies suggest that the reducing electron required for

TEMPO$^{\bullet}$ binding also derives from a $[cat]^{2-}$ ligand to generate $[sq^{\bullet}]^{-}$ complex intermediates. The parallels to the Re–$O_2$ bond-forming reactions described above are striking. In all of these reactions, the ability of the redox-active ligands to mediate $1e^{-}$ transfer imparts a remarkable radical-like reactivity to the closed-shell $[Re^{V}(O)(cat)_2]^{-}$ fragment, which in turn keys efficient Re–O bond formation via reactions with oxygen radicals.

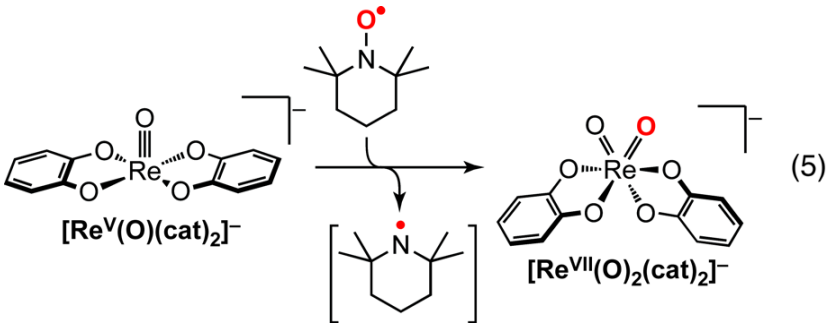


(5)

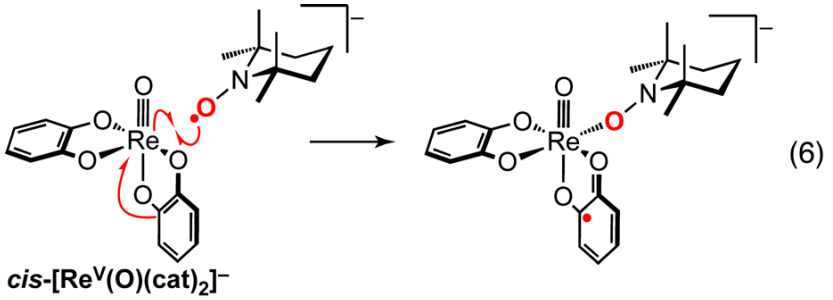


(6)

### 2.3.3 $1e^{-}$ Versus $2e^{-}$ Redox in $O_2$ Homolysis

The thermodynamic driving force for $O_2$ homolysis by $[Re^{V}(O)(cat)_2]^{-}$ and its derivatives is a function of the $Re^{VII}$=O bond dissociation enthalpies (BDEs) of the resulting dioxorhenium(VII) products.[41,42] All of $[Re^{V}(O)(cat)_2]^{-}$, $[Re^{V}(O)(Br_4cat)_2]^{-}$, and $[Re^{V}(O)(ap^{Ph})_2]^{-}$ are rapidly oxidized to the corresponding dioxo products with

stoichiometric addition of 1 equiv of strong oxo donors, such as pyridine *N*-oxide, DMSO, or $OAsPh_3$. The dioxo species are all reduced by $PPh_3$ to regenerate the respective oxorhenium(V) anions. Together, these results bracket the $Re^{VII}$=O BDEs of $[Re^{VII}(O)_2(cat)_2]^-$, $[Re^{VII}(O)_2(Br_4cat)_2]^-$, and $[Re^{VII}(O)_2(ap^{Ph})_2]^-$ within the same, rather large range, 118 ± 15 kcal $mol^{-1}$.[107] An estimate of the $Re^{VII}$=O BDE in $[Re^{V}(O)(ox)_2]^-$ could not be made by this method because $[Re^{VII}(O)_2(ox)_2]^-$ is not isolable (*vide supra*). Accordingly, all of the bimetallic $O_2$ homolysis reactions are exothermic by at least 43.1 kcal $mol^{-1}$ of rhenium, and up to 73.8 kcal $mol^{-1}$ of rhenium, but uncertainty in determination of the respective BDEs precludes precise determination or comparison of the energetics of the individual reactions.

Given the large experimental uncertainty in determination of the $Re^{VII}$=O BDEs, thermodynamic contributions to the observed differences in rates of $O_2$ cleavage cannot be rigorously evaluated. Oxygen-atom addition to the oxorhenium(V) anions is formally a $2e^-$ oxidation of the metal fragment. It is probable that $[Re^{V}(O)(ap^{Ph})_2]^-$, containing the most electron-rich ligand, is most easily oxidized by $2e^-$, and therefore has the most exothermic reaction with $O_2$. However, thermodynamics alone cannot rationalize the observed rates of reactions with $O_2$. In particular, the $[Re^{V}(O)(ox)_2]^-$ anion is remarkably stable in $O_2$. But reactions with oxidants, including DMSO, rapidly decompose $[Re^{V}(O)(ox)_2]^-$, presumably via oxo group transfer to generate $[Re^{VII}(O)_2(ox)_2]^-$. Importantly, $[Re^{V}(O)(ox)_2]^-$ also deoxygenates $[Re^{VII}(O)_2(cat)_2]^-$ (eq. 4, Scheme 2.4). The driving force for these oxygen-atom transfer reaction may be the instability of the putative $[Re^{VII}(O)_2(ox)_2]^-$ product, but the fact that a reaction occurs at all suggests that equilibrium $2e^-$ oxo–group transfer to $[Re^{V}(O)(ox)_2]^-$ is not prohibitive. Accordingly, $[Re^{VII}(O)_2(cat)_2]^-$ is a competent catalyst for the aerobic decomposition of $[Re^{V}(O)(ox)_2]^-$, implying that the thermodynamics of $O_2$ cleavage by $[Re^{V}(O)(ox)_2]^-$ are favorable. The lack of a reaction with $O_2$ must, then, be kinetic in origin. It was postulated that the

source of this kinetic inhibition is the absence of a redox-active ligand to mediate the $1e^-$ redox steps that key formation of the intermediate $O_2$ adducts.

### 2.3.4 Implications for Bimetallic Activation and Assembly of $O_2$.

The mechanism of $O_2$ homolysis by $[Re^V(O)(cat)_2]^-$ and its derivatives mirrors that proposed for most biological oxygenases and models systems.[20,25,32] In particular, the net $4e^-$ reduction of $O_2$ occurs through a series of $1e^-$ steps, via superoxo and peroxo intermediates.[25] Because bimetallic $O_2$ homolysis to make two terminal metal-oxo groups is formally a $2e^-$ oxidation of each metal center, the reaction is appropriately viewed as two oxygen-atom transfers from $O_2$ to the metal ions. Accordingly, the thermodynamics of the oxygen–atom transfer reaction are determined by of the BDEs of the oxo donor and acceptor substrates, allowing for a straightforward prediction of the reaction spontaneity.[42] The utility of these $2e^-$ oxo–transfer couples in rationalizing metal-mediated oxidation reactions is well established.[41] But unlike many strong oxo donors, $O_2$ is a kinetically poor oxidant. This study suggests that the ability of the transition metal to mediate $1e^-$ transfer may be a crucial factor in determining the facility of reactions with $O_2$, because the absence of an accessible $1e^-$ redox couple can introduce a kinetic barrier to $O_2$ homolysis.

Biological oxygenases overwhelmingly utilize naturally abundant 3d transition metal ions in their catalytic active sites, so the intermediacy of partially reduced $O_2$ complexes in both natural and synthetic oxygenases is a consequence the fact that the preferred redox pathway for nearly all 3d transition metals is $1e^-$ transfer.[39] In contrast, later 4d and 5d transition metal complexes find utility in many selective bond-making and bond-breaking reactions because of their ability to mediate the transfer of multiple electrons while avoiding odd-electron intermediates. The $[Re^V(O)(cat)_2]^-$ is not structurally or electronically unique as compared to the many five coordinate oxorhenium(V) complexes that have been extensively employed as oxo-transfer

reagents,[41,49,98,99] except for one factor. The complexes reported here have redox-active ligands, which afford access a low-energy pathway for the $1e^-$ bond-forming reactions with $O_2$. By way of comparison, a 2003 review[49] of oxo transfer reactions catalyzed by oxorhenium(V) complexes with redox-inert ligands highlights (1) the scarcity of $Re^{VI}$, as compared to $Re^{V}$ and $Re^{VII}$, and the absence of free radical reactivity; (2) the general lack of reactivity with dioxygen. The few species that do react with $O_2$ do not cleanly homolyze the O–O bond to generate terminal oxo ligands.[49,108] In contrast, a comparatively large number of the isoelectronic oxomolybdenum(IV) species are oxidized by $O_2$ to afford dioxomolybdenum(VI) complexes,[41,109] but molybdenum(V) has been noted to "intervene more directly" than rhenium(VI) in oxo transfer reactions. Accordingly, for facile cleavage of $O_2$, an accessible $1e^-$ redox couple may be at least as important as an ability to deliver $2e^-$ in reactions with oxo-donor substrates.

The implications of this conclusion are far-reaching. It suggests that designs for new oxygenase-type catalysts should consider not only the $2e^-$ thermodynamic stability of the resulting oxometal fragment, but also the accessibility of a $1e^-$ redox couple. Moreover, the same electronic features that facilitate bimetallic $O_2$ homolysis are necessarily implicit in the reverse reaction, symmetric assembly of $O_2$ by coupling of two metal oxo fragments. This step is commonly invoked in proposed schemes for catalytic water oxidation.[80,82] The data presented herein suggests that coupling to redox–active ligands may provide a mechanism for accessing odd–electron intermediates in the net $4e^-$ bond-forming process. To this end, one complex with redox-active quinone ligands has been shown to have good catalytic activity for water oxidation.[110,111] It is intriguing to note that computational studies suggest quinone ligand centered redox chemistry may facilitate O–O bond formation.[110]

## 2.4 Conclusions

A series of five-coordinate oxorhenium(V) complexes with redox-active catecholate and amidophenolate ligands have been prepared and shown to effect clean bimetallic cleavage of $O_2$ to give dioxorhenium(VII) products. The rates of the $O_2$ homolysis reactions parallel the oxidation potentials of the redox–active ligands, with $[ap^{Ph}]^{2-}$ > $[cat]^{2-}$ > $[Br_4cat]^{2-}$. A structural homolog with redox–inert oxalate ligands does not react with $O_2$. The thermodynamics of $O_2$ cleavage by all of the oxorhenium(V) complexes are favorable, so thermodynamics alone cannot explain the relative rates of the reactions, especially the stability of $[Re^{V}(O)(ox)_2]^{-}$ in $O_2$.

Instead, the sum of the experimental and computational data suggest that redox-active ligands lower the kinetic barrier to bimetallic $O_2$ homolysis at five–coordinate oxorhenium(V), by giving access to $1e^{-}$ redox steps that are crucial for formation and stabilization of intermediate $O_2$ adducts. Bimetallic $O_2$ activation occurs by two sequential Re–O bond forming reactions, which generate mononuclear $\eta^1$-superoxo, and then binuclear *trans*-μ-1,2-peroxo-bridged, complexes. Formation of both Re–O bonds requires trapping of a triplet radical dioxygen species by a *cis*-$[Re^{V}(O)(cat)_2]^{-}$ anion. In each reaction the dioxygen fragment is reduced by $1e^{-}$, so generation of each new Re–O bond requires that an oxometal fragment is oxidized by $1e^{-}$. With redox–inert ligands, this $1e^{-}$ necessarily derives from the rhenium(V) center. But mononuclear oxorhenium(VI) species are rare, and oxorhenium(V) complexes are not generally prone to $1e^{-}$ transfer or free radical reactivity. The complexes containing a redox-active ligand can access a lower energy reaction pathway for the $1e^{-}$ Re–O bond forming reaction because the metal fragment can be oxidized without a change in formal rhenium oxidation state. It is also likely that redox-active ligands facilitate $O_2$ homolysis by lowering the barrier to the formally spin-forbidden reactions of triplet dioxygen with the closed shell oxorhenium(V) anions.

In sum, introduction of a redox-active ligand orthogonalizes $1e^-$ and $2e^-$ redox at oxorhenium(V), which allows high-valent rhenium to utilize a mechanism for $O_2$ activation that is more typical for oxygenase enzymes and models based on 3d transition metal ions: $O_2$ cleavage occurs by a net $2e^-$ process through a series of $1e^-$ steps. Ongoing studies in our laboratory are pursuing the use of redox-active ligand $1e^-$ redox for multielectron oxygenasetype catalysis, as well as the microscopic reverse reaction, O–O bond formation from coupling of two M=O fragments for catalytic water oxidation.

## 2.5 Experimental Details and Supplementary Material

### 2.5.1 General Considerations.

Unless otherwise specified, all manipulations were performed under anaerobic conditions using standard vacuum line techniques, or in an inert atmosphere glove box under purified nitrogen. Routine NMR spectra were acquired on a Varian Mercury 300 spectrometer (300.323 MHz for $^1$H; 75.5 MHz for $^{13}$C) or a Varian Mercury 400 spectrometer (161.9 MHz for $^{31}$P) at ambient temperature. Variable temperature NMR spectra were obtained with a Bruker AMX 400 spectrometer (400.138 MHz for $^1$H). All chemical shifts are reported in parts per million (ppm) relative to TMS, with the residual solvent peak serving as an internal reference. UV–visible absorption spectra were acquired using a Varian Cary 50 spectrophotometer. Unless otherwise noted, all electronic absorption spectra were recorded at ambient temperatures in 1 cm quartz cells. UV–vis chemical kinetics data were fit by iterative multivariate analysis using the commercially available software Specfit/32 from Spectrum Software Associates. IR spectra were obtained in KBr or Nujol using a Shimadzu 8400S Fourier transform infrared spectrophotometer or a Perkin Elmer 1000 FT-IR spectrophotometer. All mass spectra were recorded in the Georgia Institute of Technology Bioanalytical Mass Spectrometry Facility. Electrospray ionization mass spectrometry (ESI-MS) was carried out with acetonitrile solutions using a Micromass Quattro LC spectrometer. Electron

impact mass spectra (EI-MS) were obtained using a VG instruments model 70-SE spectrometer. Fast atom bombardment mass spectra (FAB-MS) were acquired in the negative mode on a VG Instruments 70-SE spectrometer. Elemental analyses were performed by Atlantic Microlab, Inc., Norcross, GA. All analyses were performed in duplicate, and the reported compositions are the average of the two runs.

**2.5.2 Methods and Materials.**

Anhydrous acetonitrile (MeCN), dichloromethane, and pentane solvents for air- and moisture-sensitive manipulations were purchased from Sigma-Aldrich and further dried by passage through columns of activated alumina, degassed by at least three freeze-pump-thaw cycles, and stored under $N_2$ prior to use. Methanol (anhydrous, 99.0%), was purchased from Honeywell Burdick and Jackson. Ethanol (anhydrous, 200 proof, 99.5%), was purchased from Sigma-Aldrich. Acetone (99.8%, extra dry) was purchased from Acros. All were used as received. Oxygen (ultra high purity) was used as received from Airgas, Inc. Deuterated acetonitrile (MeCN-*d*3) was purchased from Cambridge Isotope Laboratories, degassed by three freeze-pump-thaw cycles, vacuum distilled from $CaH_2$, and stored under a dry $N_2$ atmosphere prior to use. $[Re^{V}(O)(PPh_3)_2Cl_3]$,[84] $(Et_4N)[Re^{V}(O)(cat)_2]$,[71] $(Et_4N)[Re^{V}(O)(PPh_3)(cat)_2]$,[84] $(Et_4N)[Re^{VII}(O)_2(cat)_2]$,[71] $(nBu_4N)[Re^{V}(O)(OPPh_3)(Br_4cat)_2]$,[112] and 2,4-di-*tert*-butyl-6-(phenylamino)phenol ($H_2ap^{Ph}$; Scheme 2.2)[113] were prepared by literature methods. All characterization data matched those referenced. All other reagents were purchased from Sigma–Aldrich and used as received.

**2.5.3 Preparation of $(Me_4N)[Re^{V}(O)(ap^{Ph})_2]$.**

A 50 mL flask with a Kontes brand high-vacuum PTFE valve was charged with $[Re^{V}O(PPh_3)_2Cl_3]$ (0.251 g, 0.302 mmol), $Me_4NCl$ (0.242 g, 2.22 mmol), $H_2ap^{Ph}$ (0.181 g, 0.608 mmol), and MeOH (10 mL). $Et_3N$ (180 µL, 1.29 mmol) was slowly added with vigorous stirring to afford a green suspension. The flask was sealed and immersed in a

silicone fluid bath at 85 °C for 4 h to yield a clear, dark green solution, then slowly cooled to ambient temperature and stored under $N_2$ for 15 h to precipitate the desired product. Filtration through a fritted funnel afforded lime green crystals of $(Me_4N)[Re^{V}(O)(ap^{Ph})_2]$ (0.196 g, 0.226 mmol, 75%). UV–vis (MeCN) $\lambda_{max}$, nm ($\varepsilon$, $M^{-1}$ $cm^{-1}$): 316 (19000), 620 (40). $^1$H NMR (300 MHz, MeCN–*d*3, $): 7.34, 7.26 (br, N*Ph*: ortho, meta, 8H); 7.09 (t, *J* = 7 Hz, N*Ph*: para, 2H); 6.74 (d, *J* = 2 Hz, Ar*H*, 2H); 6.53 (d, *J* = 2 Hz, Ar*H*, 2H); 3.02 (s, *Me*$_4$N$^+$, 12H); 1.17 (s, –C(C*H*$_3$)$_3$, 9H); 1.02 (s, –C(C*H*$_3$)$_3$, 9H). Samples of $[Re^{V}(O)(ap^{Ph})_2]^-$ for elemental analysis contained 1 molecule of MeOH. MeOH is also observed in the X-ray crystal structure. The reported analysis is for $(Me_4N)[Re^{V}(O)(ap)_2]$•MeOH. Anal. Calcd for $C_{45}H_{66}N_3O_4Re$: C, 60.11; H, 7.40; N, 4.67; Found: C, 60.23; H, 7.35; N, 4.85.

**2.5.4 Preparation of $(Et_3NH)[Re^{V}(O)(PPh_3)(ox)_2]$.**

$[Re^{V}(O)(PPh_3)_2Cl_3]$ (0.251 g, 0.300 mmol) and oxalic acid dihydrate ($H_2ox$•$2H_2O$) (0.075 g, 0.590 mmol) were combined in air with anhydrous EtOH (15 mL) in a 50 mL round bottom flask, and $Et_3N$ (165 µL, 1.18 mmol) was added dropwise with vigorous stirring. The resulting green suspension was heated to reflux to give a clear green solution which became violet over for 40 min. The solution was cooled to room temperature and stored at 8 °C for 15 h to yield finely-divided purple solids, which were collected by vacuum filtration. The solids were purified by precipitation from $CH_2Cl_2$ with pentane, affording microcrystalline $(Et_3NH)[Re^{V}(O)(PPh_3)(ox)_2]$ (0.169 g, 0.223 mmol, 87%). UV–vis (MeCN) $\lambda_{max}$, nm ($\varepsilon$, $M^{-1}$ $cm^{-1}$): 550 (40), 705 (40). FTIR (KBr): 3541 (br), 3459 (br), 3059 (m), 2986 (w), 1759 (s, $ox^{2-}$ C=O), 1708 (s, $ox^{2-}$ C=O), 1670 (s, $ox^{2-}$ C=O), 1480 (w), 1435 (w), 1393 (w), 1374 (w), 1304 (m), 1250 (w), 1192 (w), 1160 (w), 1097 (m), 1046 (w), 1008 (m), 883 (m), 836 (w), 809 (m), 790 (m), 753 (m), 710 (m), 694 (m), 578 (w), 531 (m) $cm^{-1}$. $^{13}$C NMR (300 MHz, MeCN–*d*3, $): 166.43, 164.75, 161.00, 160.30 (all *ox*); 135.32 (d, *J* = 11 Hz), 133.12 (d, *J* = 2 Hz), 130.12 (d, *J* = 11 Hz) (all

P*Ph*$_3$); 47.71, 9.15 (*Et*$_3$NH$^+$). Samples of [Re$^V$(O)(PPh$_3$)(ox)$_2$]$^-$ for elemental analysis were obtained from concentrated EtOH solutions. The reported analysis is for (Et$_3$NH)[Re$^V$(O)(ox)$_2$(PPh$_3$)]•EtOH, and the presence of one EtOH in the sample was confirmed by 1H NMR spectroscopy. Anal. Calcd for $C_{30}H_{37}NO_{10}PRe$: C, 45.68; H, 4.73; N, 1.78; Found: C, 45.48; H, 4.73; N, 1.90.

**2.5.5 Preparation of (Et$_4$N)[Re$^{VII}$(O)$_2$(Br$_4$cat)$_2$].**

A 250 mL round bottom flask was charged with a clear green solution of (Et$_4$N)[Re$^V$(O)(Br$_4$Cat)$_2$(OPPh$_3$)] (1.463 g, 1.02 mmol) in acetone (75 mL) and stirred in air for 3 d, resulting in a color change to dark purple. The reaction mixture was chilled to 8 °C and purple solids precipitated from solution over 15 h. The solids were collected by vacuum filtration, washed with EtOH (2 x 15 mL, cold), and ether (2 x 15 mL), and dried *in vacuo* to give (Et$_4$N)[Re$^{VII}$(O)$_2$(Br$_4$cat)$_2$] (1.097 g, 0.917 mmol, 91%) as a purple powder. UV–vis (MeCN) $\lambda_{max}$, nm ($\varepsilon$, M$^{-1}$ cm$^{-1}$): 280 (12000), 405 (5200), 535 (5200). FAB–MS (*m/z*): 1066 [M–Et4N]$^-$. FTIR (KBr): 3957 (w), 3905 (w), 2980 (w), 2362 (w), 2327 (w), 1750 (w), 1709 (w), 1538 (w), 1515 (m), 1480 (m),1454 (w), 1436 (w), 1400 (s, Br$_4$Cat$^{2-}$ CC), 1358 (m), 1297 (w), 1255 (m, Br$_4$Cat$^{2-}$ C–O), 1234 (m), 1172 (w), 1096 (w), 1066 (w), 999 (m), 948 (s), 922 (s), 786 (w), 756 (m), 740 (m), 692 (w), 651 (w) 576 (m) cm$^{-1}$. Anal. Calcd for $C_{20}H_{20}Br_8NO_6Re$: C, 20.07; H, 1.69; N, 1.17; Found: C, 20.34; H, 1.65; N, 1.32.

**2.5.6 Preparation of (Et$_4$N)[Re$^{VII}$(O)$_2$(ap$^{Ph}$)$_2$].**

**Method 1**. Using the procedure described above for preparation of [Re$^V$(O)(ap$^{Ph}$)$_2$]$^-$, [ReO(PPh$_3$)$_2$Cl$_3$] (0.648 g, 0.780 mmol), Et$_4$NCl (0.512 g, 3.09 mmol), H$_2$ap$^{Ph}$ (0.214 g, 0.719 mmol), MeOH (20 mL), and Et$_3$N (425 µL, 3.04 mmol) were combined in a sealable 100 mL flask and heated in a silicone fluid bath at 85 °C for 4 h. The resulting clear green solution containing (Et$_4$N)[Re(O)(ap$^{Ph}$)$_2$] was slowly cooled to ambient temperature and exposed to air, effecting a color change to dark violet. Slow

evaporation of the solvent over 30 d deposited violet crystals, which were collected by vacuum filtration through a fritted funnel and washed with diethyl ether (2 % 15 mL) to afford $(Et_4N)[Re^{VII}(O)_2(ap^{Ph})_2]$ (0.122 g, 0.130 mmol, 18%). **Method 2**. A 20 mL scintillation vial was charged with $(Et_4N)[Re(O)(ap^{Ph})_2]$ (0.135 g, 0.146 mmol) and dissolved in 2 mL $CH_2Cl_2$. Slow addition of 0.406 M pyridine *N*-oxide in $CH_2Cl_2$ (400 µL, 0.16 mmol) with vigorous stirring afforded an immediate color change from a pale green to a dark violet. The solution was stirred for 24 h and the solvent was removed under reduced pressure. The resulting dark powder was washed with pentane (3 x 2 mL) and dried *in vacuo* to yield $(Et_4N)[Re^{V}(O)_2(ap)_2]$ (0.114 g, 0.121 mmol, 80%). UV–vis ($CH_2Cl_2$) $\lambda_{max}$, nm ($\varepsilon$, $M^{-1}$ $cm^{-1}$): 292 (17000), 415 (sh, 6500), 494 (7500), 602 (8000). 8! FAB–MS (*m/z*): 809 $[M–Et4N]^-$. 1H NMR (300 MHz, MeCN–*d*3, $): 7.34 (m, N*Ph*: ortho, meta, 8H); 7.04 (tt, *J* = 7, 1 Hz, N*Ph*: para, 2H); 6.43 (d, *J* = 2 Hz, Ar*H*, 2H); 6.08 (d, *J* = 2 Hz, Ar*H*, 2H); 3.42 (q, *J* = 7.3 Hz, $(CH_3CH_2)_4N^+$, 8H); 1.33 (tt, *J* = 7.3, 1.9 Hz, $(CH_3CH_2)_4N^+$, 12H) 1.25 (s, $^t$Bu, 18H); 1.10 (s, $^t$Bu, 18H). Anal. Calcd for $C_{48}H_{70}N_3O4Re$: C, 61.38; H, 7.51; N, 4.47; Found: C, 61.10; H, 7.52; N, 4.44.

**2.5.7 Reactions with Dioxygen.**

In a representative procedure, a 1.0 cm quartz cuvette fitted with a Kontes brand high-vacuum PTFE valve was charged with 2.0 mL of $[Re^{V}(O)(cat)_2]^-$ (7.5 x $10^{-5}$ M) in $CH_2Cl_2$ and sealed under $N_2$. The solution was degassed on a high-vacuum line by three freeze-pump-thaw cycles and an initial spectrum was acquired. The cuvette was then backfilled with 1 atm of $O_2$, shaken vigorously, placed in a Peltier UV–vis cell holder with a magnetic stirrer, and stirred to maintain a constant concentration of dissolved $O_2$ throughout the reaction. The reaction progress was monitored by UV–vis spectroscopy (200–900 nm) for 35 min at 48 s intervals. For reactions with air, the solutions were similarly prepared under $N_2$ and degassed prior to air exposure. For NMR kinetics

studies, a J. Young brand NMR tube with a Teflon screw cap was used in place of the sealable cuvette.

**2.5.8 X-ray Crystallography.**

Crystals of $(Et_3NH)[Re^{V}(O)(ap^{Ph})_2]$•0.25MeOH, $(Et_3NH)[Re^{V}(O)(ox)_2(PPh_3)]$•1.5EtOH, and $(Et_4N)[Re^{VII}(O)_2(ap^{Ph})_2]$ suitable for X-ray diffraction analysis were coated with Paratone N oil, suspended on a small fiber loop and placed in a cooled nitrogen gas stream at 173 K on a Bruker D8 APEX II CCD sealed tube diffractometer. Data for $(Et_4N)[Re^{VII}(O)_2(ap^{Ph})_2]$ was obtained with graphite monochromated Cu Kα (λ = 1.54178 Å) radiation. Diffraction data for $(Et_3NH)[Re^{V}(O)(ap^{Ph})_2]$•0.25MeOH and $(Et_3NH)[Re^{V}(O)(ox)_2(PPh_3)]$•1.5EtOH were collected using graphite monochromated Mo Kα (λ= 0.71073 Å) radiation. All other data collection procedures, data processing and programs were the same for all samples. Data were measured using a series of combinations of phi and omega scans with 10 s frame exposures and 0.5° frame widths. Data collection, indexing and initial cell refinements were all carried out using APEX II software.[114] Frame integration and final cell refinements were done using SAINT software.[115] The final cell parameters were determined from least–squares refinement on 9899 reflections for $(Et_3NH)[Re^{V}(O)(ap^{Ph})_2]$•0.25MeOH, 6871 reflections for $(Et_3NH)[Re^{V}(O)(ox)_2(PPh_3)]$•1.5EtOH, and 8761 reflections for $(Et_4N)[Re^{VII}(O)_2(ap^{Ph})_2]$. The structures were solved using direct methods and difference Fourier techniques using the SHELXTL program package.[116] Hydrogen atoms were placed in their expected chemical positions using the HFIX command and were included in the final cycles of least squares with isotropic Uij's related to the atoms ridden upon. All non–hydrogen atoms in $(Et_4N)[Re^{VII}(O)_2(ap^{Ph})_2]$ were refined anisotropically, but only the metal–containing fragments in $(Et_3NH)[Re^{V}(O)(ap^{Ph})_2]$•0.25MeOH and

$(Et_3NH)[Re^{V}(O)(ox)_2(PPh_3)]$•1.5EtOH were refined anisotropically. Scattering factors and anomalous dispersion corrections are taken from the *International Tables for X-Ray Crystallography*.[117] Other details of data collection and structure refinement are provided in Table 2.1.

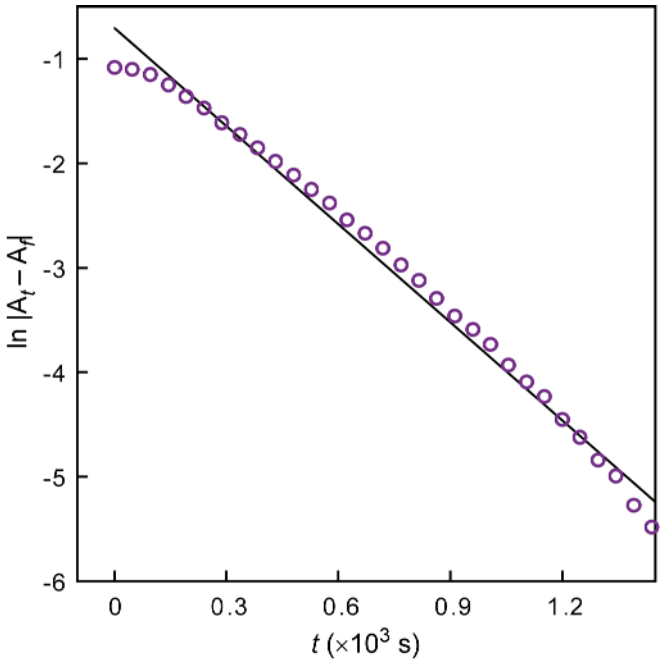


**Figure 2.10.** Plot of ln $|A_t - A_f|$ versus time for UV–vis absorption data collected at 554 nm in a reaction of 8 x $10^{-5}$ M $[Re^{V}(O)(cat)_2]^-$ with 1 atm $O_2$ in $CH_2Cl_2$ at 25 °C to generate $[Re^{VII}(O)_2(cat)_2]^-$. The solid line represents a linear fit to the data.

**Table 2.1.** Crystallographic Data and Structure Parameters for $(Et_3NH)[Re^{V}(O)(ap^{Ph})2]^{-}$ • 0.25 MeOH (A), $(Et_3NH)[Re^{V}(O)(ox)_2(PPh_3)]^{-}$ • 1.5 EtOH (B), and $(Et_4N)[Re^{VII}(O)_2(ap^{Ph})_2]$ (C).

| Complex | A | B | C |
|---|---|---|---|
| Empirical Formula | $C_{46.25}H_{67}N_3O_{3.25}Re$ | $C_{31}H_{40}NO_{10.5}PRe$ | $C_{48}H_70N_3O_4Re$ |
| Formula Weight | 923.23 | 811.81 | 939.27 |
| T (K) | 173(2) | 173(2) | 173(2) |
| Crystal System | monoclinic | triclinic | orthorhombic |
| Space Group | *P*21/*n* | *P*–1 | *Pbca* |
| Unit cell dimensions | | | |
| a (Å) | 13.6961(17) | 9.694(5) | 21.3050(4) |
| b (Å) | 23.198(3) | 13.247(6) | 11.0850(2) |
| c (Å) | 15.4092(19) | 13.851(7) | 39.1021(7) |
| α (°) | 90 | 90.283(8) | 90 |
| β (°) | 114.484(2) | 97.568(7) | 90 |
| γ (°) | 90 | 99.833(8) | 90 |
| V (Å$^3$) | 4455.6(6) | 1737.8(14) | 9234.6(3) |
| Z | 4 | 2 | 8 |
| $D_{calc}$ (g cm$^{-1}$) | 1.346 | 1.551 | 1.351 |
| Absorption coefficient (mm$^{-1}$) | 2.768 | 3.597 | 5.483 |
| Crystal size (mm) | 0.23 x 0.13 x 0.06 | 0.44 x0.32 x0.16 | 0.28 x 0.19 x 0.05 |
| θ range for data collection (°) | 1.68–28.50 | 1.48–28.17 | 2.26–66.96 |
| Index ranges | $-18 \le h \le 18$ | $-12 \le h \le 12$ | $-20 \le h \le 24$ |
| | $-30 \le k \le 30$ | $-17 \le k \le 17$ | $-12 \le k \le 12$ |
| | $-20 \le l \le 20$ | $-18 \le l \le 18$ | $-44 \le l \le 44$ |
| Reflections collected/unique | 64625/11138 | 23686/8461 | 32480/7856 |
| Goodness of fit on $F^2$ | 1.018 | 1.096 | 1.022 |
| R [I > 2σ(I)] | 0.0433 | 0.0278 | 0.0270 |
| $wR_2$ (all data) | 0.0951 | 0.0738 | 0.0645 |

## 2.6 References


[1] Sheldon, R. A.; Kochi, J. K. *Metal-Catalyzed Oxidations of Organic Compounds*; Academic Press:New York, 1981.

[2] In *Comprehensive Organic Synthesis: Selectivity, Strategy and Efficiency in Modern Organic Chemistry, Volume 7: Oxidation*; Trost, B. M., Fleming, I., Eds.; Pergamon: Oxford, UK, **1991**.

[3] In *Organic Syntheses by Oxidation with Metal Compounds*; Mijs, W. J., De Jonge, C. R. H. I., Eds. **1986**.

[4] Cavani, F.; Ballarini, N.; Luciani, S. *Top. Catal.* **2009**, *52*, 935-947.

[5] Parshall, G. W.; Ittel, S. D. *Homogeneous Catalysis, 2nd Edition. The Applications and Chemistry of Catalysis by Soluble Transition Metal Complexes*; Wiley-Interscience: New York, **1992**.

[6] Haber, J. In *Handb. Heterog. Catal. (2nd Ed.)*; Ertl, G., Ed.; Wiley-VCH: Weinheim, Germany, **2008**, 7, 3359-3384.

[7] Van Deurzen, M. P. J.; Van Rantwijk, F.; Sheldon, R. A. *Tetrahedron* **1997**, *53*, 13183-13220.

[8] Whittall, J. In *Catal. Fine Chem. Synth.*; Roberts, S., M., Whittall, J., Eds.; John Wiley & Sons Ltd.: Chichester, UK, **2007**, 5, 1-33.

[9] In *Oxygen Complexes and Oxygen Activation by Transition Metals*; Martell, A. E., Sawyer, D. T., Eds.; Plenum: New York, **1988**, 341.

[10] In *The Activation of Dioxygen and Homogeneous Catalytic Oxidation*; Barton, D., H. R., Martell, A. E., Sawyer, D. T., Eds.; Plenum: New York, **1993**.

[11] Stahl, S. S. *Science (Washington, DC, United States)* **2005**, *309*, 1824-1826.

[12] Boring, E.; Geletii, Y. V.; Hill, C. L. *Catal. Met. Complexes* **2003**, *26*, 227-264.

[13] Dijksman, A.; Arends, I. W. C. E.; Sheldon, R. A. *Platinum Met. Rev.* **2001**, *45*, 15-19.

[14] Murahashi, S.-I.; Komiya, N.; Hayashi, Y.; Kumano, T. *Pure Appl. Chem.* **2001**, *73*, 311-314.

[15] Zhan, B.-Z.; Thompson, A. *Tetrahedron* **2004**, *60*, 2917-2935.

[16] Stahl, S. S. *Angew. Chem., Int. Ed.* **2004**, *43*, 3400-3420.

[17] In *Advances in Catalytic Activation of Dioxygen by Metal Complexes*; Simandi, L. I., Ed.; Kluwer Acadmic Publishers: Norwell, MA, **2003**.

[18] Borovik, A. S.; Zinn, P. J.; Zart, M. K. In *Activation of Small Molecules: Organometallic and Bioinorganic Perspectives*; Tolman William, B., Ed.; Wiley-VCH: Weinheim, Germany, **2006**, 187-234.

[19] Meunier, B.; Editor *Biomimetic Oxidations Catalyzed by Transition Metal Complexes*, 2000.

[20] Nam, W. *Acc. Chem. Res.* **2007**, *40*, 465.

[21] Chaudhuri, P.; Wieghardt, K.; Weyhermueller, T.; Paine, T. K.; Mukherjee, S.; Mukherjee, C. *Biol. Chem.* **2005**, *386*, 1023-1033.

[22] Chaudhuri, P.; Hess, M.; Mueller, J.; Hildenbrand, K.; Bill, E.; Weyhermueller, T.; Wieghardt, K. *J. Am. Chem. Soc.* **1999**, *121*, 9599-9610.

[23] Wang, Y.; DuBois, J. L.; Hedman, B.; Hodgson, K. O.; Stack, T. D. P. *Science (Washington, D. C.)* **1998**, *279*, 537-540.

[24] Cornell, C. N.; Sigman, M. S. In *Activatino of Small Molecules: Organometallic and Bioinorganic Perspectives*; Tolman William, B., Ed.; Wiley-VCH: Weinheim, Germany, **2006**, 159-186.

[25] Special Issue on Dioxygen Activation and Metallozyme Models, *Acc. Chem. Res.* **2007**, *40*, 465-634.

[26] Que, L., Jr.; Tolman, W. B. *Nature* **2008**, *455*, 333-340.

[27] In *Porphyrin Handbook*; Kadish, K. M., Smith, K. M., Guilard, R., Eds.; Academic Press: San Diego, CA, **2000**.

[28] Mirica, L. M.; Ottenwaelder, X.; Stack, T. D. P. *Chem. Rev.* **2004**, *104*, 1013-1045.

[29] Kopp, D. A.; Lippard, S. J. *Curr. Opin.Chem. Biol.* **2002**, *6*, 568-576.

[30] Tshuva, E. Y.; Lippard, S. J. *Chem. Rev.* **2004**, *104*, 987-1012.

[31] Op't Holt, B. T.; Vance, M. A.; Mirica, L. M.; Heppner, D. E.; Stack, T. D. P.; Solomon, E. I. *J. Am. Chem. Soc.* **2009**, *131*, 6421-6438.

[32] In *Biomimetic Oxid. Catal. Transition Met. Complexes*; Meunier, B., Ed.; Imperial College: London, **2000**, 677.

[33] Lewis, E. A.; Tolman, W. B. *Chem. Rev.* **2004**, *104*, 1047-1076.

[34] Kim, E.; Chufan, E. E.; Kamaraj, K.; Karlin, K. D. *Chem. Rev.* **2004**, *104*, 1077-1134.

[35] Costas, M.; Mehn Mark, P.; Jensen Michael, P.; Que, L., Jr. *Chem. Rev.* **2004**, *104*, 939-86.

[36] Sono, M.; Roach, M. P.; Coulter, E. D.; Dawson, J. H. *Chem. Rev.* **1996**, *96*, 2841-2887.

[37] Meunier, B.; de Visser, S. P.; Shaik, S. *Chem. Rev.* **2004**, *104*, 3947-3980.

[38] MacBeth, C. E.; Golombek, A. P.; Young, V. G., Jr.; Yang, C.; Kuczera, K.; Hendrich, M. P.; Borovik, A. S. *Science* **2000**, *289*, 938-941.

[39] Greenwood, N. N.; Earnshaw, A. *Chemistry of the Elements*; Pergamon: New York, **1984**.

[40] Kolb, H. C.; Sharpless, K. B. In *Transition Met. Org. Synth. (2nd Ed.)*; Beller, M., Bolm, C., Eds.; Wiley-VCH: Weinheim, Germany, **2004**, 2, 275-298.

[41] Holm, R. H. *Chem. Rev.* **1987**, *87*, 1401-49.

[42] Holm, R. H.; Donahue, J. P. *Polyhedron* **1993**, *12*, 571-89.

[43] Enemark, J. H.; Cooney, J. J. A.; Wang, J.-J.; Holm, R. H. *Chem. Rev.* **2004**, *104*, 1175-1200.

[44] Jacobi, B. G.; Laitar, D. S.; Pu, L.; Wargocki, M. F.; DiPasquale, A. G.; Fortner, K. C.; Schuck, S. M.; Brown, S. N. *Inorg. Chem.* **2002**, *41*, 4815-4823.

[45] Nugent, W. A.; Mayer James, M. *Metal-Ligand Multiple Bonds*; John Wiley & Sons: New York, **1988**.

[46] Harlan, E. W.; Berg, J. M.; Holm, R. H. *J. Am. Chem. Soc.* **1986**, *108*, 6992-7000.

[47] Neithamer, D. R.; LaPointe, R. E.; Wheeler, R. A.; Richeson, D. S.; Van Duyne, G. D.; Wolczanski, P. T. *J. Am. Chem. Soc.* **1989**, *111*, 9056-72.

[48] Brown, S. N.; Mayer, J. M. *Inorg. Chem.* **1992**, *31*, 4091-100.

[49] Espenson, J. H. *Adv. Inorg. Chem.* **2003**, *54*, 157-202.

[50] Blackmore Karen, J.; Ziller Joseph, W.; Heyduk Alan, F. *Inorg. Chem.* **2005**, *44*, 5559-61.

[51] Haneline Mason, R.; Heyduk Alan, F. *J. Am. Chem. Soc.* **2006**, *128*, 8410-1.

[52] Blackmore, K. J.; Lal, N.; Ziller, J. W.; Heyduk, A. F. *J Am Chem Soc* **2008**, *130*, 2728-2789.

[53] Ketterer, N. A.; Fan, H.; Blackmore, K. J.; Yang, X.; Ziller, J. W.; Baik, M. H.; Heyduk, A. F. *J Am. Chem. Soc.* **2008**, *130*, 4364-74.

[54] Zarkesh Ryan, A.; Ziller Joseph, W.; Heyduk Alan, F. *Angew Chem Int Ed Engl* **2008**, *47*, 4715-8.

[55] Nguyen, A. I.; Blackmore, K. J.; Carter, S. M.; Zarkesh, R. A.; Heyduk, A. F. *J Am Chem Soc* **2009**.

[56] Bart, S. C.; Lobkovsky, E.; Bill, E.; Chirik, P. J. *J. Am. Chem. Soc.* **2006**, *128*, 5302-5303.

[57] Bouwkamp, M. W.; Bowman, A. C.; Lobkovsky, E.; Chirik, P. J. *J. Am. Chem. Soc.* **2006**, *128*, 13340-13341.

[58] Bart, S. C.; Bowman, A. C.; Lobkovsky, E.; Chirik, P. J. *J. Am. Chem. Soc.* **2007**, *129*, 7212-7213.

[59] Stanciu, C.; Jones Mary, E.; Fanwick Phillip, E.; Abu-Omar Mahdi, M. *J. Am. Chem. Soc.* **2007**, *129*, 12400-12401.

[60] Mukherjee, C.; Weyhermueller, T.; Bothe, E.; Chaudhuri, P. *Inorg. Chem.* **2008**, *47*, 2740-2746.

[61] Lu, C. C.; Weyhermuller, T.; Bill, E.; Wieghardt, K. *Inorg. Chem.* **2009**, *48*, 6055-6064.

[62] Chaudhuri, P.; Hess, M.; Weyhermuller, T.; Wieghardt, K. *Angew. Chem., Int. Ed.* **1999**, *38*, 1095-1098.

[63] Rolle, C. J.; Hardcastle, K. I.; Soper, J. D. *Inorg. Chem.* **2008**, *47*, 1892-1894.

[64] Smith, A. L.; Soper, J. D. *Polyhedron* **2009**, 29, 164-169.

[65] Pierpont, C. G.; Lange, C. W. *Prog. Inorg. Chem.* **1994**, *41*, 331-442.

[66] Pierpont, C. G. *Coord. Chem. Rev.* **2001**, *216-217*, 99-125.

[67] Kokatam, S.-L.; Chaudhuri, P.; Weyhermuller, T.; Wieghardt, K. *Dalton Trans.* **2007**, 373-378.

[68] Ray, K.; Petrenko, T.; Wieghardt, K.; Neese, F. *Dalton Trans.* **2007**, 1552-1566.

[69] Hendrickson, D. N.; Pierpont, C. G. *Top. Curr. Chem.* **2004**, *234*, 63-95.

[70] Shultz, D. A. *Comments Inorg. Chem.* **2002**, *23*, 1-21.

[71] Dilworth, J. R.; Ibrahim, S. K.; Khan, S. R.; Hursthouse, M. B.; Karaulov, A. A. *Polyhedron* **1990**, 9, 1323-9.

[72] Brudvig, G. W.; Beck, W. F.; De Paula, J. C. *Annu. Rev. Biophys. Biophys. Chem.* **1989**, *18*, 25-46.

[73] Eisenberg, R.; Gray Harry, B. *Inorg. Chem.* **2008**, *47*, 1697-9.

[74] Surendranath, Y.; Dinca, M.; Nocera, D. G. *J. Am. Chem. Soc.* **2009**, *131*, 2615-2620.

[75] Betley Theodore, A.; Wu, Q.; Van Voorhis, T.; Nocera Daniel, G. *Inorg. Chem.* **2008**, *47*, 1849-61.

[76] Renger, G. *Comprehensive Series in Photochemical & Photobiological Sciences* **2008**, *9*, 237-290.

[77] Tagore, R.; Crabtree, R. H.; Brudvig, G. W. *Inorg. Chem.* **2008**, *47*, 1815-1823.

[78] McEvoy, J. P.; Brudvig, G. W. *Chem. Rev.* **2006**, *106*, 4455-4483.

[79] Yagi, M.; Syouji, A.; Yamada, S.; Komi, M.; Yamazaki, H.; Tajima, S. *Photochem. Photobiol. Sci.* **2009**, *8*, 139-147.

[80] Ruettinger, W.; Dismukes, G. C. *Chem. Rev.* **1997**, *97*, 1-24.

[81] Liu, F.; Concepcion, J. J.; Jurss, J. W.; Cardolaccia, T.; Templeton, J. L.; Meyer, T. J. *Inorg. Chem.* **2008**, *47*, 1727-1752.

[82] Binstead, R. A.; Chronister, C. W.; Ni, J.; Hartshorn, C. M.; Meyer, T. J. *J. Am. Chem. Soc.* **2000**, *122*, 8464-8473.

[83] Kettler, P. B.; Chang, Y.-D.; Zubieta, J.; Abrams, M. J. *Inorg. Chim. Acta* **1994**, *218*, 157-65.

[84] Edwards, C. F.; Griffith, W. P.; White, A. J. P.; Williams, D. J. *J. Chem. Soc., Dalton Trans.* **1992**, 957-62.

[85] Bianchini, C.; Masi, D.; Mealli, C.; Meli, A.; Martini, G.; Laschi, F.; Zanello, P. *Inorg. Chem.* **1987**, *26*, 3683-93.

[86] Bill, E.; Bothe, E.; Chaudhuri, P.; Chlopek, K.; Herebian, D.; Kokatam, S.; Ray, K.; Weyhermueller, T.; Neese, F.; Wieghardt, K. *Chem.-Eur. J.* **2005**, *11*, 204-224.

[87] Poddel'sky, A. I.; Cherkasov, V. K.; Abakumov, G. A. *Coord. Chem. Rev.* **2009**, *253*, 291-324.

[88] Espenson, J. H. *Chemical Kinetics and Mechanism, 2nd Edition*; McGraw-Hill Inc.: New York, 1995.

[89] Becke, A. D. *J. Chem. Phys.* **1993**, *98*, 5648-52.

[90] Hay, P. J.; Wadt, W. R. *J. Chem. Phys.* **1985**, *82*, 299-310.

[91] Stephens, P. J.; Devlin, F. J.; Chabalowski, C. F.; Frisch, M. J. *J. Phys. Chem.* **1994**, *98*, 11623-7.

[92] *Jaguar*, version 6.5; Schrodinger, LLC: New York, 2006.

[93] MOLPRO, version 2006; Werner, H.-J.; Knowles, P. J.; Lindh, R.; Manby, F. R.; Schu¨tz, M.; et al.; http://www.molpro.net.

[94] *MOLEKEL*, version 5.0; Flu¨kiger, P.; Lu¨thi, H. P.; Portmann, S.; Weber, J.; Swiss National Supercomputing Centre CSCS: Manno, Switzerland, 2000.

[95] Vaska, L. *Acc. Chem. Res.* **1976**, *9*, 175-83.

[96] Gublemann, M. H.; Williams, A., F. In *Structure and Bonding 55*; Springer-Verlag: Berlin, **1983**, 1-65.

[97] Herrmann, W. A.; Kuhn, F. E. *Acc. Chem. Res.* **1997**, *30*, 169-180.

[98] Arias, J.; Newlands, C. R.; Abu-Omar, M. M. *Inorg. Chem.* **2001**, *40*, 2185-2192.

[99] Owens, G. S.; Arias, J.; Abu-Omar, M. M. *Catal. Today* **2000**, *55*, 317-363.

[100] Nicholson, T.; Zubieta, J. *Inorg. Chim. Acta* **1987**, *134*, 191-193.

[102] Landis, C. R.; Morales, C. M.; Stahl, S. S. *J. Am. Chem. Soc.* **2004**, *126*, 16302-16303.

[103] Popp, B. V.; Wendlandt, J. E.; Landis, C. R.; Stahl, S. S. *Angew. Chem., Int. Ed.* **2007**, *46*, 601-604.

[104] Pascaly, M.; Duda, M.; Schweppe, F.; Zurlinden, K.; Muller, F. K.; Krebs, B. *J. Chem. Soc. Dalton Trans.* **2001**, 828-837.

[105] Masui, H.; Lever, A. B. P.; Auburn, P. R. *Inorg. Chem.* **1991**, *30*, 2402-10.

[106] Lippert, C. A.; Soper, J. D. *Inorg. Chem.* **2010**, 49(8), 3682-3684.

[107] Holm, R. H.; Kennepohl, P.; Solomon, E. I. *Chem. Rev.* **1996**, *96*, 2239-2314.

[108] Huang, R.; Espenson, J. H. *J. Mol. Catal. A: Chem.* **2001**, *168*, 39-46.

[109] Barral, R.; Bocard, C.; de Roch, I. S.; Sajus, L. *Tetrahedron Lett.* **1972**, *13*, 1693-1696.

[110] Muckerman, J. T.; Polyansky, D. E.; Wada, T.; Tanaka, K.; Fujita, E. *Inorg. Chem.* **2008**, *47*, 1787-1802.

[111] Wada, T.; Tsuge, K.; Tanaka, K. *Inorg. Chem.* **2001**, *40*, 329-337.

[112] Edwards, C. F.; Griffith, W. P.; White, A. J. P.; Williams, D. J. *J. Chem. Soc., Dalton Trans.* **1992**, 957-62.

[113] Chaudhuri, P.; Verani, C. N.; Bill, E.; Bothe, E.; Weyhermueller, T.; Wieghardt, K. *J. Am. Chem. Soc.* **2001**, *123*, 2213-2223.

[114] APEX II, Brukers AXS, Inc., Analytical X-Ray Systems: Madison, WI, 2005.

[115] SAINT, version Version 6.45A, Brukers AXS, Inc., Analytical X-ray Systems: Madison, WI, 2003.

[116] Collins, T. J. *Acc. Chem. Res.* **2002**, *35*, 782-790.

[117] In *International Tables for X-ray Crystallography, Volume C*; Wilson, J. C., Ed.; Academic Publishers: Dordrecht, **1992**.

# Chapter 3

# Deoxygenation of Nitroxyl Radicals by Oxorhenium(V) Complexes with Redox–Active Ligands

## 3.1 Introduction

An ability to engender $1e^-$ versus $2e^-$ redox selectivity is paramount for realizing a variety of synthetically important bond-making and -breaking redox reactions.[1–3] Low-coordinate oxorhenium(V) complexes are prototypical $2e^-$ redox reagents, with particular utility for mediating oxygen-atom transfer.[4–7] We speculated that coordination to a redox-active ligand may afford access to $1e^-$ redox reactions that are atypical of oxorhenium(V) complexes, while preserving the ability of the metal to mediate $2e^-$ oxo-transfer reactivity.[8–15] This strategy was successfully applied to bimetallic $O_2$ homolysis at five-coordinate oxorhenium(V) species.[16] Reported herein are remarkable $2e^-$ deoxygenation reactions of stable nitroxyl radicals by five-coordinate oxorhenium(V) anions. Kinetics studies suggest a multistep reaction mechanism, where, by analogy to the first step of $O_2$ activation, redox-active ligands are proposed to facilitate $1e^-$ trapping of oxygen radicals.

## 3.2 Results

The addition of 2,2,6,6-tetramethylpiperidine-1-oxyl (TEMPO$^\bullet$) to tan solutions containing the five-coordinate monooxo anion $[Re^{V}(O)(cat)_2]^-$ ($[cat]^{2-}$=1,2-catecholate) in $CH_3CN$ immediately produces a dark-purple solution containing the *cis*-dioxo $[Re^{VII}(O)_2(cat)_2]^-$ complex. When the reaction is performed at 25 $^oC$ in NMR tubes containing $CD_3CN$, the oxidation is complete prior to acquisition of an initial spectrum (<10 min). Under identical conditions, the oxidation of $[Re^{V}(O)(cat)_2]^-$ with 1 atm of air requires >3 h, indicating that the observed process does not result from $O_2$ contamination. Integration of the $^1H$ NMR resonances for $[Re^{VII}(O)_2(cat)_2]^-$ confirms the stoichiometry shown in Scheme 3.1. Two new methyl resonances are also observed in a

3:1 ratio. Analysis of a similarly prepared purple $CH_3CN$ solution by gas chromatography–mass spectrometry (GC-MS) (Figures 3.1, 3.2a, and 3.2b) confirms that these correspond to 2,2,6,6–tetramethylpiperidine (TMP-H) and the N-cyanomethyl congener (TMP-$CH_2CN$) (Scheme 3.1). When the reaction is performed in $CD_3CN$, the molecular ion peaks increase by 1 and 2 atomic mass units, respectively, implicating the solvent in the reaction (Figures 3.3, 3.4a, and 3.4b). Performing a reaction of $[Re^{V}(O)(cat)_2]^-$ with 1 equiv of TEMPO$^\bullet$ in the presence of excess (13 equiv) 9,10-dihydroanthracene (DHA) as a sacrificial H$^\bullet$ source affords TMP-H as the only observable product by GC-MS (Figure 3.12). The reaction of $[Re^{V}(O)(cat)_2]^-$ with 1 equiv of TEMPO$^\bullet$ in a 80:20 $CD_3CN$:$CH_3CN$ mixture gives only the protio amine species (TMP-H and TMP-$CH_2CN$), as determined by analysis of their respective isotopic compositions by GC-MS. Assuming a detection limit of 10%, the selectivity of >90% for protio products gives an estimate of the lower limit for $k_H/k_D > 36$, which is in excellent agreement with a reported value.[17]

**Scheme 3.1.**

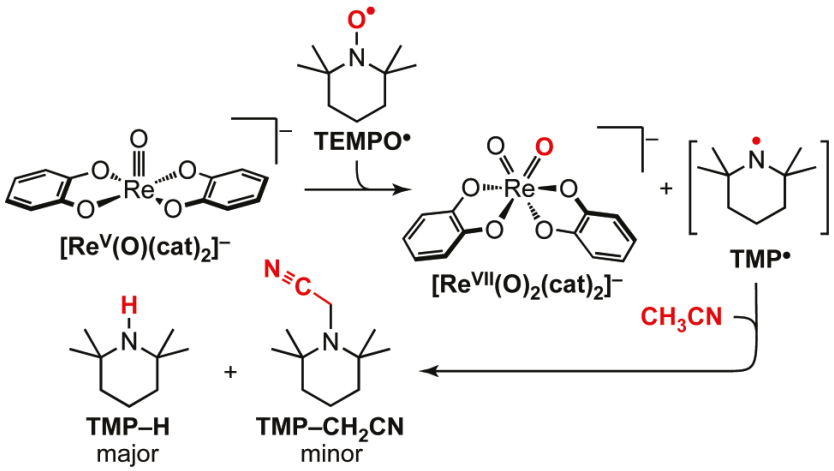

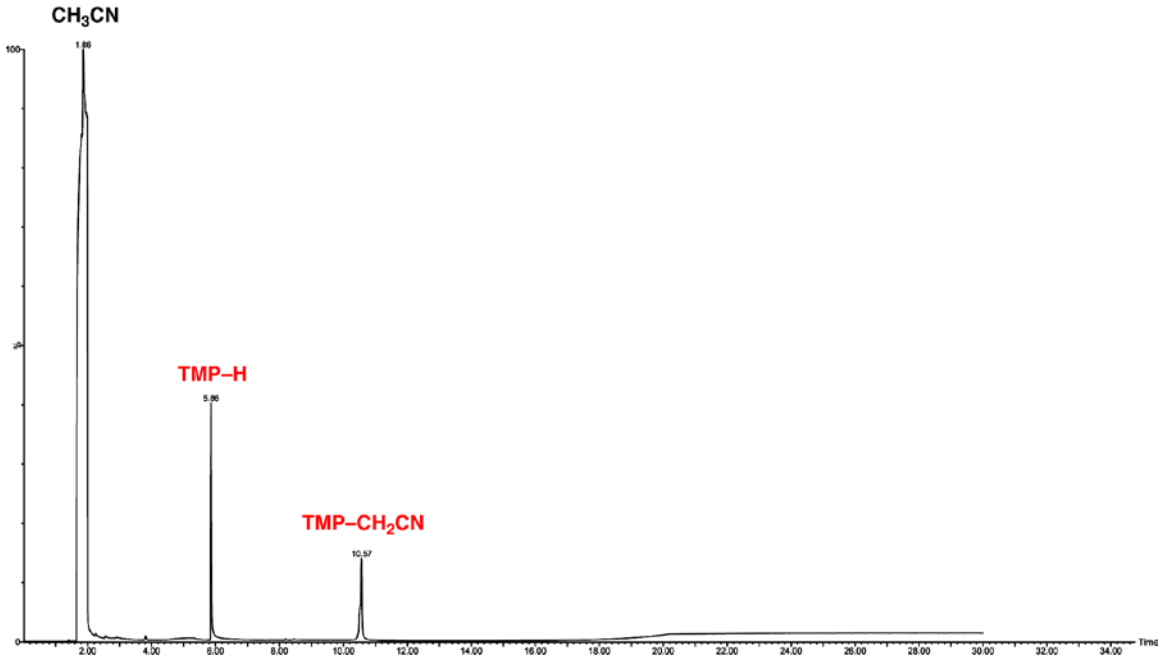


**Figure 3.1.** Gas chromatogram from a reaction of $[Re^{V}(O)(cat)_2]^-$ (0.035 mmol) with TEMPO$^{\bullet}$ (0.033 mmol) performed in $CH_3CN$. Assuming a linear response, integration of the peak areas corresponding to the TMP-H and TMP-$CH_2CN$ products suggests that they are formed in an approximate 3:1 ratio.

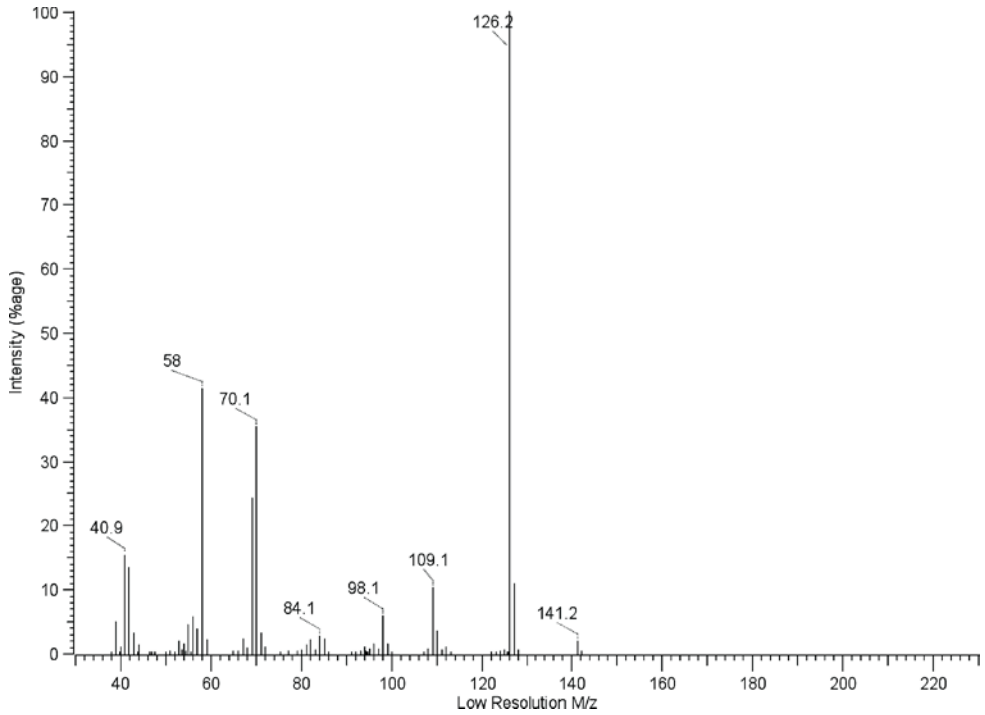


**Figure 3.2a.** Electron impact mass spectrum (EI–MS) of the TMP-H fraction from the gas chromatogram shown in Figure 3.1.

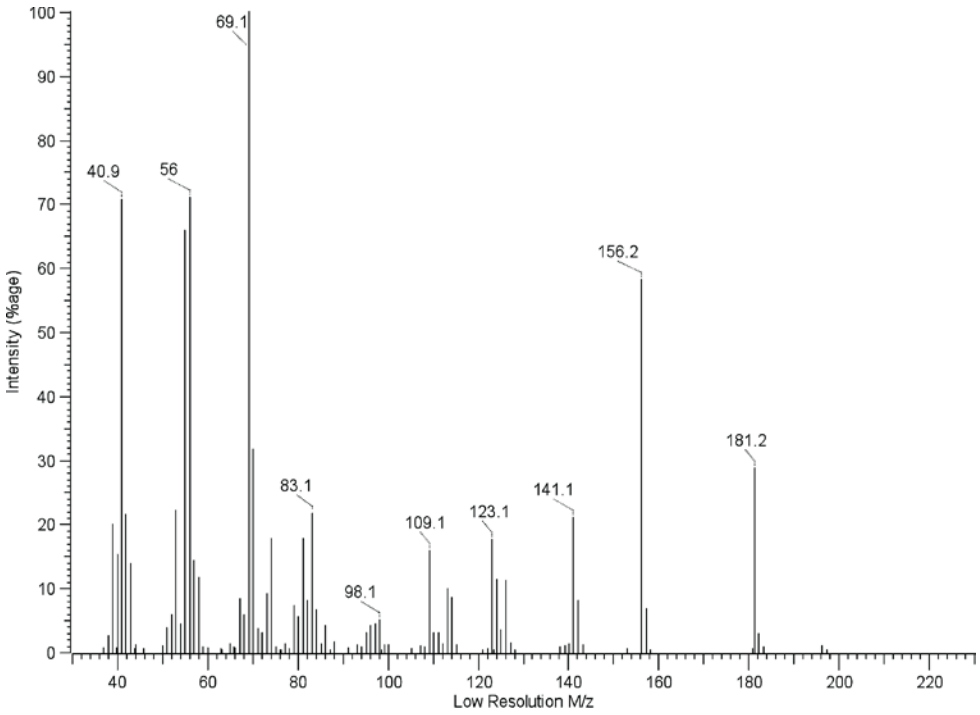


**Figure 3.2b.** Electron impact mass spectrum (EI–MS) of the TMP-$CH_2CN$ fraction from the gas chromatogram shown in Figure 3.1.

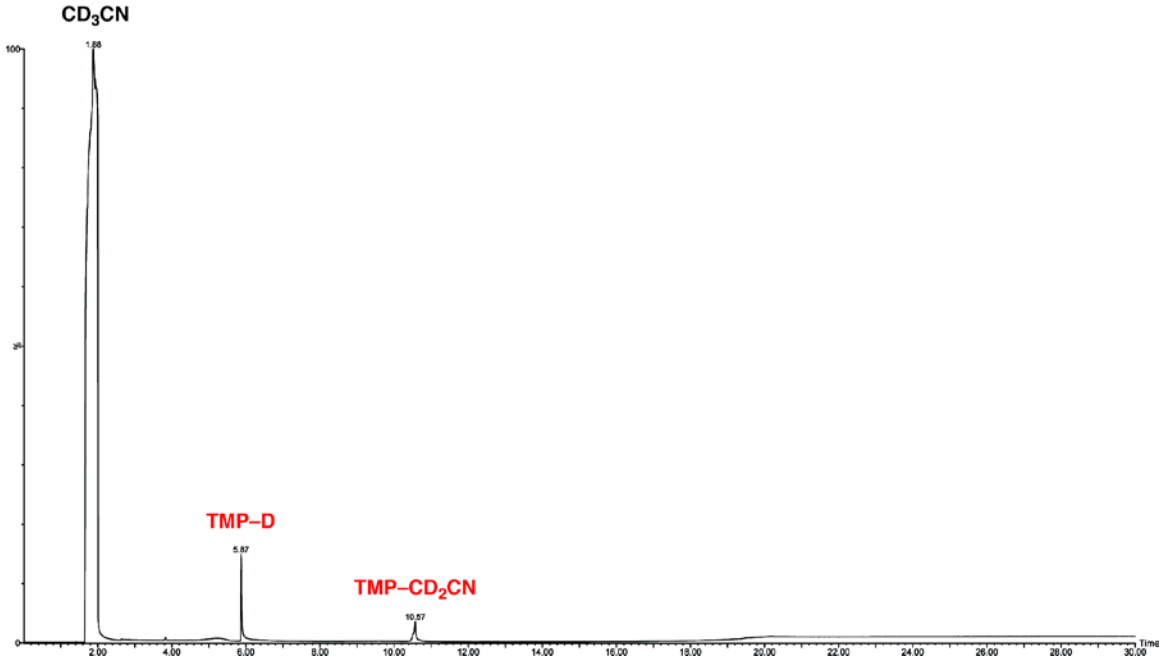


**Figure 3.3.** Gas chromatogram from a reaction of $[Re^{V}(O)(cat)_2]^-$ (0.023 mmol) with TEMPO$^{\bullet}$ (0.022 mmol) performed in $CD_3CN$. Assuming a linear response, integration of the peak areas corresponding to the TMP-D and TMP-$CD_2CN$ products suggests that they are formed in an approximate 4:1 ratio.

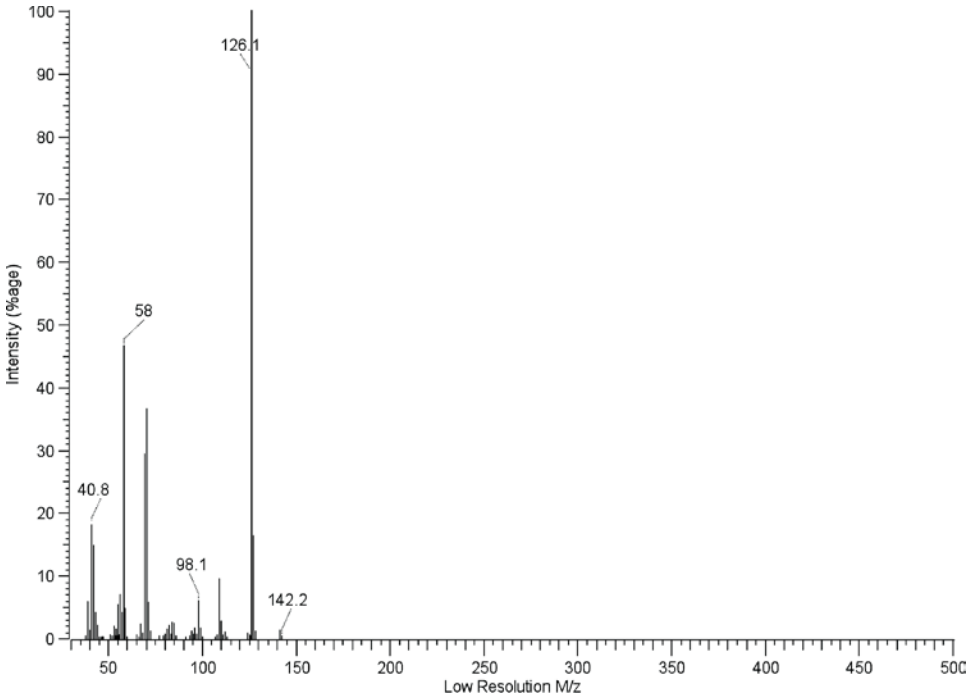


**Figure 3.4a.** Electron impact mass spectrum (EI–MS) of the TMP-D fraction from the gas chromatogram shown in Figure 3.3.

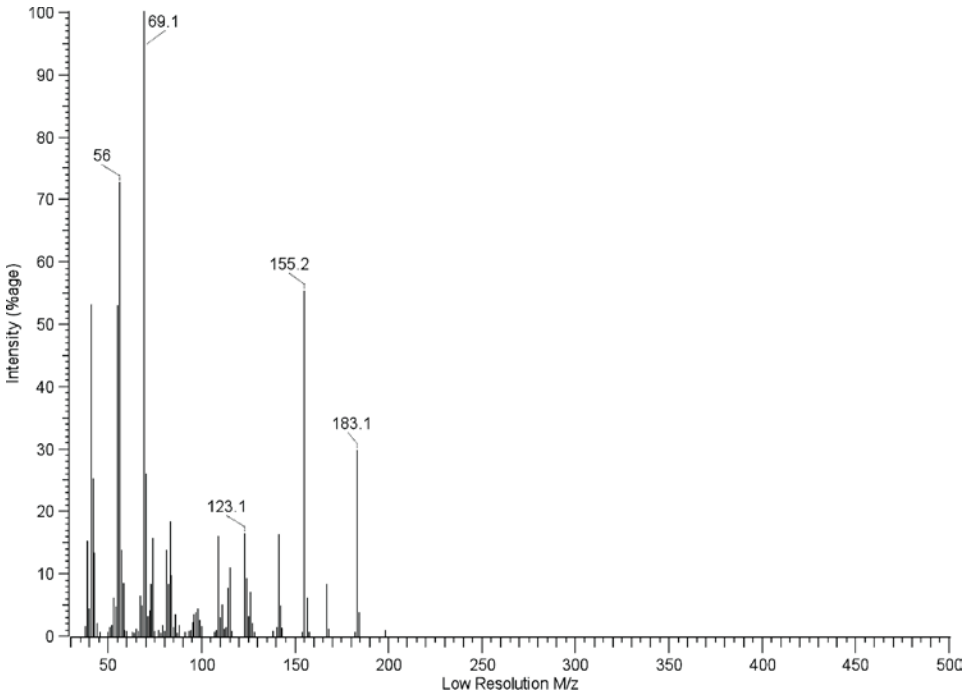


**Figure 3.4b.** Electron impact mass spectrum (EI–MS) of the TMP-$CD_2CN$ fraction from the gas chromatogram shown in Figure 3.3.

Reactions of $[Re^{V}(O)(cat)_2]^-$ with $TEMPO^{\bullet}$ in ethanol, tetrahydrofuran, or $CH_2Cl_2$ all gave clean and quantitative conversion to $[Re^{VII}(O)_2(cat)_2]^-$, as evidenced by $^1H$ NMR and UV–vis spectroscopy. All of the reactions contained TMP-H as the major $TEMPO^{\bullet}$-derived organic product (65–100%), with minor species apparently arising from radical decomposition of the solvent. Clean conversion of $[Re^{V}(O)(cat)_2]^-$ to $[Re^{VII}(O)_2(cat)_2]^-$ was similarly achieved in stoichiometric reactions with the stable di-*tert*-butylnitroxyl and *tert*-amyl-*tert*-butylnitroxyl radicals. For both, a complex mixture of amine–containing organic products was observed in neat $CH_3CN$ solutions, but reactions performed in the presence of excess DHA (10-15 equiv) gave only the expected $R_2N$–H products by GC–MS.

Structural homologues of $[Re^{V}(O)(cat)_2]^-$ were prepared by both new and previously reported methods. As detailed elsewhere,[16] $[Re^{V}(O)(OPPh_3)(Br_4cat)_2]^-$ and $[Re^{V}(O)(PPh_3)(ox)_2]^-$ ($[Br_4cat]^{2-}$ = tetrabromo-1,2-catecholate; $[ox]^{2-}$ = ethanedioate, $C_2O_4^{2-}$) have labile $OPPh_3$ and $PPh_3$ ligands, which make them precursors to the corresponding five coordinate oxorhenium(V) fragments. Square-pyramidal $(Et_4N)[Re(O)(3,5\text{-}^tBu_2cat)_2]$ ($[3,5\text{-}^tBu_2cat]^{2-}$=3,5-di-*tert*-butylcatecholate; Figure 3.5 and Table 3.3) was obtained in high yield by adaptation of a procedure for the preparation of closely related species.[16,18]

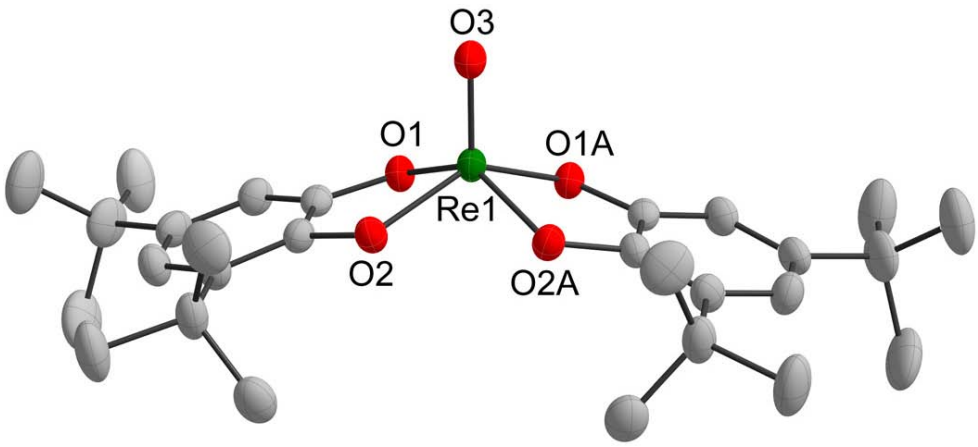


**Figure 3.5.** Solid–state structure of the anion in $(Et_4N)[Re^{V}(O)(3,5\text{-}^{t}Bu_2cat)_2]$ shown with 50% probability ellipsoids. Hydrogen atoms and countercation omitted for clarity. Selected bond lengths (Å) and angles (deg): Re1–O1 1.964(4), Re1–O2 1.968(4), Re1–O3 1.676(6), O1–Re1–O2 80.66(17), O1–Re1–O1A 85.1(2), O2–Re1–O2A 85.3(2), O1–Re1–O3 109.6(2), O2–Re1–O3 111.5(2).

The addition of 1 equiv of TEMPO$^{\bullet}$ to $CH_3CN$ solutions containing the redox-active ligand complex $[Re^{V}(O)(3,5\text{-}^{t}Bu_2\text{-}cat)_2]^{-}$ or $[Re^{V}(O)(OPPh_3)(Br_4cat)_2]^{-}$ affords clean and quantitative conversion to the corresponding dioxorhenium(VII) products. In contrast, GC-MS analysis of $CH_3CN$ solutions containing $[Re^{V}(O)(PPh_3)(ox)_2]^{-}$ and 1-3 equiv of TEMPO$^{\bullet}$ shows no TMP-H or TMP-$CH_2CN$ over 3 days at 25 $^{o}$C and <5% TMP-H after 42 h at 70 $^{o}$C. Oxidation of $[Re^{V}(O)(PPh_3)(ox)_2]^{-}$ by strong oxygen atom donors, including pyridine N–oxide, leads to rapid decomposition to $[ReO_4]^{-}$,[16] so the stability of TEMPO$^{\bullet}$ in $[Re^{V}(O)(PPh_3)(ox)_2]^{-}$ solutions implies that the $[Re^{V}(O)(ox)_2]^{-}$ core does not abstract an oxygen atom from TEMPO$^{\bullet}$.

The reaction of $[Re^{V}(O)(cat)_2]^{-}$ with TEMPO$^{\bullet}$ in a dilute $CH_3CN$ solution is sufficiently slow to permit monitoring by UV–vis absorption spectroscopy. Under pseudo-first-order conditions ($[Re^{V}]$=0.15mM; [TEMPO$^{\bullet}$]=1.5-6.0mM), the concentration-time data are clearly biphasic, indicating that an intermediate species accumulates during the reaction (Figures 3.6 and 3.7 and 3.8). Global iterative analysis of the full spectral window using an A → B → C integrated rate law model yields good first-order fits to both

the growth and decay phases of the reaction, with two exponential equations corresponding to consecutive first-order processes. The reactions performed with varied concentrations of $[Re^{V}(O)(cat)_2]^-$ and TEMPO$^\bullet$ indicate that the first phase of the reaction is first-order with respect to both reactants; the rate constant for the second reaction phase shows a zero order dependence on the TEMPO$^\bullet$ concentration (Figure 3.9 and Table 3.1 and Table 3.2). The reactions of TEMPO$^\bullet$ with $[Re^{V}(O)(3,5\text{-}^{t}Bu_2cat)_2]^-$ are also biphasic (Figure 3.10), but analogous reactions with $[Re^{V}(O)(OPPh_3)(Br_4cat)_2]^-$ are instead fit best by an A → B → C → D rate law model (Figure 3.11). The generation of $[Re^{VII}(O)_2(Br_4cat)_2]^-$ in the C→ D phase occurs very slowly, but formation of the immediate precursor occurs in two phases with distinct rates (Table 3.1 and Table 3.2).

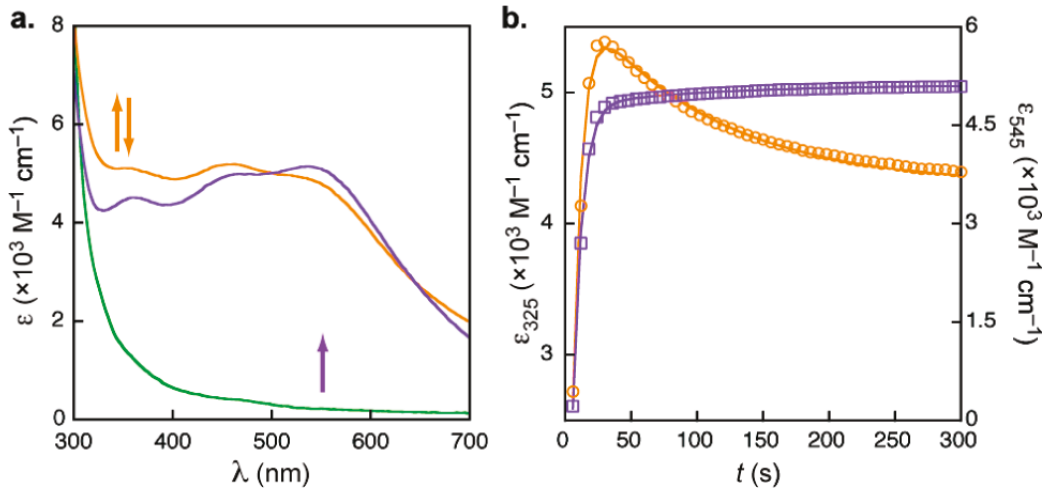


**Figure 3.6.** UV–vis absorption data for a reaction of 0.14 mM $[Re^{V}(O)(cat)_2]^-$ with 1.5 mM TEMPO$^\bullet$ at 25 °C in $CH_3CN$ to generate $[Re^{VII}(O)_2(cat)_2]^-$. (**a**) Spectra at t=0 (green line), t=30 s (orange line), and t=720 s (purple line). (**b**) Time–resolved data at 325 nm (orange ○) and 545 nm (purple □). The fits (orange and purple lines) were obtained simultaneously from iterative analysis of the full spectral window (300–700 nm) using a biexponential A → B → C integrated rate law model, giving the rate constants shown in Table 1.

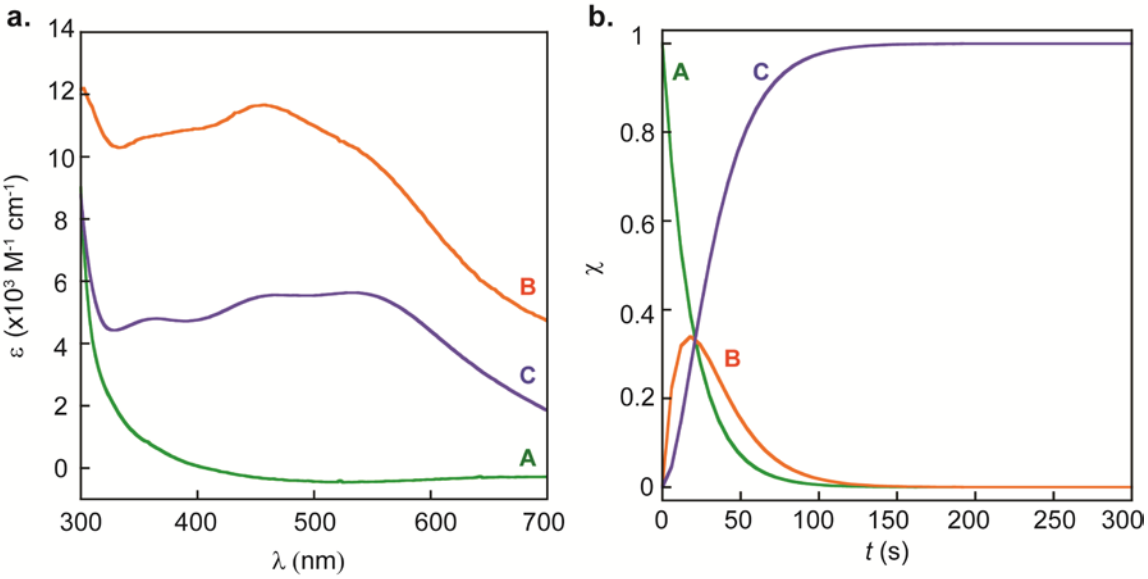


**Figure 3.7.** Computed UV–vis absorption data obtained from iterative global analysis of a reaction of 0.14 mM $[Re^{V}(O)(cat)_2]^-$ with 1.5 mM TEMPO$^\bullet$ at 25 °C in $CH_3CN$ using a biexponential A → B → C integrated rate law model. **(a)** Simulated spectra for A (green line), B (orange line), and C (purple line). **(b)** Calculated mole fraction of A (green line), B (orange line), and C (purple line) as a function of reaction time.

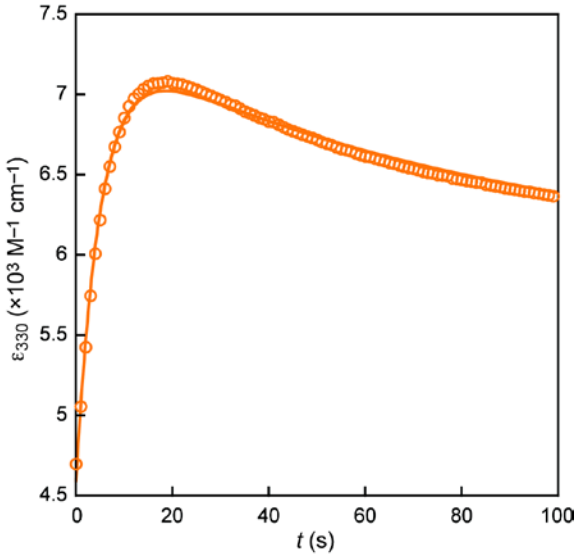


**Figure 3.8.** Time resolved UV–vis absorption data collected at 330 nm (orange ○) for a reaction of 0.14 mM $[Re^{V}(O)(cat)_2]^-$ with 1.5 mM TEMPO$^\bullet$ at 25 °C in $CH_3CN$. The fit to the data (orange line) was obtained from iterative analysis using a biexponential A → B → C integrated rate law model, giving $k_1$ = 0.20 ± 0.04 $s^{-1}$ and $k_2$ = (1.2 ± 0.2) x $10^{-2}$ $s^{-1}$.

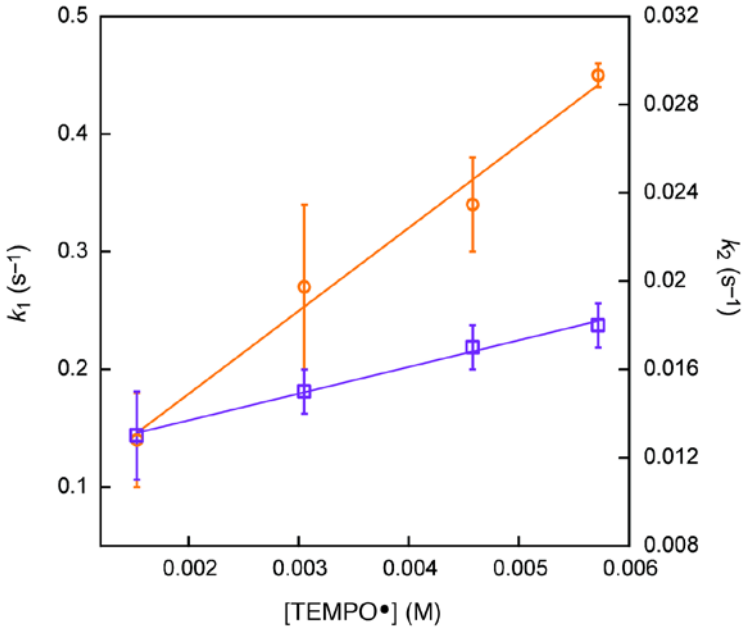


**Figure 3.9.** Plot of $k_1$ (orange ○) and $k_2$ (purple □) as a function of [TEMPO•] for reactions with 0.14 mM $[Re^{V}(O)(cat)_2]^-$ to generate $[Re^{VII}(O)_2(cat)_2]^-$ in $CH_3CN$ at 25 °C. The first–order rate constants $k_1$ and $k_2$ were obtained from iterative fitting to a biexponential A → B → C integrated rate law model, as described in Table 3.2.

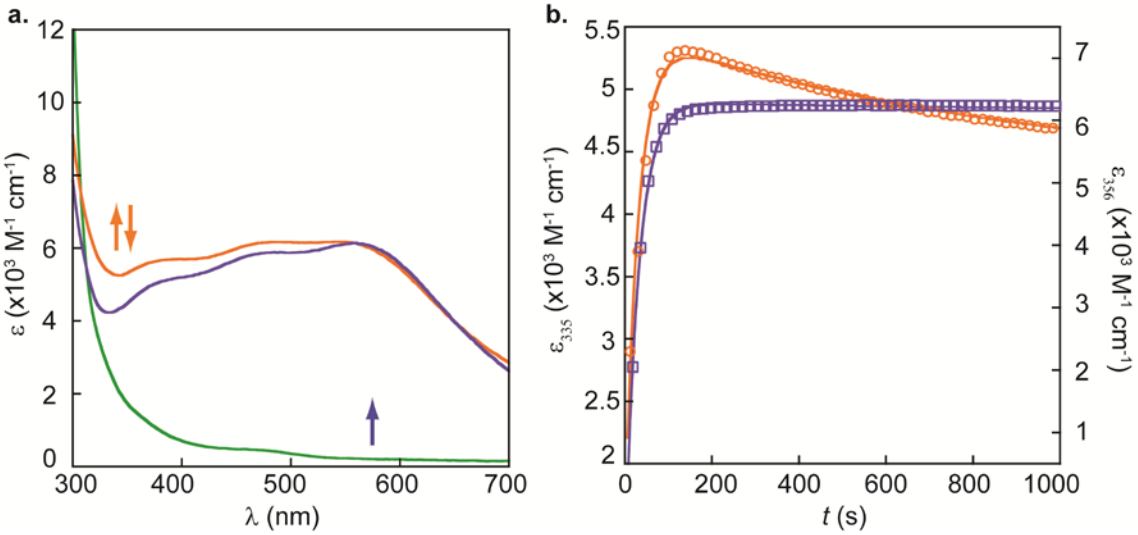


**Figure 3.10.** Selected UV–vis absorption data for a reaction of 0.14 mM $[Re^{V}(O)(3,5\text{-}{}^{t}Bu_2cat)_2]^-$ with 1.6 mM TEMPO• at 25 °C in $CH_3CN$ to generate $[Re^{VII}(O)_2(3,5\text{-}{}^{t}Bu_2cat)_2]^-$ **(a)** Spectra at $t$ = 0 (green line), $t$ = 138 s (orange line), and $t$ = 7260 s (purple line). **(b)** Time-resolved data at 335 nm (orange ○) and 560 nm (purple □). The fits (orange and purple lines) were obtained simultaneously from iterative analysis of the full spectral window (300–700 nm) using a biexponential A→ B → C integrated rate law model, giving $k_1 = (3.3 \pm 0.1) \times 10^{-2}$ s$^{-1}$ and $k_2 = (9 \pm 4) \times 10^{-4}$ s$^{-1}$.

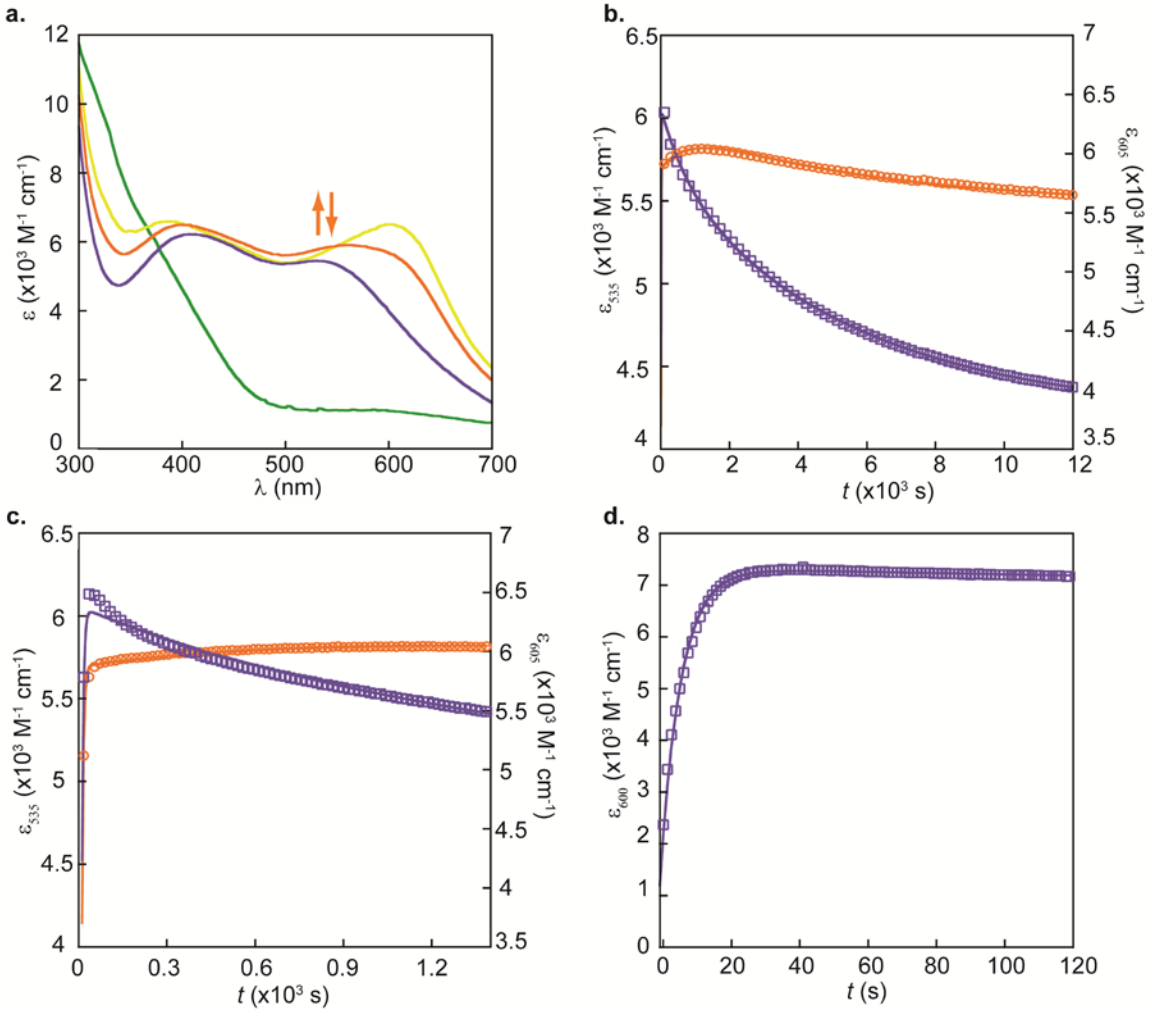


**Figure 3.11.** UV–vis absorption data for reactions of 0.14 mM $[Re^{V}(O)(Br_4cat)_2]^-$ with 1.5 mM TEMPO$^\bullet$ at 25 °C in $CH_3CN$ to generate $[Re^{VII}(O)_2(Br_4cat)_2]^-$. In each experiment, data were collected for at least 300 min, and the data between $t$ = 0 and $t$ = 300 min were used for kinetics analyses. **(a)** Spectra at $t$ = 0 (green line), $t$ = 48 s (yellow line), $t$ = 1,074 s (orange line), and $t$ = 22,110 s (purple line). **(b–c)** Time–resolved data at 535 nm (orange ○) and 605 nm (purple □). The fits (orange and purple lines) were obtained simultaneously from iterative analysis of the full spectral window (300–700 nm) using an A → B → C → D integrated rate law model. **(d)** Time–resolved data at 600 nm (purple □). The fit (purple lines) was obtained iterative analysis of the concentration–time data between $t$ = 0 and $t$ = 300 min using an A → B → C → D integrated rate law model. In total, the fits give $k_{1a}$ = 0.16 ± 0.03 $s^{-1}$, $k_{1b}$ = (1.2 ± 0.6) x $10^{-3}$ $s^{-1}$ and $k_2$ = (1.7 ± 0.5) x $10^{-4}$ $s^{-1}$.

**Table 3.1.** Rate Constants for TEMPO• Oxidations of Oxorhenium(V)[a]

| | $k_1$ ($s^{-1}$) | $k_2$ ($s^{-1}$) |
|---|---|---|
| $[Re^{V}(O)(cat)_2]^{-}$ [b] | 0.14 ± 0.04 | (1.3 ± 0.2) x $10^{-2}$ |
| $[Re^{V}(O)(3,5\text{-}^{t}Bu_2cat)_2]^{-}$ [b] | 0.033 ± 0.001 | (9 ± 2) x $10^{-4}$ |
| $[Re^{V}(O)(OPPh_3)(Br_4cat)_2]^{-}$ [c] | 0.16 ± 0.03, (1.2 ± 0.6) x $10^{-3}$ | (1.7 ± 0.5) x $10^{-4}$ |

[a]All reactions performed in $CH_3CN$ at 25 °C with $[Re^{V}]$=0.14mM and [TEMPO•]=1.5mM. [b]Fit to a biexponential A → B → C integrated rate law model. [c]Fit to an A → B → C → D rate law model. The two values of $k_1$ are the successive rate constants for formation of the immediate precursor to $[Re^{VII}(O)_2(Br_4cat)_2]^{-}$, so $k_2$ corresponds to product formation.

### 3.3 Discussion

The two amine products from the reaction with TEMPO• derive from the same piperidyl radical (TMP•) intermediate. TMP-$CH_2CN$ was previously reported from the electrochemical oxidation of TMP-H in $CH_3CN$ and was proposed to arise from the trapping of TMP• by •$CH_2CN$ (generated in situ by the net abstraction of H• from $CH_3CN$).[17-21] Assuming that radical combination is rapid compared to H• abstraction from $CH_3CN$,[20,21] the consumption of 2 equiv of TEMPO to generate 1 equiv of TMP-$CH_2CN$ and 1 equiv of TMP-H is a balanced reaction. The excess of the TMP-H product in our reactions may implicate some reaction with adventitious sources of H•.

In total, the data suggest that $[Re^{V}(O)(cat)_2]^{-}$ efficiently abstracts an oxygen atom from nitroxyl radicals to afford $[Re^{VII}(O)_2(cat)_2]^{-}$ and aminyl radical transients (Scheme 3.1). The reaction is a $2e^{-}$ oxygen atom transfer that is reminiscent of oxo transfer from amine N–oxides.[16] However, this is apparently a very unusual reaction for nitroxyl radicals, such as TEMPO•,[22-24] which are more typically $1e^{-}$ redox reagents. Because related radical Re–O bond-forming reactions proceed with the initial $1e^{-}$ oxidation of a redox-active ligand,[16] we hypothesized that this reaction may be similarly sensitive to substitution of the redox-active ligand.

We previously noted that $[Re^{VII}(O)_2(cat)_2]^-$ decomposes $[Re^{V}(O)(PPh_3)(ox)_2]^-$ by apparent oxo transfer to the $[Re^{V}(O)(ox)_2]^-$ fragment (Scheme 3.2a).[16] Because $[Re^{VII}(O)_2(cat)_2]^-$ is itself generated in reactions with TEMPO$^\bullet$ (Scheme 3.2b), $[Re^{V}(O)(cat)_2]^-$ mediates net oxo–group transfer from TEMPO$^\bullet$ to $[Re^{V}(O)(ox)_2]^-$, implying that the reaction thermodynamics are not prohibitive. The inability of $[Re^{V}(O)(PPh_3)(ox)_2]^-$ to directly deoxygenate TEMPO$^\bullet$ must then arise from a kinetic impediment.

**Scheme 3.2.**

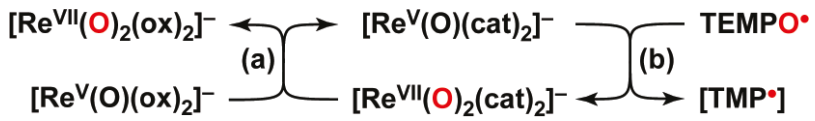


We tentatively rationalize these experimental observations by the two-step mechanism shown in Scheme 3.3. In the first reaction step, the observed first-order dependence on both reactants is consistent with the initial attack of 1 equiv of TEMPO$^\bullet$ on 1 equiv of $[Re^{V}(O)(cat)_2]^-$. The most common mode of TEMPO$^\bullet$ complexation to redox-active metal ions involves reduction to the closed-shell $[TEMPO]^-$ anion with concomitant $1e^-$ oxidation of the metal.[25- 31] In $[Re^{V}(O)(cat)_2]^-$, this $1e^-$ could derive from either the metal center or a redox-active $[cat]^{2-}$ ligand.

In attempts to isolate and further characterize the intermediate, oxyl radical sources with stronger O–R bonds and EPR spectroscopy were probed. Addition of the phenoxyl radicals galvinoxyl and 2,4,6-tri-*tert*-butylphenoxyl to solutions of $[Re^{V}(O)(cat)_2]^-$ show no reaction over days at ambient temperature. Attempts to observe a radical intermediate via EPR were also unsuccessful. Addition of 1 atm nitric oxide to

MeCN solutions of $[Re^{V}(O)(cat)_2]^{-}$ rapidly produced a dark blue/violet solution indicative of $[Re(O)_2(ap^{Ph})_2]^{-}$. Analysis of the reaction mixture by UV–vis, $^{1}H$ NMR, and MALDI–MS show a complex mixture of products. Identification of these products is ongoing, but preliminary MALDI–MS shows evidence of $[Re(O)_2(ap^{Ph})_2]^{-}$ with a peak at m/z 809 and a NO adduct with a peak at m/z 824 [M+NO+H]. This supports the radical reactivity described above, but structural characterization of the intermediate has remained elusive, so the locus of oxidation is not known.

However, $d^1$ oxorhenium(VI) complexes are comparatively rare compared to $d^0$ and $d^2$ analogues.[5] Also, computational studies of $O_2$ activation at $[Re^{V}(O)(cat)_2]^{-}$ clearly implicate ligand–centered redox in radical Re–O bond formation.[16] By analogy, we propose this nitroxyl–binding step: (1) is accompanied by the isomerization of trans-$[Re^{V}(O)(cat)_2]^{-}$ to the cis conformer; (2) occurs with oxidation of a redox–active $[cat]^{2-}$ ligand to give a semiquinonate $[sq^{\bullet}]^{-}$ free-radical intermediate. The reaction is completed by a second oxidation of the oxorhenium fragment, which homolyzes the nitroxyl-derived N–O bond. The dioxo product is $d^0$, implying that this second $1e^{-}$ step occurs with intramolecular reduction of the coordinated semiquinonate radical $[sq^{\bullet}]^{-}$ ligands. An alternative mechanism of initial outer-sphere electron transfer can be ruled out. $[Re^{V}(O)(cat)_2]^{-}$ is not a strong outer-sphere reductant; quasi-reversible oxidation of $[Re^{V}(O)(cat)_2]^{-}$ occurs at *ca.* +0.04 V versus $Fc^{+}/Fc$ in $CH_3CN$. $TEMPO^{\bullet}$ is reduced at –1.48 V versus SHE in $H_2O$. [32]

**Scheme 3.3.**

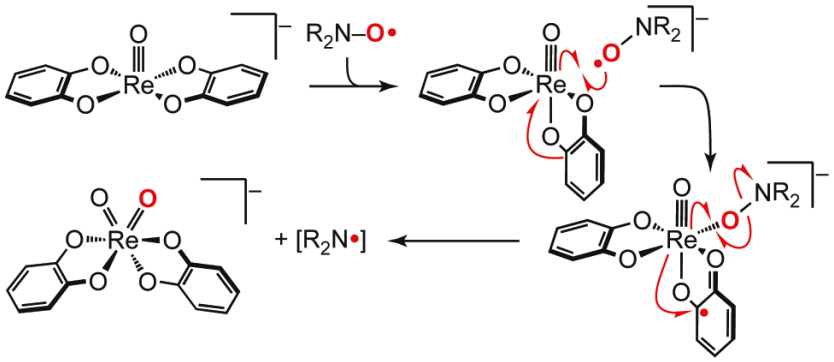


The trends in the reaction rates (Table 3.1) do not cleanly parallel the oxidation potentials of the redox–active ligands ($[3,5\text{-}^{t}Bu_2cat]^{2-}$ > $[cat]^{2-}$ > $[Br_4cat]^{2-}$).[33] The comparatively slow TEMPO• deoxygenation by $[Re^{V}(O)(3,5\text{-}^{t}Bu_2cat)_2]^{-}$ versus $[Re^{V}(O)(cat)_2]^{-}$ is surprising and suggests that steric hindrance by the *tert*-butyl groups may inhibit equilibrium formation of the $[TEMPO]^{-}$ complex intermediate. The very slow rate of $[Re^{VII}(O)_2(Br_4cat)_2]^{-}$ formation is consistent with the proposed mechanism, but generation of the precursor complex is more complex. The very fast A → B phase may reflect the enhanced Lewis acidity of the $[Re^{V}(O)(Br_4cat)_2]^{-}$ core.[16,34,35] In the context of this proposed mechanism, we attribute the kinetic inertness of $[Re^{V}(O)(ox)_2]^{-}$ toward TEMPO• to its reluctance to undergo $1e^{-}$ transfer. Binding $R_2N–O^{\bullet}$ to $[Re^{V}(O)(ox)_2]^{-}$ would require metal-centered $1e^{-}$ oxidation because the $[ox]^{2-}$ ligands are not redox-active.

To further validate our claim that redox-active ligands are essential to overcome the kinetic factors in the presented reaction we sought out to test the ability of a complex that is known to make strong M=O bonds, >167 kcal/mol, to react with TEMPO•. Studies of $WCl_2(PMe_3)_4$ have shown it to be a potent oxygen atom acceptor, forming oxo complexes upon reaction with $CO_2$ and phosphine oxides.[36] Reactions of $WCl_2(PMe_3)_4$

with TEMPO$^{\bullet}$ in $C_6D_6$ showed minimal to no reactivity, by $^1$H NMR, over days at ambient temperature. While $WCl_2(PMe_3)_4$ is known to react slowly with O atom donors, oxygen atom transfer from pyridine N–oxide showed conversion to $WOCl_2(PMe_3)_3$ and pyridine in ~90% and 100% yield respectively over hours under identical conditions as evidenced by the $^1$H NMR. Analysis of the NMR samples by UV–visible spectroscopy showed a max yield of 100% and 30% for reaction with pyridine N–oxide and TEMPO$^{\bullet}$ respectively when compared to an isolated sample of $WOCl_2(PMe_3)_3$. This provides an upper limit of reaction progress assuming $WOCl_2(PMe_3)_3$ is the only species contributing to the spectra. The strong O atom acceptor failed to deoxygenate TEMPO$^{\bullet}$ in any significant amount. The divergent reactivity with TEMPO$^{\bullet}$ arise from kinetic factors and should not be a result of differences in the thermodynamic affinity of the complexes for an O atom.

### 3.4 Conclusion

In summary, $[Re^{V}(O)(cat)_2]^-$ and its analogues exhibit a remarkable ability to deoxygenate nitroxyl radicals, which may be a function of their capacity to undergo both ligand–centered $1e^-$ and metal–centered $2e^-$ redox reactions. Metal ions that bind TEMPO$^{\bullet}$ as $[TEMPO]^-$ often cannot undergo further $1e^-$ oxidation (e.g., $Ti^{III}$),[25-27] or they have high d–electron counts that disfavor terminal oxo formation.[28-31] In contrast, most oxorhenium(V) complexes that mediate $2e^-$ oxo transfer do not undergo $1e^-$ transfer.[4,5] Ongoing efforts in our laboratory are utilizing the ability of redox-active ligands to orthogonalize $1e^-$ and $2e^-$ redox reactions for redox selectivity in other reactions with small molecules.

## 3.5 Experimental Details and Supplementary Material

### 3.5.1 General Considerations.

Unless otherwise noted, all manipulations were performed under anaerobic conditions using standard vacuum line techniques, or in an inert atmosphere glove box under purified nitrogen. NMR spectra were acquired on a Varian Mercury 300 spectrometer (300.323 MHz for $^{1}H$; 75.5 MHz for $^{13}C$) or a Varian Mercury 400 spectrometer (161.9 MHz for $^{31}P$) at ambient temperatures. All chemical shifts are reported in parts per million (ppm) relative to TMS, with the residual solvent peak serving as an internal reference. UV–visible absorption spectra were acquired using a Varian Cary 50 spectrophotometer equipped with a water jacketed cell holder fitted to a Peltier temperature controller. Unless otherwise specified, all electronic absorption spectra were recorded at 25 °C in 1 cm quartz cells. UV–vis chemical kinetics data were fit by iterative multivariate analysis using the commercially available software Specfit/32 from Spectrum Software Associates. All mass spectra were recorded in the Georgia Institute of Technology Bioanalytical Mass Spectrometry Facility. GC–MS was performed on GC–HP5890 using a J&W–DB–5 column (30 m x 0.25 mm) equipped with a VG instruments model 70–SE electron impact mass spectrometer. Cyclic voltammetric measurements were made using a CH Instruments CHI620C potentiostat in a three component cell consisting of a platinum disk working electrode, a platinum wire auxiliary electrode, and a non-aqueous $AgNO_3/Ag$ reference electrode. All electrochemical experiments were performed in $CH_3CN$ with 0.1 M $[^{n}Bu_4N][PF_6]$ as the supporting electrolyte. Electrochemical data are referenced and reported to $Fc^{+}/Fc$ as an internal standard. Elemental analyses were performed by Atlantic Microlab, Inc., Norcross, GA. All analyses were performed in duplicate, and the reported compositions are the average of the two runs.

### 3.5.2 Methods and Materials.

Anhydrous acetonitrile ($CH_3CN$), dichloromethane ($CH_2Cl_2$) and tetrahydrofuran (THF) solvents for air- and moisture-sensitive manipulations were purchased from Sigma-Aldrich and further dried by passage through columns of activated alumina, degassed by at least three freeze-pump-thaw cycles, and stored under $N_2$ prior to use. Acetone (99.8%, extra dry) was purchased from Acros. Ethanol (anhydrous, 200 proof, 99.5%) and diethyl ether (anhydrous, ACS reagent, >99.0%) were purchased from Sigma-Aldrich. All were used as received. Deuterated acetonitrile ($CD_3CN$), benzene-*d*6 ($C_6D_6$), and dicholoromethane ($CD_2Cl_2$), were purchased from Cambridge Isotope Laboratories, degassed by three freeze-pump-thaw cycles, vacuum distilled from $CaH_2$, and stored under a dry $N_2$ atmosphere prior to use. Acetone–*d*6 was used as received from Cambridge Isotope Laboratories. $Re^{V}(O)(PPh_3)_2Cl_3$,[37] $(Et_4N)[Re^{V}(O)(cat)_2]$,[38] $(Et_4N)[Re^{VII}(O)_2(cat)_2]$,[38] $(Et_4N)[Re^{V}(O)(OPPh_3)(Br_4cat)_2]$,[39] $(Et_4N)[Re^{V}(O)(PPh_3)(ox)_2]$,[16] were prepared by literature methods. All characterization data matched those referenced. All other reagents were purchased from Sigma-Aldrich and used as received.

### 3.5.3 Synthesis of $(Et_4N)[Re^{V}(O)(3,5\text{-}^{t}Bu_2cat)_2]$.

A 50 mL flask with a Kontes brand high vacuum PTFE valve was charged with $Re^{V}(O)(PPh_3)_2Cl_3$ (0.116 g, 0.140 mmol), $Et_4NCl$ (0.115 g, 0.889 mmol), 3,5-di-*tert*-butylcatechol ($3,5\text{-}^{t}Bu_2catH_2$) (0.071 g, 0.32 mmol) and MeOH (15 mL). $Et_3N$ (90 µL, 0.65 mmol) was slowly added with vigorous stirring to afford a green suspension. The flask was sealed and immersed in a silicone fluid bath at 35 °C for 6 h to yield a clear green solution. The mixture was cooled to room temperature to precipitate finely divided green solids, which were collected by vacuum filtration under $N_2$. The solids were purified by precipitation from acetone with diethyl ether to afford $(Et_4N)[Re^{V}(O)(3,5\text{-}^{t}Bu_2cat)_2]$ (0.094 g, 0.121 mmol, 87%) as tan–colored crystals suitable for analysis by X-ray diffraction.

UV–vis (MeCN) $\gamma_{max}$, nm ($\varepsilon$, $M^{-1}$ $cm^{-1}$): 295 (12,500), 475 (sh). The solid state structure of $(Et_4N)[Re^{V}(O)(3,5\text{-}^{t}Bu_2cat)_2]$ contains only one $C_s$ symmetric isomer, but the $^1$H NMR solution spectrum of the same material contains two isomers in an approx. 2:1 ratio, suggesting that a $C_2$–symmetry isomer is also present in solution. They are here arbitrarily assigned as isomer A and isomer B. The peak areas indicated below are normalized to one $[Et_4N]^+$, so the sum of the aryl and *tert*–butyl proton integrals are 4 and 36, respectively. $^1$H NMR (300 MHz, $CD_3CN$, δ): 7.03 (d, J = 2.1 Hz, Ar*H*, isomer A, 1.33H); 7.01 (d, J = 2.2 Hz, Ar*H*, isomer B, 0.66H,); 6.7 (d, J = 2.1 Hz, Ar*H*, isomers A + B, 2H); 3.39 (q, J = 7.2, $(CH_3\mathit{CH}_2)_4N^+$, 8H); 1.44 (s, $^{t}$Bu, isomer B, 6H); 1.43 (s, $^{t}$Bu, isomer A, 12H); 1.30 (s, $^{t}$Bu, 12H, isomer A); 1.29 (s, $^{t}$Bu, isomer B, 6H); 1.15 (tt, J = 7.2, J = 1.9, $(C\mathit{H}_3CH_2)_4N^+$, 12H). Anal. Calcd for $C_{36}H_{50}NO_5Re$: C, 55.93; H, 7.82; N, 1.81; Found: C, 55.99; H, 7.93; N, 1.94.

### 3.5.4 Reactions of Oxorhenium(V) Complexes with Nitroxyl Radicals. Stoichiometric Reactions.

In a representative procedure, a 5 dram scintillation vial was charged with $(Et_4N)[Re^{V}(O)(cat)_2]$ (8.0 mg, 0.015 mmol) and $CH_3CN$ (2-3 mL) was added to afford a clear, light brown solution. Slow addition of a freshly prepared solution of 0.56 M 2,2,6,6-tetramethylpiperidine-1-oxyl (TEMPO$^{\bullet}$) in $CH_3CN$ (27 µL, 0.015 mmol) with vigorous stirring gave an immediate color change to dark purple. The reaction mixture was fitted with a Teflon lined cap and stirred for 24 h under $N_2$. For GC–MS analysis, an aliquot was transferred to a 1 dram scintillation vial, sealed under $N_2$, and injected directly into the gas chromatograph. For NMR analysis, the same reactants were combined in a J. Young brand NMR tube with a Teflon screw cap, using $CD_3CN$ as the solvent. At NMR concentrations (*ca.* 13 mM), integration of the $^1$H NMR resonances for $[Re^{VII}(O)_2(cat)_2]^-$ and the TEMPO$^{\bullet}$-derived products confirms that the reaction is complete on acquisition of the first spectrum (<10 min), so no time-dependent measurements were made by this

method. **Kinetics Studies.** In a representative procedure, a 1.0 cm quartz cuvette with a PTFE screw cap containing a septum top was charged with 0.15 mM $[Re^{V}(O)(cat)2]^{-}$ (2.0 mL, 3.0 x $10^{-7}$ mol) in $CH_3CN$ and sealed under $N_2$. The cuvette was placed in a Peltier UV–vis cell holder with a magnetic stirrer. A freshly prepared solution of 0.025 M $TEMPO^{\bullet}$ in $CH_3CN$ (130 µL, 3.2 x $10^{-6}$ mol) was quickly introduced into the cuvette via a gas tight syringe with vigorous stirring to make the $[TEMPO^{\bullet}]$ = 1.5 mM and $[Re^{V}]$ = 0.14 mM. The reaction progress was monitored by UV–vis spectroscopy (300–700 nm) for 15 min at 6 s intervals.

### 3.5.5 Reactions of $W^{II}Cl_2(PMe_3)_4$ with $TEMPO^{\bullet}$.

In a representative procedure a 5 dram scintillation vial was charged with $WCl_2(PMe_3)_4$ (70.0mg, 0.1452mmol) and dissolved in 3 mL of $C_6D_6$ with 1.5 µL of hexamethyldisiloxane added as an internal standard. The stock solution was transferred to a J–Young NMR tube (750 µL, 3.63 x $10^{-5}$ mol). $TEMPO^{\bullet}$ (6.5mg, 4.1 x $10^{-5}$ mol) dissolved in $C_6D_6$ (250 µL) was added. The reaction progress was monitored by $^{1}H$ NMR spectroscopy.

**Table 3.2.** Rate Constants for Reactions of Oxorhenium(V) Complexes with TEMPO$^{\bullet}$ Obtained by Iterative Fitting to a Biexponential A → B → C Integrated Rate Law Model.[a]

| | [$Re^{V}$] (mM) | [TEMPO$^{\bullet}$] (mM) | $k_1$ ($s^{-1}$) | $k_2$ ($s^{-1}$) |
|---|---|---|---|---|
| $[Re^{V}(O)(cat)_2]^-$ | 0.072 | 1.5 | 0.16 ± 0.04[b] | 0.017 ± 0.008 |
| | 0.14 | 1.5 | 0.14 ± 0.04[c] | 0.013 ± 0.002 |
| | | 3.0 | 0.27 ± 0.07[d] | 0.015 ± 0.001 |
| | | 4.6 | 0.34 ± 0.04[d] | 0.017 ± 0.001 |
| | | 5.7 | 0.45 ± 0.01[e] | 0.018 ± 0.001 |
| $[Re^{V}(O)(3,5\text{-}^{t}Bu_2cat)_2]^-$ | 0.14 | 1.6 | 0.033 ± 0.001[f] | (9 ± 2) x $10^{-4}$ |
| $[Re^{V}(O)(Br_4cat)_2]^-$ | 0.14 | 1.5 | 0.16 ± 0.03[g,h] | (1.7±0.5) x $10^{-4}$ |
| | | | (1.2 ± 0.6) x $10^{-3}$ | |

[a]All reactions performed in $CH_3CN$ at 25 °C. All rate constants and error estimates are the averages and sample standard deviations of ≥2 sets of concentration–time data. [b]From global analysis of the full spectral data acquisition windows (300–700 nm) of three separate kinetics experiments and one single–wavelength fit to data collected at 330 nm. [c]From global analysis of the full spectral data acquisition windows (300–700 nm) of four separate kinetics experiments and one single–wavelength fit to data collected at 330 nm. [d]From global analysis of the full spectral data acquisition window (300–700 nm) of one kinetics experiment and one single–wavelength fit to data collected at 325 nm. [e]From single–wavelength fits to two sets of concentration–time data collected at 325 nm. [f]From global analysis of the full spectral data acquisition window (300–700 nm) of three separate kinetics experiments. [g]From global analysis of the full spectral data acquisition window (300–700 nm) of three separate kinetics experiments and one single–wavelength fit to data collected at 600 nm. [h]The two values of $k_1$ are the two rates constants for formation of the immediate precursor to $[Re^{VII}(O)_2(Br_4cat)_2]^-$, where $k_{1a}$ corresponds to the A → B reaction phase and $k_{1b}$ corresponds to the B → C phase in the A → B → C → D rate law model.

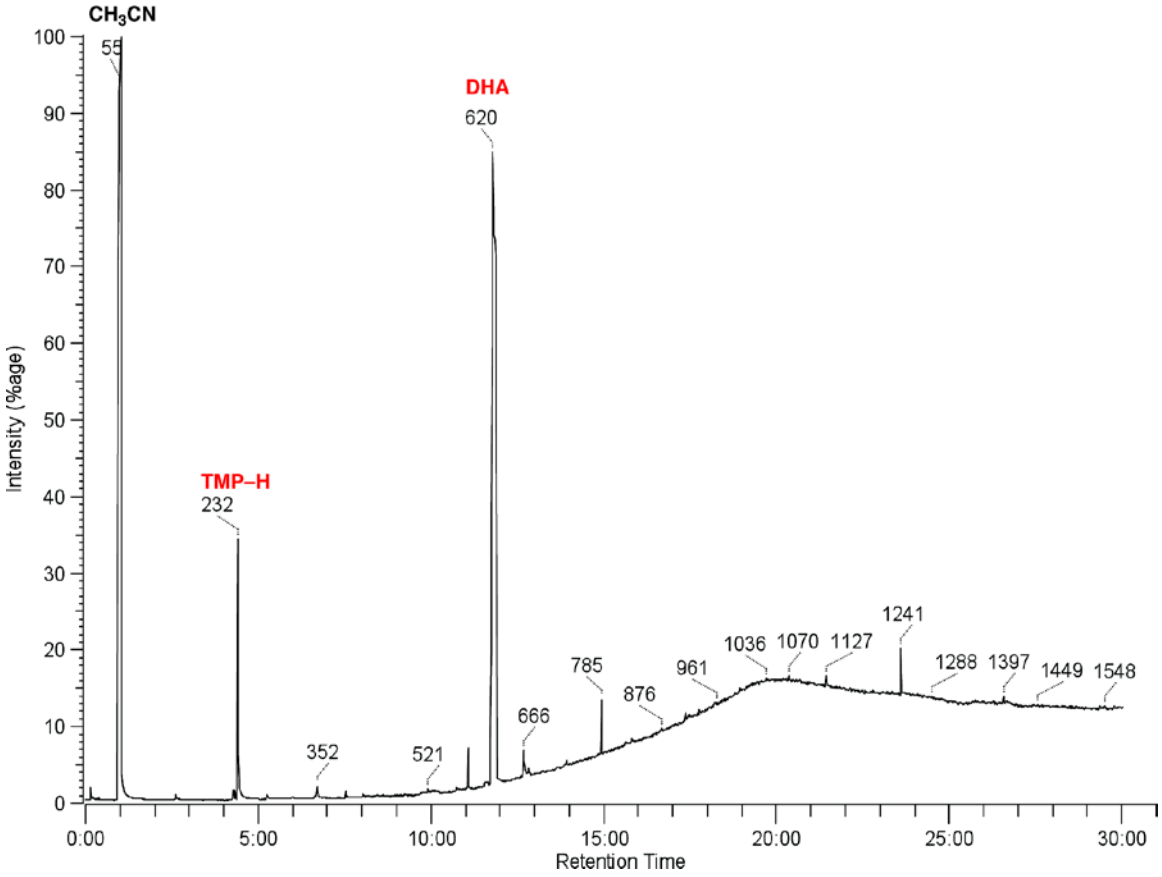


**Figure 3.12.** Gas chromatogram from a reaction of $[Re^{V}(O)(cat)_2]^-$ (0.041 mmol) with TEMPO$^{\bullet}$ (0.040 mmol) performed in $CH_3CN$ containing 9,10-dihydroanthracene (DHA) (0.52 mmol).

**Table 3.3.** Crystallographic Data and Structure Parameters for $[Re^{V}(O)(3,5\text{-}^{t}Bu_2cat)_2]^{-}$.

| Complex | $[Re^{V}(O)(3,5\text{-}^{t}Bu_2cat)_2]^{-}$ |
|---|---|
| Empirical formula | $C_{36}H_{60}NO_5Re$ |
| Formula weight | 773.05 |
| Temperature | 173(2) K |
| Crystal system | Orthorhombic |
| Space group | Pnma |
| Unit cell dimensions | |
| a (Å) | 11.6064(8) Å |
| b (Å) | 30.002(2) Å |
| c (Å) | 10.6924(7) Å |
| α (°) | $90^{o}$ |
| β (°) | $90^{o}$ |
| γ (°) | $90^{o}$ |
| V ($Å^3$) | 3723.2(4) $Å^3$ |
| Z | 4 |
| $D_{calc}$ (g $cm^{-1}$) | 1.379 $Mg/m^3$ |
| Absorption coefficient ($mm^{-1}$) | 3.302 $mm^{-1}$ |
| Crystal size (mm) | 0.55 x 0.03 x 0.03 $mm^3$ |
| θ range for data collection (°) | 1.36 to $26.7^{o}$ |
| Index ranges | $-13 \le h \le 14$ |
| | $-37 \le k \le 33$ |
| | $-13 \le l \le 13$ |
| Reflections collected/unique | 34143 |
| Goodness of fit on $F^2$ | 1.041 |
| R [$I > 2\sigma(I)$] | 0.0494 |
| $wR_2$ (all data) | 0.0972 |

## 3.7 References


[1] Sheldon, R. A.; Kochi, J. K. Metal-Catalyzed Oxidations of Organic Compounds; Academic Press: New York, **1981**.

[2] Comprehensive Organic Synthesis: Selectivity, Strategy and Efficiency in Modern Organic Chemistry, Vol. 7: Oxidation; Trost, B. M., Fleming, I., Eds.; Pergamon: Oxford, U.K., **1991**.

[3] Report of the Basic Energy Sciences Workshop on Solar Energy Utilization; U.S. Department of Energy: Washington, DC, 2005.

[4] Holm, R. H. *Chem. Rev*. **1987**, 87, 1401-1449.

[5] Espenson, J. H. Adv*. Inorg. Chem*. **2003**, 54, 157-202.

[6] Owens, G. S.; Arias, J.; Abu-Omar, M. M. *Catal. Today* **2000**, 55, 317-363.

[7] Herrmann, W. A.; Kuhn, F. E. *Acc. Chem. Res*. **1997**, 30, 169-180.

[8] Blackmore, K. J.; Ziller, J. W.; Heyduk, A. F*. Inorg. Chem*. **2005**, 44, 5559-5561.

[9] Haneline, M. R.; Heyduk, A. F. *J. Am. Chem. Soc.* **2006**, 128, 8410-8411.

[10] Zarkesh, R. A.; Ziller, J.W.; Heyduk, A. F*. Angew. Chem., Int. Ed*. **2008**, 47, 4715-4718.

[11] Bart, S. C.; Lobkovsky, E.; Bill, E.; Chirik, P. J. *J. Am. Chem. Soc.* **2006**, 128, 5302-5303.

[12] Bouwkamp, M.W.; Bowman, A. C.; Lobkovsky, E.; Chirik, P. J. *J. Am. Chem. Soc*. **2006**, 128, 13340-13341.

[13] Stanciu, C.; Jones, M. E.; Fanwick, P. E.; Abu-Omar, M. M. *J. Am. Chem. Soc*. **2007**, 129, 12400-12401.

[14] Lu, C. C.; Weyhermuller, T.; Bill, E.; Wieghardt, K. *Inorg. Chem*. **2009**, 48, 6055-6064.

[15] Smith, A. L.; Soper, J. D. *Polyhedron* **2010**, 29, 164-169.

[16] Lippert, C. A.; Arnstein, S. A.; Sherrill, C. D.; Soper, J. D. *J. Am. Chem. Soc*. **2010**, 132, 3879-3892.

[17] Ohmori, H.; Ueda, C.; Yamagata, K.; Masui, M.; Sayo, H. *J. Chem. Soc., Perkin. Trans. 2* **1987**, 1065-1069.

[18] Kettler, P. B.; Chang, Y.-D.; Zubieta, J.; Abrams, M. J. *Inorg. Chim. Acta* **1994**, 218, 157-165.

[19] Masui, M.; Yamagata, K.; Ueda, C.; Ohmori, H. *J. Chem. Soc., Chem. Commun*. **1985**, 272-273.

[20] Roberts, B. P. *Chem. Soc. Rev*. **1999**, 28, 25-35.

[21] Tsentalovish, Y. P.; Kulik, L. V.; Gritsan, N. P.; Yurkovskaya, A. V. *J. Phys. Chem. A* **1998**, 102, 7975-7980.

[22] Alper, H. *J. Org. Chem.* **1973**, 38, 1417-1418.

[23] Carloni, P.; Damiani, E.; Iacussi, M.; Greci, L.; Stipa, P.; Cauzi, D.; Rizzoli, C.; Sgarabotto, P. *Tetrahedron* **1995**, 51, 12445-12452.

[24] Lucarini, M.; Marchesi, E.; Pedulli, G. F.; Chatgilialoglu, C. *J. Org. Chem*. **1998**, 63, 1687-1693.

[25] Mahanthappa, M. K.; Huang, K.-W.; Cole, A. P.; Waymouth, R. M. *Chem. Commun.* **2002**, 502-503.

[26] Gazzi, R.; Perazzolo, F.; Sostero, S.; Ferrari, A.; Traverso, O. *J. Organomet. Chem*. **2005**, 690, 2071-2077.

[27] Schröder, K.; Hasse, D.; Saak, W.; Beckhaus, R.; Kretschmer, W. P.; Lützen, A. *Organometallics* **2008**, 27, 1859-1868.

[28] Mindiola, D. J.; Waterman, R.; Jenkins, D. M.; Hillhouse, G. L. *Inorg. Chim. Acta* **2003**, 345, 299-308.

[29] Ito, M.; Matsumoto, T.; Tatsumi, K*. Inorg. Chem*. **2009**, 48, 2215-2223.

[30] Dickman, M. H.; Doedens, R. J. *Inorg. Chem.* **1982**, 21, 682-684.

[31] Jaitner, P.; Huber, W.; Huttner, G.; Scheidsteger, O. *J. Organomet. Chem*. **1983**, 259, C1-C5.

[32] Hodgson, J. L.; Namazian, M.; Bottle, S. E.; Coote, M. L. *J. Phys. Chem. A* **2007**, 111, 13595-13605.

[33] Pascaly, M.; Duda, M.; Schweppe, F.; Zurlinden, K.; M€uller, F. K.; Krebs, B. *J. Chem. Soc., Dalton Trans*. **2001**, 828-837.

[34] Hoffman, B. M.; Eames, T. B*. J. Am. Chem. Soc*. **1969**, 91, 5168-5170.

[35] Cohen, A. H.; Hoffman, B. A. *Inorg. Chem.* **1974**, 13, 1484-1491.

[36] Brock, S. L.; Mayer, J. M. *Inorg. Chem.***1991**, 30, 2138-2143.

[37] Johnson, N. P.; Lock, C. J. L.; Wilkinson, G. *J. Chem. Soc.* **1964**, 1054-66.

[38] Dilworth, J. R.; Ibrahim, S. K.; Khan, S. R.; Hursthouse, M. B.; Karaulov, A. A. *Polyhedron* **1990**, *9*, 1323-9.

[39] Edwards, C. F.; Griffith, W. P.; White, A. J. P.; Williams, D. J. *J. Chem. Soc., Dalton Trans.* **1992**, 957-62.

# CHAPTER 4

# Redox-Active Ligand-Mediated Bond-Forming Reactions at a High-Valent Oxorhenium(V) Center.

## 4.1 INTRODUCTION

Coordination of redox-active ligands to transition metals affords complexes that can have complicated electronic properties owing to the overlap of the metal d-orbitals and the frontier ligand orbitals.[1-19] Assignment of oxidation states in these types of complexes can be particularly difficult due to their "non-innocent" nature.[20] Structural, spectroscopic, and theoretical methods have been used to probe the electronic properties of complexes containing redox-active ligands and help assign oxidation states.[1,3,5,9,11-19] In turn, there has been an increase in the studies of the synthesis and reactivity of such complexes.[21-31]

Redox-active aminophenols in particular have gained considerable interest as ligands for transition metal complexes due to their ability to do redox chemistry typically performed by metal centers.[12,14,32-35] These so called "non-innocent" ligands can coordinate as fully reduced amidophenolates $[ap]^{2-}$, partially oxidized iminosemiquinonate free radicals $[isq\bullet]^{-}$, or fully oxidized iminobenzoquinones [ibq] (Scheme 4.1).[36,37] The ability of redox-active ligands to facilitate $O_2$ activation and deoxygenation of nitroxyl radicals, in which the key intermediates are proposed to be an oxorhenium(V) complex containing a ligand-centered radical are the subjects of two previous chapters.[21,22] However, isolation of high-valent oxorhenium species containing ligand-centered radicals has remained elusive.

**Scheme 4.1.**

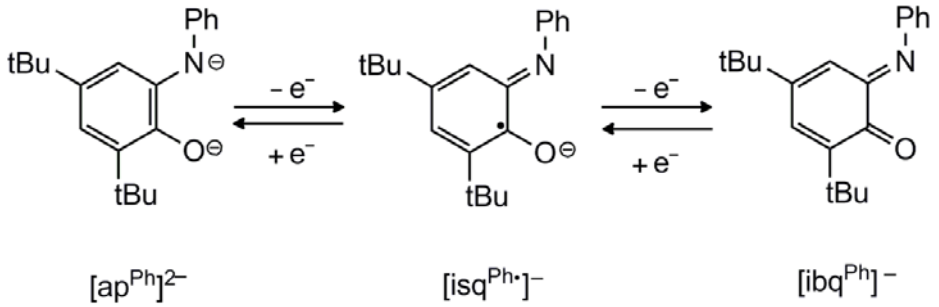


$[ap^{Ph}]^{2-}$ $[isq^{Ph\bullet}]^{-}$ $[ibq^{Ph}]^{-}$

The ability to select for $1e^-$ versus 2 $e^-$ redox reactions is of key importance in bond-making and -breaking reactions.[38-40] Oxorhenium(V) reagents have been shown to be competent $2e^-$ oxo transfer reagents to produce oxorhenium(VII) compounds.[41-43] These species tend to avoid $1e^-$ reactions that would necessarily produce a rhenium(VI) oxidation state, which is rare compared to their $d^0/d^2$ counterparts.[42] Coordination to redox-active ligands may afford access to $1e^-$ redox reactions that are atypical of oxorhenium(V) complexes.[21,22] In Chapters 2 and 3 ligand-centered $1e^-$ redox was proposed to lower the kinetic barrier to net 2e- processes by circumventing unfavorable oxidation states. However, these $1e^-$ radical trapping products were not isolable due to the thermodynamic stability of the $2e^-$ oxidized, OAT, product. Examples of high-valent rhenium complexes containing ligand centered radicals are rare,[44-46] and to our knowledge there are no examples of high-valent oxorhenium complexes containing ligand-centered radicals. Discussed herein are the syntheses, electronic properties, and reactivity of novel high-valent oxorhenium complexes containing ligand-centered radicals.

## 4.2 Results

### 4.2.1 Preparation of Oxorhenium(VI) Complexes with Ligand-Centered Radicals.

When a pale green THF solution of $(Et_4N)[Re^{V}(O)(ap^{Ph})_2]$ (**1**) was treated with 1 equiv. 2,3,4,5,6,6-hexachloro-2,4-cyclohexodiene-1-one (a source of net $[Cl]^+$) under $N_2$, an immediate color change to dark purple was observed. Purification of the purple reaction mixture by column chromatography resulted in numerous products. However, after heating at reflux for 24 hours two purple products were isolated in 71% and 12% respectively. Analysis of the two purple products by MALDI-MS gave molecular ion peaks at 1058 m/z and 828 m/z corresponding to addition of a $[OC_6Cl_5]$ and [Cl] fragment respectively (Scheme 4.2).

**Scheme 4.2.**

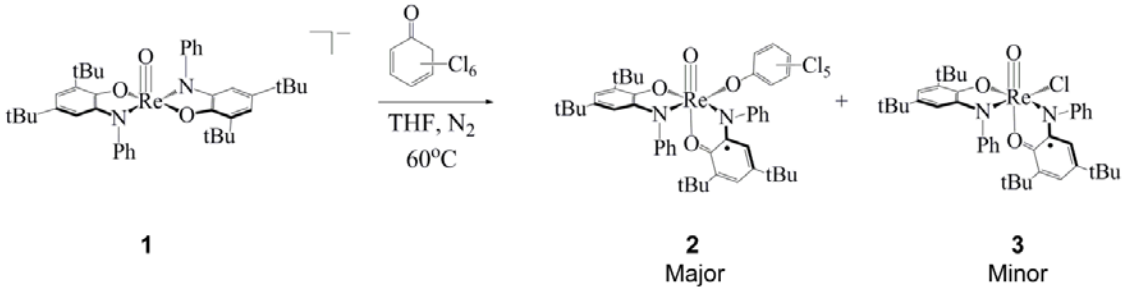


Single crystals of both products suitable for X-ray structural analysis have been obtained. Crystals of the major product were obtained from slow evaporation of a saturated MeCN solution containing a hanging wire of Chromel A at 8 °C. Its X-ray structure contains a neutral, pseudo-octahedral rhenium bound to two inequivalent aminophenol-derived ligands oriented *cis* to each other, a terminal oxo, and a phenoxide ligand oriented *cis* to the terminal oxo (Figure 4.1). The amino-phenol derived ligand *cis*

to the terminal oxo contains C–C bond distances that are equidistant within 3σ (1.40 ± 0.02 Å), and C–O and C–N bond distances of 1.360(2) 1.411(3) Å respectively, suggesting that the amino-phenol derived ligand is a fully reduced, closed-shell $[ap^{Ph}]^{2-}$ dianion (Table 4.1 and Figure 4.2).[47,48] The amino-phenol derived ligand *trans* to the terminal oxo ligand shows a loss of aromaticity with a quinoid pattern of four long and two short C–C bond distances, and shortening of the C–O and C–N bond distances to 1.303(2) and 1.350(3) Å respectively. These metrical data suggest that the ligand is best described as an iminosemiquinonate $[isq^{Ph\bullet}]^{-}$ anion (Table 4.1 and Figure 4.2).[21,47,48] The sum of these data allow for the assignment of the major product as $Re^{VI}(O)(ap^{Ph})(isq^{Ph})(OC_6Cl_5)$ (**2**).

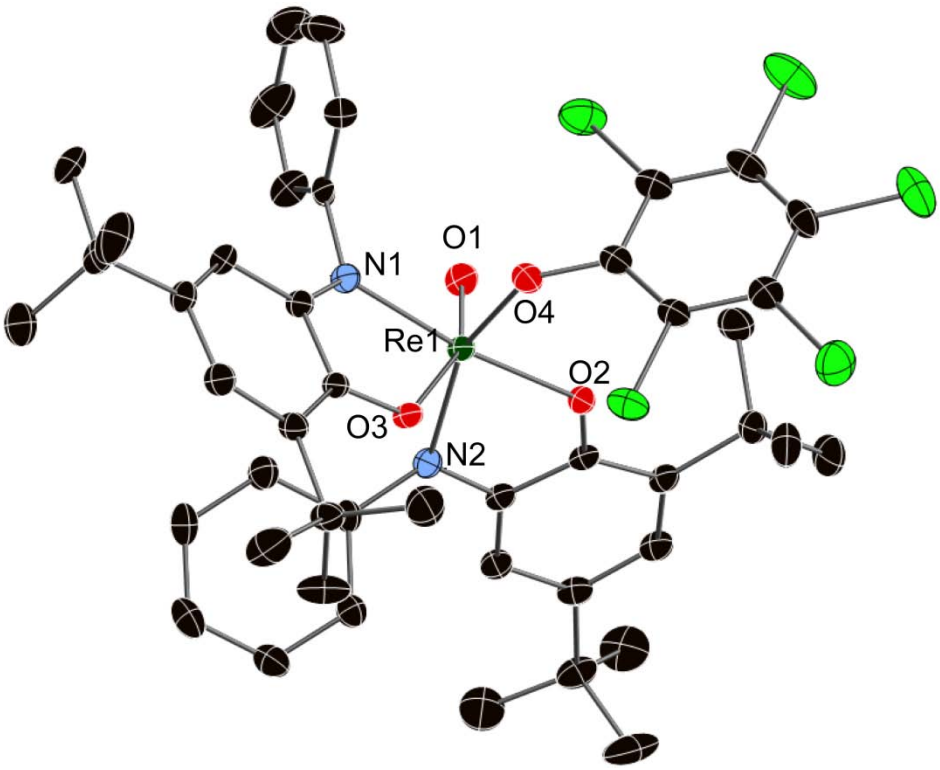


**Figure 4.1.** Solid-state structure of $Re^{VI}(O)(ap^{Ph})(isq^{Ph})(OC_6Cl_5)\bullet CH_3CN$ (**2**) shown with 50% probability ellipsoids. Hydrogen atoms and $CH_3CN$ solvate molecule omitted for clarity.

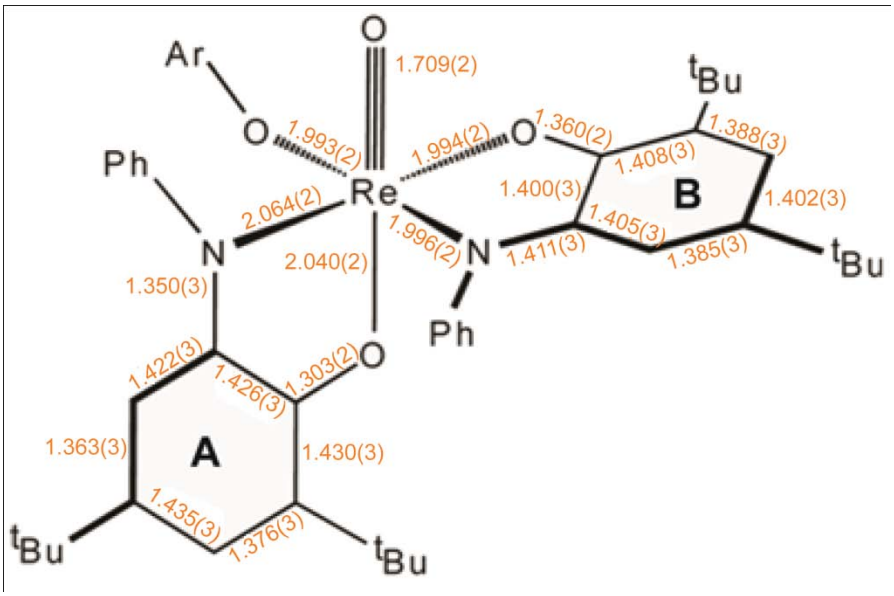


**Figure 4.2.** Schematic drawing showing the bond lengths (Å) for **2**.

Addition of the oxidant $[N(C_6H_4Br\text{-}4)_3][SbCl_6]$ to a MeCN solution of **1** immediately produces a color change from a pale green/yellow to a dark purple. Purification of the purple solution by column chromatography allows for the isolation of a purple species who UV-vis matches that of the minor product from the reaction described above exactly. Single crystals of X-ray quality were grown over 6 months from an acetonitrile solution at –20 $^{o}$C. The structure shown is Figure 4.3 is analogous to **2** consisting of a neutral, pseudo-octahedral rhenium center with two inequivalent aminophenol-derived ligands in the *cis* orientation to each other, a terminal oxo, and a chloride *cis* to the oxo. The aminophenol-derived ligands show similar bond distances to **2**. The aminophenol-derived ligand *cis* to the oxo contains C-C distances that are equidistant within 3σ (1.40 ± 0.02 Å), and C–O and C–N bond distances of 1.361(4) and 1.381(4) Å respectively, suggesting that the amino-phenol derived ligand is a fully reduced, closed-shell $[ap^{Ph}]^{2-}$ dianion. The aminophenol-derived ligand *trans* to the terminal oxo shows similar bond

distances as that of complex **2** that can be assigned to loss of aromaticity. Two C-C bond distances show shortening to 1.375(4) and 1.347(6) Å while the other 4 show elongation and the C-O shows significant contraction with a bond distance 1.311(2) Å. The C-N bond distance shows an unexpected elongation atypical of quinoid-like structures from 1.381(4) to 1.390(6) Å (Table 4.1). The sum of these bond distances suggests for the assignment of the complex as $Re^{VI}(O)(ap^{Ph})(isq^{Ph})(Cl)$ (**3**).[21,47,48]

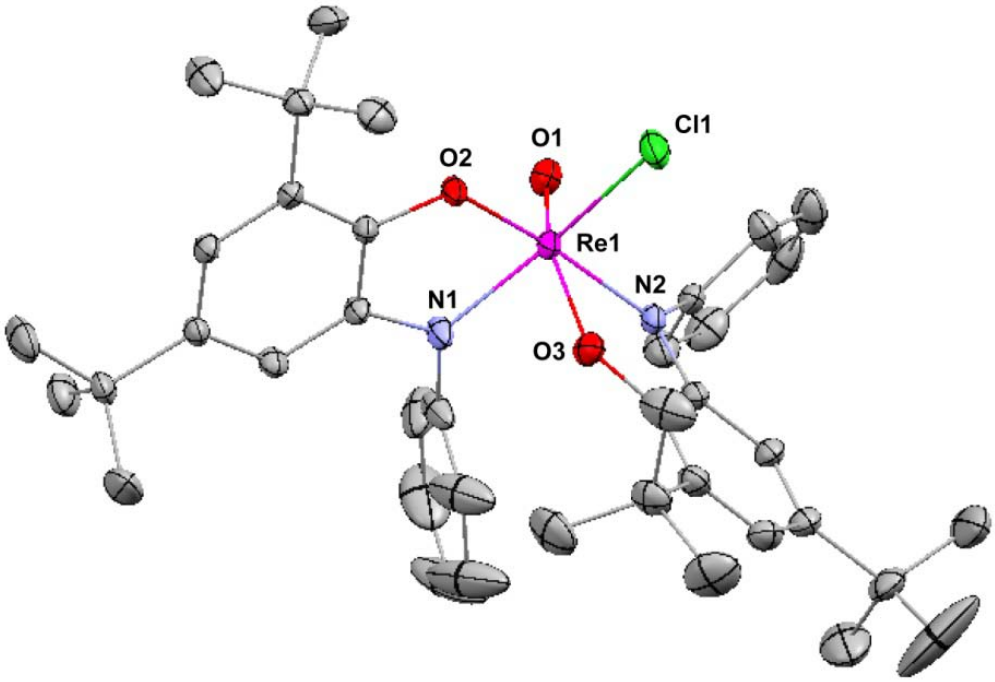


**Figure 4.3.** Solid-state structure of $Re^{VI}(O)(ap^{Ph})(isq^{Ph})(Cl)$ (**3**) shown with 50% probability ellipsoids. Hydrogen atoms omitted for clarity.

**Table 4.1.** Selected bond lengths (Å) for $Re^{VI}(O)(ap^{Ph})(isq^{Ph})(OC_6Cl_5)\bullet CH_3CN$ and $Re^{VI}(O)(ap^{Ph})(isq^{Ph})Cl$.

| $Re^{VI}(O)(ap^{Ph})(isq^{Ph})(OC_6Cl_5)\bullet CH_3CN$ | | | |
|---|---|---|---|
| $Re1\text{-}O1_{oxo}$ | 1.709(16) | $Re1\text{-}O3_{isq}$ | 2.0403(15) |
| $Re1\text{-}O2_{ap}$ | 1.9515(15) | $Re1\text{-}N2_{isq}$ | 2.0641(18) |
| $Re1\text{-}N1_{ap}$ | 1.9958(18) | $Re1\text{-}O4_{phenolate}$ | 1.9935(16) |
| $[ap^{ph}]^{2-}$ Ligand | | | |
| C7-O2 | 1.360(2) | C9-C10 | 1.402(3) |
| C12-N1 | 1.411(3) | C10-C11 | 1.385(3) |
| C7-C8 | 1.408(3) | C11-C12 | 1.405(3) |
| C8-C9 | 1.388(3) | C7-C12 | 1.400(3) |
| $[isq^{Ph\bullet}]^{-}$ Ligand | | | |
| C27-O3 | 1.303(2) | C29-C30 | 1.435(3) |
| C32-N2 | 1.350(3) | C30-C31 | 1.363(3) |
| C27-C28 | 1.430(3) | C31-C32 | 1.422(3) |
| C28-C29 | 1.376(3) | C27-C32 | 1.426(3) |
| $Re^{VI}(O)(ap^{Ph})(isq^{Ph})Cl$ | | | |
| $Re1\text{-}O1_{oxo}$ | 1.7125 | $Re1\text{-}O3_{isq}$ | 2.0727 |
| $Re1\text{-}O2_{ap}$ | 1.9744 | $Re1\text{-}N2_{isq}$ | 2.0248 |
| $Re1\text{-}N1_{ap}$ | 1.9882 | Re1-Cl1 | 2.3620 |
| $[ap^{Ph}]^{2-}$ Ligand | | | |
| C1-O2 | 1.361(4) | C3-C4 | 1.401(5) |
| C6-N1 | 1.381(4) | C4-C5 | 1.399(5) |
| C1-C2 | 1.399(5) | C5-C6 | 1.391(5) |
| C2-C3 | 1.404(5) | C1-C6 | 1.396(5) |
| $[isq^{Ph\bullet}]^{-}$ Ligand | | | |
| C21-O3 | 1.311(2) | C23-C24 | 1.430(7) |
| C26-N2 | 1.390(6) | C24-C25 | 1.347(6) |
| C21-C22 | 1.415(3) | C25-C26 | 1.409(9) |
| C22-C23 | 1.375(4) | C21-C26 | 1.447(7) |

Complex **2** and **3** show a Re-$O_{oxo}$ bond distance of 1.712 ± 0.003 Å comparable to the Re-$O_{oxo}$ bond distance of 1.715(3) Å in $[Re(O)(ap^{Ph})_2]^-$ and is consistent with a Re-$O_{oxo}$ bond order of 3.[21] A report by Gray, Brudvig and coworkers show a $d^1$ dioxorhenium(VI) complex that contains Re-$O_{oxo}$ bond distances that are near identical to the $d^2$ Re(V) congener.[49] The $d^0$ dioxorhenium(VII) congener, $[Re(O)_2(ap^{Ph})_2]^-$, contains Re-$O_{oxo}$ bond distances of 1.737 ± 0.005 Å with a bond order of 2.5 at each oxo.[21] The sum of these data suggest that **2** and **3** are best assigned as a Re(VI) metal center with a ligand-centered radical and not the Re(VII) congener with two fully reduced ligands.

Compound **2** and **3** are both air and thermally stable showing no signs of decomposition over days in solution, in air, at 70 $^oC$. Addition of excess aqueous HCl to purple **2** produced a darker purple solution that matched the UV-vis of **3** exactly. Analysis of the purple reaction mixture by MALDI-MS in the positive mode shows the appearance of a peak at *m/z* 828 corresponding to the chlorine adduct **3**, and the disappearance of the parent peak at *m/z* 1058. These results are consistent with substitution of the phenolate ligand by chloride (Scheme 4.3).

**Scheme 4.3.**

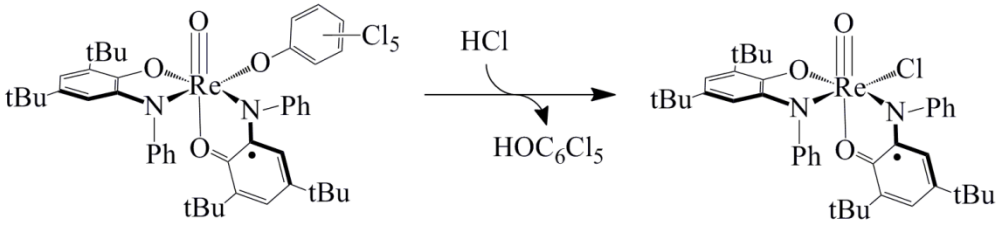


**2** **3**

### 4.2.2 Electronic Properties.

4.2.2.1 Nuclear Magnetic Resonance Spectroscopy.

The diamagnetic ground state is clearly evidenced by $^{1}$H NMR spectroscopy. The two ligands, $[ap^{Ph}]^{2-}$ and $[isq^{Ph\bullet}]^{-}$, are inequivalent and in the *cis* arrangement which gives rise to unique resonances for each. Complex **2** shows 12 resonances between 6-8 ppm at 300 MHz that correspond to the 14 aryl protons. At 500 MHz two new peaks are observed producing a 14 line spectrum, all of area one suggesting that two of the signals overlap in the lower frequency spectrum. Four singlets are observed between 0.97 and 1.2 ppm corresponding to the four *tert*-butyl groups which suggest that only one stereoisomer is present in solution, or they interconvert rapidly on the NMR timescale. One $^{t}$Bu signal shows an upfield shift of ~0.2 ppm versus the other 3 signals and broadening (ΔFWHM = 2.2 Hz) suggesting some interaction with radical spin density.

The $^{1}$H NMR spectrum of complex **3** shows a similar pattern of resonances in the aromatic region between 6-8 ppm. At room temperature, complex **3** produces 12 resonances (Figure 4.4a). However, when a spectrum is obtained at –20 °C, new resonances are observed between 7.0 and 7.2 ppm producing 14 resonances all of area one corresponding to the 14 aryl protons (Figure 4.4b). The $[ap^{Ph}]^{2-}$ and $[isq^{Ph}]^{-}$ ligands both produce two sets of triplets of doublets corresponding to the *meta*-N*Ph* protons, a set of triplets of triplets corresponding to the *para*-N*Ph* protons, and two sets of doublets corresponding to the *ortho*-N*Ph* protons. Four unique signals are again observed for the four $^{t}$Bu groups suggesting the presence of only one stereoisomer.

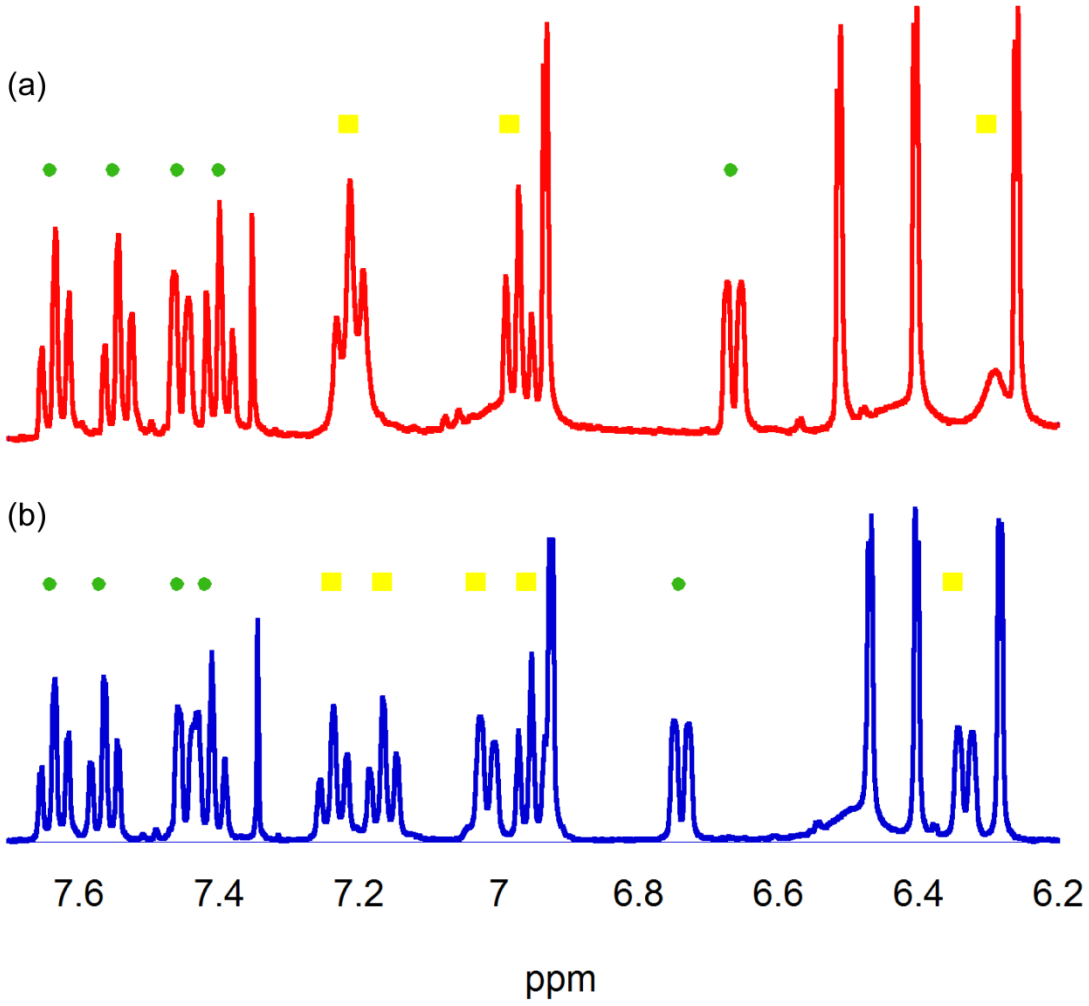


**Figure 4.4.** Variable temperature $^{1}$H NMR of $Re^{VI}(O)(ap^{Ph})(isq^{Ph})(Cl)$ in $CD_2Cl_2$ at (**a**) 20 °C (red spectrum) and (**b**) –20 °C (blue spectrum) of the aromatic region (L = green ●, L' = yellow ■).

The complex structural properties of **2** and **3,** which produce complicated 1D-NMR spectra, were further elucidated utilizing the two dimensional NMR technique correlation spectroscopy (COSY). The 2D spectra of complex **2** showed that peaks A, B, C, and F correspond to the N*Ph* protons of a single ligand while peaks D, E, H, and L correspond to the N*Ph* protons of the other ligand (Figure 4.5). Complex **3** showed a very similar spectrum with peaks A, B, C, and D corresponding to one ligand and peaks

E, F, and H corresponding to the other ligand (Figure 4.6). The two dimensional COSY NMR in conjunction with the variable temperature $^{1}$H NMR clarified the chemical structure of **2** and **3**. The 2D spectra further verified that the two ligands $[ap^{Ph}]^{2-}$ and $[isq^{Ph\bullet}]^{-}$ are in unique chemical environments.

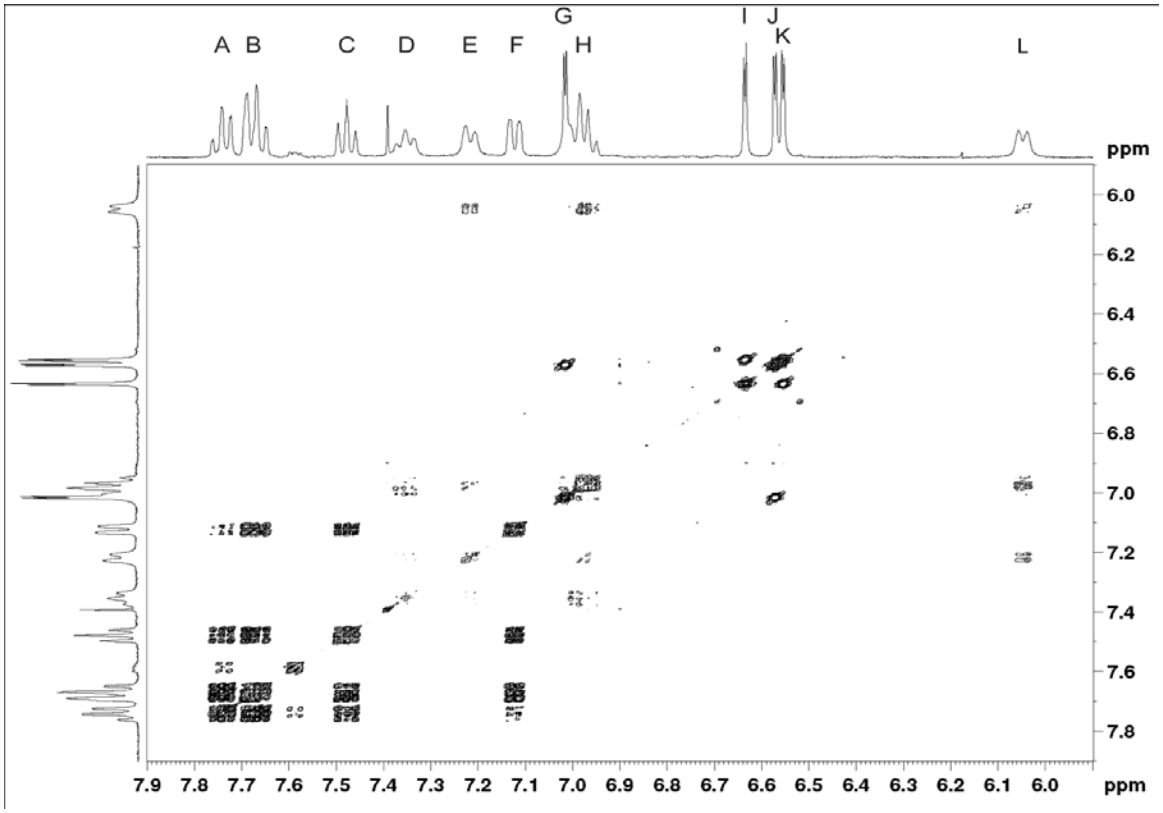


**Figure 4.5.** Two dimensional NMR (COSY) spectrum of $Re(O)(ap^{Ph})(isq^{Ph})(OC_6Cl_5)$.

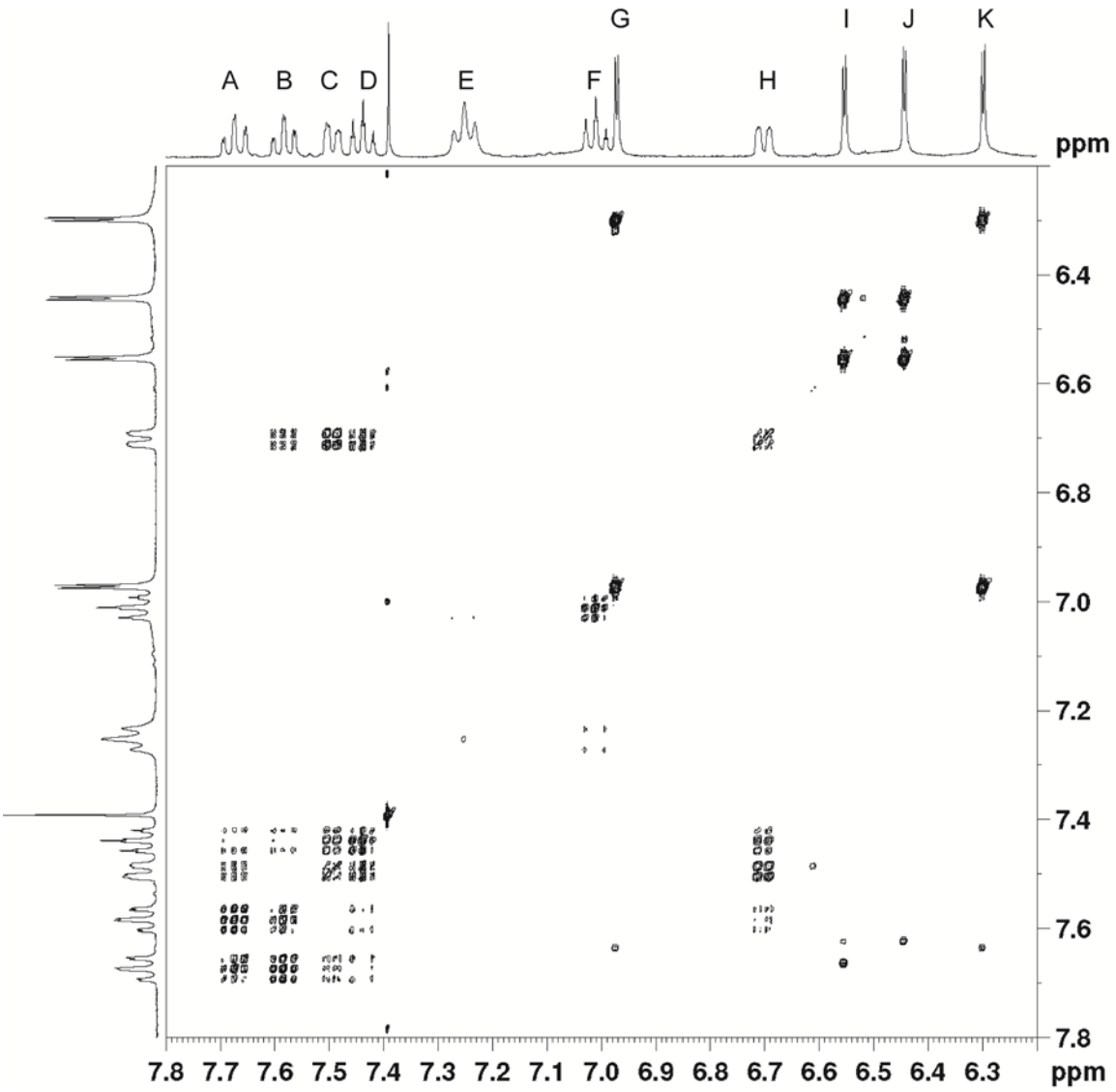


**Figure 4.6.** Two dimensional NMR (COSY) spectrum of Re(O)(ap$^{Ph}$)(isq$^{Ph}$)(Cl).

4.2.2.2 Magnetism.

The diamagnetism of complex **2** and **3** is evident in solution by the presence of $^{1}$H NMR resonances at 298 K and 240 K. However, the identification and assignment of the ligand-centered radical is from the solid state structure at 173 K. In order to confirm the oxidation state assignments from the solid state structure at 173 K correspond to the diamagnetic solution behavior at 298 K, SQUID magnetometry measurements from 5-

400 K were utilized. The magnetic measurement shows that complex **3** is diamagnetic over the entire temperature range confirming that the solid state and solution state are in accordance with each other (Figure 4.7). Complex **3** can best be described as an antiferromagnetically coupled diradical system between a $d^1$ Re(VI) and a ligand-centered radical.

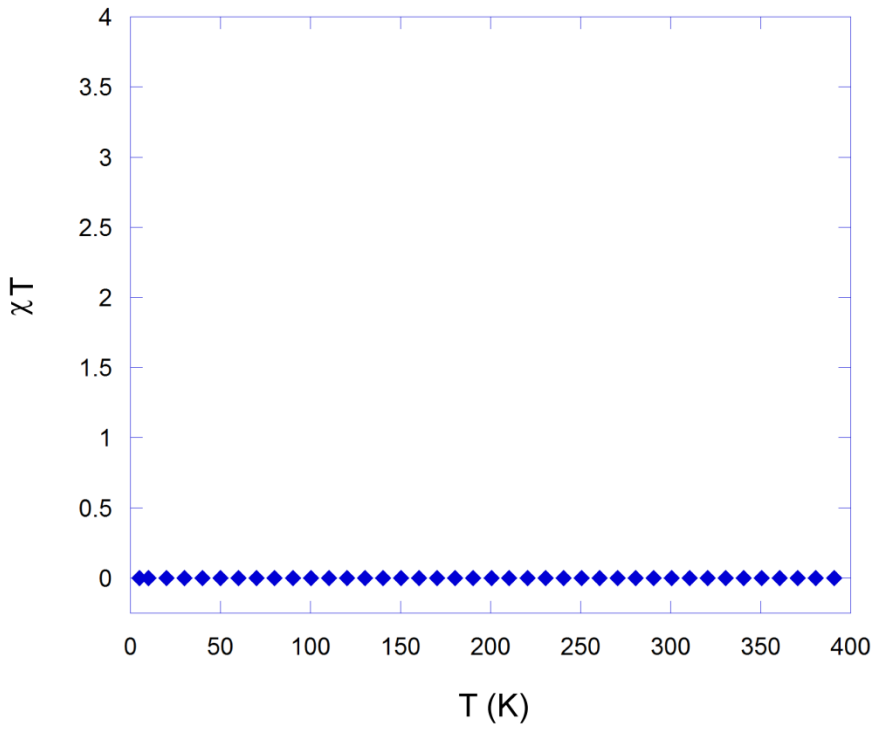


**Figure 4.7.** Magnetic susceptibility of $Re^{VI}(O)(ap^{Ph})(isq^{Ph})(Cl)$.

4.2.2.3 Electrochemistry.

Electrochemistry was utilized to probe the redox behavior of **2** and **3**. Cyclic voltammograms of **3** in MeCN solutions containing 0.1 M $[^nBu_4N][PF_6]$ supporting electrolyte display a reversible $1e^-$ redox couple centered at +0.7 V and a quasi-reversible $1e^-$ redox couple at –0.55 V and an irreversible oxidation at $E_{pa}$ = –0.15 V versus $Fc^+/Fc$ (Figure 4.8). Cyclic voltammograms of **2** are complicated and not clean,

however, they display a reversible redox event at 0.7 V and an quasi-reversible redox event at –0.53 V versus $Fc^{+}/Fc$ (Figure 4.9). When the scan rate is increased to 0.50 V $s^{-1}$, the cathodic and anodic current densities of the redox event centered at –0.53 V vs $Fc^{+}/Fc$ does not approach unity suggesting that the phenoxide anion is labile.

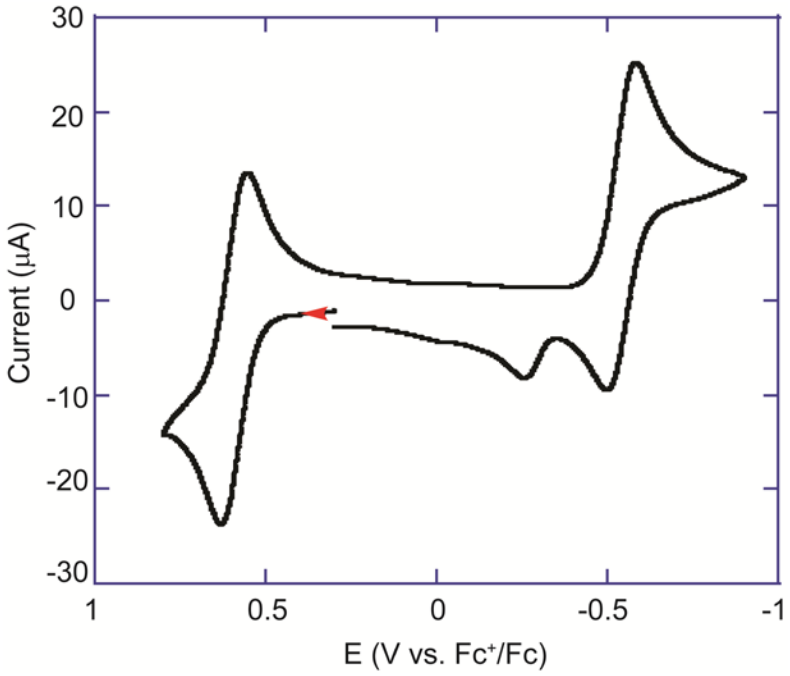


**Figure 4.8.** Cyclic voltammograms of MeCN solutions of $Re^{VI}(O)(ap^{Ph})(isq^{Ph})(Cl)$ in 0.1M $[Bu_4N][PF_6]$ supporting electrolyte at a 10 mm Pt electrode. Scan Rate: 0.1 V $s^{-1}$. Temperature: 25 $^{o}$C.

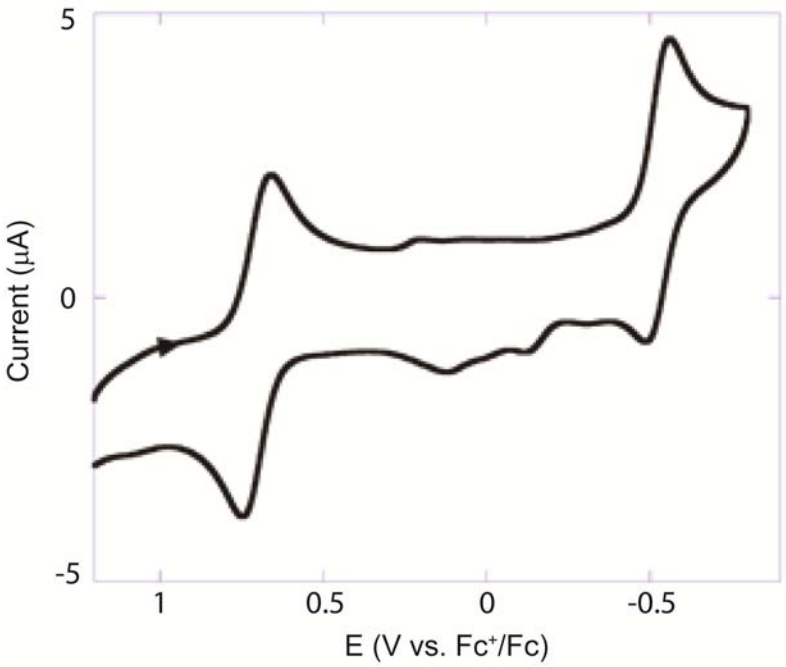


**Figure 4.9.** Cyclic voltammograms of $Re^{VI}(O)(ap^{Ph})(isq^{Ph})(OC_6Cl_5)$ in 0.1M $[Bu_4N][PF_6]$ supporting electrolyte at a 10 mm Pt electrode. Scan Rate: 0.1 V $s^{-1}$. Temperature: 25 $^oC$.

### 4.2.3 Attempted preparation of the S = ½ Congener.

The quasi-reversible behavior of **3** in the cyclic voltametry studies suggest that the $1e^-$ reduced, S = ½, anion or the 5-coordinate neutral species may be accessible. Addition of ferrocene to $CH_2Cl_2$ or MeCN solutions of **3** showed no reaction over days at ambient temperature supporting the assignment of the redox event at –0.53 V versus $Fc^+/Fc$ in Figure 1.4 to reduction of **3**. Addition of an excess of the strong reducing agents Na/Hg, cobaltocene, or bis(benzene)chromium in $CH_2Cl_2$ or MeCN rapidly produces a color change from purple to green. Work-up of the green solution and analysis by $^1H$ NMR produced a spectrum that matched authentic samples of **1**.

Addition of 1 equiv. of cobaltocene or bis(benzene)chromium to acetonitrile solutions of **3** rapidly produced a colorless solution with a dark precipitate. However,

when the reaction was performed in $CH_2Cl_2$ a rapid color change, over seconds, from a dark, vibrant purple to a dull brown-purple was observed (Figure 4.10). When the dark precipitate from the reaction in MeCN was dissolved in $CH_2Cl_2$ and analyzed by UV-vis an identical spectrum was produced.

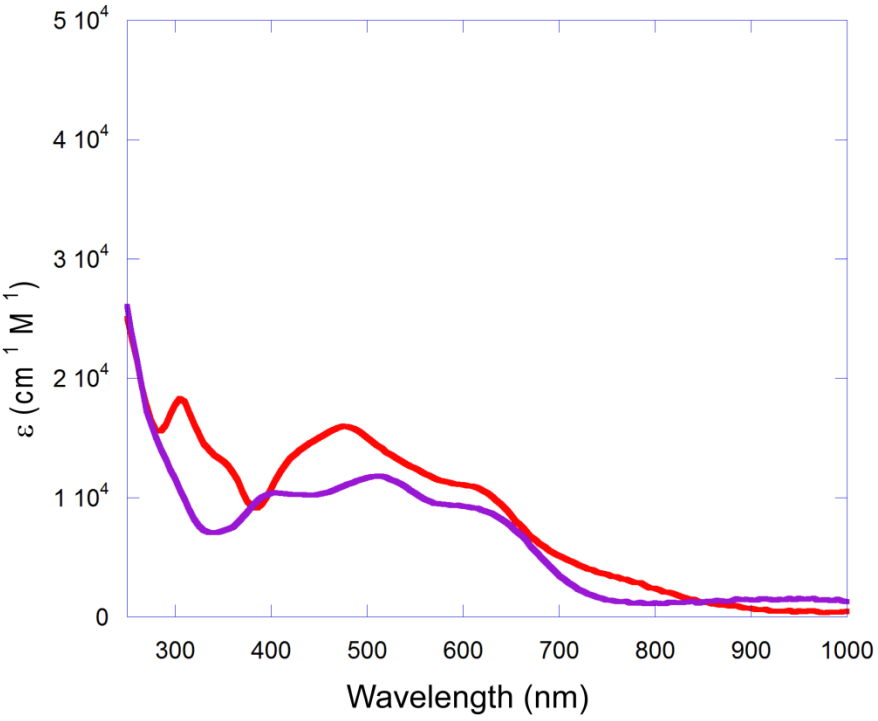


**Figure 4.10.** UV-vis absorption data in $CH_2Cl_2$ for $Re^{VI}(O)(ap^{Ph})(isq^{Ph})(Cl)$ (purple line) and the isolated product from a reaction of $Re^{VI}(O)(ap^{Ph})(isq^{Ph})(Cl)$ with 1 equiv of bis(benzene)chromium (red line).

Oxidation of **1** by $[N(C_6H_4Br\text{-}4)_3]BF_4$ in $CH_2Cl_2$ rapidly produces a color change from pale green to dull brown-purple. Analysis of the reaction mixture by UV-vis produced an identical spectrum to the reaction of **3** with bis(benzene)chromium. When $[N(C_6H_4Br\text{-}4)_3]BF_4$ is titrated into a solution containing **1** and monitored via UV-vis, a maximum yield is reached at 1 equiv of oxidant added. However, as excess oxidant is

added decomposition starts occurring as evidenced by a decrease in $\lambda_{max}$ at 480 nm. This suggests that **1** reacts with $1e^-$ oxidants in a 1:1 stoichiometry. Alternatively, when a $CH_2Cl_2$ solution of **1** is added to 1 equiv **3** in $CH_2Cl_2$ a dull brown-purple color is rapidly produced. Analysis of this solution by UV–vis produces a spectrum identical to that in Figure 4.10 (red line). The sum of these data indicate that the above three reactions (oxidation of **1**, reduction of **3**, and reaction of **1** and **3**) produce the same product.

Single crystals of X–ray quality were grown of the reduction product of **3** and the oxidation product of **1** by vapor diffusion of MeCN into $CH_2Cl_2$ solutions of the dull-purple product. Both crystals produced the same dimeric structure (**4**) (Figure 4.11). The complex is a charge neutral bis(μ-oxo)dirhenium complex where each rhenium center contains two aminophenol-derived ligands. One MeCN molecule is contained in the unit cell, but is not bound to the rhenium. Formation of the bis(μ-oxo) dimer requires one of the two *trans* $[ap^{Ph}]^{2-}$ ligands in the $[Re^{V}(O)(ap^{Ph})_2]^-$ core to twist to a *cis* conformation. For the purpose of this thesis we will assign oxidation state changes to the ligand, which would give $Re^{V}_2(\mu\text{-}O)_2(ap^{Ph})_2(isq^{Ph})_2$. However, initial metal oxidation to generate $Re^{VI}_2(\mu\text{-}O)_2(ap^{Ph})_4$ is just as likely. This isomerization parallels that implemented in the reaction of **1** with $PPh_3$, $O_2$, or $TEMPO^{\bullet}$ discussed in Chapters 2 and 3. The quality of the crystal is poor which prohibits the assignment of ligand oxidation states from the bond distances. Attempts to grow crystals of better quality in order to assign oxidation states are ongoing.

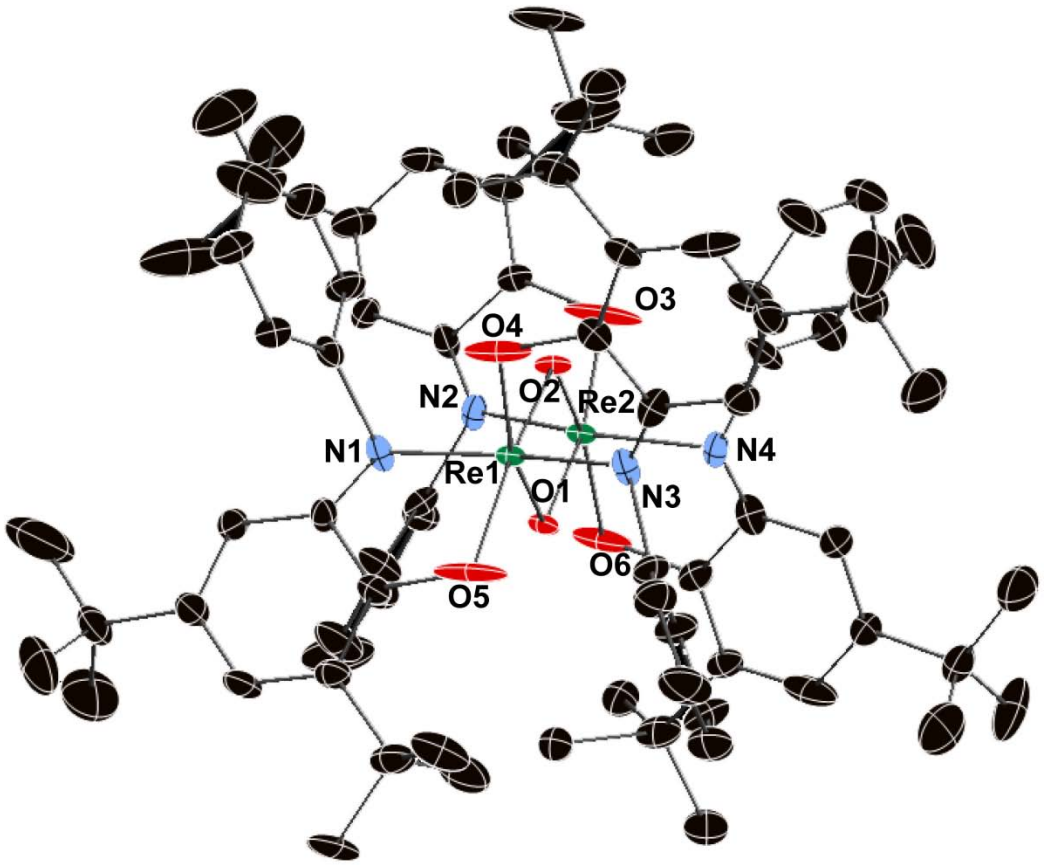


**Figure 4.11**. Solid state structure of **4**. Shown with 50% probability ellipsoids. Hydrogen atoms omitted for clarity.

Cyclic voltammagrams of **1** in $CH_3CN$ and **4** in $CH_2Cl_2$ with $[^nBu_4N][PF_6]$ supporting electrolyte show remarkably similar voltammagrams (Figure 4.12a). Both **1** and **4** show an irreversible oxidation at $E_{pa}$ = –0.35 V and an irreversible reduction at $E_{pc}$ = –1.03 V versus $Fc^+/Fc$. These data suggest that **1** and **4** are interconverted rapidly on the electrochemical timescale. Oxidation of **1** rapidly dimerizes to generate **4**, while reduction of the dimer results in dissociation and generation of the 5-coordinate anion **1**. This also suggest that the S = ½, 5-coordinate neutral species, $Re(O)(ap^{Ph})(isq^{Ph})$ is not isolable under these conditions.

Cyclic voltammagrams of **4** were run in [$^{n}Bu_4N$][Cl] supporting electrolyte in attempts to trap Re(O)($ap^{Ph}$)($isq^{Ph}$) by generating [Re(O)($ap^{Ph}$)($isq^{Ph}$)Cl]$^{-}$. At higher scan rates, reduction of **4** is preceded by an irreversible reduction at $E_{pc}$ = -0.6 V versus $Fc^{+}$/Fc (Figure 4.12b). This is near the potential for the expected reduction of Re(O)($ap^{Ph}$)($isq^{Ph}$) which is not observed in Figure 4.12a. It was initially thought that the $Cl^{-}$ electrolyte prevented dimerization via transient formation of [Re(O)($ap^{Ph}$)($isq^{Ph}$)Cl]$^{-}$, however CV of isolated **3** shows a quasi-reversible reduction centered at –0.55 V versus $Fc^{+}$/Fc. Chemical reduction of **3** requires a strong reductant, Cr($\eta^{6}$-$C_6H_6$)$_2$ (–1.15 V in $CH_2Cl_2$), therefore the redox event at –0.55 V is assigned to the reduction of **3** to generate [Re(O)($ap^{Ph}$)($isq^{Ph}$)Cl]$^{-}$ (Figure 4.12c). At higher scan rates the ratio of cathodic and anodic current densities approach unity suggesting that the halide quickly dissociates but is observable at faster scan rates. The sum of these data suggest that the irreversible reduction at $E_{pc}$ = –0.6 V in Figure 5.12b is not due to reduction of [Re(O)($ap^{Ph}$)($isq^{Ph}$)Cl]$^{-}$. The reduction of **3** occurs at $E_{pc}$ = –0.55 V, therefore reduction [Re(O)($ap^{Ph}$)($isq^{Ph}$)Cl]$^{-}$ requires potentials below –0.6 V.

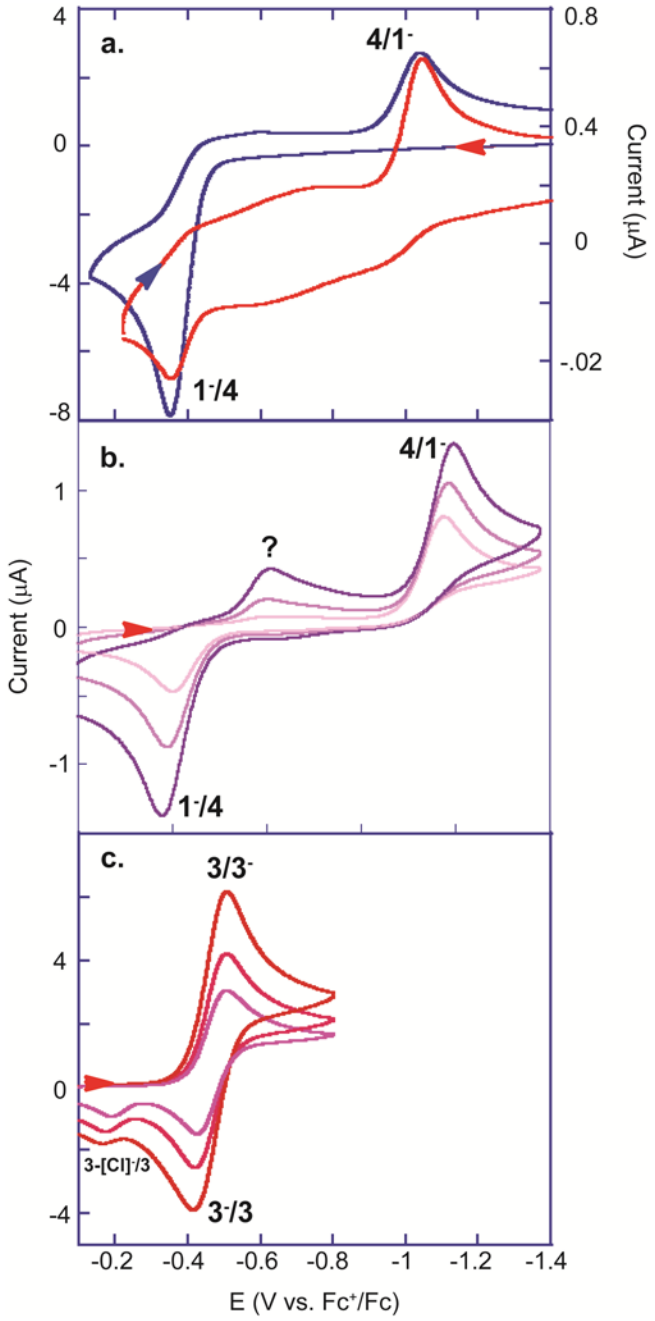


**Figure 4.12.** Cyclic voltammograms of (a) $[Re^{V}(O)(ap^{Ph})_2]^{-}$ (blue) $CH_3CN$ in and $Re^{V}_2(\mu\text{-}O)_2(ap^{Ph})_2(isq^{Ph})_2$ (red, x5) in $CH_2Cl_2$ containing 0.1 M $[^{n}Bu_4N][PF_6]$ at 100 mV $s^{-1}$ scan rate; (b) $Re^{V}_2(\mu\text{-}O)_2(ap^{Ph})_2(isq^{Ph})_2$ in $CH_2Cl_2$ containing $[^{n}Bu_4N][Cl]$ at 25 (faint purple), 50 (light purple), and 100 (purple) mV $s^{-1}$ scan rates; and (c) $Re^{VI}(O)(ap^{Ph})(isq^{Ph})Cl$ in $CH_3CN$ containing $[^{n}Bu_4N][Cl]$ 50 (purple), 100 (light red), and 250 (dark red) mV $s^{-1}$ scan rates. All CV scans were measured at 25 $^{o}$C using a 10 mm Pt electrode.

## 4.3. Discussion

### 4.3.1 Structural Parameters of Oxorhenium Complexes Containing Ligand-Centered Radicals

Addition of chemical oxidants to **1** in the presence of traps produced complexes consisting of a $d^1$, oxorhenium(VI) metal center and a ligand-centered radical. The solid state structures of **2** and **3** provide rare opportunity to compare structural parameters of high-valent oxorhenium species containing ligand-centered radicals.

Complex **2** has two crystallographically unique ligands which, along with the bond distances, suggests that the ligand-centered radical is localized only on the *trans* aminophenol-derived ligand. Complex **3** shows a similar trend in bond distances of the two ligands with some minor differences. There is no change in the C–N bond within 3σ in **3** versus a 0.06 Å contraction in **2**. The crystallographic data for **3** also suggest that the radical density is localized on the *trans* aminophenol-derived ligand. This is likely a function of the strong *trans* influence of the oxo and the weaker σ basicity of the monoanionic $[isq^{Ph}]^{\bullet -}$ radical as compared to the $[ap^{Ph}]^{2-}$ dianion.

The diamagnetic ground state conveniently allowed for the solution state behavior to be monitored by $^1$H NMR. Both **2** and **3** show complicated NMR spectra consistent with two inequivalent aminophenol-derived ligands. The 500 MHz spectrum of **2** contains 14 aromatic resonances of equal intensity which suggests that there is restricted rotation about the NPh bond at room temperature. The hindered rotation can be explained due to the steric bulk of the $OC_6Cl_5$ ligand, and the *cis* arrangement of the two aminophenol-derived ligands. The oxygen of the amidophenolate ligand (Figure 4.2, Ligand B) is *trans* to the nitrogen of the iminosemiquinonate ligand (Figure 4.2, Ligand A) which directs the NPh group of the amidophenolate towards the $^t$Bu of the iminosemiquinonate (Figure 4.1). This is unlike the six-coordinate dioxorhenium(VII) congener, $[Re^{VII}(O)_2(ap^{Ph})_2]^-$, where the oxygen of both ligands are *trans* to each other

directing the NPh groups away from the $^{t}$Bu groups allowing rotation about the NPh N–C bond (Figure 4.13).[21]

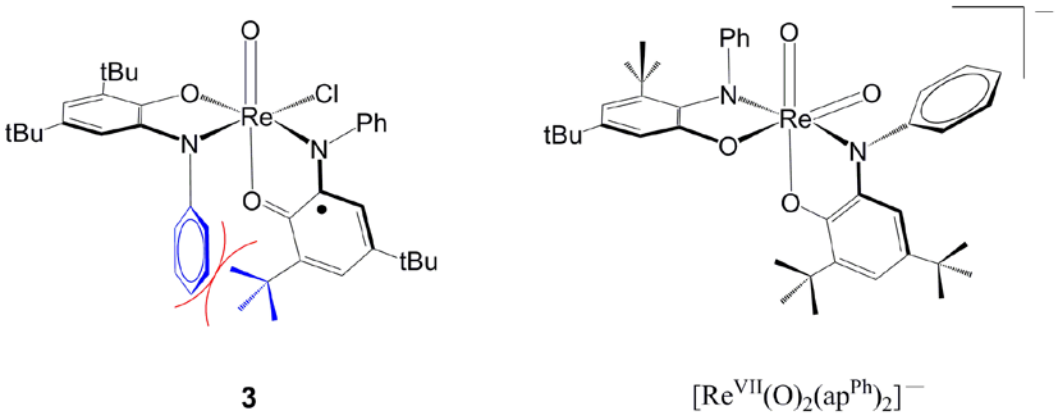


**Figure 4.13.** Schematic representation of sterics in **3** and $[Re^{VII}(O)_2(ap^{Ph})]^-$.

The 12 aryl resonances of complex **3** integrate to 14 protons. However, no new peaks are observed when a higher frequency magnetic field is used suggesting that peaks are not overlapping, but have in fact coalesced. At room temperature the NPh is able to rotate about the N–C bond giving rise to coalescence that is observed in the $^{1}$H NMR spectrum. When the spectrum is obtained at –20 °C this rotation is inhibited and locks the NPh group in place which allows for observation of all 14 resonances. The $[OC_6Cl_5]^-$ ligand of **2** is significantly bulky compared to the $[Cl]^-$ ligand of **3** which could obstruct the rotation about the NPh group.

### 4.3.2 Ligand Radical Involvement in Re-X Bond-Forming Reactions

Addition of a net source of $[Cl]^+$ to **1** produces **3**, a $2e^-$ redox process that is analogous to oxo transfer to **1** to produce $[Re(O)_2(ap^{Ph})_2]^-$. In both bond-forming reactions the new Re–X bond occurs *cis* to the oxo ligand which requires a *trans* to *cis*

isomerization of the $[ap^{Ph}]^{2-}$ ligands. As the $X^-$ ligand becomes larger, $[O]^{2-}$ < $[Cl]^-$ < $[OC_6Cl_5]^-$, the $[ap^{Ph}]^{2-}$ become significantly more sterically congested as evidenced by their respective $^1$H NMR.

Geometrically, $[Re(O)_2(ap^{Ph})_2]^-$ and **3** are analogous, and both are products of $2e^-$ oxidation, however, they have different electronic structures. Oxo transfer to **1** removes the $2e^-$ from the metal center while $[Cl]^+$ addition removes one electron from the metal center and one from a redox-active $[ap^{Ph}]^{2-}$ ligand to generate **3**. This formulation suggests that **3** is a diradical consisting of metal-based and ligand-based radical spin density. However, the diamagnetism of **3** implies that the two unpaired spins are antiferromagnetically coupled. In order to minimize the dπ–pπ repulsion caused by the strong π-donor $[O]^{2-}$ ligands in the c*is* arrangement the metal assumes a $d^0$ configuration. The $Cl^-$ ligand in **3** is a poor π-donor therefore not causing a significant amount of dπ–pπ repulsion as well as being unsuitable for stabilization of a high-valent Re(VII) metal center. Because the $Cl^-$ is unable to stabilize a $d^0$ configuration, the rhenium center assumes a $d^1$ that is further stabilized through antiferromagnetically coupling to the ligand radical.

The ability of redox-active ligands to facilitate Re–O bond-forming reactions was discussed in chapters 2 and 3. The involvement of the ligand in supplying $1e^-$ in radical-type reactions at **1** was proposed based on kinetic studies and computational results, but without direct experimental observation of ligand-centered radicals. The generation and isolation of **2** and **3** provide experimental evidence for the ability of redox-active ligands to supply $1e^-$ for Re–X bond-forming reactions. The Re–X bond-forming reaction to generate **2** and **3** parallels the computed intermediates of $O_2$ addition to **1**. The computed product of $O_2$ addition to **1** contained a $\eta^1$-superoxide $[O_2^{\bullet}]^-$ ligand and a semiquinonate $[isq^{Ph\bullet}]^-$ ligand radical localized *trans* to $Re–O_{oxo}$ (Scheme 4.4a). Addition of a net source of $[Cl]^+$ to **1** generated a similar 6-coordinate **2** and **3**. Analysis of **2** and **3**

by X-ray crystallography confirmed that the $[isq^{Ph\bullet}]^-$ ligand radical density was again localized *trans* to the Re–$O_{oxo}$ (Scheme 4.4b). The localization of the $[isq^{Ph\bullet}]^-$ ligand *trans* to the oxo group is likely due to the strong *trans* influence of the oxo ligand and the weaker σ basicity of $[isq^{Ph\bullet}]^-$ versus $[ap^{Ph}]^{2-}$. In order for the diradical **3** to be diamagnetic, the two unpaired spin densities must be strongly antiferromagnetically coupled. This requires the ligand radical orbitals to mix with the π-symmetry orbitals of the metal. When the Re–$O_{oxo}$ is coincident with the z-axis the metal radical is located in the $d_{xy}$ orbital. Only the *trans* ligand has sufficient symmetry to allow antiferromagnetic coupling with the $d_{xy}$ orbital containing the metal radical (Figure 4.14).

**Scheme 4.4.**

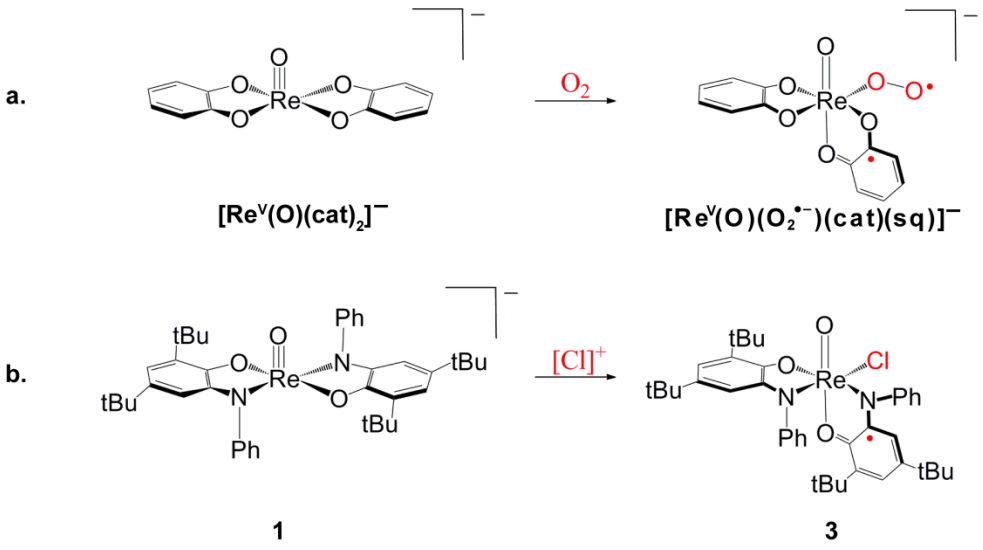

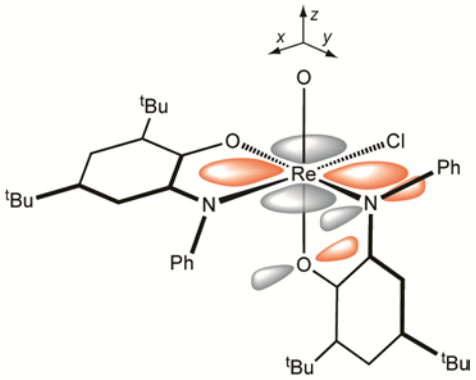


**Figure 4.14.** Qualitative π orbital interactions in **3**.

## 4.4. Conclusion

Oxidation of oxorhenium(V) complexes containing redox-active amidophenolates by strong chemical oxidants in the presence of traps that are not capable of stabilizing dioxorhenium(VII) produce isolable six-coordinate oxorhenium(VI) complexes containing ligand centered radicals. The Re–X bond-forming step occurs with isomerization of the $[isq^{Ph\bullet}]^{-}$ ligand. This is consistent with previously reported Re–O bond forming reactions at an oxorhenium(V) metal centers containing redox-active ligands. These species contain two radicals, a ligand-centered radical, and a metal radical that are antiferromagnetically coupled. Complex **2** and **3** provides valuable insight into the properties and reactivity of oxorhenium complexes containing ligand-centered radicals. Specifically, observation of ligand radicals in **3** and **4** provide experimental evidence for the ability of redox-active ligands to facilitate bond-forming reactions at high-valent oxorhenium centers. However, the locus of the initial oxidation to be metal-based or ligand-based remains unknown. The S = ½ reduced species $Re(O)(ap^{Ph})(isq^{Ph})$ would serve as a better electronic mimic of the proposed intermediates in reactions at

oxorhenium(V) with oxygenic radicals. Unfortunately, this species is not isolable under the provided conditions.

## 4.5 Experimental Details and Supplementary Material.

### 4.5.1 General Considerations.

Unless otherwise specified, all manipulations were performed under anaerobic conditions using standard vacuum line techniques, or in an inert atmosphere glove box under purified nitrogen. Routine NMR spectra were acquired on a Varian Mercury 300 spectrometer (300.323 MHz for $^{1}$H) at ambient temperature. Variable temperature NMR and 2–D NMR spectra were obtained with a Bruker AMX 400 spectrometer (400.138 MHz for 1H). All chemical shifts are reported in parts per million (ppm) relative to TMS, with the residual solvent peak serving as an internal reference. UV–visible absorption spectra were acquired using a Varian Cary 50 spectrophotometer. Unless otherwise noted, all electronic absorption spectra were recorded at ambient temperatures. All mass spectra were recorded in the Georgia Institute of Technology Bioanalytical Mass Spectrometry Facility. Matrix-assisted laser desorption/ionization mass spectrometry was obtained using an Applied Biosystems 4700 Proteomics Analyzer. Cyclic voltammetric measurements were made using a CH Instruments CHI620C potentiostat in a three component cell consisting of a platinum disk working electrode, a platinum wire auxiliary electrode, and a non-aqueous $AgPF_6$/Ag reference electrode. Electrochemical data are referenced and reported to $Fc^+$/Fc as an internal standard. Magnetism data were recorded using a Quantum Design MPMS-5S SQUID magnetometer. Complex **3** was analyzed using 5-10 mg of powdered material loaded into a 0.5 mm by 1.5 mm gelatin capsule, wrapped in Kapton tape, and inserted into a plastic straw. The experiment for complex **3** was performed using a 100 G field between 5 and 400 K. Elemental analyses were performed by Atlantic Microlab, Inc., Norcross,

GA. All analyses were performed in duplicate, and the reported compositions are the average of the two runs.

### 4.5.2 Methods and Materials.

Anhydrous acetonitrile, dichloromethane, and THF solvents for air- and moisture-sensitive manipulations were purchased from Sigma-Aldrich and further dried by passage through columns of activated alumina, degassed by at least three freeze-pump-thaw cycles, and stored under $N_2$ prior to use. Methanol (anhydrous, 99.0%), was purchased from Honeywell Burdick and Jackson. Acetone (99.8%, extra dry) was purchased from Acros. All were used as received. Deuterated acetonitrile ($CD_3CN$) and dichloromethane ($CD_2Cl_2$) were purchased from Cambridge Isotope Laboratories, degassed by three freeze-pump-thaw cycles, vacuum distilled from $CaH_2$, and stored under a dry $N_2$ atmosphere prior to use. $(Et_4N)[Re^{V}(O)(ap)_2]$ (**1**) was prepared by literature methods.[21] All characterization data matched those referenced. All other reagents were purchased from Sigma-Aldrich and used as received.

### 4.5.3 Synthesis of $Re^{VI}(O)(ap^{Ph})(isq^{Ph})(OC_6Cl_5)$ (2).

A 150 mL flask with a Kontes brand high vacuum PTFE valve was charged with $(Et_4N)[Re^{V}(O)(ap^{Ph})_2]$ (568.2 mg, 0.616 mmol) and THF (40 mL). 2,3,4,5,6,6-hexachloro-2,4-cyclohexodiene-1-one (222.5 mg, 0.742 mmol) dissolved in THF (3 mL) was added to generate a dark purple solution. The reaction mixture was stirred at 80 $^{o}$C for 4 h. The mixture was exposed to air and the solvent removed under reduced pressure. The dark residue was dissolved in $CH_2Cl_2$ and subjected to column chromatography on a silica gel column (230-400 mesh) prepared with hexanes. A dark purple band was eluted as the major fraction ($2^{nd}$) with a hexanes-$CH_2Cl_2$ (70/30) mixture. Solvent removal from the eluate followed by freeze drying from a benzene solution afforded **1**. (364.2 mg, 0.34 mmol, 71%). $^{1}$H NMR (300 MHz, $CD_2Cl_2$, $\delta$): 7.7 (td, J = 7 Hz, J = 2 Hz, N*Ph*: meta, 1H); 7.64 (d, J = 8 Hz, N*Ph*: ortho, 1H); 7.63 (td, J = 7Hz, J = 2 Hz, N*Ph*: meta, 1H); 7.44 (tt, J

= 7 Hz, J = 1 Hz, NPh: para, 1H); 7.32 (t, J = 7 Hz, N*Ph*: meta, 1H); 7.18 (d, J = 7 Hz, N*Ph*: ortho, 1H); 7.08 (d, J = 8Hz, N*Ph*: ortho, 1H); 6.98 (d, J = 2 Hz, Ar*H*, 1H); 6.97 (t, J = 7 Hz, N*Ph*: meta, 1 H); 6.95 (t, J = 7Hz, N*Ph*: para, 1H); 6.59 (d, J = 2 Hz, Ar*H*, 1H); 6.53 (d, J = 2 Hz, Ar*H*, 1H); 6.51 (d, J = 2 Hz, Ar*H*, 1H); 6.00 (d, J = 8 Hz, N*Ph*: ortho, 1H); 1.23 (s, tBu 9H); 1.19 (s, tBu, 9H); 1.17 (s, tBu, 9H); 0.98 (s, br, tBu, 9H). UV–vis (MeCN) $\lambda_{max}$, nm ($\varepsilon$, $M^{-1}$ $cm^{-1}$): 231 (50,000), 413 (13,300), 523 (17,100), 613 (sh), 894 (3,500). MALDI-MS (*m/z*): 1058. FTIR (ATR): 2953 (m), 2923 (m), 2866 (m), 1590 (vw), 1532 (vw), 1479 (m), 1458 (m), 1386 (vs), 1359 (s), 1313 (vw), 1299 (vw), 1252 (m), 1225 (w), 1203 (w),1164 (w), 1135 (w), 1108 (w), 1077 (w), 1027 (w), 989 (s), 934 (s), 924 (s), 894 (w), 880 (w), 864 (w), 830 (vs), 778 (s), 711 (s), 674 (vs), 608 (vw), 553 (s), 426 (m). The reported analysis is for [$Re^{VI}$(O)($ap^{Ph}$)($isq^{Ph}$)($OC_6Cl_5$)]•Benzene and the presence of benzene in the sample was confirmed by $^1$H NMR. Anal. Calcd for $C_{53}H_{64}Cl_5N_2O_4Re$: C, 55.04; H, 5.58; N, 2.42; Found: C, 55.19; H, 5.22; N, 2.40. Crystals of X-ray quality were grown by slow evaporation of a saturated acetonitrile solution at 8 $^oC$ over two weeks from a hanging wire of Chromel A®.

**4.5.4 Synthesis of $Re^{VI}$(O)($ap^{Ph}$)($isq^{Ph}$)Cl (3).**

**Method 1.** Compound **2** was isolated as a minor product from the above procedure. (62.4 mg, 0.075 mmol, 12%). **Method 2.** A 20-dram scintillation vial was charged with ($Et_4N$)[$Re^V$(O)($ap^{Ph}$)$_2$] (25.9 mg, 0.0281 mmol), dissolved in MeCN (5 mL), and cooled to -20 $^oC$. A second 20-dram scintillation vial was charged with [N($C_6H_4$Br-4)$_3$][$SbCl_6$] (25.8 mg, 0.0316 mmol), dissolved in MeCN (2 mL), and cooled to –20 $^oC$. The two solutions were quickly mixed while cold with vigorous stirring and stored at -20 $^oC$. Dark purple crystals of X-ray quality deposited over six months at –20 $^oC$. (2.7 mg, 3.26 mmol, 11%). **Method 3.** A 20-dram scintillation vial was charged with **1** (30.0 mg) and dissolved in a $CH_2Cl_2$-MeCN (50/50) mixture. Excess concentrated HCl was added dropwise (6 drops, 200-300 µL). The reaction mixture was stirred at room temperature,

in air, for 15 hours. The reaction mixture was washed with water (5 mL) to remove unreacted HCl. The organic layer was separated and washed two more times with water (5 mL) and the organic layer was collected and dried over $MgSO_4$. Removal of the solvent under reduced pressure gave a purple residue of **2** in quantitative yield. $^1$H NMR (293 K, 400 MHz, $CD_2Cl_2$, $\delta$): 7.63 (td, J = 7.5 Hz, J = 2 Hz, N*Ph*: meta, 1H); 7.54 (td, J = 7.5 Hz, J = 2 Hz, N*Ph*: meta, 1H); 7.45 (d, J = 8 Hz, N*P*h: ortho, 1H); 7.40 (tt, J = 7.4 Hz, J = 1.2 Hz, N*Ph*: para, 1H); 7.2 (t, J = 8 Hz, N*Ph'*: meta, 2H); 6.97 (tt, J = 7.4 Hz, J = 1.2, N*Ph'*: ortho, para, 2H); 6.93 (d, J = 2.1 Hz, Ar*H*, 1 H); 6.66 (d, J = 8.5 Hz, N*Ph:* ortho, 1H); 6.52 (d, J = 2.1 Hz, Ar*H,* 1H); 6.4 (d, J = 2.1 Hz, Ar*H*, 1H); 6.29 (br, N*Ph'*: ortho, 1H) 6.26 (d, J = 2.1 Hz, Ar*H*, 1H); 1.48 (s, $^t$Bu Hz, 9H); 1.22 (s, $^t$Bu Hz, 9H); 1.20 (s, $^t$Bu, 9H); 1.18 (s, $^t$Bu, 9 H). $^1$H NMR (253 K, 400 MHz, $CD_2Cl_2$, $\delta$): 7.63 (t, J = 7 Hz, N*Ph*: meta, 1H); 7.56 (t, J = 7 Hz, N*Ph*: meta, 1H); 7.44 (d, J = 7 Hz, N*Ph*: ortho, 1H); 7.41 (t, J = 7 Hz, N*Ph*: para, 1H); 7.24 (t, J = 7 Hz, N*Ph'*: meta, 1H); 7.17 (t, J = 7 Hz, N*Ph'*: meta, 1H); 7.01 (d, J = 7 Hz, N*Ph'*: ortho 1H); 6.96 (t, J = 7 Hz, N*Ph'*: para, 1H); 6.92 (d, J = 2 Hz, Ar*H*, 1H); 6.75 (d, J = 7 Hz, N*Ph*: ortho 1H); 6.47 (d, J = 2 Hz, Ar*H* 1H); 6.40 (d, J = 2Hz, Ar*H*, 1H); 6.33 (d, J = 7 Hz, N*Ph'*: ortho, 1H); 6.28 (d, J = 2 Hz, Ar*H*, 1H); 1.48 (s, $^t$Bu, 9H); 1.17 (s, $^t$Bu, 18H); 1.15 (s, $^t$Bu, 9H). UV–vis ($CH_2Cl_2$) $\lambda_{max}$, nm ($\varepsilon$, $M^{-1}$ $cm^{-1}$): 295 (sh), 410 (10,500), 515 (12,300), 605 (sh), 920 (1700). MALDI-MS (*m/z*): 828. FTIR (ATR): 2958 (m), 2905 (m), 2868 (m), 1588 (m), 1532 (m), 1481 (s), 1451 (m), 1407 (w), 1391 (m), 1362 (s), 1320 (m), 1302 (m), 1264 (s), 1250 (s), 1176 (s), 1111 (w), 1070 (w), 1027 (m), 995 (s), 928 (vs), 915 (vs), 859 (s), 834 (m), 772 (m), 758 (m), 741 (w), 714 (vs), 703 (vs), 671 (m), 652 (m), 643 (s), 616 (s), 555 (m), 541 (m), 503 (m), 474 (w). The reported analysis is for [$Re^{VI}$(O)($ap^{Ph}$)($isq^{Ph}$)(Cl) )] • 0.5 Benzene and the presence of benzene in the sample was confirmed by $^1$H NMR. The sample for elemental analysis was prepared by method 3 which produces an equivalent of the pentachlorophenol as

an impurity and is required for a passing elemental. Anal. Calcd for $C_{47.8}H_{53.8}Cl_5N_2O_{3.8}Re$: C, 53.13; H, 5.02; N, 2.59; Found: C, 53.06; H, 5.15; N, 2.70.

### 4.5.5 Synthesis of $Re_2(\mu\text{-}O)_2(ap^{Ph})_2(isq^{Ph})_2$ (4)

**Method 1.** To a $CH_2Cl_2$ (5 mL) solution of $Re^{VI}(O)(ap^{Ph})(isq^{Ph})(Cl)$ (25.6 mg, 0.031 mmol) in a 20-dram scintillation vial was added bis(benzene)chromium (6.3 mg, 0.031 mmol) in $CH_2Cl_2$ (5 mL). The reaction mixture was stirred for 20 min at which point the solvent was removed under vacuum. The resulting purple residue was extracted with ether and the solvent removed under vacuum to afford **4** (19.3 mg, 79 %). Single crystals of X-ray quality were grown from slow evaporation of a $CH_2Cl_2$ solution. **Method 2**. To a MeCN (10 mL) solution of $[Re(O)(ap^{Ph})_2]^-$ (0.3272 g, 0.355 mmol) in a 20-dram scintillation vial was added $[N(C_6H_4Br\text{–}4)_3][BF_4]$ (0.1963 g, 0.345 mmol) in MeCN (5 mL). The reaction was stirred for 30 min at which point $Re_2(\mu\text{-}O)_2(ap^{Ph})_2(isq^{Ph})_2$ was collected as a dark purple powder via filtration (0.5323 g, 97 %). Single crystals of X-ray quality were grown by vapor diffusion of MeCN into a $CH_2Cl_2$ solution of $Re_2(\mu\text{-}O)_2(ap^{Ph})_2(isq^{Ph})_2$. **Method 3.** To a $CH_2Cl_2$ (5 mL) solution of $Re^{VI}(O)(ap^{Ph})(isq^{Ph})(Cl)$ (8.9 mg, 0.01 mmol) in a 20-dram scintillation vial was added $[Re(O)(ap^{Ph})_2]^-$ (10.7 mg, 0.012) in $CH_2Cl_2$ (5 mL). The reaction mixture was stirred for 10 min at which point the solvent was removed under vacuum. The resulting purple residue was extracted with ether and the solvent removed under vacuum to give $Re_2(\mu\text{-}O)_2(ap^{Ph})_2(isq^{Ph})_2$ as a dark purple powder (15.23 mg, 96 %). Single crystals of X-ray quality were grown from slow evaporation of a benzene solution. $^1$H NMR (300 MHz, $C_6D_6$, $\delta$): 6.8-7.0 (m, 28 Ar*H*); 1.27 (s, $^t$Bu*H*, 36 H); 1.1 (s, $^t$Bu*H*, 36 H). UV–vis ($CH_2Cl_2$) $\lambda_{max}$, nm ($\varepsilon$, $M^{-1}$ $cm^{-1}$): 300 (sh), 420 (sh), 480 (33,000), 610 (22,700). MALDI-MS(*m/z*): 1586. FTIR (ATR): 2953 (s), 2902 (m), 2865 (m), 1589 (m), 1484 (s), 1463 (m), 1391 (m), 1361 (s), 1247 (vs), 1201 (m), 1163 (m), 1024 (m), 994 (s), 928 (m), 888 (s), 861 (s), 832 (s), 765 (s), 708 (vs),

687 (w), 645 (vs), 621 (s), 570 (s), 545 (m), 502 (m), 483 (s), 400 (m). Anal. Calcd for $C_{80}H_{100}N_4O_4Re_2$: C, 60.58; H, 6.35; N, 3.53; Found: C, 60.03; H, 6.35; N, 3.44.

**4.5.6. X-ray Crystallography.**

Crystals of $Re^{VI}(O)(ap^{Ph})(isq^{Ph})(OC_6Cl_5)$, $Re^{VI}(O)(ap^{Ph})(isq^{Ph})(Cl)$, and $Re_2^{V}(\mu\text{-}O)_2(ap^{Ph})_2(isq^{Ph})_2$ suitable for X-ray diffraction analysis were coated with Paratone N oil, suspended on a small fiber loop and placed in a cooled nitrogen stream at 173 K on Bruker D8 APEX II CCD sealed tube diffractometer. Data were collected using graphite monochromated Mo Kα (λ = 0.71073 Å) radiation. Data were measured using a series of combinations of phi and omega scans with 10 s fame exposures and 0.5$^o$ frame widths. Data collection, indexing and initial cell refinements were done using APEX II software.[50] Frame integration and final cell refinements were done using SAINT software.[51] The structures were solved using direct methods and difference Fourier techniques using the SHELXTL program package, V6.12. Hydrogen atoms were placed in their expected chemical positions using the HFIX command and were included in the final cycles of least squares with isotropic $U_{ij}$'s related to the atoms ridden upon. All non-hydrogen atoms were refined anisotropically except for C19, C24, and the N and O atoms in $Re_2^{V}(\mu\text{-}O)_2(ap^{Ph})_2(isq^{Ph})_2$ Scattering factors and anomalous dispersion corrections are taken from the *International Tables for X-Ray Crystallography*.[52] Other details of data collection and structure refinement are provided in Table 4.1.

**Table 4.1.** Crystallographic Data and Structure Parameters for **2**•$CH_3CN$ and **3**.

| Complex | **2**•$CH_3CN$ | **3** |
|---|---|---|
| Empirical formula | $C_{48}H_{53}Cl_5N_3O_4Re$ | $C_{40}H_{50}ClN\ O_3Re$ |
| Formula weight | 1099.38 | 828.47 |
| Temperature | 173(2) K | 173(2) K |
| Crystal system | Triclinic | Triclinic |
| Space group | P-1 | P-1 |
| Unit cell dimensions | | |
| a (Å) | 11.9967(14) | 9.322(4) |
| b (Å) | 12.6993(15) | 12.209(5) |
| c (Å) | 16.7812(19) | 17.354(7) |
| α (°) | 100.583(2) | 86.153(5) |
| β (°) | 107.213(2) | 75.923(5) |
| γ (°) | 90.282(2) | 83.290(5) |
| V ($Å^3$) | 2395.8(5) | 1901.2(12) |
| Z | 2 | 2 |
| $D_{calc}$ (g $cm^{-1}$) | 1.524 | 1.447 |
| Absorption coefficient ($mm^{-1}$) | 2.86 | 3.304 |
| Crystal size (mm) | 0.59 x 0.38 x 0.21 | 0.32 x 0.13 x 0.12 |
| θ range for data collection (°) | 1.86–32.52 | 1.21–30.36 |
| Index ranges | $-17 \le h \le 17$ | $-12 \le h \le 13$ |
| | $-18 \le k \le 18$ | $-17 \le k \le 17$ |
| | $-25 \le l \le 24$ | $23 \le l \le 23$ |
| Reflections collected/unique | 5150 | 35407 |
| Goodness of fit on $F^2$ | 1.06 | 1.007 |
| R [$I > 2\sigma(I)$] | 0.0304 | 0.0431 |
| $wR_2$ (all data) | 0.0765 | 0.1163 |

## 4.6. References


[1] Ghosh, M.; Weyhermüller, T.; Wieghardt, K. *Dalton. Trans*. **2010**, 39, 1996-2007.
[2] Chirik, P. J.; Wieghardt, K. *Science* **2010**, 327, 794-795.

[3] Boyer, J. L.; Rochford, J.; Tsai, M.-K.;Muckerman, J. T.; Fujita, *E. Coord. Chem. Rev*. **2010**, 254, 309-330.

[4] Van der Vlugt, J. I.; Reek, J.N.H. *Angew. Chem., Int. Ed*. **2009**, 48, 8832-8846.

[5] Kaim, W.; Lahiri,G. K. *Angew. Chem., Int. Ed*. **2007**, 46, 1778-1796.

[6] de Bruin, B.; Hetterscheid, D. G. H. Eur. J. *Inorg. Chem*. **2007**, 211-230.

[7] Butin, K. P.;Beloglazkina,E.K.; Zyk, N. V. *Russ.Chem. Rev*. **2005**, 74, 531-553.

[8] Ward, M. D.; McCleverty, J. A. *J. Chem. Soc., Dalton Trans*. **2002**, 275-288.

[9] Ray, K.; Petrenko, T.; Wieghardt, K.; Neese, F. *Dalton Trans.* **2007**, 1552-1566.

[10] Remenyi, C.; Kaupp, M. *J. Am. Chem. Soc.* **2005**, 127, 11399-11413.

[11] Chaudhuri, P.; Verani, C. N.; Bill, E.; Bothe, E.; Weyhermüller, T.; Wieghardt, K. *J. Am. Chem. Soc.* **2001**, 123, 2213-2223.

[12] Pierpont, C. G. *Coord. Chem. Rev.* **2001**, *216-217*, 99-125.

[13] Kokatam, S.-L.; Chaudhuri, P.; Weyhermueller, T.; Wieghardt, K. *Dalton Trans.* **2007**, 373-378.

[14] Ray, K.; Petrenko, T.; Wieghardt, K.; Neese, F. *Dalton Trans.* **2007**, 1552-1566

[15] Hendrickson, D. N.; Pierpont, C. G. *Top. Curr. Chem.* **2004**, *234*, 63-95.

[16] Shultz, D. A. *Comments Inorg. Chem.* **2002**, *23*, 1-21.

[17] Crabtree, R.H. *The Organometallic Chemistry of the Transition Metals* **2005**, 15.

[18] Sazama, G.T.; Betley, T.A. *Inorg. Chem.* **2010**, *49*, 2512.

[19] Evan R. King, E. R.; Betley T. A. *J. Am. Chem. Soc*. **2009**, 131, 14374-14380

[20] Jørgensen, C. K. *Coord. Chem. Rev.* **1966**, 1, 164-178.

[21] Lippert, C. A.; Arnstein, S. A.; Sherrill, C. D.; Soper, J. D. *J. Am. Chem. Soc*. **2010**, 132, 3879-3892.

[22] Lippert, C. A., Soper, J. D. *Inorg. Chem.*, **2010**, 49, 3682-3684.

[23] Rolle, C. J.; Hardcastle, K. I.; Soper, J. D. *Inorg. Chem.* **2008**, *47*, 1892-1894.

[24] Smith, A. L.; Soper, J. D. *Polyhedron* **2010**, *29*, 164-169.

[25] Nguyen, A. I.; Blackmore, K. J.; Carter, S. M.; Zarkesh, R. A.; Heyduk, A. F. *J. Am. Chem. Soc.* **2009**.

[26] Blackmore, K. J.; Lal, N.; Ziller, J. W.; Heyduk, A. F. *J. Am. Chem. Soc.* **2008**, *130*, 2728-2729.

[27] Ketterer, N. A.; Fan, H.; Blackmore, K. J.; Yang, X.; Ziller, J. W.; Baik, M. H.; Heyduk, A. F. *J. Am. Chem. Soc.* **2008**, *130*, 4364-74.

[28] Mukherjee, C.; Weyhermüeller, T.; Bothe, E.; Chaudhuri, P. *Inorg. Chem.* **2008**, *47*, 2740-2746.

[29] Stanciu, C.; Jones, M. E.; Fanwick, P. E.; Abu-Omar, M. M. *J. Am. Chem. Soc.* **2007**, *129*, 12400-12401.

[30] Bart, S. C.; Bowman, A. C.; Lobkovsky, E.; Chirik, P. J. *J. Am.Chem. Soc.* **2007**, *129*, 7212-7213.

[31] Lippert, C. A.; Soper, J. D. *Inorg. Chem.* **2010**, 49, 3682-3684.

[32] Blackmore, K. J.; Ziller, J. W.; Heyduk, A. F. *Inorg. Chem.* **2005**, 44, 5559-5561.

[33] Blackmore, K. J.; Sly, M. B.; Haneline, M. R.; Ziller, J. W.; Heyduk, A. F. *Inorg. Chem.* **2008**, 47, 10522-10532.

[34] Zarkesh, R. A.; Heyduk, A. F. *Organometallics*, **2009**, 28, 6629-6631.

[35] Mukherjee, C.; Weyhermüller, T.; Bothe, E.; Chaudhuri, P. *C. R. Chimie*, **2007**, 10, 313-325.

[36] Pierpont, C. G.; Lange, C. W. *Prog. Inorg. Chem.* **1994**, *41*, 331-442.

[37] Pierpont, C. G. *Coord. Chem. Rev.* **2001**, *216-217*, 99-125.

[38] Sheldon, R. A.; Kochi, J. K. *Metal-Catalyzed Oxidations of Organic Compounds*; Academic Press: New York, **1981**.

[39] *Comprehensive Organic Synthesis: Selectivity, Strategy and Efficiency in Modern Organic Chemistry*, Vol. 7: Oxidation; Trost, B. M., Fleming, I., Eds.; Pergamon: Oxford, U.K., **1991**.

[40] *Report of the Basic Energy Sciences Workshop on Solar Energy Utilization*; U.S. Department of Energy: Washington, DC, **2005**.

[41] Holm, R. H. *Chem. Rev*. **1987**, 87, 1401-1449.

[42] Espenson, J. H. Adv. *Inorg. Chem*. **2003**, 54, 157-202.

[43] Herrmann, W. A.; Kuhn, F. E. *Acc. Chem. Res*. **1997**, 30, 169-180.

[44] Sproules, S.; Bemedito, F. L.; Bill, E. Weyhermüller, T.; DeBeer, G. Wieghardt, K. *Inorg. Chem.* **2009**, 48, 10926-10941.

[45] Al-Mowali, A. H.; Porte, A. L. *J. Chem. Soc., Dalton Trans.* **1975**, 250-252.

[46] Gerber, T. I. A.; Luzipo, D.; Mayer, P. Van Brecht, B. J. A. M.; Du Preez, J. G. H. *J. Coord. Chem.* **2003**, 56, 1049-1061.

[47] Bill, E.; Bothe, E.; Chaudhuri, P.; Chlopek, K.; Herebian, D.; Kokatam, S.; Ray, K.; Weyhermueller, T.; Neese, F.; Wieghardt, K. *Chem. –Eur. J.* **2005**, *11*, 204-224.

[48] Poddel'sky, A. I.; Cherkasov, V. K.; Abakumov, G. A. *Coord. Chem. Rev.* **2009**, *253*, 291-324.

[49] Brewer, J. C.; Thorp, H. H.; Slagle, K. M.; Brudvig, G. W.; Gray, H. B. *J. Am. Chem. Soc.* **1991,** *113,* 3173-3174.

[50] *APEX II*; Brukers AXS, Inc., Analytical X-Ray Systems: Madison, WI, **2005**.

[51] *SAINT*, version 6.45A; Brukers AXS, Inc., Analytical X-ray Systems: Madison, WI, **2003**.

[52] *In International Tables for X-ray Crystallography, Volume C*; Wilson, J. C., Ed.; Academic Publishers: Dordrecht, The Netherlands, **1992**.

# Chapter 5

# "Masked" Oxyl Radicals: Synthesis and Reactivity

## 5.1 Introduction

Selecting for $1e^-$ and/or $2e^-$ redox transformations in bond-making and -breaking reactions is of paramount importance for selective activation of small molecules.[1-3] Transition metals are often employed as catalysts for selective redox control due to their ability to mediate the transfer of multiple redox equivalents while avoiding odd electron intermediates.[1,4-8] Later 4d and 5d metals are typically utilized for this purpose owing to their tendency to facilitate $2e^-$ reactions with organic substrates while avoiding odd d electron counts.[1,4-6]

Catalysis that incorporates free radical intermediates have some synthetic utility but tend to be unselective, or selective for less desirable products.[1,2,4,5] This is due to the fact that radical reactions often have low kinetic barriers. As discussed in Chapter 1, biological reactions access the low barrier pathways of radical reactions while maintaining redox control and selectivity in the activation of small molecules.[9-11] For example, the ability of P450 to hydroxylate strong C–H bonds is often ascribed to the diradical ground state of the $Fe^{IV}$=O intermediate, which contains a porphryin ligand radical.[12] It appears that using redox-active ligands in concert with metal centers helps control the selectivity of radical reactions.

The use of redox-active ligands to store and deliver multiple redox equivalents has received a lot of attention in recent years.[13-25] There has been great success in utilizing these ligands in stoichiometric and catalytic activation of small molecules. The majority of these systems have focused on exploiting low energy ligand-metal CT for multielectron reactions at coordinatively unsaturated 3d metal centers.[13-20,24,25] For example, $2e^-$ pseudo oxidative addition and reductive elimination reactions at $d^0$ or later

first row metals, where the redox equivalents derive from the redox-ligand, have been demonstrated.[13,20,25]

A complimentary application of this strategy is discussed in Chapters 2-4 wherein redox-active ligands facilitate activation of $O_2$, deoxygenation of nitroxyl radicals, and Re–X bond forming reactions at five-coordinate oxorhenium(V) complexes.[21-23] In these reactions the ligand radicals have been proposed to impart a $1e^-$, radical-like reactivity to the net $2e^-$ oxo-transfer and Re–X bond forming reactions which gives access to a low barrier pathway. However, in all of these reactions the reactivity occurs at the metal center to make Re–O and Re–X bonds. In the context of catalysts for O-O bond formation this is undesirable because bond formation requires coupling of two metal oxyl fragments. Accordingly, new strategies are needed to direct radical reactivity towards the terminal oxo ligand and to produce oxyl-like character in order to facilitate radical coupling O–R bond forming reactions.

This chapter discusses use of coordinatively saturated oxorhenium complexes in attempts to direct the radical reactivity towards the oxo ligand giving it oxyl-like behavior. Generation of an oxyl radical typically requires population of a metal-oxo π*-antibonding orbital by a single electron or removal of an electron from a metal-oxo π-bonding orbital. The latter approach is usually energetically prohibitive due to the bonding orbitals being low in energy. A different approach that will be discussed here is to delocalize a ligand radical $L^{\bullet}$ hole of semiquinonate-type ligand into the $Re–O_{oxo}$ π system through symmetry allowed mixing of the orbitals. In the extreme case where the hole is completely delocalized, $[O]^{2-} \rightarrow [L]^{\bullet-}$, the $Re–O_{oxo}$ bond order decreases from 3.0 to 2.5 generating an oxyl radical (Figure 5.1). This is most likely a high-energy process, depending on the ligand oxidation potentials, but it is not unreasonable to expect that mixing the $[L]^{\bullet-}$ SOMO with a Re≡O π -bond may give oxyl radical character. We term these “masked” oxyls. The following criteria are required for a “masked” oxyl: (1) a

ligand-based radical, (2) a Re–$O_{oxo}$ π-bond, and (3) mixing of the $[L]^{\bullet-}$ SOMO with the Re≡O π-bond.

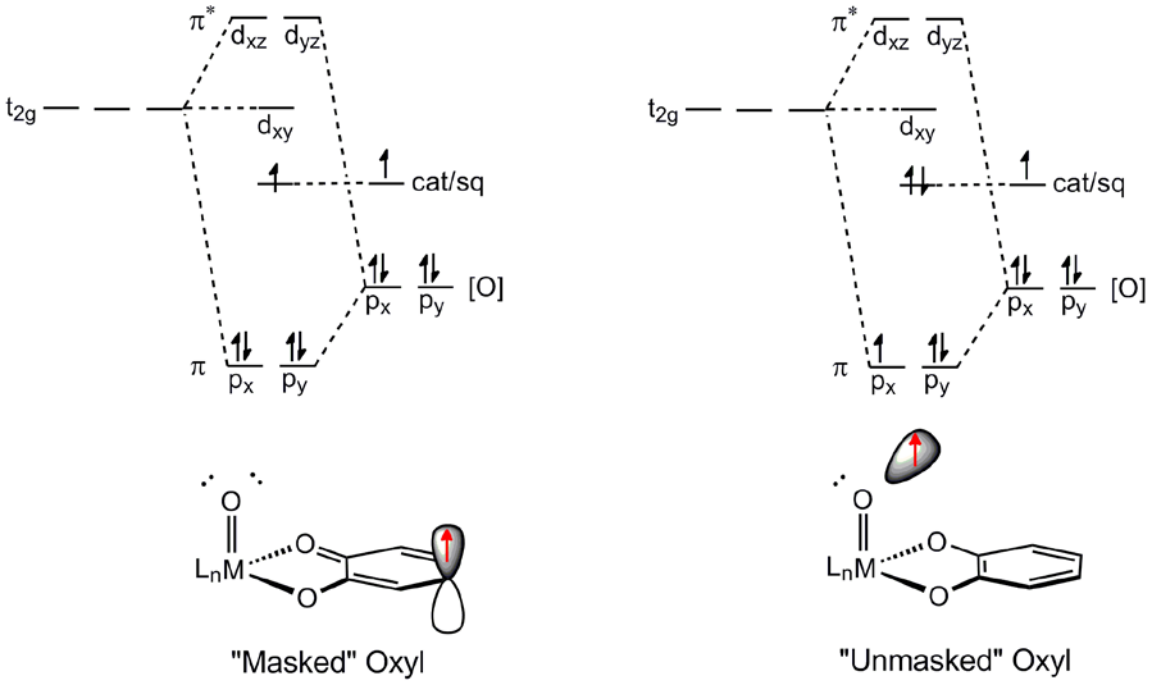


**Figure 5.1.** Qualitative MO of (**a**) a $d^0$ M=$O_{oxo}$ containing a ligand radical with a corresponding schematic representation of a "masked" oxyl and (**b**) the strong limit case of intraligand charge transfer generating an oxyl radical and corresponding schematic representation.

## 5.2 Results

### 5.2.1 Preparation and Characterization of Coordinatively Saturated Oxorhenium Complexes.

Addition of 1.1 equiv. catecholborane (1,2-catecholborane or 3,5-di-*tert*-butyl-catecholborane) to a benzene solution of $TpRe^{V}(O)(OMe)_2$ [Tp = tris(pyrazolyl)borate] resulted in a color change from vibrant blue to brown over one hour at ambient temperature. The two brown products were isolated in high yield by slow evaporation of

an ether solution at –50 $^{O}$C (> 80%). Analysis of the brown powders by MALDI-MS gave parent ion peaks at m/z 526 and 636, respectively, corresponding to substitution of the two $[OMe]^-$ ligands with $[cat]^{2-}$ or $[3,5\text{-}^tBu_2cat]^{2-}$ respectively ($[cat]^{2-}$ = 1,2-catecholate, $[3,5\text{-}^tBu_2cat]^{2-}$ = 3,5-di-*tert*-butylcatecholate) (eq. 1). Analysis of the brown powders by $^1$H NMR gave the expected peaks corresponding to coordination of a catecholate or 3,5-di-*tert*-butylcatecholate to a rhenium(V) metal center. Purification by silica gel chromatography allowed $TpRe^V(O)(^tBu_2cat)$ to be collected as an analytically pure brown solid. The same brown products were also obtained by addition of excess $Et_3N$ and the corresponding catechol to $TpRe(O)(OMe)_2$ and stirring for three days (eq. 2). However, even in the presence of excess ligand and base the reaction gave low yields (~50%).

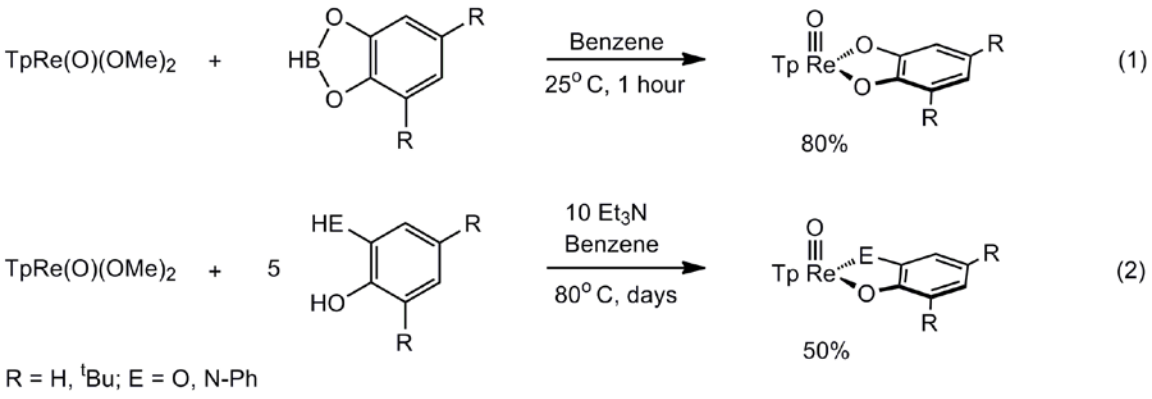


Two derivatives containing $[ap^{Ph}]^{2-}$ and $[OCH_2CH_2O]^{2-}$ ligands ($[ap^{Ph}]^{2-}$ =2,4-di-*tert*-butyl-6-(phenylamido)phenolate) were prepared by reactions of $TpRe^V(O)(OMe)_2$ and $TpRe^V(O)(Cl)_2$, respectively with the acid ligand precursor in basic benzene and basic MeCN, respectively. Slow evaporation of an ether/pentane solution of $TpRe^V(O)(ap^{Ph})$ at –10 $^{O}$C deposited dark brown crystals suitable for x-ray diffraction. A

single crystal structure is provided in Figure 5.2. It contains a pseudo-octahedral rhenium bound to a facially capping Tp ligand and an aminophenol-derived ligand *cis* to a terminal oxo ligand. The ligand C–C bond distances are equal within 3$\sigma$ (1.40 ± 0.02 Å), and the C–O and C–N bond distances of 1.371(8) and 1.407(8) Å, respectively, suggest that the aminophenol-derived ligand is a fully reduced, closed-shell $[ap^{Ph}]^{2-}$ dianion.[26,27] The assignment of this complex as rhenium(V) is additionally supported by the diamagnetic $^{1}$H NMR spectrum and analytical data.

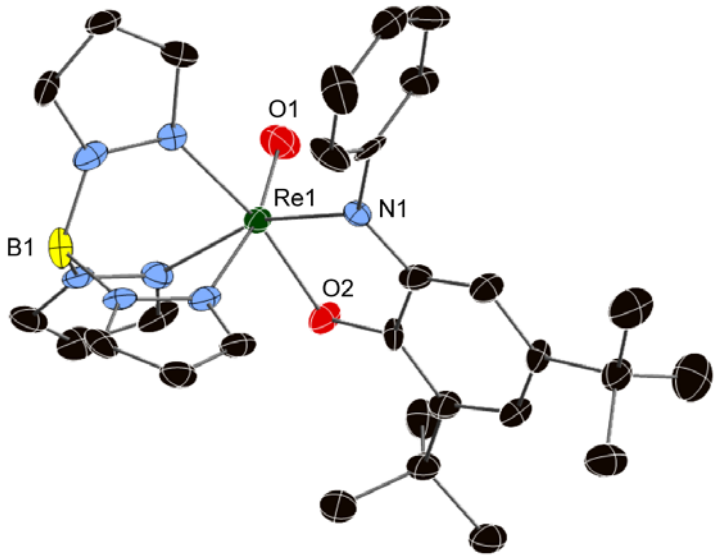


**Figure 5.2.** Solid-state structure of $TpRe^{V}(O)(ap^{Ph})$•0.3 Pentane shown with 50% probability ellipsoids. Hydrogen atoms and solvent molecule omitted for clarity. Selected bond lengths (Å): Re1–O1 1.690(5), C1–O2 1.371(8), C6–N1 1.407(8).

Crystals of $TpRe^{V}(O)(OCH_2CH_2O)$ obtained from a concentrated $CH_2Cl_2$ solution were also analyzed by x-ray diffraction. As shown in Figure 5.3, the complex contains a pseudo-octahedral geometry. As in the $[ap^{Ph}]^{2-}$ complex described above, the ethylene glycolate ligand is located *cis* to the terminal oxo ligand. The $[OCH_2CH_2O]^{2-}$ ligand

contains C–O bond distances of 1.475(14) and 1.452(11) Å typical of diolates. The $Re{\equiv}O_{oxo}$ bond length of 1.686(7) Å is consistent with the Re–O triple bond expected for a monooxo $d^2$ ion in a tetragonal ligand field.[28] Similar to $TpRe^{V}(O)(ap^{Ph})$, the rhenium(V) oxidation state of $TpRe^{V}(O)(OCH_2CH_2O)$ is supported by the diamagnetic $^1H$ NMR spectrum and analytical data.

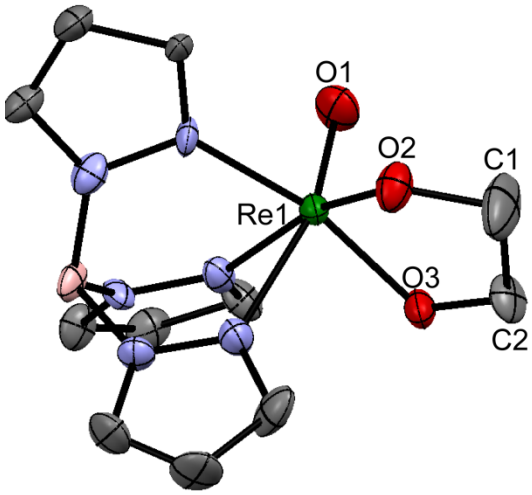


**Figure 5.3.** Solid-state structure of $TpRe^{V}(O)(OCH_2CH_2O)$ shown with 50% probability ellipsoids. Hydrogen atoms omitted for clarity. Selected bond lengths (Å): Re1-O1 1.686(7), Re1-O2 1.961(6), Re1-O3 1.941(6), C1-O2 1.475(14), C2-O3 1.452(11).

Cyclic voltammograms of TpRe(O)(L) (L = $[cat]^{2-}$, $[3,5\text{-}^{t}Bu_2cat]^{2-}$, $[ap^{Ph}]^{2-}$, $[O_2(CH_2)_2]^{2-}$) are shown in Figure 5.4. In $CH_3CN$ with $[^{n}Bu_4N][PF_6]$ supporting electrolyte, irreversible oxidation of TpRe(O)(cat) occurs at $E_{pa}$ = 0.77 V versus $Fc^{+}/Fc$ (Figure 5.3a). A reversible redox event occurs at –1.77 V versus $Fc^{+}/Fc$ and because the ligand is fully reduced it is assigned to the $Re^{V}/Re^{IV}$ couple. The voltammogram for TpRe(O)(3,5-$^{t}Bu_2$cat) shows a reversible event centered at 0.6 V versus $Fc^{+}/Fc$ and the potential shifts to 0.3 V versus $Fc^{+}/Fc$ upon ligand substitution from $[3,5\text{-}^{t}Bu_2cat]^{-}$ to $[ap^{Ph}]^{2-}$ (Figure

5.3b). The $[ap^{Ph}]^{2-}$ ligand is more electron rich and therefore more easily oxidized, and so the redox event is assigned to the ligand.[29] Although, a metal based redox event cannot be ruled out, metal based oxidation would generate a $d^1$ monooxorhenium(VI) complex. These are rare and thermodynamically unfavorable compared to their $d^0/d^2$ counterparts.[30]

A voltammogram of $TpRe(O)(OCH_2CH_2O)$ containing the redox-inert glycol ligand is shown in Figure 5.3b. It has a reversible redox event centered at 0.56 V versus $Fc^+/Fc$ which is necessarily assigned to the $Re^V/Re^{VI}$ couple. From this datum we are unable to undoubtedly assign the redox event of $TpRe^V(O)(3,5\text{-}^tBu_2cat)$ as a ligand- or metal-based event.

The ability of the six-coordinate dioxorhemium(VII) complex[31] $[Re^{VII}(O)_2(ap^{Ph})_2]^-$ to undergo electron transfer was also investigated by cyclic voltammetry. A reversible oxidation is observed centered at –0.125 V versus $Fc^+/Fc$ (Figure 5.3c). The complex contains a $d^0$ metal center, therefore a ligand-based oxidation is the only reasonable option.

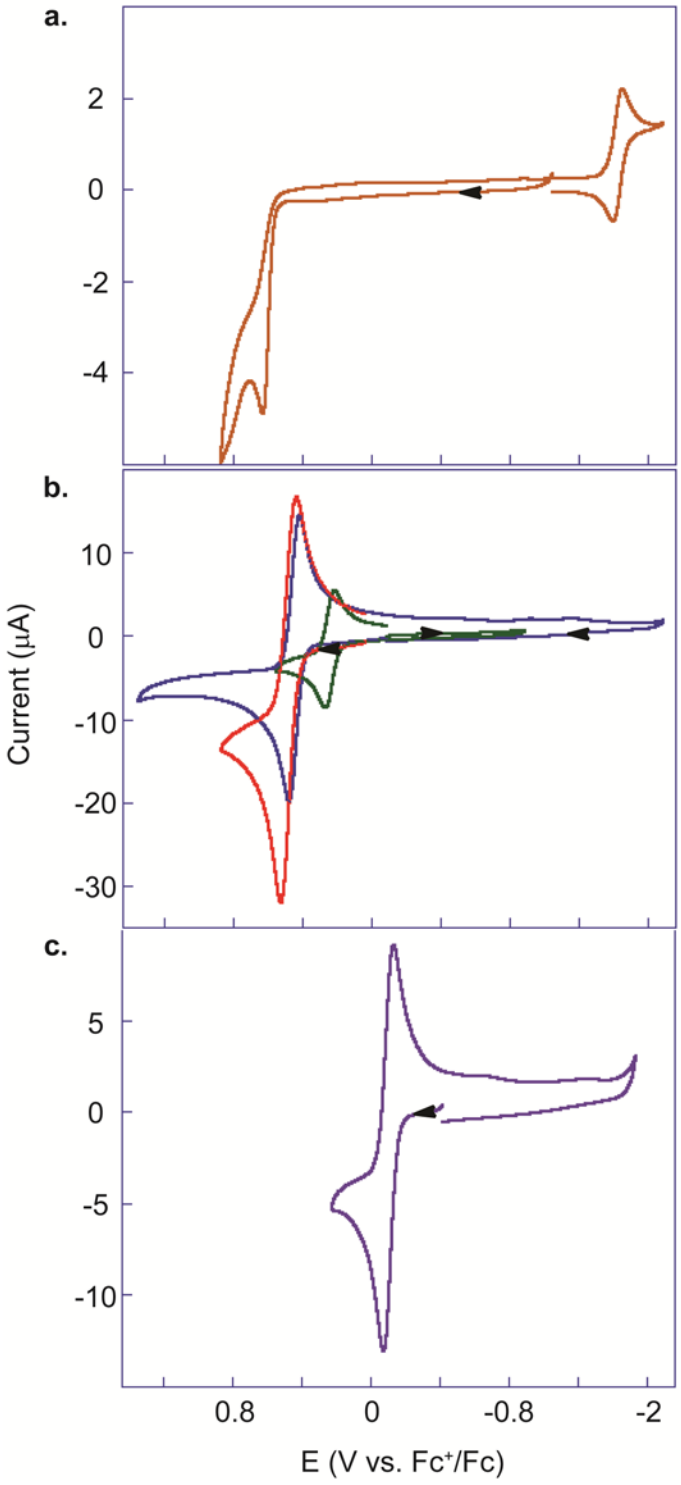


**Figure 5.4.** Cyclic voltammograms of (**a**) TpRe(O)(cat), (**b**) TpRe(O)(3,5-$^{t}$Bu$_2$cat) (red), TpRe(O)(ap$^{Ph}$) (green), and TpRe(O)(OCH$_2$CH$_2$) (blue), and (**c**) [Re$^{VII}$(O)$_2$(ap$^{Ph}$)$_2$]$^-$ in CH$_3$CN containing [$^{n}$Bu$_4$N][PF$_6$] at 100 mV s$^{-1}$ scan rates. All CV scans were measured at 25 $^{o}$C using a 10 mm Pt electrode.

### 5.2.2 Attempted Synthesis of $[Re(O)(ap^{Ph})(isq^{Ph})(Cl)]^{-}$.

In Chapter 4 $[Re^{V}(O)(ap^{Ph})(isq^{Ph})]^{-}$ was shown to rapidly dimerize making it non-isolable. We therefore attempted to trap the $[Re^{V}(O)(ap^{Ph})(isq^{Ph})]^{-}$ monomer with $Cl^{-}$ to generate $[Re^{V}(O)(ap^{Ph})(isq^{Ph})(Cl)]^{-}$. Chemical oxidation of $[Re^{V}(O)(ap^{Ph})_2]^{-}$ in the presence of $Cl^{-}$ salts, or by direct addition of $Cl^{\bullet}$ failed to produce $[Re^{V}(O)(ap^{Ph})(isq^{Ph})(Cl)]^{-}$. This is not too unexpected considering the quasi-reversible behavior of $[Re^{VI}(O)(ap^{Ph})(isq^{Ph})(Cl)]$ reduction. However, addition of 2.4 equiv $Me_3SiCl$ to $CH_2Cl_2$ solutions of $[Re^{V}(O)(ap^{Ph})_2]^{-}$ and heating at 65 $^{o}$C resulted in a color change from pale yellow-green to dark maroon. The maroon product was conveniently purified by silica gel chromatography. Single crystals suitable for X-ray diffraction were grown by slow evaporation of concentrated $CH_2Cl_2$ solutions (Figure 5.5). The solid state structure reveals a pseudo-octahedral, six-coordinate neutral *cis*-dichlororhenium ion with two aminophenol-derived ligands in the *trans* position. The C–O and C–N bond lengths average 1.32 Å and 1.36 Å respectively, which are contracted compared to the $[ap^{Ph}]^{2-}$ ligands in $[Re^{V}(O)(ap^{Ph})_2]^{-}$, $Re^{VI}(O)(ap^{Ph})(isq^{Ph})(OC_6Cl_5)$, and $Re^{VI}(O)(ap^{Ph})(isq^{Ph})(Cl)$ but elongated compared to the $[isq^{Ph}]^{\bullet-}$ ligand in $Re^{VI}(O)(ap^{Ph})(isq^{Ph})(OC_6Cl_5)$ and $Re^{VI}(O)(ap^{Ph})(isq^{Ph})(Cl)$. The C–C bonds also show a loss of aromaticity with a quinoid-like distortion of four long and two short C–C bonds. The sum of the bond distances are in good agreement with the arithmetic mean of those expected for one $[ap^{Ph}]^{2-}$ and one $[isq^{Ph}]^{\bullet-}$ ligand.[32,33] Further support for a S = ½ ground state is evidenced by a solution magnetic moment of 1.77 $\mu_B$ at 25 $^{o}$C in $CD_3CN$ and the absence of well-resolved diamagnetic resonances in the $^{1}$H NMR spectrum. The sum of these data suggest that the complex is best described as $Re^{V}(Cl)_2(ap^{Ph})(isq^{Ph})$ containing a single ligand-centered radical with a S = ½ ground state. It is unknown if the unpaired electron is localized on a single ligand similar to $Re^{VI}(O)(ap^{Ph})(isq^{Ph})(Cl)$ and

$Re^{VI}(O)(ap^{Ph})(isq^{Ph})(OC_6Cl_5)$ or if it is delocalized throughout both of the aminophenol ligands. Both possibilities are just as reasonable.

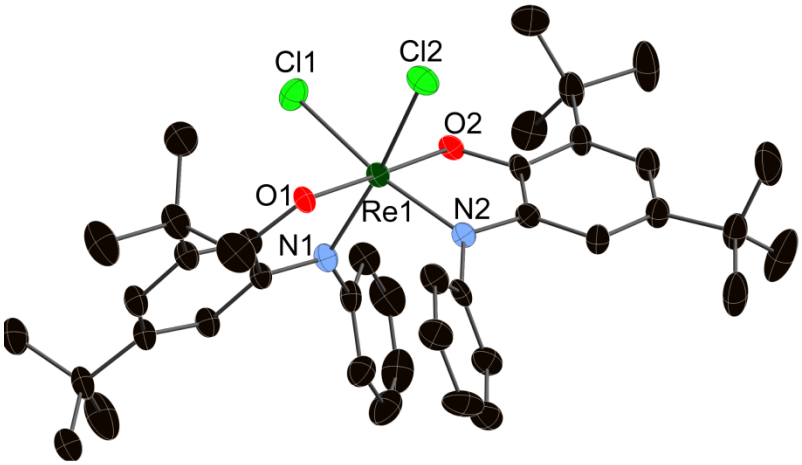


**Figure 5.5.** Solid state structure of $[Re(Cl)_2(ap^{Ph})(isq^{Ph})]$•0.65 $CH_2Cl_2$ show with 50% probability ellipsoids. The hydrogen atoms and $CH_2Cl_2$ solvate are omitted for clarity. Selected bond lengths (Å): Re1-Cl1 2.3681(12), Re1-Cl2 2. 3616(13), C1-O1 1.319(6), C6-N1 1.360(6), C7-O2 1.324(5), C12-N2 1.366(6).

### 5.2.3 Preparation and Characterization of "Masked" Oxyl Radicals.

The electrochemical data for $TpRe^{V}(O)(ap^{Ph})$ and $[Re^{VII}(O)_2(ap^{Ph})_2]^-$ suggested that they are reasonable candidates for generation of "masked" oxyls (Figure 5.1). Since they both show reversible redox events at relatively modest potentials, chemical oxidations were pursued. Addition of 1 equiv $AgBF_4$ to a THF solution of $TpRe^{V}(O)(ap^{Ph})$ gave a gradual color change from brown to green over 15 hours. Removal of solvent followed by washing with ether gave a green solid. Analysis of the green solid by MALDI-MS gave a peak at m/z 711 that matches the neutral starting material consistent with an electron transfer product. However, the UV-vis of $CH_2Cl_2$ solutions of the starting material and green product are significantly different (Figure 5.6). Also, the green solid is

insoluble in ether and pentane suggesting that it is a salt, which is expected for $1e^-$ oxidation of $TpRe^{V}(O)(ap^{Ph})$.

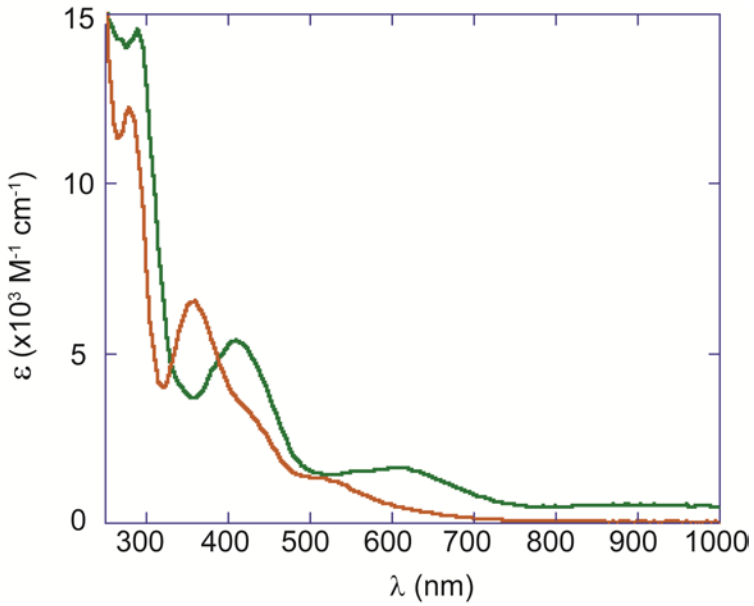


**Figure 5.6.** UV-vis absorption spectra of 2 x $10^{-5}$ M $TpRe(O)(ap^{Ph})$ (brown line) and $[TpRe(O)(isq^{Ph})][BF_4]$ (green line) in MeCN.

Single crystals of the green solid suitable for X-ray analysis were obtained by slow diffusion of ether into a $CH_2Cl_2$ solution. As shown in Figure 5.7, the cation contains rhenium with pseudo-octahedral geometry similar to $TpRe^{V}(O)(ap^{Ph})$ with a Tp ligand and an aminophenol-derived ligand *cis* to a terminal oxo and a $BF_4$ counter anion. While it is structurally similar to $TpRe^{V}(O)(ap^{Ph})$, it is significantly different electronically. The aminophenol-derived ligand has contracted C–O and C–N bond distances of 1.300(13) and 1.371(15) Å, and a quinoid-type pattern of four long and two short C–C bonds, so the metrical data best match those for the $[isq^{Ph}]^{\bullet -}$ radical. This ligand oxidation state implies that the complex is best formulated as $[TpRe^{V}(O)(isq^{Ph})][BF_4]$ containing a ligand

radical. Consistent with this S = ½ radical ground state the solution magnetic moment is 1.72 $\mu_B$ in $CD_3CN$ at 25 $^oC$.

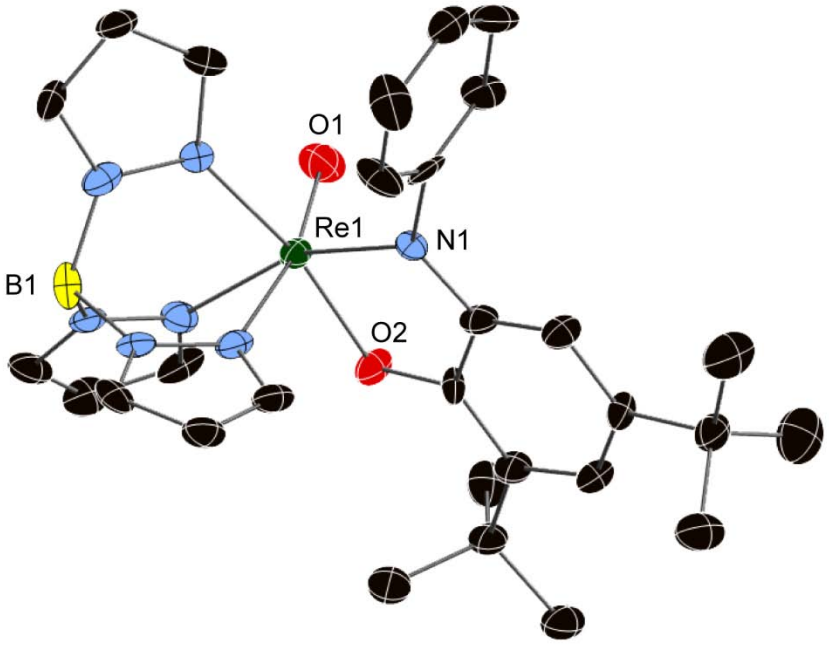


**Figure 5.7.** Solid-state structure of $[TpRe^{V}(O)(isq^{Ph})][BF_4]$•0.28 $CH_2Cl_2$ shown with 50% probability ellipsoids. Hydrogen atoms, $BF_4$ counter anion, and solvent molecule omitted for clarity. Selected bond lengths (Å): Re1-O1 1.662(9), C10-O2 1.300(13), C15-N1 1.371(15).

Addition of 1 equiv $AgBF_4$ to an acetone solution of $[Re(O)_2(ap^{Ph})_2]^-$ rapidly produced a color change from violet to green. Reduction of volume and cooling to –20 $^oC$ produced a green solid. MALDI-MS analysis of the green solid shows a peak at m/z 809 that matches the anionic starting material and as expected for an electron transfer product the lack of NMR signals suggests the presence of a paramagnetic species. Since $[Re(O)_2(ap^{Ph})_2]^-$ contains a $d^0$ metal center the oxidation is necessarily ligand-based producing $Re(O)_2(ap^{Ph})(isq^{Ph})$, but structural data are needed to confirm the

assignment (Scheme 5.1). Dissolving the green material in acetone and stirring overnight at ambient temperature results in a color change to dark purple. Analysis of the purple material by MALDI-MS gave a peak at m/z 1602 corresponding to the dirhenium complex shown in Scheme 5.1.

**Scheme 5.1.**

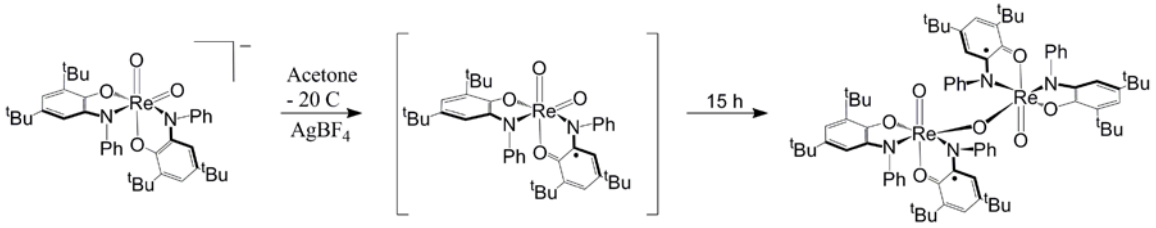


Single crystals suitable for X-ray analysis were grown by slow evaporation of an MeCN solution at –20 $^{o}$C. The structure reveals a neutral dirhenium complex with each rhenium center containing a pseudo-octahedral geometry consisting of two aminophenol-derived ligands in a *cis* arrangement, a terminal oxo ligand and a bridging oxo (Figure 5.8). One MeCN solvent molecule is contained in each unit cell, but is not bound to either rhenium. The two rhenium centers are symmetrical with the bridging oxo occupying a *cis* site to the terminal oxo ligand. Both aminophenol-derived ligands *cis* to the terminal oxos have C–C bond distances that are equidistant within 3σ (1.40 ± 0.02 Å) and has C–O and C–N bond distances of 1.358 ± 0.02 and 1.384 ± 0.03 Å, respectively, suggesting the aminophenol-derived ligands are the fully reduced, closed-shell $[ap^{Ph}]^{2-}$ dianions.[26,27] The amino-phenol derived ligands *trans* to the terminal oxo ligands show a loss of aromaticity with a quinoid pattern of four long and two short C–C bond distances, and shortening of the C–O and C–N bond distance to 1.303 ± 0.03 and 1.367 ± 0.05 Å respectively. These

distances suggest that the ligand is best described as an iminosemiquinonate $[isq^{Ph\bullet}]^{-}$ anion.[33,34] The $Re{\equiv}O_{oxo}$ bond distances of 1.699 ± 0.01 Å are within the anticipated range for a Re–O triple bond in Re(V) and Re(VI) complexes.[35] The sum of these data suggest that the purple product is best described as a $Re_2^{VI}(O)_2(\mu\text{-}O)(ap^{Ph})_2(isq^{Ph})_2$ dimer. The assignment of the purple species as $Re_2^{VI}(O)_2(\mu\text{-}O)(ap^{Ph})_2(isq^{Ph})_2$ means that the reaction in Scheme 5.1 is not balanced. One route to this observed dimer is a reaction of $Re^{VII}(O)_2(ap^{Ph})(isq^{Ph})$ with $Re^{V}(O)(ap^{Ph})(isq^{Ph})$. This requires a net loss of $[O]^{2-}$ (Scheme 5.2). Accordingly, addition of 0.5 equiv $PPh_3$ to $CH_2Cl_2$ solutions of $[Re^{VII}(O)_2(ap^{Ph})(isq^{Ph})]$ resulted in a rapid color change to dark purple. Analysis of the dark purple solution by UV-vis produced a spectrum that was identical to authentic samples of $Re_2^{VI}(O)_2(\mu\text{-}O)(ap^{Ph})_2(isq^{Ph})_2$ (Scheme 5.2a). Mixing excess $PPh_3$ (*ca.* 10 eq.) produces an immediate color change from green to dull-purple. Analysis of the dull-purple solution by UV-vis generated a spectrum that was identical to authentic samples of $Re_2^{V}(\mu\text{-}O)_2(ap^{Ph})_2(isq^{Ph})_2$ (Scheme 5.2b). Addition of excess $PPh_3$ to $[Re^{VII}(O)_2(ap^{Ph})(isq^{Ph})]$ should generate 1 equiv of $Re^{V}(O)(ap^{Ph})(isq^{Ph})$ which is known to rapidly dimerize into $Re_2^{V}(\mu\text{-}O)_2(ap^{Ph})_2(isq^{Ph})_2$. This suggests that $Re_2^{VI}(O)_2(\mu\text{-}O)(ap^{Ph})_2(isq^{Ph})_2$ is produced through dimerization of a $Re^{VII}(O)_2(ap^{Ph})(isq^{Ph})$ transient and a $Re^{V}(O)(ap^{Ph})(isq^{Ph})$ fragment.

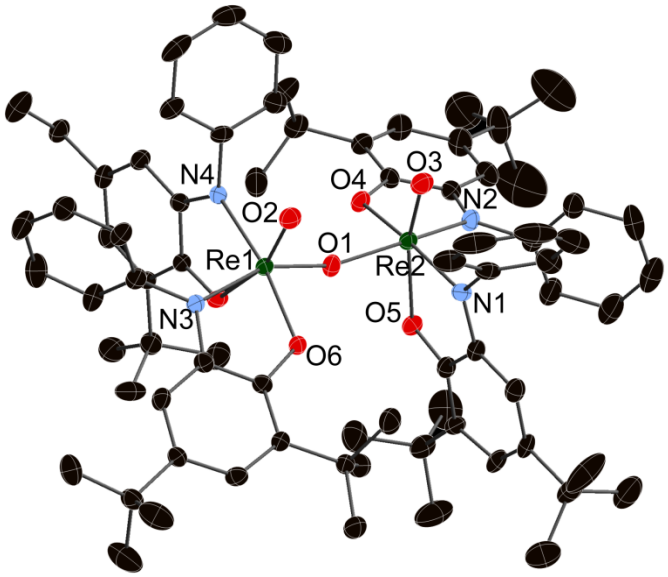


**Figure 5.8.** Solid state structure of $Re_2^{VI}(O)_2(\mu\text{-}O)(ap^{Ph})_2(isq^{Ph})_2$ shown with 50% probability ellipsoids. Hydrogen atoms omitted for clarity. Selected bond lengths (Å): Re1-O2 1.710(3), Re2-O3 1.698(3), Re1-O1 1.885(3), Re2-O1 1.898(3).

**Scheme 5.2.**

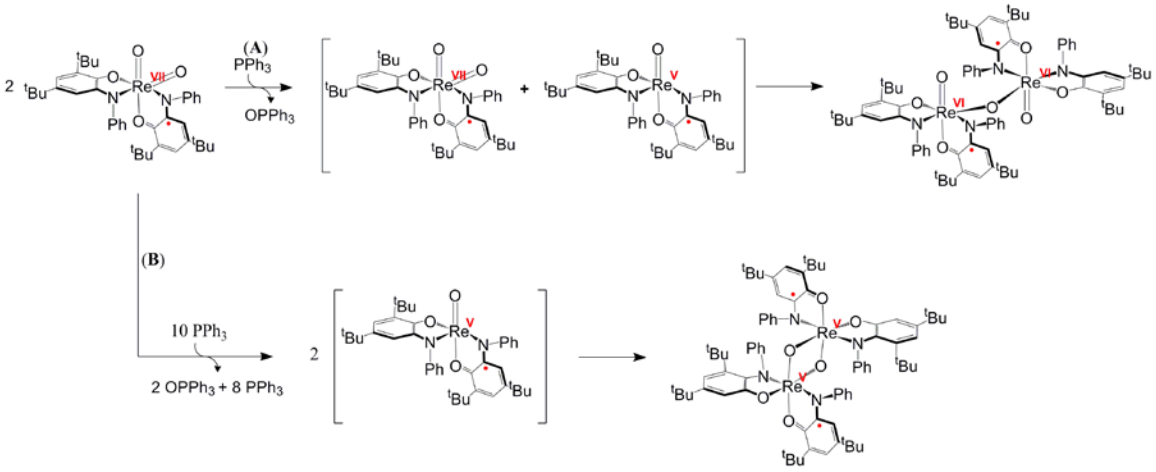

### 5.2.4 Radical Coupling of "Masked" Oxyls.

Based on the criteria defining "masked" oxyl species described in section 5.1, five "masked" oxyl species have been synthesized: $Re^{VI}(O)(ap^{Ph})(isq^{Ph})(Cl)$, $Re^{VI}(O)(ap^{Ph})(isq^{Ph})(OC_6Cl_5)$, $[TpRe(O)(isq^{Ph})]^+$, $Re^{VII}(O)_2(ap^{Ph})(isq^{Ph})$, and $Re_2{}^{VI}(O)_2(\mu\text{-}O)(ap^{Ph})_2(isq^{Ph})_2$ (Table 5.1.). The reactivity of the new "masked" oxyl complexes described above along with $Re^{VI}(O)(ap^{Ph})(isq^{Ph})(Cl)$ described in Chapter 4, were tested with a variety of reagents capable of supplying radicals: $H^\bullet$, $O^\bullet$, $B^\bullet$, $Si^\bullet$, and $C^\bullet$ (Table 5.2). Only a broad and incomplete study has been performed to date, and this section will not go into great detail of the majority of this reactions. However, two reactions showed promise towards oxyl-like radical coupling and will be discussed in more detail in the following section.

**Table 5.1.** List of “masked” oxyl sources.

| Entry | "Masked" Oxyl Source | Name |
|---|---|---|
| 1 | 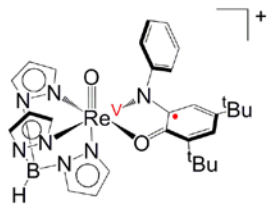 | $[TpRe^{V}(O)(isq^{Ph})][BF_4]$ |
| 2 | 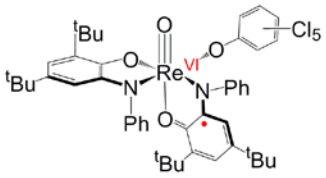 | $Re^{VI}(O)(ap^{ph})(isq^{Ph})(OC_6Cl_5)$ |
| 3 | 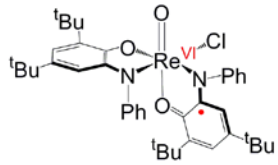 | $Re^{VI}(O)(ap^{ph})(isq^{Ph})(Cl)$ |
| 4 | 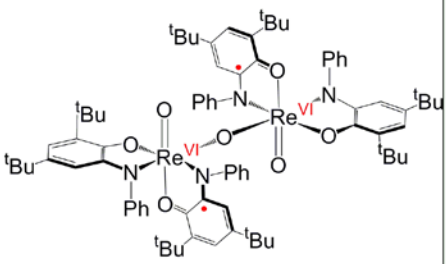 | $Re_2^{VI}(O)_2(\mu\text{-}O)(ap^{Ph})_2(isq^{Ph})_2$ |
| 5 | 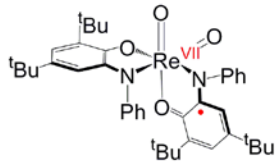 | $Re^{VII}(O)_2(ap^{Ph})(isq^{Ph})$ |

**Table 5.2.** List of Radical Sources and Corresponding "Masked" Oxyl Source for Radical Coupling Reactions.

| "Masked" Oxyl Source | Radical Source | Net Radical |
|---|---|---|
| $[TpRe^{V}(O)(isq^{Ph})][BF_4]$<br>$Re_2^{VI}(O)_2(\mu\text{-}O)(ap^{Ph})_2(isq^{Ph})_2$<br>$Re^{VI}(O)(ap^{ph})(isq^{Ph})(Cl)$ | $Bu_3SnH$ | $[H^{\bullet}]$ |
| $[TpRe^{V}(O)(isq^{Ph})][BF_4]$<br>$Re^{VI}(O)(ap^{ph})(isq^{Ph})(Cl)$ | $TEMPO^{\bullet}$ | $[O^{\bullet}]$ |
| $[TpRe^{V}(O)(isq^{Ph})][BF_4]$<br>$Re^{VI}(O)(ap^{ph})(isq^{Ph})(Cl)$ | $^{t}BuO–O^{t}Bu$ | $[O^{\bullet}]$ |
| $[TpRe^{V}(O)(isq^{Ph})][BF_4]$<br>$Re_2^{VI}(O)_2(\mu\text{-}O)(ap^{Ph})_2(isq^{Ph})_2$<br>$Re^{VI}(O)(ap^{ph})(isq^{Ph})(Cl)$ | Azobisisobutyronitrile | $[C^{\bullet}]$ |
| $[TpRe^{V}(O)(isq^{Ph})][BF_4]$<br>$Re_2^{VI}(O)_2(\mu\text{-}O)(ap^{Ph})_2(isq^{Ph})_2$<br>$Re^{VII}(O)_2(ap^{Ph})(isq^{Ph})$ | $PhMe_2SiB(N^{i}Pr_2)_2$ | $[Si^{\bullet}],[B^{\bullet}]$ |
| $Re^{VI}(O)(ap^{ph})(isq^{Ph})(Cl)$ | Gomberg's Dimer | $[C^{\bullet}]$ |

5.2.4.1 Reactions with a Hydrogen Atom Donor, $H^{\bullet}$

Addition of $Bu_3SnH$ to a MeCN solution of $[TpRe(O)(isq^{Ph})]^{+}$ resulted in a rapid color change from green to brown. Analysis of the brown solution by UV-vis and $^{1}H$ NMR matched that of $TpRe(O)(ap^{Ph})$ exactly suggesting that an electron transfer event occurred with no radical coupling. It is possible that a radical coupling event occurred to generate $[TpRe^{V}(OH)(ap^{Ph})]^{+}$ which rapidly loses a proton to produce $TpRe(O)(ap^{Ph})$. One possible explanation for the instability of the hydroxo complex could be that weaker π donation by the $[OH]^{-}$ ligand would be unsuitable to stabilize the high rhenium oxidation state (Scheme 5.3). Addition of $Bu_3SnH$ to $Re_2^{VI}(O)_2(\mu\text{-}O)(ap^{Ph})_2(isq^{Ph})_2$ and $Re^{VI}(O)(ap^{Ph})(isq^{Ph})(Cl)$ gave a complex mixture of unidentifiable organic and inorganic products by MALDI-MS, GC-MS, and $^{1}H$ NMR spectroscopy.

**Scheme 5.3.**

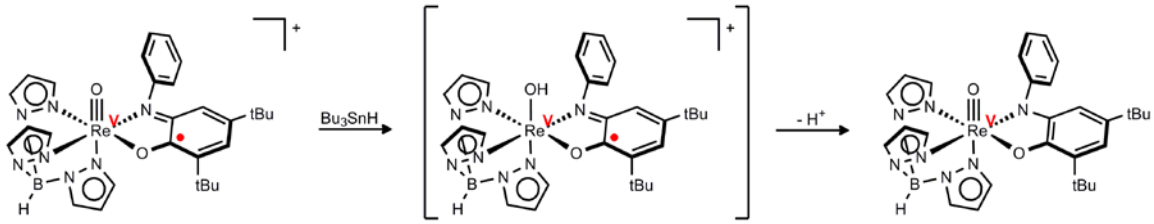


5.2.4.2 Reactions with Azobisisobutyronitrile, C•

Addition of Azobisisobutyronitrile (AIBN) to toluene solutions of $[TpRe(O)(isq^{Ph})]^{+}$, $Re_2^{VI}(O)_2(\mu\text{-}O)(ap^{Ph})_2(isq^{Ph})_2$, and $Re^{VI}(O)(ap^{Ph})(isq^{Ph})(Cl)$ gave no reaction over days at ambient temperatures. However, upon heating to 80 $^{o}$C the diazo compound thermolyses to generate two equiv of $CN(CH_3)_2C^{\bullet}$ and $N_2$ gas.[36,37] The three "masked" oxyl species behaved differently towards the net $[C]^{\bullet}$ source. As with the $H^{\bullet}$ reaction above, $[TpRe^{V}(O)(isq^{Ph})]^{+}$ produced $TpRe^{V}(O)(ap^{Ph})$ as evidenced by comparison of the UV-vis and $^{1}$H NMR spectra to authentic samples of the isolated brown product. Both $Re_2^{VI}(O)_2(\mu\text{-}O)(ap^{Ph})_2(isq^{Ph})_2$, and $Re^{VI}(O)(ap^{Ph})(isq^{Ph})(Cl)$ gave a slow color change from dark purple to a dull-purple. Analysis of the dull-purple by GC-MS, MALDI-MS, and $^{1}$H NMR gave a complex mixture of unidentifiable products. Analysis of the same reaction mixtures by UV-vis produced a spectrum matching $Re_2^{V}(\mu\text{-}O)_2(ap^{Ph})_2(isq^{Ph})_2$.

5.2.4.3 Reactions with $PhMe_2SiB(N^{i}Pr_2)_2$, Si• and B•

Exposure of $PhMe_2SiB(N^{i}Pr_2)_2$ to ultraviolet radiation below 320 nm results in photolysis to generate $PhMe_2Si^{\bullet}$ and $^{\bullet}B(N^{i}Pr_2)_2$.[38] Addition of 1 equiv $PhMe_2SiB(N^{i}Pr_2)_2$ to benzene solutions of $[TpRe^{V}(O)(isq^{Ph})]^{+}$ results in a rapid color change to brown. Analysis of the brown reaction mixture by UV-vis matched that of $TpRe(O)(ap^{Ph})$ exactly while GC-MS of the same solution gave a complex mixture of organic products. This suggests that, similar to reaction with $Bu_3SnH$, only an electron transfer event occurs to

reduce $[TpRe^{V}(O)(isq^{Ph})]^{+}$ to $TpRe(O)(ap^{Ph})$. The fate of the $PhMe_2SiB(N^{i}Pr_2)_2$ reagent is unknown. Addition of 1 equiv $PhMe_2SiB(N^{i}Pr_2)_2$ to benzene solutions of $[Re(O)_2(ap^{Ph})(isq^{Ph})]$ results in a rapid color change to purple. Analysis of the purple solution by GC-MS, MALDI, MS, and $^{1}H$ NMR gave a complex mixture of unidentifiable products. Analysis of the same reaction mixtures by UV-vis produced a spectrum that did not match any isolated rhenium complexes described in this thesis.

Addition of 0.5-2.0 equiv $PhMe_2SiB(N^{i}Pr_2)_2$ to a benzene solution of $Re_2^{VI}(O)_2(\mu\text{-}O)(ap^{Ph})_2(isq^{Ph})_2$ gave no reaction over days at ambient temperature in the absence of light. However, when the reaction mixture was irradiated with UV light for 5 h a color change from dark purple to dull-purple was observed. Analysis of the reaction mixture by UV-vis produced a spectrum matching $Re_2^{V}(\mu\text{-}O)_2(ap^{Ph})_2(isq^{Ph})_2$, while MALDI-MS of the same solution gave peaks at m/z 944, 1079, and 1586. The peaks at m/z 944 and 1079 correspond to a $[Re(O)_2(L)_2]$ (L = aminophenol-derived) core plus one and two $[PhMe_2Si]$ fragments respectively while the peak at m/z 1586 corresponds to the known $Re_2^{V}(\mu\text{-}O)_2(ap^{Ph})_2(isq^{Ph})_2$ dimer (Scheme 5.4). The two siloxy containing metal species would be expected to be brightly colored, and the observation of mainly $Re_2^{V}(\mu\text{-}O)_2(ap^{Ph})_2(isq^{Ph})_2$ in the UV-vis suggests that they are formed in comparatively low yield. Analysis of the same reaction mixture by GC-MS revealed $PhMe_2SiOH$ and $(PhMe_2Si)_2O$ as the major products (Scheme 5.4). Minor products in the GC-MS included $PhMe_2SiH$, $(PhMe_2Si)_2$, $PhMe_2Si(C_6H_5)$, and $HB(N^{i}Pr_2)_2$. The sum of these data suggests that an oxo transfer reaction has occurred. Photolysis of $PhMe_2SiB(N^{i}Pr_2)_2$ in the presence of $O_2$ did not show any production of $PhMe_2SiOH$ by GC-MS. Interestingly, $Re_2^{VI}(O)_2(\mu\text{-}O)(ap^{Ph})_2(isq^{Ph})_2$ does not react with excess $PPh_3$ (*ca.* 20 equiv) over days at ambient temperature, suggesting that $Re_2^{VI}(O)_2(\mu\text{-}O)(ap^{Ph})_2(isq^{Ph})_2$ is not a strong thermodynamic oxo donor.

**Scheme 5.4.**

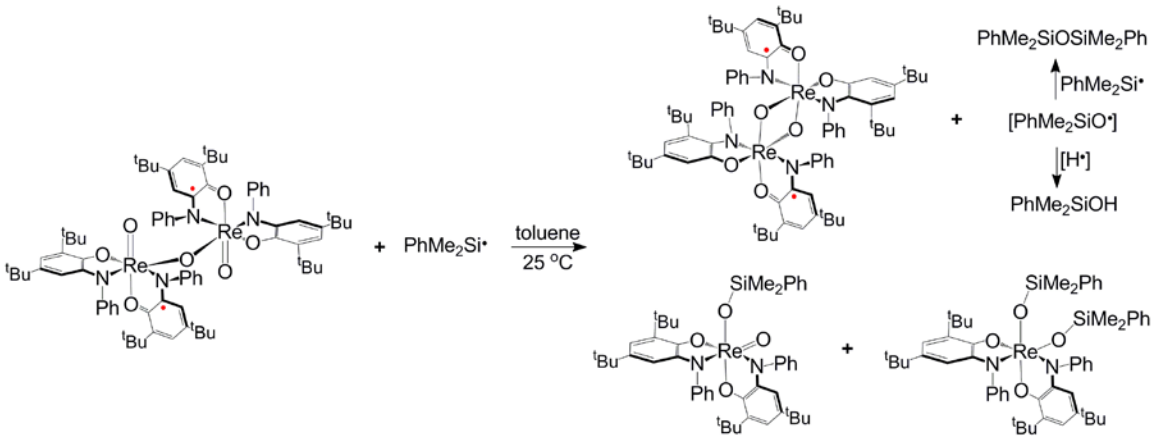


As illustrated in Scheme 5.4, the immediate product of net oxo transfer from $Re_2^{VI}(O)_2(\mu\text{-}O)(ap^{Ph})_2(isq^{Ph})_2$ to $PhMe_2Si^{\bullet}$ is a dimethylphenylsiloxyl $PhMe_2SiO^{\bullet}$ radical. Generation of $PhMe_2SiOH$ requires net addition of 1 equiv $H^{\bullet}$ while generation of $(PhMe_2Si)_2O$ could result from radical trapping of the dimethylphenylsiloxyl $PhMe_2SiO^{\bullet}$ radical by another $PhMe_2Si^{\bullet}$ generated through photolysis of $PhMe_2SiB(N^iPr_2)_2$. Mixing $[Re^V(O)(ap^{Ph})_2]^-$ or $[Re^{VII}(O)_2(ap^{Ph})_2]^-$ with 2 equiv $PhMe_2SiB(N^iPr_2)_2$ gave no reaction over days at ambient temperature in the dark, and no reaction after 5 h of irradiation with UV light. The implications of these results for the mechanism of oxo transfer in Scheme 5.4 are discussed in section 5.3.

5.2.4.4 Reaction with Gomberg's Dimer, $C^{\bullet}$

Addition of 1.1 equiv triphenylmethyl radical $Ph_3C^{\bullet}$ to a benzene solution of $Re^{VI}(O)(ap^{Ph})(isq^{Ph})Cl$, with exclusion of ambient light, results in a slow color change from dark violet to red-purple over 1 week at ambient temperature. Stoichiometric amounts of $Ph_3C^{\bullet}$ were used, however, the actual concentration of the free radical in benzene is 2% of the Gomberg dimer.[39] Analysis of the reaction mixture by GC-MS revealed triphenylmethanol $PH_3COH$ as the major product in 69% yield based on limiting

rhenium. Minor products include benzophenone and triphenylmethane, which make up <10% of the total $Ph_3C^{\bullet}$-derived material. The red-purple solution contained three rhenium products which were separated and isolated by column chromatography. These are unreacted $Re^{VI}(O)(ap^{Ph})(isq^{Ph})Cl$ starting material, $Re_2^{V}(\mu\text{-}O)_2(ap^{Ph})_2(isq^{Ph})_2$ dimer, and $Re^{V}(Cl)_2(ap^{Ph})(isq^{Ph})$, and the identity of all three was confirmed by comparison of the UV-vis spectra to authentic samples prepared independently. The yields of both organic and rhenium products are suggestive of an oxo transfer reaction (Scheme 5.5).

**Scheme 5.5.**

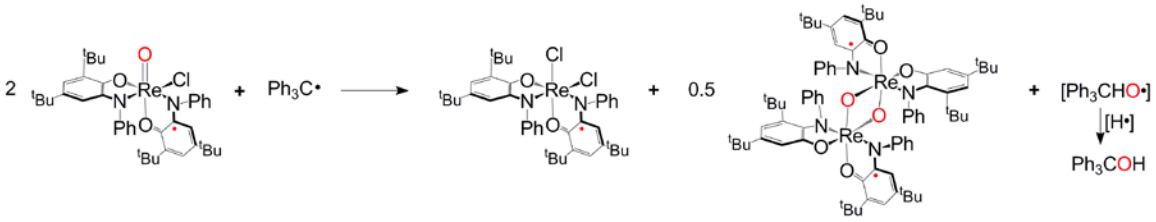


The immediate product of net oxo transfer from $Re^{VI}(O)(ap^{Ph})(isq^{Ph})Cl$ to $Ph_3C^{\bullet}$ is a triphenylmethoxyl radical $Ph_3CO^{\bullet}$. However, this species undergoes a rapid 1,2-phenyl shift to produce α-phenoxydiphenylmethyl radical.[40,41] The observation of $Ph_3COH$ in high yield suggests that free $Ph_3CO^{\bullet}$ radical is not an intermediate in the reaction. The production of $Ph_3COH$ from a net source of $Ph_3CO^{\bullet}$ requires addition of 1 equiv $H^{\bullet}$. The source of the $H^{\bullet}$ is unknown. Exposure of the $Ph_3C^{\bullet}$ radical to $O_2$ under analogous conditions did not produce any $Ph_3COH$. Mixing $Re_2^{V}(\mu\text{-}O)_2(ap^{Ph})_2(isq^{Ph})_2$ and $Ph_3C^{\bullet}$ or $[Ph_3C][BF_4]$ (1-30 eq.) over 2-6 days at ambient temperature gave negligible change in

the UV-vis spectra and analysis of the reaction mixture by GC-MS showed no production of $Ph_3COH$.

Addition of 1 equiv $Ph_3C^{\bullet}$ to $[Re^{V}(O)(ap^{Ph})_2]^{-}$ in benzene gave slow conversion over 24 h to a slightly darker yellow-green solution that contained 15-30% of the $1e^{-}$ oxidized product $Re^{V}_2(\mu\text{-}O)_2(ap^{Ph})_2(isq^{Ph})_2$. Analysis of the same reaction mixture by GC-MS again showed no production of $Ph_3COH$. Mixing 1 equiv $[Ph_3C][BF_4]$ to a benzene solution of $[Re^{V}(O)(ap^{Ph})_2]^{-}$ results in a rapid color change from pale yellow-green to dull-purple. Analysis of the purple reaction mixture by MALDI-MS and UV-vis spectroscopy after 24 h at ambient temperature confirmed the identity of the purple material as $Re_2^{V}(\mu\text{-}O)_2(ap^{Ph})_2(isq^{Ph})_2$ in 90% isolated yield based on rhenium. No $Ph_3COH$ is formed during the reaction suggesting that the $[Ph_3C]^{+}$ is a competent $1e^{-}$ oxidant for $[Re^{V}(O)(ap^{Ph})_2]^{-}$ but the two are unsuitable for an oxo transfer reaction. Exposure of $[Re^{VII}(O)_2(ap^{Ph})_2]^{-}$ in a 90:10 benzene:MeCN solution to 1 equiv $Ph_3C^{\bullet}$ resulted in no obvious color change and no $Ph_3COH$ production by GC-MS.

## 5.3 Discussion

### 5.3.1 Re–O Bond Formation via Metal-Centered Radical Trapping

The propensity for the five-coordinate “masked” oxyl complexes to dimerize directed us to pursue isolation of coordinatively-saturated complexes that fit the criteria to be “masked” oxyl radicals. However, oxidation of $[Re^{VII}(O)_2(ap^{Ph})_2]^{-}$ by chemical oxidants ultimately lead to a dimerized product. Unlike the previous dimer, sufficient X-ray data was obtained to assign oxidation states of the metal and ligands as a neutral $Re_2^{VI}(O)_2(\mu\text{-}O)(ap^{Ph})_2(isq^{Ph})_2$. The dimer complex and corresponding oxidation states are unexpected from the reaction conditions and warrant further discussion. The dimerized product requires a net loss of an [O] atom and reduction of the Re(VII) to Re(VI). As described above it is believed that the generation of the dimer proceeds through a $[Re^{VII}(O)_2(ap^{Ph})(isq^{Ph})]$ intermediate. Loss of an [O] atom from $Re^{VII}(O)_2(ap^{Ph})(isq^{Ph})$

would generate $Re^{V}(O)(ap^{Ph})(isq^{Ph})$ which is known to rapidly dimerize to $Re_2^{V}(\mu\text{-}O)_2(ap^{Ph})_2(isq^{Ph})_2$; the fate of the [O] atom is unknown. From this result it is not unreasonable that $Re^{V}(O)(ap^{Ph})(isq^{Ph})$ and $[Re^{VII}(O)_2(ap^{Ph})(isq^{Ph})]$ would dimerize to produce $Re_2^{VI}(O)_2(\mu\text{-}O)(ap^{Ph})_2(isq^{Ph})_2$. This draws parallels to radical trapping of oxygenic radicals, such as $O_2$ and $TEMPO^{\bullet}$, by $[Re^{V}(O)(ap^{Ph})_2]^{-}$ to form a Re–O bond, suggesting that $[Re^{VII}(O)_2(ap^{Ph})(isq^{Ph})]$ has oxyl-like behavior. Reactions of $[Re^{VII}(O)_2(ap^{Ph})(isq^{Ph})]$ with oxo acceptors suggest that the reaction of $[Re^{VII}(O)_2(ap^{Ph})(isq^{Ph})]$ with $Re^{V}(O)(ap^{Ph})(isq^{Ph})$ is a reasonable route to the dimer (Scheme 5.2). When excess $PPh_3$ (*ca.* 10 eq.) is added to $Re^{VII}(O)_2(ap^{Ph})(isq^{Ph})$ an OAT reaction occurs rapidly producing $Re^{V}(O)(ap^{Ph})(isq^{Ph})$ which rapidly dimerizes into $Re_2^{V}(\mu\text{-}O)_2(ap^{Ph})_2(isq^{Ph})_2$. However, when a sub stoichiometric amount of $PPh_3$ (0.5 eq.) is added slowly the $Re_2^{VI}(O)_2(\mu\text{-}O)(ap^{Ph})_2(isq^{Ph})_2$ dimer is produced. This would generate 0.5 equiv of $Re^{V}(O)(ap^{Ph})(isq^{Ph})$ which could rapidly interact with the remaining $Re^{VII}(O)_2(ap^{Ph})(isq^{Ph})$ to produce the observed dimeric complex. This supports that the $Re^{VII}(O)_2(ap^{Ph})(isq^{Ph})$ being trapped by $Re^{V}(O)(ap^{Ph})(isq^{Ph})$ in mechanism (i) of Scheme 5.6 to make $Re_2^{VI}(O)_2(\mu\text{-}O)(ap^{Ph})_2(isq^{Ph})_2$. This is only one possible mechanism that explains formation of dimer and the reaction with $PPh_3$. Mechanism (iii) can be ruled because there is no evidence of $O_2$ evolution or generation of $Re^{VI}(\mu\text{-}O)_2(ap^{Ph})_2(isq^{Ph})_2$. Electron transfer shown in mechanism (ii) is downhill by *ca.* 1 kcal $mol^{-1}$, so it is just as likely and cannot be ruled out. This reaction has not been the topic of a complete study and more experiments are needed to develop a thorough discussion of the reaction mechanism.

**Scheme 5.6.**

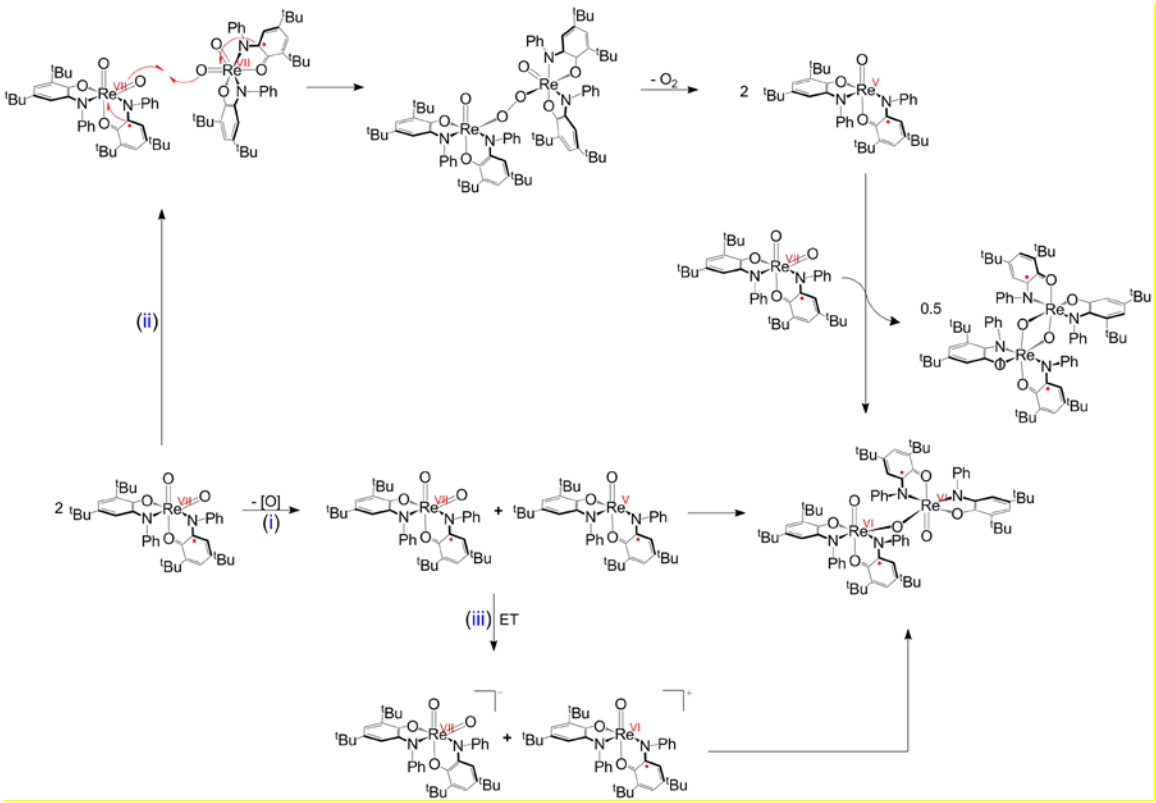

The comproportion reaction of $Re^{VI}(O)(ap^{Ph})(isq^{Ph})Cl$ and $[Re^{V}(O)(ap^{Ph})_2]^{-}$ to generate $Re_2^{V}(\mu\text{-}O)_2(ap^{Ph})_2(isq^{Ph})_2$ deserves further consideration. There are three possible mechanisms, shown in Scheme 5.7, for the generation of $Re_2^{V}(\mu\text{-}O)_2(ap^{Ph})_2(isq^{Ph})_2$ by mixing $Re^{VI}(O)(ap^{Ph})(isq^{Ph})Cl$ and $[Re^{V}(O)(ap^{Ph})_2]^{-}$. Mechanism (*i*) of initial $Cl^{-}$ dissociation followed by electron transfer can be ruled out due to the rate of the reaction being unaffected by addition of excess $Cl^{-}$ (as 100 eq. $[Et_4N]Cl$) to the reaction mixture. $Re^{VI}(O)(ap^{Ph})(isq^{Ph})Cl$ is reduced at $E_{pc}$ = –0.59 V and $[Re^{V}(O)(ap^{Ph})_2]^{-}$ is oxidized at $E_{pa}$ = –0.35 V, so initial outer-sphere electron transfer in mechanism (*ii*) is

thermodynamically uphill by *ca.* 6 kcal mol$^{-1}$. Independent experiments have shown that the resulting electron transfer products Re$^{V}$(O)(ap$^{Ph}$)(isq$^{Ph}$) and [Re$^{V}$(O)(ap$^{Ph}$)(isq$^{Ph}$)Cl]$^{-}$ will rapidly dimerize to Re$_2^{V}$(μ-O)$_2$(ap$^{Ph}$)$_2$(isq$^{Ph}$)$_2$, so mechanism (*ii*) cannot be ruled out.

**Scheme 5.7.**

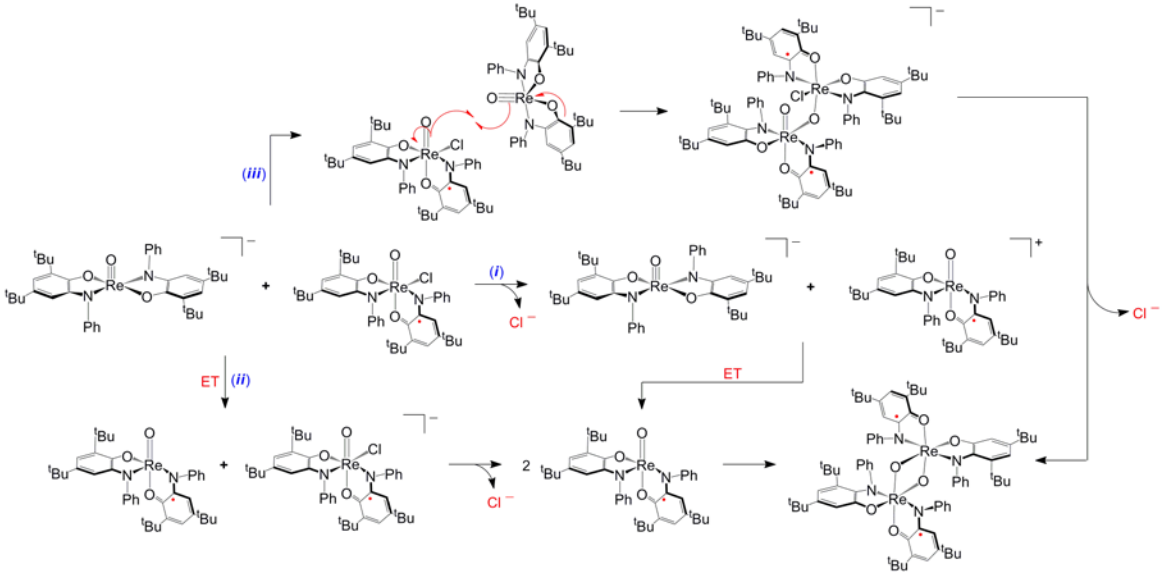


Mechanism (*iii*) invokes direct attack of the oxo ligand in Re$^{VI}$(O)(ap$^{Ph}$)(isq$^{Ph}$)Cl on [Re$^{V}$(O)(ap$^{Ph}$)$_2$]$^{-}$ to initially generate an asymmetric μ-oxo dimer, followed by loss of Cl$^{-}$ and collapse of the dimer to generate the second Re–O bond in Re$_2^{V}$(μ-O)$_2$(ap$^{Ph}$)$_2$(isq$^{Ph}$)$_2$. The first step of this proposed mechanism is particularly interesting because it too parallels the trapping of oxygenic radicals to generate new Re–O bonds discussed in Chapters 2-4. An intriguing consequence of this proposal is that it requires Re$^{VI}$(O)(ap$^{Ph}$)(isq$^{Ph}$)Cl be a source of an oxyl metal fragment.

### 5.3.2 Radical Coupling at Oxyl-Like Terminal Oxo Ligands

The capacity of six-coordinate oxorhenium complexes containing ligand radicals to undergo radical coupling at the oxo ligand is revealed by their reactions with $PhMe_2Si^{\bullet}$ and trityl $Ph_3C^{\bullet}$ radicals. As described above, the rhenium and organic products of Scheme 5.4 are suggestive of net oxo transfer from $Re^{VI}(O)_2(\mu\text{-}O)(ap^{Ph})_2(isq^{Ph})_2$ to $PhMe_2Si^{\bullet}$. The net source of $[Si]^{\bullet}$ is only formed upon photolysis and high-energy UV light is required for the reaction to occur, suggesting that the O–Si bond-forming event proceeds through a radical mechanism at the oxo ligand in $Re^{VI}(O)_2(\mu\text{-}O)(ap^{Ph})_2(isq^{Ph})_2$. This would generate a dimethylphenylsiloxide complex $[Re^{V}(OSiMe_2Ph)(ap^{Ph})(isq^{Ph})(\mu\text{-}O)Re^{VI}(O)(ap^{Ph})(isq^{Ph})]$ which could likely fragment, facilitated by both steric constraints and electronic requirements needed to stabilize the high oxidation state, into the two monomers $Re^{VI}(O)(OSiMe_2Ph)(ap^{Ph})(isq^{Ph})$ and $Re^{V}(O)(ap^{Ph})(isq^{Ph})$ where the latter is known to rapidly dimerize into $Re_2{}^{V}(\mu\text{-}O)_2(ap^{Ph})_2(isq^{Ph})_2$ (Scheme 5.8). The $Re^{V}(O)(OSiMe_2Ph)(ap^{Ph})(isq^{Ph})$ monomer would be structural similar to $Re^{VI}(O)(ap^{Ph})(isq^{Ph})(Cl)$ and it proposed based on molecular ion peaks observed in the MALDI-MS that match theoretical isotopic distribution for addition of a $[PhMe_2Si]$ fragment to a monomeric dioxorhenium core with two aminophenol-derived ligands (Figure 5.11). The observation of multiple rhenium and organic products in variable yields makes it impossible to delineate a mechanism without a more detailed study.

**Scheme 5.8.**

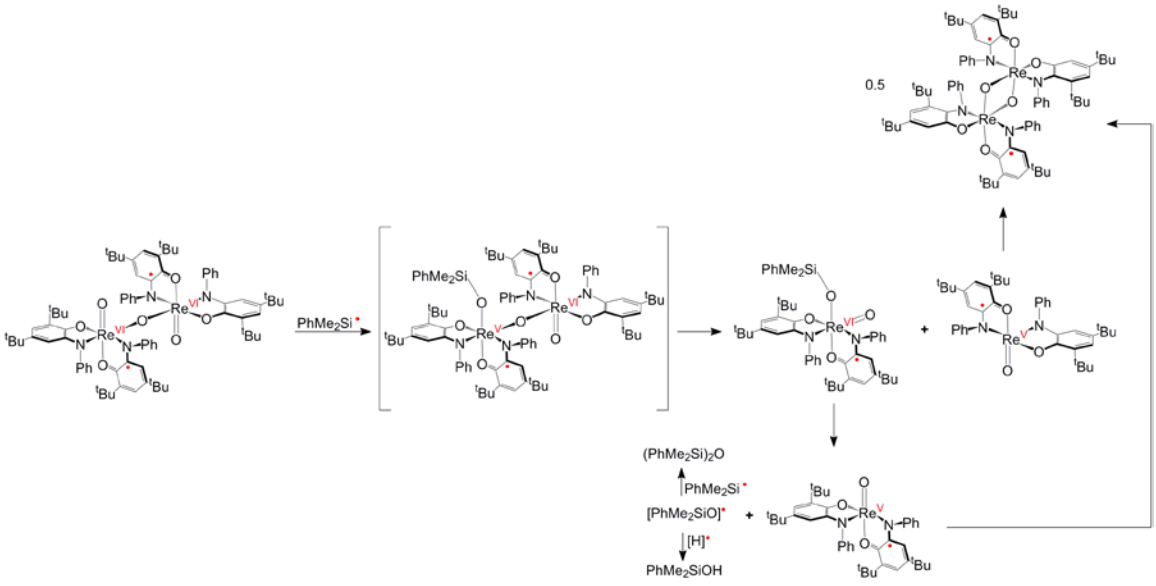

Formation of $PhMe_2SiOH$ from the putative siloxide complex requires 1 equiv $H^{\bullet}$, but added reductants were not needed to observe $PhMe_2SiOH$. Generation of $(PhMe_2Si)_2O$ could occur by three routes (Scheme 5.9.). One possibility is (a) dissociation of the siloxyl radical $PhMe_2SiO^{\bullet}$ which is rapidly trapped by another molecule of $PhMe_2Si^{\bullet}$ generated through photolysis to make the disiloxane. Pathway (b) may be a possible side route to the silanol and disiloxane, but it cannot be the major pathway due to lack of formation of the $Re_2^{V}(\mu\text{-}O)_2(ap^{Ph})_2(isq^{Ph})_2$ dimer. Pathway (c) leads to the correct products and cannot be confirmed or ruled out without a more detailed mechanistic study. The multitude of products and lack of yields make it unfeasible to decipher a mechanism. It is most likely that multiple pathways are occurring simultaneously.

**Scheme 5.9.**

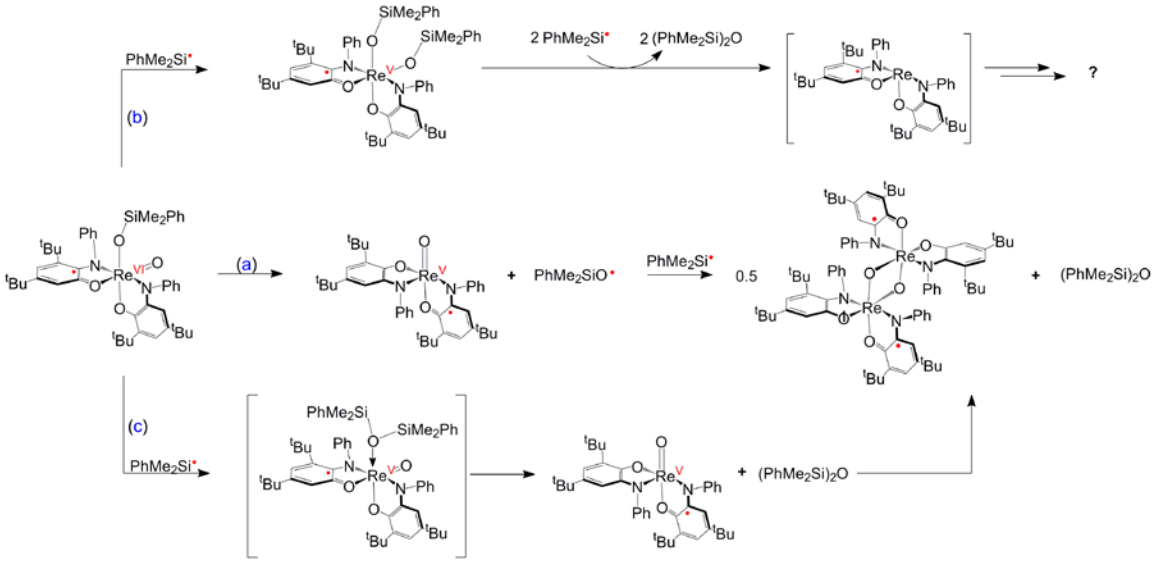


The oxyl-like behavior of these types of complexes is further supported by the ability of $Re^{VI}(O)(ap^{Ph})(isq^{Ph})Cl$ to undergo a radical coupling reaction with trityl $Ph_3C^{\bullet}$ at the terminal oxo ligand. Similar to the reaction of $Re^{VI}(O)_2(\mu\text{-}O)_2(ap^{Ph})_2(isq^{Ph})_2$ with $Si^{\bullet}$, the products in Scheme 5.5 are consistent with net oxo transfer from $Re^{VI}(O)(ap^{Ph})(isq^{Ph})Cl$ to $Ph_3C^{\bullet}$. The net product of O atom transfer would produce a triphenylmethoxyl $Ph_3CO^{\bullet}$ radical which is known to degrade rapidly in solution suggesting that a tripenylmethoxide complex, $Re^{V}(OCPh_3)(ap^{Ph})(isq^{Ph})Cl$, is formed prior to $Ph_3COH$ generation. Even though $Re^{V}(OCPh_3)(ap^{Ph})(isq^{Ph})Cl$ is never observed during the course of the reaction it holds remarkable similarities to the dimethylphenylsiloxide complex, $Re^{VI}(O)(OSiMe_2Ph)(ap^{Ph})(isq^{Ph})$, discussed above.

Two mechanistic possibilities for formation of the putative alkoxide complex are shown in Scheme 5.10. The product of electron transfer (ET) from $Re^{VI}(O)(ap^{Ph})(isq^{Ph})Cl$ to $Ph_3C^{\bullet}$ would produce $[Re^{VI}(O)(ap^{Ph})(isq^{Ph})Cl]^{-}$ and $[Ph_3C]^{+}$. The anionic complex, $Re^{VI}(O)(ap^{Ph})(isq^{Ph})Cl]^{-}$, is known to rapidly dimerize into $Re_2{}^{V}(\mu\text{-}O)_2(ap^{Ph})_2(isq^{Ph})_2$ which

is inert towards $[Ph_3C]^+$ therefore making mechanism (*i*) unlikely unless $Re^{VI}(O)(ap^{Ph})(isq^{Ph})Cl]^-$ is rapidly trapped by $[Ph_3C]^+$. Mechanism (*ii*) of radical trapping of $Ph_3C^\bullet$ by $Re^{VI}(O)(ap^{Ph})(isq^{Ph})Cl$ is more reasonable. It is not rare for metal oxo complexes to react with carbon radicals to make C–O bonds. For example, $Cr(O)_2Cl_2$ complexes are known to form alkoxide species upon $R^\bullet$ addition.[42] There is also relevant literature supporting a hydroxyl rebound-type mechanism for $Ph_3CH$ oxidation that produces the C–O bond in $Ph_3COH$ by trapping $Ph_3C^\bullet$ at a M–OH transient.[43-46] Generation of $PH_3COH$ from the alkoxide complex requires 1 equiv $H^\bullet$ similar to $PhMe_2SiOH$ formation described above, but added reductants were not needed to observe $Ph_3COH$.

**Scheme 5.10.**

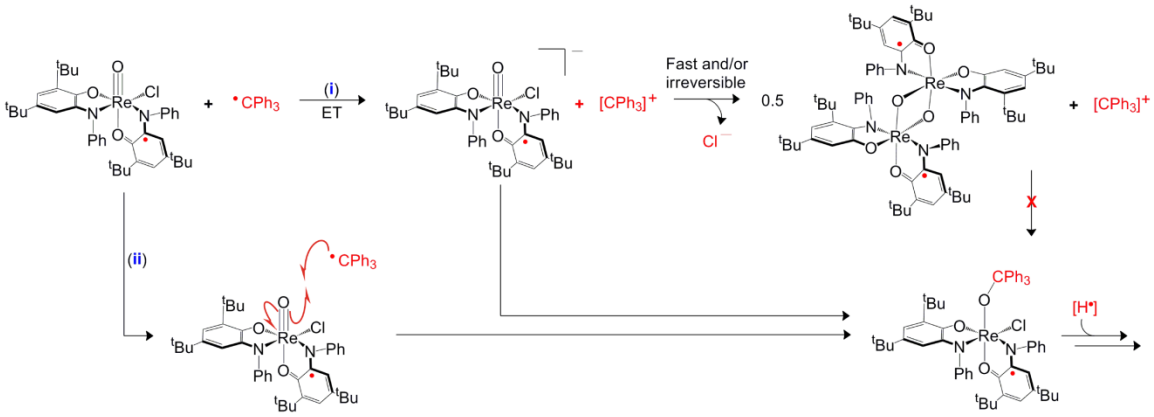


There is a distinctive divergence of reactivity between the closed-shell oxorhenium complexes and the “masked” oxyl, oxorhenium complexes containing a ligand radical. The closed-shell complexes $[Re^V(O)(ap^{Ph})_2]^-$ and $[Re^{VII}(O)_2(ap^{Ph})_2]^-$ react as typical $2e^-$ O atom acceptors and donors respectively while the “masked” oxyl

complexes $Re_2^{VI}(O)_2(\mu\text{-}O)_2(ap^{Ph})_2(isq^{Ph})_2$ and $Re^{VI}(O)(ap^{Ph})(isq^{Ph})(Cl)$ are poor thermodynamic oxo donors evidenced by their inability to oxidize $PPh_3$. However, they are able to perform oxygen atom transfer reactions to radical substrates. Although Mayer and coworkers have convincingly argued that unpaired spin density at oxygen is not a prerequisite for radical $R^{\bullet}$ addition at a terminal oxo group, recent literature reports continue to suggest that complexes with ligand free radicals are competently active for radical bond-making and bond-breaking reactions at ligands.[21-23] In those regards, the O-Si and O-C bond forming reactions at the oxo ligand described in this chapter are unusual radical scavengers in that they are not strong oxidants nor a ground state oxyl radicals.

### 5.3.3 Common Properties of "Masked" Oxyls Capable of Radical Coupling at a Terminal Oxo Ligand

Comparing the structural and electronic properties of the series of "masked" oxyl species that were successful at radical coupling at the terminal oxo ligand to those that were not reveals a trend. Of the various types of isolated "masked" oxyls in Table 5.1, only $Re^{VI}(O)(ap^{Ph})(isq^{Ph})(Cl)$ and $Re_2^{VI}(O)_2(\mu\text{-}O)(ap^{Ph})_2(isq^{Ph})_2$ were reactive towards radical coupling at the oxo ligand. Both have a $d^1$, Re(VI) metal center, a terminal oxo ligand, and an $[isq^{Ph}]^{\bullet-}$ ligand radical *trans* to the terminal oxo. $Re^{VI}(O)(ap^{Ph})(isq^{Ph})(OC_6Cl_5)$ would most likely be capable of radical coupling at the oxo, but was not explored due to the lability of the phenoxide ligand. The complexes that were unsuccessful at radical coupling reactions are $[TpRe(O)(isq^{Ph})]^{+}$ which consisted of a $d^2$, Re(V) center with a terminal oxo ligand and an $[isq^{Ph}]^{\bullet-}$ ligand radical *cis* to the terminal oxo and $Re^{VII}(O)_2(ap^{Ph})(isq^{Ph})$. The $Re^{VII}(O)_2(ap^{Ph})(isq^{Ph})$ is very oxidizing and unstable is solution.

It appears that a $d^1$ metal center with a terminal oxo ligand having a *trans* $[isq^{Ph}]^{\bullet-}$ ligand radical is required to give oxyl-like character to the oxo ligand. It is unknown why

a *cis* orientation does not work. Both orientations should allow mixing of the $[isq^{Ph}]^{\bullet-}$ SOMO with the Re≡O π-bond. The *trans* configuration of the $[isq^{Ph}]^{\bullet-}$ ligand allows the unpaired electron to be in a π-symmetry orbital that overlaps with the $d^1_{xy}$ as well as one of the two $d_{xy,yz}$ orbitals used to form the Re≡O π -bonds (Figure 5.9). Perhaps this arrangement, which allows for antiferromagnetic coupling, is what drives the complex to have oxyl-like behavior.

In the extreme case of strong intraligand charge transfer the hole is localized on the oxo ligand generating an oxyl radical (Figure 5.10.). Both $Re^{VI}(O)(ap^{Ph})(isq^{Ph})(Cl)$ and $Re_2^{VI}(O)_2(\mu\text{-}O)(ap^{Ph})_2(isq^{Ph})_2$ are not appropriately described as ground state oxyl radicals, but it is not unreasonable to expect that the symmetry allowed mixing of the orbitals may generate oxyl radical character which gives rise to the observed reactivity. Conceivably, the *cis* configuration in $[TpRe(O)(isq^{Ph})]^+$ may limit the intraligand charge transfer thereby prohibiting oxyl-like behavior.

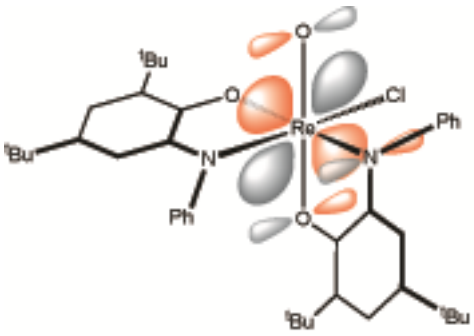


**Figure 5.9.** Qualitative π orbital interactions in $Re^{VI}(O)(ap^{Ph})(isq^{Ph})(Cl)$.

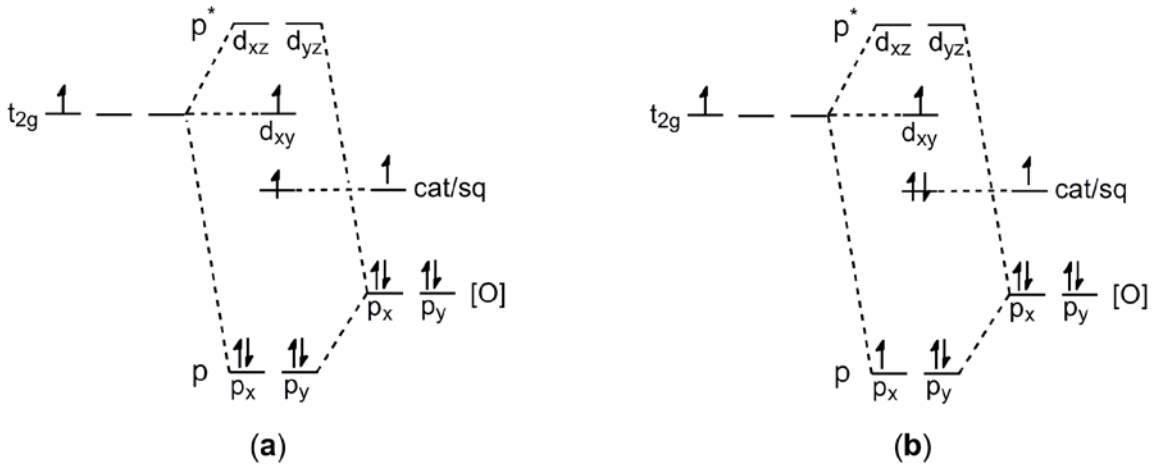


**Figure 5.10.** Qualitative π-bonding MO of (**a**) $Re^{VI}(O)(ap^{Ph})(isq^{Ph})(Cl)$ and (**b**) with the limit of strong intraligand charge transfer generating an oxyl radical.

## 5.4 Conclusion

The capacity for $Re^{VI}(O)(ap^{Ph})(isq^{Ph})(Cl)$ and $Re_2{}^{VI}(O)_2(\mu\text{-}O)(ap^{Ph})_2(isq^{Ph})_2$ to undergo radical coupling at a terminal oxo ligand has been shown. These two species are capable of facile oxo transfer to $Ph_3C^{\bullet}$ and $PhMe_2Si^{\bullet}$ respectively. This is unusual because neither is a strong outer-sphere oxidant or a ground state oxyl radical, and both are poor oxo transfer reagents. It is postulated that symmetry allowed mixing of a populated Re≡O π -bond with an $[isq]^{\bullet-}$ ligand radical gives rise the oxyl radical character. This allows the closed-shell oxo ligands to undergo a net $2e^-$ oxo transfer reaction via low barrier radical ligand mediated bond-forming steps. This draws parallels to trapping of oxygenic radicals at $[Re^{V}(O)(ap^{Ph})_2]^-$ and its derivatives.

The ability of $[isq]^{\bullet-}$ ligand radical orbitals to mix with a populated Re≡O π -bond shows a new method of making oxyl radicals. Harnessing this intraligand charge transfer for radical reactions demonstrates a novel method to utilize redox-active ligands for small molecule activation. This strategy holds exciting implications for the design of kinetically reactive oxidants to use low barrier radical redox steps in selective

multielectron redox transformations to make and break bonds. The results described in this chapter lay the foundation and molecular design to develop catalysts capable of efficiently making and breaking O–O bonds.

## 5.5 Experimental Detail and Supplementary Material

### 5.5.1 General Considerations.

Unless otherwise specified, all manipulations were performed under anaerobic conditions using standard vacuum line techniques, or in an inert atmosphere glove box under purified nitrogen. Routine NMR spectra were acquired on a Varian Mercury 300 spectrometer (300.323 MHz for $^{1}$H) at ambient temperature. $^{11}$B NMR was acquired on a Bruker AMX 400 spectrometer (400.138 MHz for 1H). All chemical shifts are reported in parts per million (ppm) relative to TMS, with the residual solvent peak serving as an internal reference. UV–visible absorption spectra were acquired using a Varian Cary 50 spectrophotometer. Unless otherwise noted, all electronic absorption spectra were recorded at ambient temperatures. All mass spectra were recorded in the Georgia Institute of Technology Bioanalytical Mass Spectrometry Facility. Matrix-assisted laser desorption/ionization mass spectrometry was obtained using an Applied Biosystems 4700 Proteomics Analyzer. All photochemical reactions were carried out with a 150 watt Powersun UV mercury vapor bulb purchased from Petsmart with quartz glassware. Cyclic voltammetric measurements were made using a CH Instruments CHI620C potentiostat in a three component cell consisting of a platinum disk working electrode, a platinum wire auxiliary electrode, and a non-aqueous $AgPF_6$/Ag reference electrode. Electrochemical data are referenced and reported to $Fc^{+}$/Fc as an internal standard. Elemental analyses were performed by Atlantic Microlab, Inc., Norcross, GA. All analyses were performed in duplicate, and the reported compositions are the average of the two runs.

### 5.5.2 Methods and Materials.

Anhydrous acetonitrile, dichloromethane, toluene, benzene, and THF solvents for air- and moisture-sensitive manipulations were purchased from Sigma-Aldrich and further dried by passage through columns of activated alumina, degassed by at least three freeze-pump-thaw cycles, and stored under $N_2$ prior to use. Methanol (anhydrous, 99.0%), was purchased from Honeywell Burdick and Jackson. Acetone (99.8%, extra dry) was purchased from Acros. All were used as received. Deuterated acetonitrile ($CD_3CN$), toluene ($C_7D_8$), benzene ($C_6D_6$) and dichloromethane ($CD_2Cl_2$) were purchased from Cambridge Isotope Laboratories, degassed by three freeze-pump-thaw cycles, vacuum distilled from $CaH_2$, and stored under a dry $N_2$ atmosphere prior to use. $(Et_4N)[Re^{V}(O)_2(ap)_2]$,[22] $TpRe(O)(Cl)_2$,[47] $TpRe(O)(OMe)_2$,[47] $Re(O)(ap^{Ph})(isq^{Ph})(Cl)$,[23] 3,5-di-*tert*-butylcatecholborane, triphenylmethyl radical,[48] triphenylmethyl tetrafluroborate,[49] and dimethylphenylsilylbis(diisopropylamino)borane[38] were prepared by literature methods. All characterization data matched those referenced. All other reagents were purchased from Sigma-Aldrich and used as received.

### 5.5.3 Synthesis of $TpRe^{V}(O)(cat)$.

A 20 mL scintillation vial was charged with $TpRe(O)(OMe)_2$ (0.1 g, 0.2 mmol) and benzene (10 mL). Slow addition of 1M catecholborane in THF (0.2 mL, 0.2 mmol) and stirring for 1 h afforded a color change from violet to brown. The solvent was removed under reduced pressure and the dark residue was dissolved in $CH_2Cl_2$ and subjected to column chromatography on a silica gel column (230-400 mesh) prepared with hexanes. A brown band was eluted as the major product with a $CH_2Cl_2$-hexanes (70/30) mixture. The solvent was removed under vacuum and TpRe(O)(cat) was isolated by precipitation from an ether solution at –50 $^{o}$C (0.96 g, 87 %).$^{1}$H NMR (300 MHz, $CD_2Cl_2$, $\delta$): 8.04 (d, J = 2 Hz, Tp*H*, 2 H); 7.99 (dd, J = 2 Hz, J = 1 Hz, Tp*H*, 2 H); 7.44 (dd, J = 2 Hz, J = 1 Hz, Tp*H*, 1 H); 7.20 (m, Ar*H*, 2 H); 7.15 (d, J = 2 Hz, Tp*H*, 1 H); 6.81

(m, Ar*H*, 2 H); 6.52 (t, J = 2 Hz, Tp*H*, 2 H); 5.91 (t, J = 2 Hz, Tp*H*, 1 H). UV–vis ($CH_2Cl_2$) $\lambda_{max}$, nm ($\varepsilon$, $M^{-1}$ $cm^{-1}$): 270 (10,800), 315 (4,500), 385 (sh). MALDI-MS (*m/z*): 526 $[M]^+$. FTIR (ATR): 3147 (vw), 3132 (w), 2496 (w), 1506 (m), 1469 (s), 1408 (s), 1313 (s), 1230 (vs), 1211 (vs), 1186 (s), 1119 (s), 1099 (s), 1050 (vs), 1017 (m), 994 (m), 964 (vs), 930 (w), 861 (w), 802 (m), 763 (vs), 745 (vs), 711 (vs), 681 (vs), 651 (vs), 613 (s), 565 (w), 548 (m), 456 (w). Anal. Calcd for TpRe(O)(cat) $C_{15}H_{14}BN_6O_3Re$: C, 34.43; H, 2.70; N, 16.06; Found: C, 35.02; H, 3.11; N, 15.83.

**5.5.4 Synthesis of TpRe$^{V}$(O)(3,5-$^{t}$Bu$_2$cat).**

**Method 1.** A 20 mL scintillation vial was charged with TpRe(O)$(OMe)_2$ (0.1 g, 0.2 mmol), benzene (10 mL), $Et_3N$ (400 µL, 2.9 mmol) and 3,5-di-*tert*-butylcatechol (0.2615 g, 1.2 mmol). The mixture was stirred at room temperature for 3 d at which point the solvent was removed under vacuum. The dark residue was dissolved in $CH_2Cl_2$ and subjected to column chromatography on a silica gel column (230-400 mesh) prepared with hexanes. A brown band was eluted as the major product with a $CH_2Cl_2$-hexanes (70/30) mixture. The solvent was removed under vacuum and TpRe(O)(3,5-$^{t}$Bu$_2$cat)) was isolated by precipitation from an ether solution at – 50 $^{o}$C (0.1378 g, 54 %). **Method 2.** A 20 mL scintillation vial was charged with TpRe(O)$(OMe)_2$ (0.5136 g, 1.1 mmol), Benzene (10 mL), and 3,5-di-*tert*-butylcatecholborane (0.2651 g, 1.2 mmol). The mixture was stirred at room temperature for 1 h at which point the solvent was removed under vacuum. The dark residue was dissolved in $CH_2Cl_2$ and subjected to column chromatography on a silica gel column (230-400 mesh) prepared with hexanes. A brown band was eluted as the major product with a $CH_2Cl_2$-hexanes (70/30) mixture. The solvent was removed under vacuum and TpRe(O)(3,5-$^{t}$Bu$_2$cat) was isolated by precipitation from an ether solution at –50 $^{o}$C (0.56 g, 82 %).$^{1}$H NMR (300 MHz, Acetone-*d*6, $\delta$): 8.28 (t, J = 2 Hz, Tp*H*, 2 H); 8.11 (d, J = 2 Hz, Tp*H*, 1 H); 8.07 (d, J = 2

Hz, Tp*H*, 1 H); 7.67 (d, J = 2 Hz, Tp*H*, 1 H); 7.15 (d, J = 2 Hz, Tp*H*, 1 H); 7.10 (d, J = 2 Hz, Ar*H*, 1 H); 6.85 (d, J = 2 Hz, Ar*H*, 1 H); 6.65 (d, J = 2 Hz, Tp*H*, 1 H); 6.63 (d, J = 2 Hz, Tp*H*, 1 H); 6.00 (t, J = 2 Hz, Tp*H*, 1 H); 1.44 (s, $^{t}$Bu*H*, 9 H); 1.35 (s, $^{t}$Bu*H*, 9 H). UV–vis ($CH_2Cl_2$) $\lambda_{max}$, nm ($\varepsilon$, $M^{-1}$ $cm^{-1}$): 275 (14,200), 340, (7,000), 405 (sh). MALDI-MS (*m/z*): 636 $[M]^+$. FTIR (ATR): 3118 (vw), 3108 (w), 2896 (w), 1506 (m), 1479 (s), 1407 (s), 1313 (s), 1234 (vs), 1217 (vs), 1184 (s), 1120 (s), 1095 (s), 1050 (vs), 988 (m), 977 (vs), 933 (w), 856 (w), 812 (m), 763 (vs), 710 (vs), 663 (vs), 650 (vs), 611 (s), 565 (w), 550 (m). Anal. Calcd for TpRe(O)(3,5-t$Bu_2$cat) • 0.4 diethyl ether $C_{24.6}H_{34}BN_6O_{3.4}Re$: C, 44.42; H, 5.15; N, 12.63; Found: C, 44.54; H, 5.06; N, 12.96.

**5.5.5 Synthesis of TpRe$^{V}$(O)(ap$^{Ph}$).**

A 20 mL scintillation vial was charged with TpRe(O)$(OMe)_2$ (0.3006 g, 0.63 mmol), Benzene (10 mL), $Et_3N$ (600 µL, 4.3mmol) and $H_2ap^{Ph}$ (0.6129 g, 2.1 mmol). The mixture was heated at reflux for 48 h. The solvent of the resulting brown solution was removed under vacuum. The dark residue was dissolved in $CH_2Cl_2$ and subjected to column chromatography on a silica gel column (230-400 mesh) prepared with hexanes. A brown band was eluted as the major product with a $CH_2Cl_2$-hexanes (70/30) mixture. The solvent was removed under vacuum and TpRe(O)(ap$^{Ph}$) was isolated by precipitation from an ether solution at – 50 $^{o}$C (0.1492 g, 33 %). Crystals of X-ray quality were grown by slow evaporation of an ether/pentane solution at – 10 $^{o}$C. $^{1}$H NMR (293 K, 300 MHz, $CD_2Cl_2$, $\delta$): 8.02 (d, J = 2 Hz, Tp*H* 1H); 7.86 (d, J = 2 Hz, Tp*H* 1H); 7.78 (d J = 2 Hz, Tp*H* 1H); 7.53 (d, J = 2 Hz, Tp*H* 1H); 7.48 (d, J = 2 Hz, Tp*H* 1H); 7.29 (br, N*Ph*, 4H); 7.07 (t, J = 7Hz, *p*-N*Ph*, 1H); 6.75 (d, J = 2 Hz, Ar*H,* 1H); 6.68 (d, J = 2 Hz, Tp*H* 1H); 6.45 (d, J = 2 Hz, Ar*H*, 1H); 6.44 (t, J = 2 Hz, Tp*H* 1H); 6.07 (t, J = 2Hz, Tp*H* 1H); 6.00 (t, J = 2 Hz, Tp*H* 1H); 1.44 (s, $^{t}$Bu, Tp*H* 9 H); 1.21 (s, $^{t}$Bu, Tp*H* 9H). UV–vis ($CH_2Cl_2$) $\lambda_{max}$, nm ($\varepsilon$, $M^{-1}$ $cm^{-1}$): 280 (12,000), 360 (6,500), 430 (sh), 518 (1000). MALDI-MS

(*m/z*): 711 $[M]^+$. FTIR (ATR): 2949 (w), 2901 (w), 2859 (w), 1405 (s), 1391 (m), 1311 (s), 1213 (s), 1117 (s), 1048 (vs), 988 (vs), 934 (vs), 890 (s), 777 (s), 761 (vs), 715 (vs), 653 (m), 616 (m), 557 (m). Anal. Calcd for TpRe(O)($ap^{Ph}$)•0.3 Pentane $C_{30.5}H_{38.6}BN_7O_2Re$: C, 50.02; H, 5.31; N, 13.39; Found: C, 49.85; H, 5.36; N, 13.11.

**5.5.6 Synthesis of $TpRe^{V}(O)(O_2C_2H_4)$.**

A 50 mL round bottom flask was charged with $TpRe(O)(Cl)_2$ (0.2507 g, 0.52 mmol) and dissolved in 25 mL of MeCN. Ethylene glycol (115 µL, 2.0 mmol), and $Et_3N$ (290 µL, 2.1 mmol) were added and the mixture was heated at reflux for 27 h. The solvent was removed under vacuum and the purple residue was taken up in 10 mL $CH_2Cl_2$. The purple solution was washed with water (3 x 10 mL) and dried over $MgSO_4$. The $MgSO_4$ was removed via filtration and the solvent of the filtrate was removed under vacuum to leave a blue-purple powder of $TpRe(O)(O_2C_2H_4)$ (0.1638, 66 %). Crystals of X-ray quality were grown from a concentrated $CH_2Cl_2$ solution. $^1H$ NMR (300 MHz, $CD_2Cl_2$, $\delta$): 7.93 (d, J = 2 Hz, Tp*H*, 2 H); 7.90 (d, J = 2 Hz, Tp*H*, 2 H); 7.55 (d, J = 2 Hz, Tp*H*, 1 H); 7.37 (d, J = 2 Hz, Tp*H*, 1 H); 6.44 (t, J = 2 Hz, Tp*H*, 2 H); 5.97 (t, J = 2 Hz, Tp*H*, 1 H); 5.09 (m, OC$H_2$$CH_2$O, 2 H); 4.82 (m, $OCH_2$C$H_2$O, 2 H). UV–vis ($CH_2Cl_2$) $\lambda_{max}$, nm ($\varepsilon$, $M^{-1}$ $cm^{-1}$): 280 (60) FAB–MS (*m/z*): 476 $[M]^+$. FTIR (ATR): 3080 (w), 2857 (w), 2532 (w), 1504 (m), 1406 (s), 1312 (s), 1207 (s), 1113 (m), 1050 (vs), 1018 (vs), 963 (vs), 899 (vs), 766 (vs), 714 (s), 677 (m), 651 (vs), 618 (vs), 542 (s). Anal. Calcd for $TpRe(O)(O_2C_2H_4)$ $C_{11}H_{14}BN_6O_3Re$: C, 27.80; H, 2.97; N, 17.68; Found: C, 28.24; H, 3.01; N, 17.31.

**5.5.7 Synthesis of $[TpRe^{V}(O)(isq^{Ph})][BF_4]$•0.28 $CH_2Cl_2$.**

A 20 mL scintillation vial was charged with TpRe(O)($ap^{Ph}$) (0.4346 g, 0.61 mmol), THF (10 mL), and $AgBF_4$ in THF (0.1231 g, 0.63 mmol). The mixture was stirred for 15 h at ambient temperature. The solvent was removed under vacuum and the green residue

was washed with ether (3 x 5 mL) leaving behind [TpRe(O)(isq$^{Ph}$)][$BF_4$] as a green powder (0.3996 g, 82 %). Crystals of X-ray quality were grown by slow diffusion of ether into a $CH_2Cl_2$ solution of [TpRe(O)(isq$^{Ph}$)][$BF_4$]. UV–vis ($CH_2Cl_2$) $\lambda_{max}$, nm ($\varepsilon$, $M^{-1}$ $cm^{-1}$): 290 (14,500), 410 (5,300), 610 (1600), 910 (530). ESI-MS (*m/z*): 711 $[M]^+$. FTIR (ATR): 3122 (vw), 2958 (vw), 1507 (m), 1485 (m), 1406 (m), 1366 (w), 1315 (m), 1250 (m), 1213 (s), 1180 (m), 1121 (m), 1050 (vs), 998 (m), 957 (vs), 862 (w), 785 (s), 769 (s), 708 (s), 649 (s), 615 (s), 542 (w), 520 (w), 506 (w). Anal. Calcd for [TpRe(O)(ap$^{Ph}$)][$BF_4$]•0.5 $BF_4$ $C_{29}H_{35}B_{2.5}F_6N_7O_2Re$: C, 41.42; H, 4.20; N, 11.66; Found: C, 41.47; H, 4.36; N, 11.41.

**5.5.8 Synthesis of $Re^{VII}(O)_2(ap^{Ph})(isq^{Ph})$.**

A 20 mL scintillation vial was charged with $[Re(O)_2(ap^{Ph})_2]^-$ (33.3 mg, 0.040 mmol), Acetone (10 mL), and $AgBF_4$ (8.3 mg, 0.043 mmol). The mixture was allowed to warm to room temperature while stirring over 10 min. The resulting green solution was filtered through celite. The filtrate was reduced under vacuum to ~2 mL and stored at –20 $^oC$ overnight. $Re(O)_2(ap^{Ph})(isq^{Ph})$ was collected as a green precipitate via filtration (16.2 mg, 50%). MALDI-MS (*m/z*): 809 $[M]^+$.

**5.5.9 Synthesis of $Re_2^{VI}(O)_2(\mu\text{-}O)(ap^{Ph})_2(isq^{Ph})_2$.**

A 20 mL scintillation vial was charged with $[Re(O)_2(ap^{Ph})_2]^-$ (0.2270 g, 0.24 mmol), Acetone (10 mL), and $AgBF_4$ (1.1 mL, 0.24 mmol). The mixture was stirred for 15 h at which point the solvent was removed under vacuum. The dark residue was extracted with ether and filtered leaving a white precipitate. The solvent of the purple filtrate was removed under vacuum leaving $Re_2(O)_2(\mu\text{–}O)(ap^{Ph})_2(isq^{Ph})_2$ as a purple powder (0.165 g, 43 %). Crystals of X-ray quality were grown by slow evaporation of an acetonitrile solution at –20 $^oC$. MALDI-MS (*m/z*): 1602 $[M]^+$. Anal. Calcd for $Re_2^{VI}(O)_2(\mu\text{-}O)(ap^{Ph})_2(isq^{Ph})_2$•0.8 $BF_4$, $CH_3CN$ $C_{82}H_{103}B_{0.8}F_{3.2}N_5O_7Re_2$: C, 57.51; H, 6.06; N, 4.09; Found: C, 57.31; H, 7.07; N, 3.96.

### 5.5.10 Synthesis of $Re^{V}(Cl)_2(ap^{Ph})(isq^{Ph})$.

**Method 1**. A 50 mL flask with a Kontes brand high-vacuum PTFE valve was charged with $[Re(O)(ap^{Ph})_2]^-$ (0.4841 g, 0.524 mmol) and $CH_2Cl_2$ (25 mL). $Me_3SiCl$ (160 µL, 1.26 mmol) was added to afford a red-orange solution. The flask was sealed and immersed in a silicone fluid bath at 65 $^oC$ for 3 h to yield a clear, dark maroon solution, then cooled to ambient temperature. The mixture was exposed to air and the solvent removed under reduced pressure. The residue was dissolved in $CH_2Cl_2$ (2 mL) and subjected to column chromatography on a silica gel column (230-400 mesh) prepared with hexanes. A dark maroon band was eluted as the major fraction ($1^{st}$) with $CH_2Cl_2$. Solvent removal from the eluate afforded $Re(Cl)_2(ap^{Ph})(isq^{Ph})$ as a maroon powder (0.3987 g, 90 %). Single crystals of X-ray quality were grown from slow evaporation of a $CH_2Cl_2$ solution. **Method 2.** To a $CH_2Cl_2$ (10 mL) solution of $[Re(O)_2(ap^{Ph})_2]^-$ (33.4 mg, 0.036 mmol) in a 20-dram scintillation vial was added excess aqueous HCl (5 mL, 0.1M). The reaction mixture was stirred vigorously at ambient temperature for 24 h. The mixture was washed with $H_2O$ (3 x 5 mL) and dried over $MgSO_4$. Filtration followed by solvent removal of the filtrate afforded $Re(Cl)_2(ap^{Ph})(isq^{Ph})$ as a maroon powder (19.2 mg, 63 %). UV–vis ($CH_2Cl_2$) $\lambda_{max}$, nm ($\varepsilon$, $M^{-1}$ $cm^{-1}$): 264 (18,800), 385 (8,100), 490 (29,300). MALDI-MS(*m/z*): 847 $[M]^+$. FTIR (ATR): 2951 (s), 2904 (m), 2865 (m), 1585 (m), 1540 (m), 1485 (vs), 1454 (vs), 1393 (w), 1361 (vs), 1305 (w), 1251 (vs), 1231 (m), 1199 (m), 1164 (m), 1109 (w), 1074 (w), 1025 (m), 997 (m), 912 (m), 864 (m), 828 (w), 768 (vs), 735 (vs), 706 (vs), 651 (m), 604 (m), 543 (m), 497 (s), 399 (m). Anal. Calcd for $C_{40}H_{50}Cl_2N_2O_2Re$: C, 56.66; H, 5.94; N, 3.30; Found: C, 56.52; H, 6.28; N, 3.27.

### 5.5.11 Radical Coupling with Dimethylphenylsilylbis(diisopropylamino)borane.

In a representative procedure a 20-dram vial was charged with $Re(O)_2(\mu\text{–}O)(ap^{Ph})_2(isq^{Ph})_2$ (24.6 mg, 0.015 mmol) and benzene (2 mL). Dimethylphenylsilylbis(diisopropylamino)borane (12.2 mg, 0.035 mmol) was added and

the mixture was transferred to a quartz J. Young brand NMR tube with a Teflon screw cap. The sample was irradiated with UV radiation for 5 h. A 1 mL aliquot of the reaction mixture was transferred to a 2 mL GC autosampler vial and analyzed via GC-MS to determine the organic product distribution and MALDI-MS.

**5.5.12 Radical Coupling with Triphenylmethyl Radical.**

In a representative procedure a 20-dram vial was charged with $Re^{VI}(O)(ap^{PH})(isq^{Ph})(Cl)$ (78.5 mg, 0.1 mmol) and benzene (10 mL). $Ph_3C^{\bullet}$ in benzene (0.0725 M, 700 µL, 0.1 mmol $Ph_3C^{\bullet}$) was added. The vial was wrapped in Al foil and the reaction mixture was stirred at ambient temperature for 1 week. The presence of $Ph_3COH$ (0.066 mmol, 69 % based on initial [Re]) was verified via GC-MS. The solvent was removed under vacuum and the dark residue was washed with MeCN (3 x 5 mL) to give a red-purple solution and a dark precipitate of $Re_2(\mu\text{-}O)_2(ap^{Ph})_2(isq^{Ph})_2$ (28.5 mg, 0.018 mmol) which was collected via filtration. The red-purple solution was subjected to column chromatography on a silica gel column (230-400 mesh) prepared with hexanes. A dark purple band was eluted as the 1$^{st}$ fraction with a $CH_2Cl_2$/hexanes mixture (70/30). Solvent removal from the eluate followed by freeze drying from a benzene solution afforded $Re^{VI}(O)(ap^{Ph})(isq^{Ph})(Cl)$ (22.9 mg, 0.028 mmol). A maroon band was eluted as the 2$^{nd}$ fraction using $CH_2Cl_2$. Solvent removal from the eluate under reduced pressure gave a dark maroon powder consisting of $Re(Cl)_2(ap^{Ph})(isq^{Ph})$ (22.9, 0.027).

**5.5.13 X-ray Crystallography.**

Crystals of $TpRe^{V}(O)(ap^{Ph})$, $[TpRe^{V}(O)(isq^{Ph})][BF_4]\bullet 0.28\ CH_2Cl_2$, $TpRe^{V}(O)(OH_2CH_2O)$, and $Re_2{}^{VI}(O)_2(\mu\text{-}O)(ap^{Ph})_2(isq^{Ph})_2$ suitable for X-ray diffraction analysis were coated with Paratone N oil, suspended on a small fiber loop and placed in a cooled nitrogen stream at 173 K on Bruker D8 APEX II CCD sealed tube diffractometer. Data were collected using graphite monochromated Mo Kα (λ = 0.71073 Å) radiation. Data were measured using a series of combinations of phi and omega

scans with 10 s fame exposures and 0.5$^{o}$ frame widths. Data collection, indexing and initial cell refinements were done using APEX II software.[50] Frame integration and final cell refinements were done using SAINT software.[51] The structures were solved using direct methods and difference Fourier techniques using the SHELXTL program package, V6.12. Hydrogen atoms were placed in their expected chemical positions using the HFIX command and were included in the final cycles of least squares with isotropic $U_{ij}$'s related to the atoms ridden upon. All non-hydrogen atoms were refined anisotropically except for C2S in $Re^{V}(Cl)_2(ap^{Ph})(isq^{Ph})$•0.66 $CH_2Cl_2$. Scattering factors and anomalous dispersion corrections are taken from the *International Tables for X-Ray Crystallography*.[52] Other details of data collection and structure refinement are provided in Table 5.3. and Table 5.4.

**Table 5.3.** Crystallographic Data and Structure Parameters for $TpRe^{V}(O)(ap^{Ph})$, $[TpRe^{V}(O)(isq^{Ph})][BF_4]$•0.28 $CH_2Cl_2$, and $TpRe^{V}(O)(O_2(CH_2)_2)$.

| Complex | $TpRe(O)(ap^{Ph})$ | $[TpRe(O)(isq^{Ph})][BF_4]$ | $TpRe(O)(O_2(CH_2)_2)$ |
|---|---|---|---|
| Empirical formula | $C_{29}H_{35}BN_7O_2Re$ | $C_{29.28}H_{35.56}B_2Cl_{0.56}F_4N_7O_2Re$ | $C_{11}H_{14}BN_6O_3Re$ |
| Formula weight | 710.65 | 821.24 | 475.29 |
| Temperature | 173(2) K | 173(2) K | 173(2) K |
| Crystal system | Monoclinic | Orthorhombic | Orthorhombic |
| Space group | P2(1)/c | Iba2 | Iba2 |
| Unit cell dimensions | | | |
| a (Å) | 12.425(7) | 15.26(2) | 15.7088(18) |
| b (Å) | 14.267(9) | 19.41(3) | 16.6032(19) |
| c (Å) | 17.487(10) | 21.91(3) | 12.9355(15) |
| α (°) | 90 | 90 | 90 |
| β (°) | 108.094(10) | 90 | 90 |
| γ (°) | 90 | 90 | 90 |
| V ($Å^3$) | 2947(3) | 6488(15) | 3373.8(7) |
| Z | 4 | 8 | 8 |
| $D_{calc}$ (g $cm^{-1}$) | 1.602 | 1.681 | 1.871 |
| Absorption coefficient ($mm^{-1}$) | 4.162 | 3.854 | 14.272 |
| Crystal size (mm) | 0.18 x 0.08 x 0.05 | 0.27 x 0.13 x 0.06 | 0.28 x 0.07 x 0.03 |
| θ range for data collection (°) | 1.72-29.57 | 1.86-27.87 | 3.87-66.24 |
| Index ranges | $-17 \le h \le 17$ | $-20 \le h \le 20$ | $-18 \le h \le 18$ |
| | $-19 \le k \le 19$ | $-25 \le k \le 25$ | $-19 \le k \le 18$ |
| | $-24 \le l \le 24$ | $-28 \le l \le 28$ | $-15 \le l \le 14$ |
| Reflections collected/unique | 55042 | 53154 | 11450 |
| Goodness of fit on $F^2$ | 1.002 | 1.052 | 1.021 |
| R [$I > 2\sigma(I)$] | 0.0547 | 0.0587 | 0.0341 |
| $wR_2$ (all data) | 0.1365 | 0.1472 | 0.1197 |

**Table 5.4.** Crystallographic Data and Structure Parameters for $[Re^{V}(Cl)_2(ap^{Ph})(isq^{Ph})]$•0.65 $CH_2Cl_2$ and $[Re_2^{VI}(O)_2(\mu\text{-}O)(ap^{Ph})_2(isq^{Ph})_2]$•0.5$CH_3CN$.

| Complex | $Re^{V}(Cl)_2(ap^{Ph})(isq^{Ph})$ | $Re_2^{VI}(O)_2(\mu\text{-}O)(ap^{Ph})_2(isq^{Ph})_2$ |
|---|---|---|
| Empirical formula | $C_{40.65}H_{51.3}Cl_{3.3}N_2O_2Re$ | $C_{81}H_{101.5}N_{4.5}O_7Re_2$ |
| Formula weight | 903.12 | 1632.14 |
| Temperature | 173(2) K | 173(2) K |
| Crystal system | Monoclinic | Triclinic |
| Space group | P2(1)/c | P-1 |
| Unit cell dimensions | | |
| a (Å) | 10.5294(15) | 13.979(3) |
| b (Å) | 40.534(6) | 21.762(4) |
| c (Å) | 10.4408(15) | 26.405(5) |
| α (°) | 90 | 84.897(3) |
| β (°) | 107.828(2) | 83.355(3) |
| γ (°) | 90 | 77.683(3) |
| V ($Å^3$) | 4242.1(10) | 7778(3) |
| Z | 4 | 4 |
| $D_{calc}$ (g $cm^{-1}$) | 1.414 | 1.394 |
| Absorption coefficient ($mm^{-1}$) | 3.106 | 3.164 |
| Crystal size (mm) | 0.40 x 0.23 x 0.08 | 0.29 x 0.26 x 0.13 |
| θ range for data collection (°) | 2.01-32.55 | 1.19-29.34 |
| Index ranges | $-15 \le h \le 15$ | $-19 \le h \le 19$ |
| | $-59 \le k \le 60$ | $-29 \le k \le 30$ |
| | $-15 \le l \le 15$ | $-36 \le l \le 36$ |
| Reflections collected/unique | 91051 | 147107 |
| Goodness of fit on $F^2$ | 1.13 | 1.025 |
| R [$I > 2\sigma(I)$] | 0.0549 | 0.0423 |
| $wR_2$ (all data) | 0.1243 | 0.1154 |

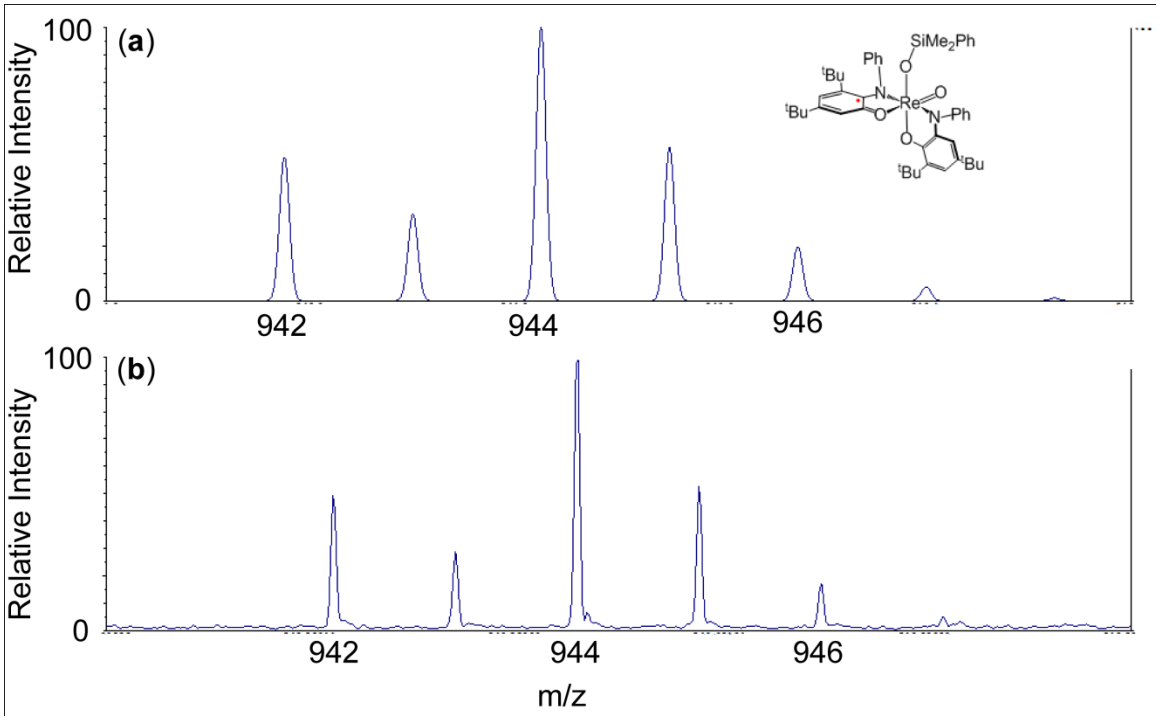


**Figure 5.11.** (**a**) Theoretical splitting pattern for $Re^{VI}(O)(OSiMe_2Ph)(ap^{Ph})(isq^{Ph})$ and (**b**) experimental MALDI-MS of a reaction with $Re^{VI}(O)_2(\mu\text{-}O)(ap^{Ph})_2(isq^{Ph})_2$ and $PhMe_2Si^{\bullet}$.

## 5.7 References


[1] Sheldon, R. A.; Kochi, J. K. Metal-Catalyzed Oxidations of Organic Compounds; Academic Press: New York, **1981**.

[2] Comprehensive Organic Synthesis: Selectivity, Strategy and Efficiency in Modern Organic Chemistry, Vol. 7: Oxidation; Trost, B. M., Fleming, I., Eds.; Pergamon: Oxford, U.K., **1991**.

[3] Report of the Basic Energy Sciences Workshop on Solar Energy Utilization; U.S. Department of Energy: Washington, DC, **2005**.

[4] *Organic Syntheses by Oxidation with Metal Compounds*; Mijs, W. J., De Jonge, C. R. H. I., Eds.; Plenum: New York, **1986**.

[5] Cavani, F.; Ballarini, N.; Luciani, S. *Top. Catal.* **2009**, *52*, 935-947.

[6] Parshall, G. W.; Ittel, S. D. Homogeneous Catalysis. *The Applications and Chemistry of Catalysis by Soluble Transition Metal Complexes*, 2nd ed.; Wiley-Interscience: New York, **1992**.

[7] Van Deurzen, M. P. J.; Van Rantwijk, F.; Sheldon, R. A. *Tetrahedron* **1997**, *53*, 13183-13220.

[8] Whittall, J. In *Catalysts for Fine Chemical Synthesis*; Roberts, S. M., Whittall, J., Eds.; John Wiley & Sons Ltd.: Chichester, U.K., **2007**, 5, 1-33.

[9] *Biomimetic Oxidations Catalyzed by Transition Metal Complexes*; Meunier, B., Ed.; Imperial College: London, **2000**.

[10] Lippard, S. J.; Berg, J. M. *Principles of Bioinorganic Chemistry*, University Science Books, **1994**.

[11] Cornell, C. N.; Sigman, M. S. In *ActiVation of Small Molecules: Organometallic and Bioinorganic Perspectives*; Tolman William, B., Ed.; Wiley-VCH: Weinheim, Germany, **2006**; 159-186.

[12] Ortiz de Montellano, P. R. (ed.) *Cytochrome P450. Structure, Mechanism, and Biochemistry.* Plenum Press, New York, **1995.**

[13] Blackmore, K. J.; Ziller, J. W.; Heyduk, A. F. *Inorg. Chem*. **2005**, 44, 5559–5561.

[14] Haneline, M. R.; Heyduk, A. F. *J. Am. Chem. Soc*. **2006**, 128, 8410-8411.

[15] Zarkesh, R. A.; Ziller, J.W.; Heyduk, A. F. *Angew. Chem., Int. Ed*. **2008**, 47, 4715-4718.

[16] Bart, S. C.; Lobkovsky, E.; Bill, E.; Chirik, P. J. *J. Am. Chem. Soc*. **2006**, 128, 5302-5303.

[17] Bouwkamp, M.W.; Bowman, A. C.; Lobkovsky, E.; Chirik, P. J. *J. Am. Chem. Soc*. **2006**, 128, 13340-13341.

[18] Stanciu, C.; Jones, M. E.; Fanwick, P. E.; Abu-Omar, M. M. *J. Am. Chem. Soc*. **2007**, 129, 12400-12401.

[19] Lu, C. C.; Weyhermuller, T.; Bill, E.; Wieghardt, K. *Inorg. Chem*. **2009**, 48, 6055-6064.

[20] A. L.; Soper, J. D. *Polyhedron* **2010**, 29, 164-169.

[21] Lippert, C. A.; Soper, J. D. *Inorg. Chem.*, **2010**, 49, 3682-3684.

[22] Lippert, C. A.; Arnstein, S. A.; Sherrill, C. D.; Soper, J. D. J. Am. Chem. Soc. **2010**, 132, 3879-3892.

[23] Lippert, C. A; Hardcastle, K. H.; Soper, J. D. *Inorg. Chem.* **2011**, *Submitted.*

[24] Rolle, C. J.; Hardcastle, K. I.; Soper, J. D. *Inorg. Chem.* **2008**, *47*, 1892-1894.

[25] Smith, A. L.; Hardcastle, K. I.; Soper, J. D. *J. Am. Chem***.** Soc. **2010**, *132*, 14358-14360

[26] Bill, E.; Bothe, E.; Chaudhuri, P.; Chlopek, K.; Herebian, D.; Kokatam, S.; Ray, K.; Weyhermueller, T.; Neese, F.; Wieghardt, K. *Chem.sEur. J.* **2005**, *11*, 204-224.

[27] Poddel'sky, A. I.; Cherkasov, V. K.; Abakumov, G. A. *Coord. Chem. Rev*. **2009**, *253*, 291-324.

[28] Nugent, W. A.; Mayer, J. M. *Metal-Ligand Multiple Bonds*; John Wiley & Sons: New York, **1988**.

[29] Pascaly, M.; Duda, M.; Schweppe, F.; Zurlinden, K.; M€uller, F. K.; Krebs, B. *J. Chem. Soc., Dalton Trans.* **2001**, 828-837.

[30] Espenson, J. H. *Adv. Inorg. Chem.* **2003**, *54*, 157-202.

[31] Lippert, C. A.; Arnstein, S. A.; Sherrill, C. D.; Soper, J. D. *J. Am. Chem. Soc*. **2010**, 132, 3879-3892.

[32] Poddel'sky, A. I.; Cherkasov, V. K.; Fukin, G. K.; Bubnov, M. P.; Abakumova, L. G.; bakumov, G. A. *Inorg. Chim. Acta* **2004**, *357*, 3632-3640.

[33] Bill, E.; Bothe, E.; Chaudhuri, P.; Chlopek, K.; Herebian, D.; Kokatam, S.; Ray, K.; Weyhermüller, T.; Neese, F.; Wieghardt, K. *Chem. Eur. J.* **2005**, *11*, 204-224.

[34] Poddel'sky, A. I.; Cherkasov, V. K.; Abakumov, G. A. *Coord. Chem. Rev.* **2009**, *253*, 291-324.

[35] Brewer, J. C.; Thorp, H. H.; Slagle, K. M.; Brudvig, G. W.; Gray, H. B. *J. Am. Chem. Soc.* **1991,** *113,* 3173-3174.

[36] Engel, P. S. *Chem. Rev.* **1980**, 80, 99-150.

[37] Zawalski, R. C.; Lisiak, M.; Kovacic, P.; Luedtke, A.; Timberlake, J. W. *Tetrahedron Lett*, **1980**, 21, 425- 428.

[38] Matsumoto, A; Ito, Y. J. Org. Chem. **2000**, 65, 5707-5711.

[39] March, Jerry **1985**, *Advanced Organic Chemistry: Reactions, Mechanisms, and Structure* (3rd ed.), New York: Wiley.

[40] Falvey, D. E.; Khambatta, B. S.; Schuster, G. B. J. Phys. Chem. **1990**, 94, 1056-1059.

[41] Bryant, J. R.; Matsuo, T.; Mayer, J. M. Inorg. Chem. 2004, 43, 1587-1592.

[42] Rappet, A. K.; Goddard, W. A. *J. Am. Chem. Soc.* **1982**,*104 3287*-3294.

[43] Prokop, K. A.; de Visser, A. P.; Goldberg, D. P. *Angew. Chem. Int. Ed*. **2010**, 49, 5091-5095.

[44] Seo, M. S.; Jang, H. G.; Kim, J.; Nam, W. *Bull. Korean Chem. Soc*. **2005**, 26, 971-974.

[45] Paine, T. K.; Costas, M.; Kaizer, J.; Que, L. *J. Biol. Inorg. Chem*. **2006,** 11, 272-276.

[46] Eric Vanover, V.; Huang, Y.; Xu, L.; Newcomb, M.; Zhang, R. *Org. Lett.,* 12, **2010,** 2246-2249.

[47] Seymore, S. B. and Seth N. Brown, S. N. *Inorg. Chem.*, **2000**, 39, 325-332.

[48] Gomberg, M. *J. Am. Chem. Soc.* **1900**, 22, 11, 757-771.

[49] Sharp, D.; Shepard, N. "Complex Fluorides. Part VIII". *University Chemical Laboratory, Cambridge*: **1956,** 674-682.

[50] *APEX II*; Brukers AXS, Inc., Analytical X-Ray Systems: Madison, WI, **2005**.

[51] *SAINT*, version 6.45A; Brukers AXS, Inc., Analytical X-ray Systems: Madison, WI, **2003**.

[52] *In International Tables for X-ray Crystallography, Volume C*; Wilson, J. C., Ed.; Academic Publishers: Dordrecht, The Netherlands, **1992**.

# Chapter 6

# Conclusions and Future Directions

## 6.1 Conclusions and Summary

Orthogonalizing $1e^-$ and $2e^-$ redox at high-valent oxorhenium centers by the utilization of radical ligands opens novel avenues for control of low barrier redox transformation of small molecule substrates. This is accomplished through coordination to redox-active ligands. A key aspect of all of this chemistry is the ability of the redox-active ligands to mediate single electron oxidation state changes at oxorhenium centers that are not generally prone to $1e^-$ or radical reactivity without perturbing the metal-centered $2e^-$ oxo transfer process. More specifically, the ligand radicals are able to facilitate radical-like reactivity at distal sites in the same molecule. This has lead to new methods of forming Re–X and O–R bonds using radical reagents such as $O_2$, $TEMPO^{\bullet}$, $Ph_3C^{\bullet}$, and $PhMe_2Si^{\bullet}$.

We believe radical ligands to be important in facilitating radical-like bond-forming reactions at distal sites within the same molecule, specifically at a terminal oxo ligand to provide oxyl like character. This has relevance towards the RC hypothesis of water oxidation where two metal oxyl fragments combine to form a new O–O bond. Therefore, the most important future avenues for research will focus on elaborating the capacity of redox-active ligand radicals to effect oxyl like reactions.

## 6.2 Future Directions

The oxorhenium complexes discussed in this thesis have two significant problems related to bimetallic RC O-O bond formation. 1) Our studies of $O_2$ homolysis show that the microscopic reverse reaction of $O_2$ assembly is prohibitively uphill. Oxorhenium(V) complexes containing redox-active ligands produce dioxorhenium(VII) complexes with $O_2$ addition. The new Re=O bond is substantially strong with a BDE of

118 ± 15 kcal $mol^{-1}$, therefore coupling of two Re=O to make an O–O bond is thermodynamically unfavorable. 2) Radical coupling of two monomeric metal oxyls is statistically unlikely. Metal oxyls are predicted to be extremely reactive and would most likely deactivate through unwanted radical side reactions before coming into contact with another metal oxyl fragment.

Future investigations would involve overcoming the above two challenges. One such solution for the former would be to use metal centers that can maintain the kinetic $1e^-$ pathway from coordination to redox-active ligands, but invert the thermodynamics by producing weaker and more thermodynamically reactive M=O bonds. For example, as discussed in chapter 1 iron, ruthenium, and iridium would be well suited towards this goal by utilizing the molecular design criteria developed in this thesis: utilizing redox-active ligands to store and deliver electron equivalents at distal site in the same molecule. The second challenge will require the development of dinuclear metal complexes containing redox-active ligands. Future investigations would involve generation of ligands capable of coordinating two metals simultaneously, thereby orienting the terminal oxo ligands in a cofacial arrangement to facilitate O–O bond formation. This category of ligands has been termed “pacman” ligands and there is relevant literature that supports the development of these types of complexes.[1-3] The most exciting and important outcome, if the above challenges can be overcome, would be the development of a superior electrocatalytic water oxidation catalyst.

Another interesting area of investigation involves the activation of kinetically inert small molecules. It would be of interest to see if the strategy of orthogonalizing $1e^-$ and $2e^-$ redox at oxorhenium centers to activate $O_2$ and $TEMPO^{\bullet}$ is transferable to other systems. Would it be possible for these types of complexes to access low barrier radical redox steps in selective multielectron transformations of other radical or kinetically inert small molecules? One such example would be the deoxygenation of nitrous oxide to

produce a metal oxo. Analogous to enzymatic $O_2$ activation discussed in Chapter 2, activation of $N_2O$ is believed to proceed via a similar bimetallic pathway through a series of single-electron steps.[4]

While the above only list a few examples of the possibilities for future investigations, they represent the significance and utility such research has on new catalysts development.

## 6.3 References


[1] Muckerman,J. T.; Polyansky, D. E.; Wada, T.; Tanaka, K.; Fujita, E. *Inorg. Chem.* **2008,** 1787-1802.

[2] Deng, Z.; Tseng, H.; Ruifa Zong, Wang, D.; Thummel, R. *Inorg. Chem.* **2008**, 1835-1848.

[3] Betley, T. A.; Wu, Q.; Voorhis, T. V.; Nocera, D. G. *Inorg. Chem.* **2008**, 1849-1861.

[4] Tolman, W. B. *Angew. Chem. Int. Ed.* **2010**, 49, 1018-1024.

# Appendix A

# Catalytic Aerobic Alcohol Oxidation by Oxorhenium Complexes Containing Redox-Active Ligands

## A.1 Introduction

The selective oxidation of alcohols plays vital roles in organic syntheses in laboratories as well as chemical industries. Alcohol oxidation is capable of producing a range of useful products such as aldehydes, ketones, and carboxylic acids for use in pharmaceuticals, agriculture, and fine chemicals.[1-2] Stoichiometric oxygen donors such as chromate or permanganate are typically utilized, but these reagents are expensive and have serious toxicity issues associated with them.[1,4-7] Molecular oxygen would be the ideal terminal oxidant as it is abundant and cheap, and if reduced completely to water, generates environmentally benign coproducts. However, the preference for unselective radical reactions and its kinetic inertness make the use of $O_2$ as an oxidant challenging.[8]

Transition metal oxos are typically employed to impart selective, partial oxidation of alcohols, among many others.[134] Unfortunately, these reactions tend to be carried out under stoichiometric conditions. The generation of metal oxos from $O_2$ would provide an ideal route to the catalytic aerobic oxidation of alcohols (Scheme A.1). While the use of $O_2$ as a transition metal mediated oxidant is not unheard of,[9-22] its large overpotential and tendency to generate highly oxidizing species upon partial reduction highlight challenges of utilizing $O_2$ as a terminal oxidant.[8] The features that engender $O_2$ activation are not readily transferable to other oxidation systems. We have recently reported on the chemical features that promote selective $O_2$ reduction which provides precedent for the development of a transition metal oxo oxidation catalyst utilizing $O_2$.[23]

**Scheme A.1.**

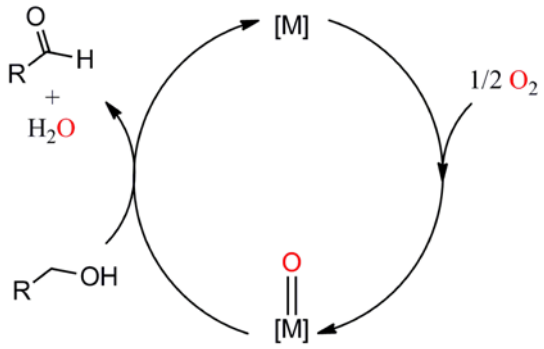


## A.2 Results

Exposure of a methanolic solution of $[Et_4N][Re(O)(cat)_2]$ (**1**) to air gives a color change from green to bright blue ($\mathbf{I_B}$) in *ca.* 100 min which slowly converts to a bright purple solution containing $[Et_4N][Re(O)_2(cat)_2]$ (**2**) over 50 h (Figure A.1). The aerobic oxidation of **1** to produce **2** in MeOH at UV-vis concentrations occurs with a 30% spectroscopic yield suggesting that significant decomposition occurs during the reaction in MeOH. However, when the reaction is performed at higher concentrations and monitored by $^1$H NMR spectroscopy in MeOH-*d*4 the yield of **2** increased to 75%.

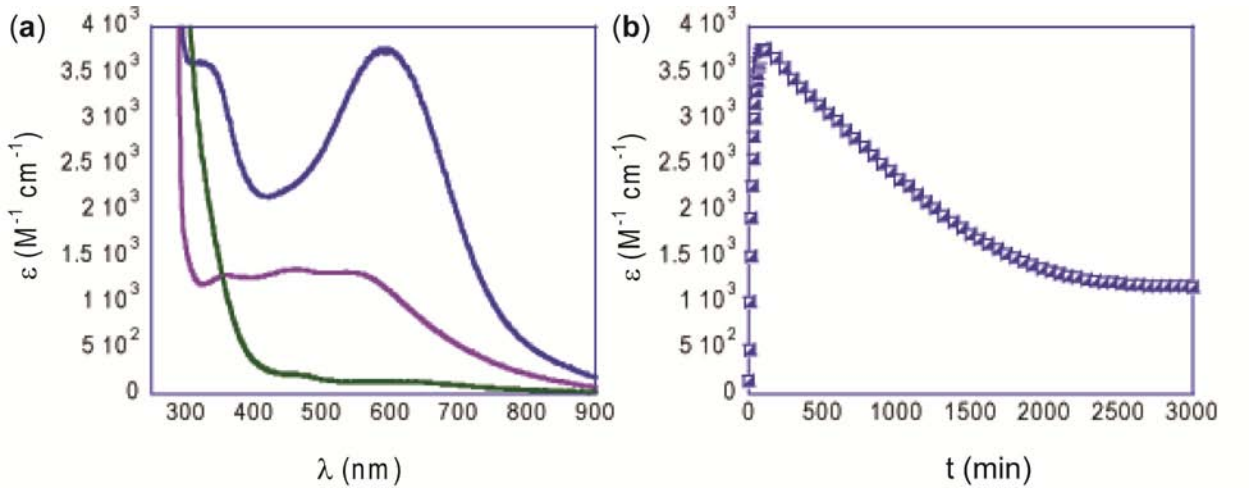


**Figure A.1. (a)** UV-vis absorption spectra for a reaction of 4.5 × $10^{-4}$ M **1** (green line) with 1 atm air in MeOH at 25 °C to generate blue intermediate $\mathbf{I_B}$ (blue line) in 100 min and **2** (purple line) in 3000 min. **(b)** Time-resolved data for the formation and decay of $\mathbf{I_B}$ with λ at 600 nm (blue □).

When 1 eq. of **1** dissolved in MeOH was added to a solution of **2** in MeOH under $N_2$, the purple solution rapidly turned bright blue producing a UV-vis spectrum identical to that in the reaction of **1** with air in MeOH. Over the course of days the blue solution gradually became a pale green that was identified as **1** by $^1$H NMR spectroscopy. When **1** and **2** are mixed in MeCN, THF, DMSO or $CH_2Cl_2$, no color change is observed indicating that MeOH is an essential component. At constant concentrations of **2**, the yield of blue in MeOH seemed to be independent of **1**, only the rate of formation of $\mathbf{I_B}$ increased with higher concentrations of **1** (Figure A.2).

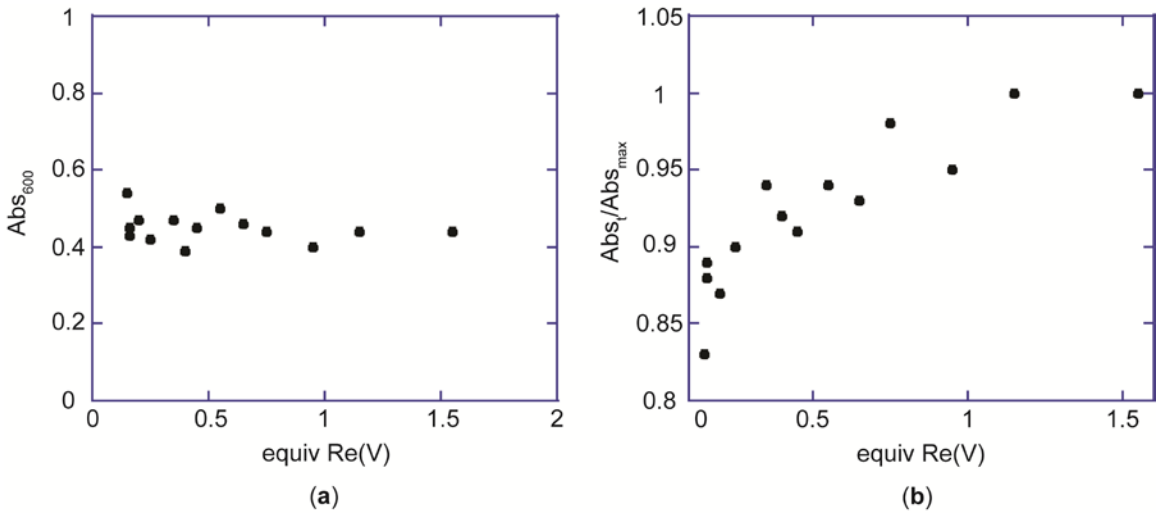


**Figure A.2.** (**a**) Plot showing maximum absorbance for a reaction of 1.5 × $10^{-4}$ M **2** and variable concentrations of **1**, and (**b**) ratio of absorbance after 300 s compared to $Abs_{max}$ at 600nm in MeOH at 25 °C

If the sum of the concentrations **1**+**2** was constant, the yield of blue only increased with **2** while the rate of formation increased with **1**, suggesting that $\mathbf{I_B}$ is only a function of [**2**] but the formation can be accelerated by higher [**1**] (Figure A.3).

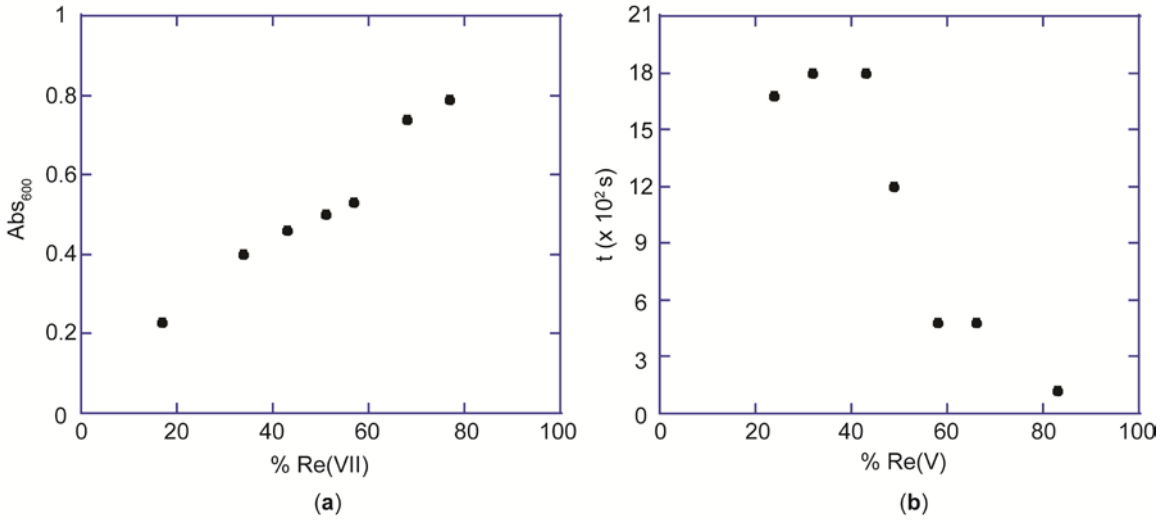


**Figure A.3.** (**a**) Plot of maximum absorbance at 600 nm ($\mathbf{I_B}$) for a reaction of 4.0 × $10^{-4}$ M total [Re] with variable ratios of **1** and **2**, and (**b**) rate of $I_B$ formation as a function of [**1**] in MeOH at 25 °C.

When 10 mol% of **1** were added to a benzyl alcohol (BnOH) solution of **2** under $N_2$, a color change from purple to green was produced over 1 hour at ambient temperature. Analysis of the green solution by $^1$H NMR shows **1** as the only metal containing product and integration of the $^1$H NMR resonances shows quantitative formation of **1** from **2**. Analysis of the same reaction mixture by GC-MS shows formation of benzaldehyde (PhCHO) as the only organic product in 58% yield (Table A.1).

NMR tubes containing **2**, 0.1 eq. **1**, and 5 eq. BnOH in MeOH-*d*4 under $N_2$ rapidly produce a blue solution that slowly fades to a pale green over days at ambient temperature. During the course of the reaction, new signals appear in the aromatic region at 6.74 ppm and 6.41 ppm that do not match **1** or **2** and cannot be assigned. In addition, a peak at 10.0 ppm was observed and corresponds to the formation of PhCHO. Integration of the PhCHO and **1** resonances indicate that *ca.* 0.5 eq. of aldehyde vs. metal and 50% **1** are formed. The remaining 50% of metal containing product can be accounted for by formation of $[ReO_4]^-$ as evidenced by a peak at *m/z* 250 in the ESI-MS, and roughly 50% free ligand evidenced by peaks in the $^1$H-NMR at 6.64 ppm and 6.55 ppm. To verify that these decomposition products are not the active species in alcohol oxidation, mixtures of $[ReO_4]^-$, $[ReO_4]^-$ + **1**, and $[ReO_4]^-$ + **2** were dissolved in BnOH and MeOH, separately. Analyses of these mixtures by NMR, GC-MS, and UV-vis show no aldehyde production or formation of a blue intermediate within 15 h, respectively. This supports the hypothesis that the alcohol oxidation is a result from the intact metal complexes and not from highly oxidizing decomposition products, such as $[ReO_4]^-$, produced during the reaction.

Since a blue solution of **2** and 0.1 eq. **1** in MeOH can be instantaneously quenched by the addition of excess BnOH, it is assumed that $\mathbf{I_B}$ is the active catalyst because the color change is accompanied by the formation of PhCHO observed by GC-MS.

We have previously reported on the ability of oxorhenium(V) complexes containing redox-active ligands to homolytically cleave dioxygen producing dioxorhenium(VII) complexes. The ability of these oxorhenium complexes to activate $O_2$ allows for the development of an aerobic alcohol oxidation catalyst. When a BnOH solution of **1** was stirred under 1 atm of air at ambient temperature, a slow color change from pale green to dark purple was observed. Analysis of the reaction mixture by $^1$H NMR after 24 h showed complete consumption of **1** while analysis of the same reaction mixture by GC-MS showed production of PhCHO in 120 % yield vs. metal. This is roughly double the yield compared to stoichiometric conditions indicating that there is a small amount of turnover (Table A.1).

The low yield and presence of oxidized decomposition products suggest that the yield and rate of alcohol oxidation may be sensitive to substitution of the redox-active ligand. When 10 mol% of $[Re(O)(OPPh_3)(Br_4cat)_2]^-$ (**3**) was added to a BnOH solution of $[Re(O)_2(Br_4cat)_2]^-$ (**4**) under $N_2$ a color change from dark purple to pale green was produced over 1.5 hours at ambient temperature. Analysis of the green solution by UV-vis and FAB-MS shows complete consumption of **4**. Analysis of the same reaction mixture by GC-MS shows formation of PhCHO as the only organic product in 93 % yield (Table A.1). When the reaction was performed under the catalytic conditions described earlier, PhCHO was produced in 720% yield vs. metal, over 1 week, indicating a significant increase in turnover. When base was added to the reaction at catalytic conditions, the yield vs. metal can be significantly increased, suggesting that base stabilizes certain species during the oxidation process which leads to higher turnover numbers (Table A.2).

**Table A.1.** Oxidation of BnOH to PhCHO by oxorhenium complexes.

| $Re^{V}$ (mM) | $Re^{VII}$ (mM) | ligand | substrate | conditions | GC yield (%) | TON |
|---|---|---|---|---|---|---|
| 1 | 9.4 | $cat^{2-}$ | BnOH | $N_2$ | 58 | n/a |
| 8.8 | 0 | $cat^{2-}$ | BnOH | air | 120 | 1 |
| 0.09 | 9.4 | $Br_4cat^{2-}$ | BnOH | $N_2$ | 93 | n/a |
| 8.4 | 0 | $Br_4cat^{2-}$ | BnOH | air | 726 | 7 |

**Table A.2.** Catalytic oxidation of BnOH to PhCHO by $[Re(O)(cat)_2]^-$ in the presence of base.

| $Re^{V}$ (mM) | equiv BnONa | time (h) | GC yield (%) | TON |
|---|---|---|---|---|
| 4.3 | 0 | 27 | 130 | 1 |
| 4.0 | 1 | 21 | 420 | 4 |
| 4.3 | 17 | 27 | 510 | 5 |
| 4.0 | 89 | 21 | 1390 | 13 |

The formation of $\mathbf{I_B}$ was investigated via UV-vis spectrometry starting with a pure solution of **2** by pre-treatment with 0.2 equiv pyridine-N-oxide to oxidize small quantities of **1** present in **2**.[40] The pure solution of **2** was then treated with base or **1** which leads to a faster formation of $\mathbf{I_B}$, whereas the increase in kinetics was larger when **1** was added compared to base (Figure A.4).

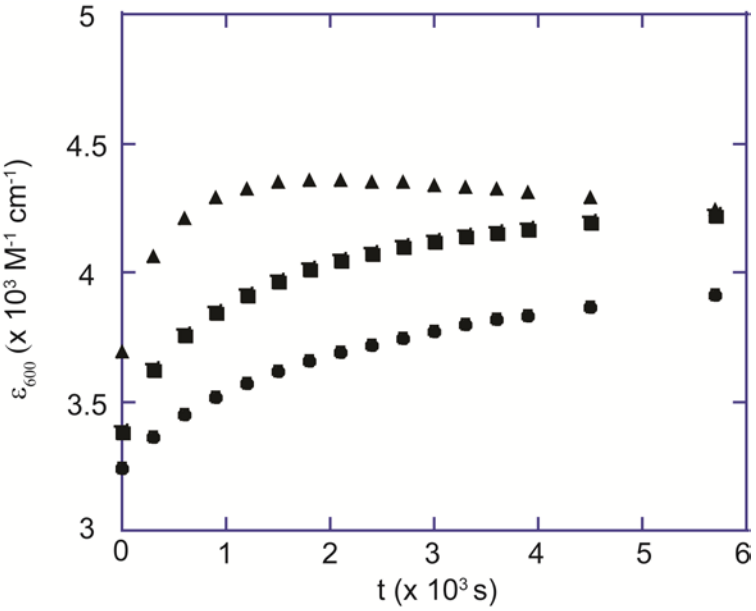


**Figure A.4.** Time-resolved data for the formation and decay of $\mathbf{I_B}$ in reactions of 3.6 × $10^{-4}$ M **2** with 0.2 equiv pyridine oxide (●), 20 equiv LiMeOH (■), and 1 equiv **1** (▲) in MeOH at 25 °C.

The formation of a similar blue species is also achieved by a combination of $(Et_4N)[Re^{VII}(O)_2(^tBu_2cat)_2]$ and $(Et_4N)[Re^{V}(O)(^tBu_2cat)_2]$ in MeOH which eventually yields a pale green solution after 1 day. Analysis of the green solution by $^1$H NMR reveals the formation of $(Et_4N)[Re^{V}(O)(^tBu_2cat)_2]$. A combination of **3** and **4** in MeOH does not generate a blue solution within 24 hours.

The catalytic oxidation of phenylethanol and benzylamine by **1** leads to the formation of acetophenone and benzaldehyde, respectively (observed qualitatively by GC-MS). This expands the substrate range to include secondary alcohols, although the relative reaction rate increases to seven days compared to hours with BnOH.

## A.3 Discussion

High-valent rhenium complexes have been shown to be effective alcohol oxidation catalyst.[24- 29] However, they are typically limited by the use of stoichiometric

co-oxidants such as $H_2O_2$ or PhIO to generate the oxidizing oxorhenium or peroxorhenium species.[24-28] The use of molecular oxygen would be the ideal co-oxidant, but high-valent oxorhenium(V) complexes are usually inert towards $O_2$ due to the electronic requirements of dioxygen activation. Activation of molecular oxygen is a $4e^-$ process that is typically carried out by multiple single electron steps. This would require a $1e^-$ oxidation of oxorhenium(V) to oxorhenium(VI), but oxorhenium(VI) complexes are extremely rare compared to their $d^0/d^2$ counterparts. The use of redox-active ligands provides a $1e^-$ pathway that does not require the formation of unfavorable $d^1$, oxorhenium(VI) complexes. This provides a methodology for utilizing $O_2$ as a co-oxidant for catalytic alcohol oxidations.

### A.3.1 Mechanistic Insights

Redox-active ligands facilitate $O_2$ homolysis by providing a lower energy pathway consisting of multiple $1e^-$ events necessary to overcome the kinetic barrier of triplet oxygen. Bimetallic homolysis of $O_2$ by oxorhenium(V) complexes containing redox-active ligands produces dioxorhenium(VII) complexes. A mixture of oxorhenium(V) and dioxorhenium(VII) in the presence of alcohols produce an oxidizing species that is capable of selectively oxidizing primary alcohols to their corresponding aldehydes and converting the dioxorhenium(VII) to oxorhenium(V) completing the catalytic cycle.

The oxorhenium(V) complexes are five-coordinate and therefore contain an open site for coordination of a $6^{th}$ ligand. There is relevant literature showing the ability of five-coordinate oxorhenium(V) complexes containing redox-active catechol ligands to coordinate a MeOH molecule in its empty coordination site. It is conceivable that this MeOH ligand can hydrogen bond to a catechol-oxygen of $[Re^{VII}(O)_2(cat)_2]^-$ forming a close contact, leading to a methanol transfer to the dioxo and the formation of the active species $\mathbf{I_B}$.[30] This hypothesis has been supported from previously reported, isolated

dinuclear rhenium complexes that are bridged by Lewis bases and/or hydrogen bonding interactions.[31- 35]

The absorption at 600 nm is only dependent on the concentration of **1** which suggests that $\mathbf{I_B}$ only derives from $[Re^{VII}(O)_2(cat)_2]^-$. Since the formation of $I_B$ is faster with higher concentrations of **1**, it seems that $[Re^{V}(O)(cat)_2]^-$ is only a catalyst to form $\mathbf{I_B}$ but itself is not part of the active, oxidizing species. In the absence of an easily oxidizable alcohol, $I_B$ decomposes to perrhenates and **1** (Scheme A.2). If the reaction is carried out in benzyl alcohol, **1** transfers BnOH instead of MeOH which leads to a seven-coordinate Re(VII) species similar to that in the catalytic cycles of methyltrioxorhenium (Scheme A.3).[36,37]

**Scheme A.2.**

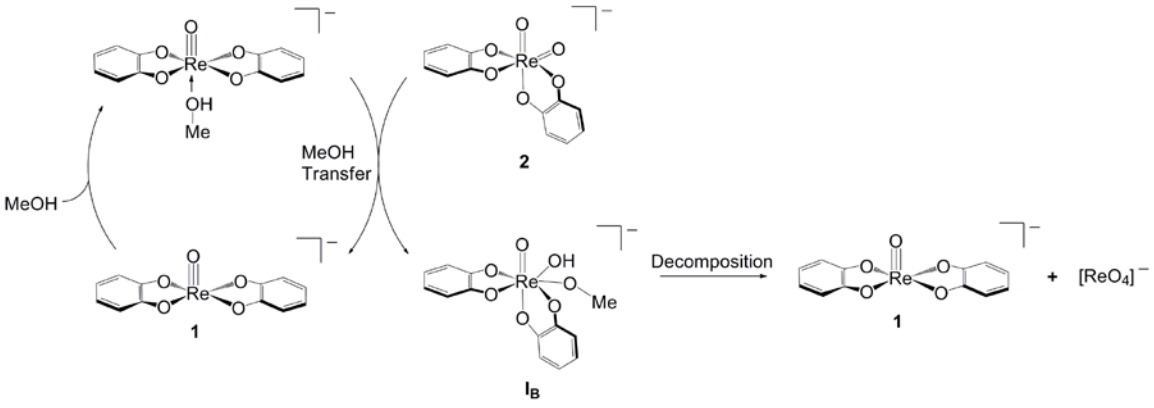

**Scheme A.3.**

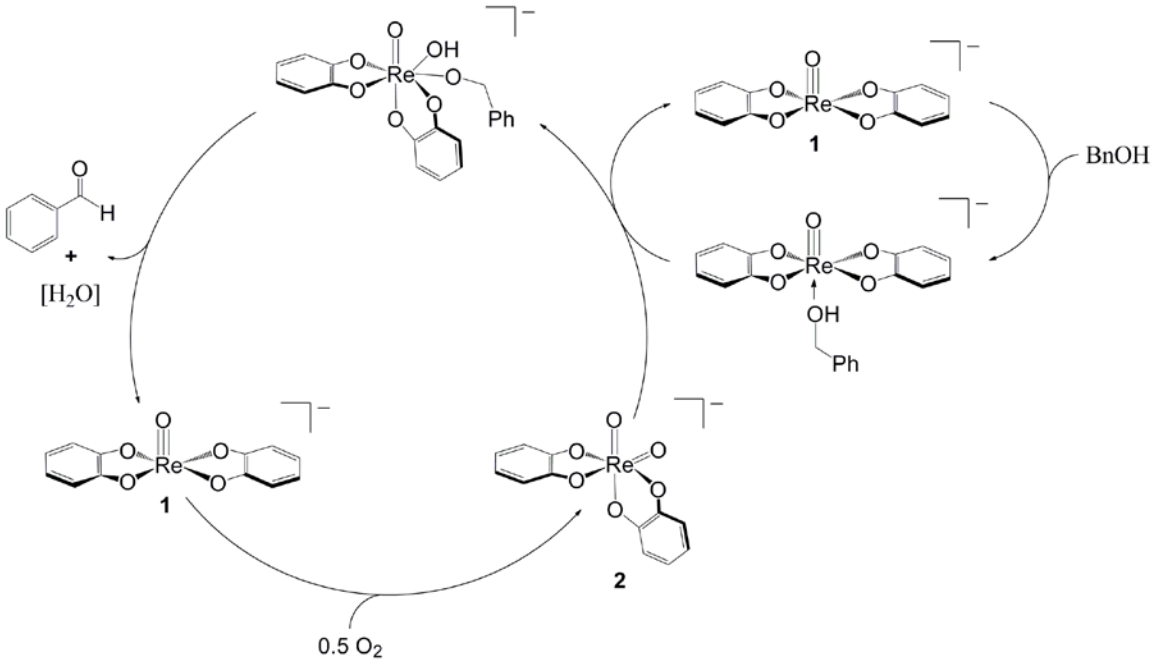


The seven-coordinate hydroxo-alkoxo Re(VII) species oxidizes BnOH to PhCHO generating $H_2O$ and **1**, although production of water has yet to be confirmed. Oxidation by $O_2$ to form **2** completes the catalytic cycle. The higher turnover numbers with the presence of base can be explained by faster formation of the alkoxo species. The addition of the more nucleophilic $BnO^-$, which might also be pre-coordinated by $[Re^V(O)(cat)_2]^-$ , leads to a faster formation of the active complex (Scheme A.4). If the decomposition pathway is significantly slower than oxidation to aldehyde, then catalytic yields should be higher.

**Scheme A.4.**

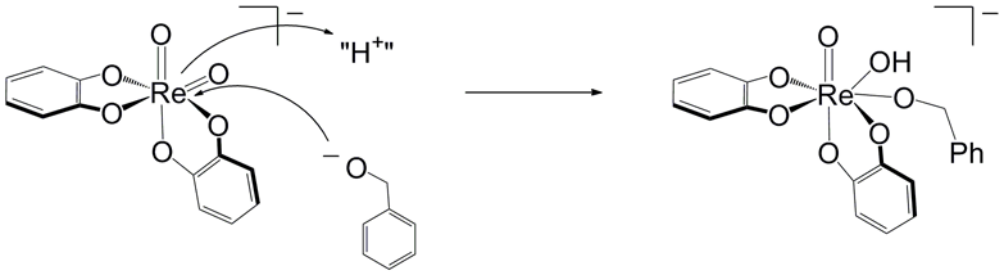


**A.3.2 Ligand Effects on Alcohol Oxidation**.

The presence of non-alcohol derived products during the course of the reaction suggests that the oxidizing system should be tunable based on the redox potential of the redox-active ligands. Substitution of the $[cat]^{2-}$ ligands with the harder to oxidize, electron poor $[Br_4cat]^{2-}$ ligand gave a decrease in oxidized, decomposition products which lead to a near quantitative yield of aldehyde formation (Table A.1). The two oxorhenium complexes Containing $[cat]^{2-}$ or $[Br_4cat]^{2-}$ ligands oxidize BnOH at the same relative rate, 75 ± 15 min.

The redox potential of the redox-active ligand appears to have negligible effect on the relative rate of alcohol oxidation, but ligands with higher redox potentials make a more robust catalyst that is less susceptible to unwanted degradative oxidations and thus provides a higher yield of aldehyde formation. However, the same trait that enables such high yields of aldehyde and robustness also provides catalytic limitations. The relative rates of alcohol oxidation of the two complexes are nearly identical which suggest that the catalytic limiting factor is the reaction with dioxygen to produce dioxorhenium(VII). The rate-limiting step appears to change based on the nature of the

ligand utilized. When the $[cat]^{2-}$ ligand is used the rate determining step appears to be alcohol oxidation. Complex **1** reacts rapidly with $O_2$ and deactivates itself by converting every molecule of **1** to **2** and cannot form the active species fast enough compared to degradation necessary for alcohol oxidation. On the other hand, complex **3** reacts slowly with $O_2$ and therefore takes extended reaction times for catalytic oxidation. The catalytic oxidation of secondary alcohols by **1** also led to the respective carbonyl compounds but at much slower rates than for primary substrates. This suggests that with increased steric bulk of the substrates the kinetics of the oxidation decrease due to steric hindrance.

## A.4 Conclusion

In sum, high-valent oxorhenium(V) and dioxorhenium(VII) complexes containing redox-active ligands afford selective oxidation of BnOH to PhCHO. The oxidizing species is an hydroxo-alkoxo rhenium(VII) complex formed by alcohol transfer from oxorhenium(V) to dioxorhenium(VII). The ability of five-coordinate oxorhenium(V) complexes containing redox-active ligands to activate dioxygen to produce dioxorhenium(VII) bestows the means for selective, catalytic aerobic oxidation of alcohols. The redox potentials of the various redox-active ligands provide a means for fine tuning of selective alcohol oxidation by matching the rate of $O_2$ activation to the rate of the alcohol oxidation.

## A.5 Experimental Details and Supplementary Material

### A.5.1 General Considerations

Unless otherwise specified, all manipulations were performed under anaerobic conditions using standard vacuum line techniques, or in an inert atmosphere glove box under purified nitrogen. Routine NMR spectra were acquired on a Varian Mercury 300 spectrometer (300.323 MHz for $^1H$). All chemical shifts are reported in parts per million (ppm) relative to TMS, with the residual solvent peak serving as an internal reference.

UV-visible absorption spectra were acquired using a Varian Cary 50 spectrophotometer. Unless otherwise noted, all electronic absorption spectra were recorded at ambient temperatures in 1 cm quartz cells. All mass spectra were recorded in the Georgia Institute of Technology Bioanalytical Mass Spectrometry Facility. Electrospray ionization mass spectrometry (ESI-MS) was carried out with acetonitrile solutions using a Micromass Quattro LC spectrometer. Fast atom bombardment mass spectra (FAB-MS) were acquired in the negative mode on a VG Instruments 70-SE spectrometer. GC-MS was performed on GC-HP5890 using a J&W-DB-5 column (30 m x 0.25 mm) equipped with a VG instruments model 70-SE electron impact mass spectrometer.

**A.5.2 Methods and Materials**

Anhydrous acetonitrile (MeCN), dichloromethane, and pentane solvents for air- and moisture-sensitive manipulations were purchased from Sigma-Aldrich and further dried by passage through columns of activated alumina, degassed by at least three freeze-pump-thaw cycles, and stored under $N_2$ prior to use. Methanol (anhydrous, 99.0%), was purchased from Honeywell Burdick and Jackson. Ethanol (anhydrous, 200 proof, 99.5%), was purchased from Sigma-Aldrich. Acetone (99.8%, extra dry) was purchased from Acros. All were used as received. Deuterated acetonitrile (MeCN-*d*3), dichloromethane ($CD_2Cl_2$), and methanol (MeOH-*d*4) were purchased from Cambridge Isotope Laboratories, degassed by three freeze-pump-thaw cycles, vacuum distilled from $CaH_2$, and stored under a dry $N_2$ atmosphere prior to use. $(Et_4N)[Re^{V}(O)(cat)_2]$,[38] $(Et_4N)[Re^{VII}(O)_2(cat)_2]$,[38] $(Et_4N)[Re^{V}(O)(OPPh_3)(Br_4cat)_2]$,[39] $(Et_4N)[Re^{V}(O)_2(OPPh_3)(Br_4cat)_2]$,[23] $(Et_4N)[Re(O)(^tBu_2cat)_2]$,[40] and $(Et_4N)[Re(O)_2(^tBu_2cat)_2]$[24] were prepared by literature methods. All characterization data matched those referenced. All other reagents were purchased from Sigma-Aldrich and used as received.

### A.5.3 Reactions with Dioxygen in MeOH

A 1.0 cm quartz cuvette fitted with a Kontes brand high-vacuum PTFE valve was charged with 2.0 mL of a $4.5 \times 10^{-4}$ M solution of **1** in MeOH and sealed under $N_2$. The solution was degassed on a high-vacuum line by three freeze-pump-thaw cycles and an initial spectrum was acquired. The cuvette was then backfilled with 1 atm of air, shaken vigorously, placed in a Peltier UV-vis cell holder with a magnetic stirrer, and stirred to maintain a constant concentration of dissolved $O_2$ throughout the reaction. The reaction progress was monitored by UV-vis spectroscopy (200-900 nm) for 3000 min at 5 min intervals. For NMR kinetics studies, a J. Young brand NMR tube with a Teflon screw cap was used in place of the sealable cuvette.

### A.5.4 Formation of $I_B$ With Constant 2 and Variable 1

A 1.0 cm quartz cuvette fitted with a Kontes brand high-vacuum PTFE valve was charged with 2.2 mL of $[Re^{VII}(O)_2(cat)_2]^-$ ($1.5 \times 10^{-4}$ M) and $[Re^{V}(O)(cat)_2]^-$ ($0.2\text{-}2.4 \times 10^{-4}$ M) in MeOH and sealed under $N_2$. The cuvette was shaken vigorously and placed in a Peltier UV-vis cell holder. The reaction progress was monitored by UV-vis spectroscopy (300-1000 nm) at 2 min intervals.

### A.5.5 Formation of $I_B$ With Constant [Re]

A 1.0 cm quartz cuvette fitted with a Kontes brand high-vacuum PTFE valve was charged with 2.2 mL of $[Re^{VII}(O)_2(cat)_2]^-$ ($0.7\text{-}3.1 \times 10^{-4}$ M) and $[Re^{V}(O)(cat)_2]^-$ ($0.9\text{-}3.3 \times 10^{-4}$ M) in MeOH to give a total metal concentration of $4 \times 10^{-4}$ M and sealed under $N_2$. The cuvette was shaken vigorously and placed in a Peltier UV-vis cell holder. The reaction progress was monitored by UV-vis spectroscopy (300-1000 nm) at 2 min intervals.

### A.5.6 Formation of $I_B$ From Pure Solution of 2

A 1.0 cm quartz cuvette fitted with a Kontes brand high-vacuum PTFE valve was charged with 2.2 mL of a $3.6 \times 10^{-4}$ M solution of **2** and pyridine oxide ($0.7 \times 10^{-4}$ M) in

MeOH and sealed under $N_2$. The experiment was repeated with LiOMe ($7.1 \times 10^{-3}$ M), and again with $[Re^{V}(O)(cat)_2]^-$ ($3.6 \times 10^{-4}$ M). The cuvette was shaken vigorously and placed in a Peltier UV-vis cell holder. The reaction progress was monitored by UV-vis spectroscopy (300-1000 nm) for 95 min at 5 min intervals.

**A.5.7 Stoichiometric Alcohol Oxidation**

In a representative procedure, a 20-mL scintillation vial was charged with 4 mL of a 12.1 mM solution of **2** and 1 mL of a 5 mM solution of **1** in BnOH to give a final concentration of 9.4 mM and 1.0 mM respectively. The reaction mixture was stirred at ambient temperature for 15 h. For GC-MS analysis an aliquot was transferred to a 1.5 mL screw top vial, sealed under $N_2$ with a screw cap with a septum top, and injected directly into the gas chromatograph. For NMR analysis, the same reactants were combined in a J. Young brand NMR tube with a Teflon screw cap, using MeOH-*d*4 as the solvent. The reaction was monitored over 48 h.

**A.5.8 Catalytic Alcohol Oxidation**

In a representative procedure, a 20-mL scintillation vial was charged with 5 mL of a 8.8 mM solution of **1** in BnOH and stirred under 1 atm of air for 15 h. For GC-MS analysis an aliquot was transferred to a 1.5 mL screw top vial, sealed with a screw cap with a septum top, and injected directly into the gas chromatograph.

**A.5.9 Catalytic Alcohol Oxidation in the Presence of Base**

In a representative procedure, a 20-mL scintillation vial was charged with 2 mL of a 10 mM solution of **1** in a BnOH/$BnO^-$ solution (100 mM $BnO^-$) and stirred under 1 atm of air for 15 h. For GC-MS analysis an aliquot was transferred to a 1.5 mL screw top vial, sealed with a screw cap with a septum top, and injected directly into the gas chromatograph.

## A.6 References


[1] Sheldon, R. A.; Kochi, J. K. *Metal Catalyzed Oxidations of Organic Compounds*, Acedemic Press, New York, **1981,** 1.

[2] Ley, S. V.; Griffith, W. P.; Marsden, S. P. *Synthesis* **1994**, 639.

[3] Sheldon, R. A.; Arends, I. W. C. E.; Dijisman, D. *Catal. Today* **2000**, 157.

[4] March, Jerry **1985**, *Advanced Organic Chemistry: Reactions, Mechanisms, and Structure* (3rd ed.), New York: Wiley.

[5] Pillai, U. R.; Sahle-Demessie, E. *Appl. Catal., A* **2003**, *245*, 103.

[6] Griffith, W. P.; Joliffe, J. M. *Stud. Surf. Sci. Catal.* **1991**, *66*, 395.

[7] Cainelli, G.; Cardillo, G. *Chromium Oxidants in Organic Chemistry*; Springer: Berlin, **1984**.

[8] Collman, J. P.; Devaraj, N. K.; Decreau, R. A.; Yang, Y.; Yan, Y. L.; Ebina, W.; Eberspacher, T. A.; Chidsey, C. E. D. *Science* **2007**, *315*, 1565.

[9] *Oxygen Complexes and Oxygen Activation by Transition Metals*; Martell, A. E., Sawyer, D. T., Eds.; Plenum: New York, **1988**.

[10] *The Activation of Dioxygen and Homogeneous Catalytic Oxidation*; Barton, D., H. R., Martell, A. E., Sawyer, D. T., Eds.; Plenum: New York, **1993**.

[11] Boring, E.; Geletii, Y. V.; Hill, C. L. *Catal. Met. Complexes* **2003**, *26*, 227-264.

[12] Dijksman, A.; Arends, I. W. C. E.; Sheldon, R. A. *Platinum Met. Rev.* **2001**, *45*, 15-19.

[13] Murahashi, S.-I.; Komiya, N.; Hayashi, Y.; Kumano, T. *Pure Appl. Chem.* **2001**, *73*, 311-314.

[14] Zhan, B.-Z.; Thompson, A. *Tetrahedron* **2004**, *60*, 2917-2935.

[15] Stahl, S. S. *Angew. Chem., Int. Ed.* **2004**, *43*, 3400-3420.

[16] Stahl, S. S. *Science* **2005**, *309*, 1824-1826.

[17] *Advances in Catalytic Activation of Dioxygen by Metal Complexes*; Simandi, L. I., Ed.; Kluwer Acadmic Publishers: Norwell, MA, **2003**.

[18] Borovik, A. S.; Zinn, P. J.; Zart, M. K. In *Activation of Small Molecules: Organometallic and Bioinorganic Perspectives*; Tolman, W. B., Ed.; Wiley-VCH: Weinheim, Germany, **2006**, 187-234.

[19] Nam, W. *Acc. Chem. Res.* **2007**, *40*, 465.

[20] Chaudhuri, P.; Wieghardt, K.; Weyhermueller, T.; Paine, T. K.; Mukherjee, S.; Mukherjee, C. *Biol. Chem.* **2005**, *386*, 1023-1033.

[21] Chaudhuri, P.; Hess, M.; Mueller, J.; Hildenbrand, K.; Bill, E.; Weyhermueller, T.; Wieghardt, K. *J. Am. Chem. Soc.* **1999**, *121*, 9599-9610.

[22] Wang, Y.; DuBois, J. L.; Hedman, B.; Hodgson, K. O.; Stack, T. D. P. *Science* **1998**, *279*, 537-540.

[23] Lippert, C. A.; Arnstein, S. A.; Sherrill, C. D.; Soper, J. D. J. Am. Chem. Soc. **2010**, 132, 3879-3892.

[24] Praskevopoulou, P.; Psaroudakis, N.; Koinis, S.; Stavropoulos, P.; Mertis, K. *J. Mol. Catal. A:Chem* **2005**, 240, 27-32.

[25] Hermann, W. A.; Zoller, J. P.; Fischer, R. W. *J. Organomet. Chem.* **1999**, 404-407.

[26] Zauche, T. H.; Espenson, J. H. *Int. J. Chem. Kinet.***1998**, 381-385.

[27] Zauche, T. H.; Espenson, J. H. *Inorg. Chem.* **1998**, 37, 6827-6831.

[28] Espenson, J. H.; Zhu, Z.; Zauche, T. H. *J. Org. Chem.* **1999**, 64, 1191-1196.

[29] Buonomenna, M. G.; Drioli, E. Org. *Process Res. Dev.* **2008**, 12, 982-988.

[30] Edwards, C. F.; Griffith, W. P.; White A. J. P.; Williams, D. J. *J. Chem. Soc., Dalton Trans.* **1992**, 957-962.

[31] Machura, B.; Dziegielewski, J. O.; Michalik, S.; Kruszynksi, R.; Bartczal, T. J.; Kusz, *Trans. Met. Chem.* **2003**, 28, 939-947.

[32] Backes-Dahmann, G.; Enemark, J. H. *Inorg. Chem.* **1987**, 26, 3960-3962.

[33] Machura, B.; Jaworka, M.; Kruszynski, R. *Inorg. Chim. Acta.* **2006**, 359, 1303-1313.

[34] Tadokoro, M.; Inoue, T.; Tamaki, S. Fujii, K.; Isogai, K.; Nakazawa, H.; Takeda, S.; Isobe, K.; Koga, N.; Ichimura, A.; Nakasuji, K. *Angew. Chem. Int. Ed.* **2007**, 46, 5938-5942.

[35] Jacob, J.; Lente, G.; Guzei, L. A.; Espenson, J. H. *Inorg. Chem.* **1999**, 38, 3762-3763.

[36] Herrmann, W. A.; Fischer, R. W.; Marz D. W. *Angew. Chem. Int. Ed.* **1991**, *30*, 1638-1641.

[37] Herrmann, W. A.; Fischer, R. W.; Scherer, W.; Rauch, M. U. *Angew. Chem. Int. Ed.* **1993**, *32*, 1157-1160.

[38] Dilworth, J. R.; Ibrahim, S. K.; Khan, S. R.; Hursthouse, M. B.; Karaulov, A. A. *Polyhedron* **1990**, *9*, 1323-1329.

[39] Edwards, C. F.; Griffith, W. P.; White, A. J. P.; Williams, D. J. *J. Chem. Soc., Dalton Trans.* **1992**, 957-962.

[40] Lippert, C. A.; Soper, J. D. *Inorg. Chem.* **2010**, 49, 3682-3684.